Prophylaxis of Renal Ischaemia Reperfusion Injury: Ischaemic Preconditioning and Drug Repurposing

David Foxwell, MBBCh, MRCP(UK), MRCGP

Thesis presented for the Degree of Philosophiae Doctor

April 2023

Wales Kidney Research Unit
Division of Infection & Immunity
School of Medicine
Cardiff University
Heath Park
Cardiff, CF14 4XN

Acknowledgements

I would like to express my gratitude and sincere thanks to my supervisors and colleagues. Without your guidance I could never have completed this PhD.

To *Professor Tim Bowen*, whose steadfast support and belief in me has been the foundation of this journey. Thank you for being my teacher, my sounding board and most importantly, my friend. Your attention to detail and care for your students is what makes you a fantastic supervisor. Without you I could not have achieved this piece of work.

To *Professor Donald Fraser*, your encouragement, mentorship, and counsel has given me direction throughout this PhD. I will always be thankful for the faith you have shown in me. Thank you for your constant support and ability to always see the positives!

To *Mr Rafael Chavez,* who believed that you could teach a medic to be a surgeon. Your wit, intelligence, and help with my PhD has never wavered. I will always remember our conversations in your office. Thank you for your encouragement and inspiration over the years.

Special thanks to Mr Usman Khalid, your enormous patience when teaching me the experimental techniques was key to my PhD. Dr Robert Andrews, for your time and instruction when analysing the transcriptomics data. Dr Gilda Pino-Chavez, for your kindness when examining the histology scoring. Dr Soma Meran and Dr Chantal Colmont for your wisdom and guidance over the years. To Debbie and Kerry (JBIOS) thank you for your advice and infinite understanding.

To Sarah,

Whose love, patience, and care

has filled my heart

and made this all possible

To Emmy,

Your wonderful smile

and belief in your dad

gave me the strength to follow my dreams

&

To my mum, Lesley,

Your endless love and support for me

has never wavered

Thesis Summary

Acute Kidney Injury (AKI) is a devastating condition leading to the morbidity and mortality in millions of sufferers each year. The commonest cause of AKI is ischaemic reperfusion injury (IRI), which often complicates organ transplantation and sepsis. Despite extensive scientific research, no effective preventative treatments are currently available for IRI in humans. In *in* vivo models, IRI in the rat kidney mimics the functional and histological injury seen in the human kidney following IRI. A preventative treatment for IRI called ischaemic preconditioning (IPC) has, in some instances, been shown to ameliorate IRI *in vivo.* However, the detailed molecular mechanisms underlying IPC function remain unknown, and this technique has failed to translate to the clinical setting.

The purpose of the work carried out in this thesis was to investigate alterations in gene expression profiles caused by IRI, to characterise changes to this IRI-specific gene expression profile resulting from IPC treatment, and to investigate pharmacological agents which could be used to attenuate IRI. The work first used an established *in vivo* rat model of IRI to optimise a suitable IPC protocol. Next generation sequencing (NGS) was then used to perform an unbiased analysis of the transcriptomic profiles elicited by IRI and IPC. Bioinformatic analysis of IRI revealed enrichment of pathways linked to cytokine dysregulation, nuclear signalling, extra cellular matrix/cytoskeleton signalling and leucocyte trafficking. Two different IPC strategies were compared computationally and were found to act via similar response pathways. Using the transcriptional profile data for IRI and IPC, a pathway-based mapping analysis was used to identify candidate drugs to prevent IRI by recapitulating the effects of IPC. Six drugs were validated *in vivo*, revealing in particular the beneficial effects of the drug pirfenidone in renal IRI prevention.

Publications, Presentations Arising from this Thesis

Peer- reviewed Publications:

- **Foxwell D**, Pradhan S, Zouwail S, Rainer TH, Phillips AO. Epidemiology of emergency department acute kidney injury. Nephrology (Carlton). 2020 Jun;25(6):457-466. doi: 10.1111/nep.13672. Epub 2019 Nov 27. PMID: 31654593.

- Phillips A, **Foxwell D**, Pradhan S, Zouwail S, Rainer TH. Derivation of a prediction model for emergency department acute kidney injury. Am J Emerg Med. 2020 Dec 13;40:64-69. doi: 10.1016/j.ajem.2020.12.017. Epub ahead of print. PMID: 33348226.

Oral Presentations at Conferences

- **Foxwell D**, Khalid U, Andrews R, Pino-Chavez G, Chavez R, Bowen T, Fraser D. Renal Ischaemic Preconditioning: Total RNA Sequencing, The Hunt for The Mechanism Continues. Welsh Association of Renal Physicians and Surgeons (WARPS) Annual Meeting, 23rd June 2017.

- **Foxwell D**, Khalid U, Andrews R, Pino-Chavez G, Chavez R, Bowen T, Fraser D. Peripheral Ischaemic Preconditioning – A method to reduce kidney Ischaemia Reperfusion Injury 18th Congress of the European Society for Organ Transplantation, Barcelona, Spain, 24-27 September 2017.

- **Foxwell D**, Khalid U, Andrews R, Pino-Chavez G, Chavez R, Bowen T, Fraser D. Total RNA Sequencing and Ingenuity Pathway Analysis Reveal Shared Gene Expression Profiles for Protection Conferred by Direct and Indirect Ischaemic Preconditioning. UK Kidney Week annual conference 2018, Harrogate, UK, 19th – 21st June 2018.

Poster Presentations at Conferences

- **Foxwell D**, Khalid U, Andrews R, Pino-Chavez G, Chavez R, Bowen T, Fraser D. Ischaemic Preconditioning of the Kidney: Total RNA Sequencing and Ingenuity Pathway Analysis. American Society of Nephrology (New Orleans, LA, USA) annual meeting, Oct 31 - Nov 5, *2017.*

- **Foxwell D**, Khalid U, Andrews R, Pino-Chavez G, Chavez R, Bowen T, Fraser D.. Identification of novel drugs that mimic ischaemic preconditioning in the treatment of kidney ischaemia reperfusion injury. British Transplantation Society (Belfast, NI), annual meeting, 4th-6th March 2020.

- **Foxwell D**, Khalid U, Andrews R, Pino-Chavez G, Chavez R, Bowen T, Fraser D. Pirfenidone confers effective prophylaxis of renal ischaemia reperfusion injury. American Society of Nephrology (Orlando, FL, USA), 3th-6th November 2022.

Abbreviations and Acronyms

ADQI	Acute Dialysis Quality Initiative
AKI	Acute Kidney Injury
AKIN	Acute Kidney Injury Network
ARF	Acute Renal failure
ATP	Adenosine Triphosphate
BAD	BCL2 Associated Agonist Of Cell Death
BAK	Bcl-2 Homologous Antagonist Killer
BAX	Bcl-2-Associated X Protein
BCL-2	B-cell Lymphoma 2
CA-AKI	Community Acquired Acute Kidney Injury
CABG	Coronary Artery Bypass Graft Surgery
CAT	Catalase
CCL2	Monocyte Chemoattractant Protein-1, MCP-1
CCR1	C-C Chemokine Receptor Type 1
CCR7	C-C Chemokine Receptor Type 7
cGMP-PKC	Cyclic Guanosine Monophosphate/Protein Kinase C
CKD	Chronic Kidney Disease
CP	Chemical Preconditioning
CXCL-1	C-X-C Motif Chemokine Ligand 1
DAMP	Damage Associated Molecular Patterns
DC	Dendritic Cells
de-novo CKD	New Onset Chronic Kidney Disease
DEG	Differentially Expressed Gene
DISC	Death-Induced Signalling Complex
DNA	Deoxyribonucleic Acid
DR	Death Receptor
ECM	Extracellular Matrix
ED-AKI	Emergency Department Acute Kidney Injury
eGFR	estimated Glomerular Filtration Rate
ESRD	End Stage Renal Disease
ETC	Electron Transport Chain
FASL	Fas Ligand
FPKM	Fragments Per Kilobase of transcript per Million mapped
Fut7	Fucosyltransferase Type 7
GFR	Glomerular Filtration Rate
GM-CSF	Granulocyte-Macrophage Colony-Stimulating Factor
GO	Gene Ontology
GPCR	G-protein Coupled Receptors
GSA	Gene Set Analysis
GSK3	Glycogen Synthase Kinase-3 Beta
HA-AKI	Hospital Acquired Acute Kidney Injury

HMGB1	High Mobility Group Box 1
HO-1	Heme Oxygenase-1
HR	Hazard Ratio
I-POC	Ischaemic Postconditioning
IBD	Inflammatory Bowel Disease
IC	Ischaemic Conditioning
ICAM-1	Intracellular Adhesion Molecule-1
ICU-AKI	Intensive Care Unit Acute Kidney Injury
IFN	Interferon
IFN-γ	Interferon Gamma
IL-1	Interleukins-1
IL-12	Interleukins-12
IL-1β	Interleukin-1 beta
IL-4	Interleukins-4
IL-6	Interleukin-6
IPA	Ingenuity Pathway Analysis
IPC	Ischaemic Preconditioning
IRI	Ischaemic Reperfusion Injury
KDIGO	Kidney Disease: Improving Global Outcomes
KEGG	Kyoto Encyclopaedia of Genes and Genomes
log_2FC	log_2 Fold Change
MA	Meta-Analysis
MAC	Membrane Attack Complex
MAC-1	Macrophage-1 Antigen
MCP-1	Monocyte Chemoattractant Protein-1
MtDNA	Mitochondrial DNA
MDRD	Modification of Diet in Renal Disease
MHC-II	Major Histocompatibility Complex Class II
MIP-2	Macrophage Inflammatory Protein-2
MK(ATP)	Mitochondrial Potassium Channel
MLKL	Mixed Kinase-Like Protein
MPTP	Mitochondrial Permeability Transition Pore
MRNA	Messenger RNA
Myd88	Marrow Differentiation Factor 88
NADPH Oxidases	Nicotinamide Adenine Dinucleotide Phosphate Oxidase Enzyme Complex
NFκB	Nuclear Factor Kappa B
NGS	Next Generation Sequencing
NHS	National Health Service
NLR	Nucleotide-Binding Oligomerization Domain-Like Receptors
NOD1	Nucleotide Binding Oligomerization Domain Containing 1
NOD2	Nucleotide Binding Oligomerization Domain Containing 2
non-AKI	No Acute Kidney Injury
NQO-1	NADPH-Quinone Oxidoreductase-1

NRF2	Nuclear Factor Erythroid 2–Related Factor 2
NSF	National Kidney Foundation
OSM	Oncostatin-M
P13K-Akt	Phosphatidylinositol-3-OH Kinase
PA	Pathway Analysis
PCA	Principal Component Analysis
PECAM-1	Platelet Endothelial Cell Adhesion Molecule 1
PKC	Protein Kinase C
PKG	Protein Kinase G
PMP	Per Million Population
PRR	Pattern Recognition Receptors
PSGL-1	P-Selectin Ligand Glycoprotein 1
RCT	Randomised Controlled Trials
RIFLE	Risk, Injury, Failure, Loss and End-Stage Renal Disease
RIN	RNA Integrity Number
RIPK1	Receptor-Interacting Protein Kinase 1
RISK	Reperfusion Injury Salvage Kinase
RNA	Ribonucleic Acid
ROS	Reactive Oxygen Species
RRT	Renal Replacement Therapy
sCr	Serum Creatinine
SOD	Superoxide Dismutase
TH	CD4+ T-Helper Cells
TLRs	Toll-Like Receptors
TNF-α	Tumour Necrosis Factor Alpha
TNFR1	TNF-Receptor Type 1
TRADD	TNF Receptor-Associated Death Domain
TRAF6	TNF Receptor-Associated Factor 6
TREM1	Triggering Receptor Expressed On Myeloid Cells
UK	United Kingdom
VCAM-1	Vascular Cell Adhesion Molecule 1
VDR	Vitamin D Receptor
WGP	The Wales Cancer Research Centre: Wales Gene Park
WT	Wild Type

Table of Contents

Chapter 1

Introduction

1.1 The Kidney

In humans, the kidneys are a pair of organs approximately 12 cm in length that reside on the left and right side of the body, posterior to the peritoneal lining of the abdomen. These innocuous, red, soft, bean shaped structures are one of the principal power houses sustaining homeostasis of the entire body's extracellular electrolyte composition and fluid balance[1; 2].

Structurally, the kidney can be divided into its outer portion, called the cortex, and its inner structure, the medulla. Each kidney has a renal artery that branches throughout the medulla and cortex delivering blood to the functional unit of the kidney, the nephron. Each kidney contains over 1 million nephrons.

At its most basic level, the nephron is composed of a renal corpuscle and a tubule. The corpuscle, located in the renal cortex, is a highly vascular structure of capillaries collectively termed the glomerulus, which is surrounded and supported by mesangial cells. The primary function of the glomerulus is to act as a filtration barrier, which in turn is enclosed by a cup-like structure called the Bowman's capsule[3]. The filtrate collects in the Bowman's capsule, passing through the capsule's lumen to the renal tubule.

The renal tubule can be broadly divided into 4 different segments that extend from the cortex to the medulla of the kidney. The first segment is the proximal convoluted tubule (found in the renal cortex) which leads to the Loop of Henle (mostly found in the medulla), which returns to the renal cortex as it delivers the filtrate to the distal convoluted tubule, culminating in the collecting tubule in the medulla[4]. Surrounding the tubules is a network of peritubular capillaries, called the vasa recta, which surround the Loop of Henle as it dives into the medulla, Figure 1.1. This interconnecting network of tubules and peritubular capillaries facilitates reabsorption of filtered electrolytes, solutes, and fluid, and excretes wastes and excessive

electrolytes and water. There is a complex interplay between the above segments and related structures through which physiological regulation and homeostasis is achieved [1; 5].

The importance of the nephron cannot be underestimated. Simply put, the kidney filters approximately 180 litres of blood a day, returning 99% of electrolytes and fluid to the circulation. This role in maintaining whole body physiology is critical to life[6]. If the kidneys fail, death is inevitable without replacement therapy.

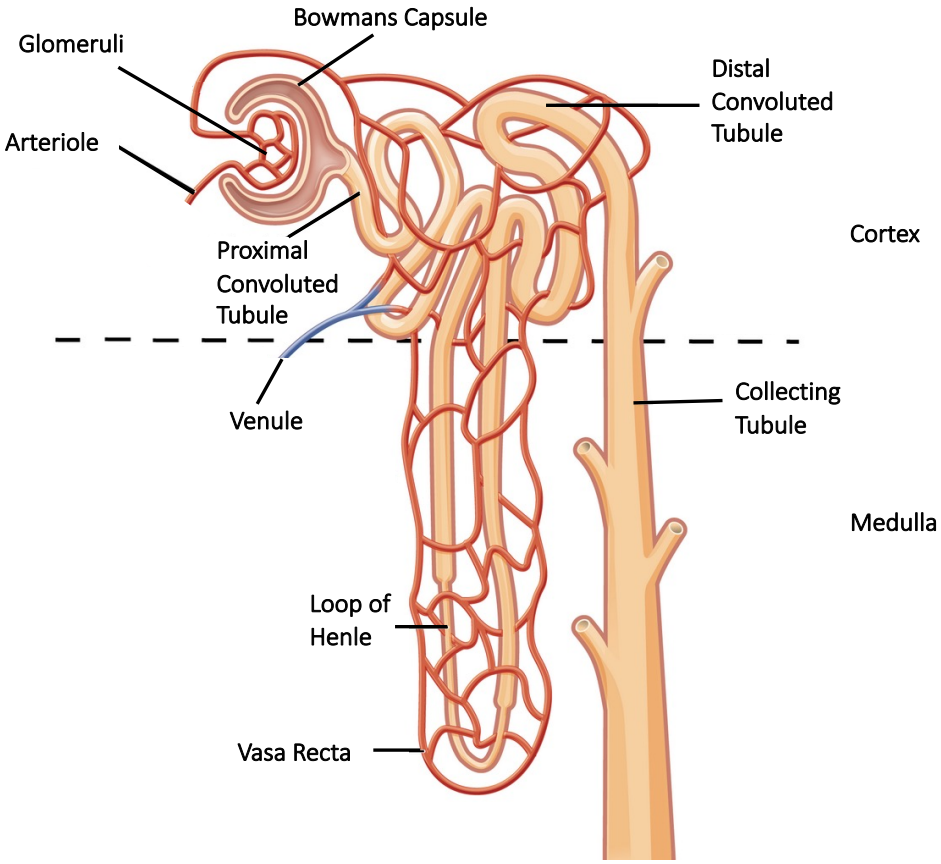

Figure 1.1 The Nephron

Anatomical representation of a single nephron of the kidney. The glomerulus and the bowman's capsule together are called the renal corpuscle and the rest of the nephron is collectively referred to as the renal tubule. The glomeruli creates 180 liters of filtrate of which 99% is reabsorbed into the systemic circulation through a complex mechanism of retention in the renal tubules.
(Adapted from https://open.oregonstate.education)

1.1.1 Kidney Disease

Kidney disease is defined as "an abnormality of kidney structure or function with implications for the health of an individual, which can occur abruptly, and either resolve or become chronic"[7]. In 2019, kidney disease was ranked the 10th leading cause of death in the world equating to an annual worldwide mortality of 1.3 million, an increase of 487,000 deaths compared to 2000[8]. Kidney disease can be broadly subdivided into acute (disease state occurring within days or weeks) or chronic (months to years). An understanding of the origins of kidney disease have been a result of over 200 years of intense scientific investigation and nomenclature evolution.

1.1.2 Acute Renal Failure

The modern notion of kidney disease was first described by Richard Bright (1827) who reported a clinical case series of patients found to have varying degrees of leg swelling (peripheral oedema), reduced urine output (oliguria) and albumin in the urine (reflecting failure of glomerular filtration to retain large molecules) which he attributed to acute reversable kidney failure[9]. Over the 19th century medical knowledge advanced and Bright's disease was divided into acute and chronic stages based on clinical examination and autopsy findings[10-12]. What Bright originally described was the whole spectrum of kidney disease caused by a multitude of causative insults spanning both acute and chronic disease[13]. For the next 100 years multiple apparently unrelated renal diseases were described leading to a syndrome of oliguria, anaemia, and hyperkalaemia, Figure 1.2 [12].

Before World War II		After World War II	
1760	Ischuria renalis	1941	Crush syndrome
1879	Renal inadequacy	1941	Pressure ischemia
1888	Hysterical ischuria	1942	Traumatic anuria
	Acute Bright's disease		Compressive syndrome
1917	Vasomotoric nephrosis	1944	Crush kidney syndrome
	War nephritis	1945	Traumatic uremia
1918	Toxic tubular nephritis	1946	Lower nephron nephrosis
1923	Toxic degenerative nephrosis	1947	Hemoglobinuric nephrosis
	Toxic nephritis	1948	Shock kidney
	Necrotizing nephrosis	1949	Acute uremia
1934	Acute tubular nephrosis	1951	Acute renal failure
1937	Traumatic nephritis		
1938	Acute hematogenous interstitial nephritis		
1938	Acute toxic nephrosis		
1940	Transfusion kidney		

Figure 1.2 Evolving terminology for Acute Renal Failure

Historical terms used to describe clinical observations consistent with renal failure, adapted from (Eknoyan 2002)[12]

It took until the 1950's for these multiple different diseases to be defined collectively. Smith et al. (1951) recognised that these seemingly unrelated diseases shared a common phenotype of oliguria, anaemia, and hyperkalaemia. In attempt to collate these diseases Smith termed their shared clinical presentation as "Acute Renal failure," which he defined as a condition causing a rapid decline in renal filtration leading to negative clinical endpoints[14]. Swann et al. (1953) went further in an attempt to reclassify these diseases into one clinical disease phenotype defined not by their aetiology, but by their common clinical presentation, defining for the first time, Acute Renal Failure (ARF)[15].

1.1.3 Measuring Renal Failure

In parallel to the advent of the clinical phenotype of ARF, molecular markers of renal function were under intense study. The first marker of reduced renal function was blood urea

nitrogen (BUN) a nitrogenous waste product of protein and amino acid metabolism. Richard Bright in 1827 first reported on the association between increasing concentrations of urea in the blood and oliguria[14]. However, BUN concentrations vary according to dietary intake, catabolic states, and is readily absorbed by the renal tubules even in the case of advanced renal failure[16]. The limitations to detect subtle changes in renal damage meant its interpretation was challenging and research focused upon the identification of a new marker.

Serum creatinine (sCr) a by-product of muscle metabolism is primarily excreted renally through a combination of glomerular filtration and proximal tubular secretion. Little tubular reabsorption of creatinine occurs and in the context of a stable renal function, creatinine remains in a constant state of equilibrium between the rate of synthesis and excretion. Due to its stability and ease of measurement at low cost, sCr became an important surrogate marker of renal function and revolutionised patient access to renal care, shaping future ARF research.

sCr has proved to be an excellent surrogate marker of kidney function in the context of ARF, but its use as a marker of excretory function in long term renal disease has drawbacks. The most accurate monitoring of kidney function requires measurement of the plasma concentration and urine clearance of an exogenous peptide, for example inulin, providing precise calculation of the glomerular filtration rate of the kidney[17; 18]. This method is labour intensive and impractical for routine clinical medicine. Using sCr concentrations to estimate glomerular filtration rate (GFR) was challenging, as sCr varies with muscle bulk, and thus different sCr levels are observed in individuals of different sex, ages, and race. To circumvent these challenges, formulae were developed which aimed to correct for these limitations and provided an estimated glomerular filtration rate (eGFR). Two leading equations emerged, the first, Cockcroft-Gault equation published in 1976, attempted to control for factors like age and body weight[19]. However, although accurate the need for medical staff to supply information

to facilitate calculation was a limitation. The modification of diet in renal disease (MDRD) equation, introduced in 1999, represented the first means of eGFR calculation using only routinely collated data (age and gender)[20].

The routine use of sCr and eGFR in medicine allowed for significant re-examination of renal disease and the notion of an acute, or chronic decline in renal function based on changes in measurable biochemical indices became applicable as a standard of care.

1.1.4 Acute Kidney Injury (AKI)

Following Swann's original description of ARF[15] and the discovery of sCr as a reliable marker of renal function it became clear that ARF based on clinical findings alone only described the extreme end of the disease. In fact, there existed a sub-clinical, asymptomatic form which accounted for the vast majority of ARF cases. What emerged was over 35 published criteria for the diagnosis of ARF all involving varying degrees of sCr accumulation, reduced eGFR and decline in urine output[21]. Although each definition differed, they facilitated research into the epidemiology of ARF exposing that even small increases in sCr can significantly increase the odds of mortality[22; 23]. The recognition that small changes in function may influence outcome was a significant shift in thinking[24]. Three consensus publications followed which aimed to define ARF diagnostic criteria.

The first criteria of ARF were published in 2004 by the Acute Dialysis Quality Initiative (ADQI) Group who proposed the RIFLE acute kidney failure (AKF) criteria. The criteria classified the increasing severity of ARF as, **R**isk, **I**njury, **F**ailure and, the two outcome measures of ARF as, **L**oss and **E**nd-Stage Renal Disease[25]. In 2007, the RIFLE criteria were endorsed by a group of AKF researchers belonging to the Acute Kidney Injury Network (AKIN). This group recommended changes to reflect the entire spectrum of the ARF syndrome. AKIN recognised

that small changes in sCr (≥26.5 µmol/l within 48 hours) can have significant adverse outcomes and further updated the term, ARF to acute kidney injury (AKI), to reflect the potentially reversibility of the disease. Finally, the kidney disease: improving global outcomes (KDIGO) AKI Work Group, combined RIFLE, and AKIN criteria, adding decline of eGFR over 7 days and recognition of those patients <18 years old with a eGFR <35ml/min as stage 3 AKI. Taken together, these renewed definitions transformed our thinking of AKI and represent one of the most important clinical developments in renal disease in the last 100 years[26], Figure 1.3.

RIFLE Criteria 2004			AKIN Criteria 2007		
Stage	**sCr/GFR**	**Urine Output**	**Stage**	**sCr**	**Urine Output**
Risk	sCr ↑ x1.5 or GFR ↓ >25%	<0.5ml/kg/hr x6 hrs	**1**	sCr ↑ x1.5 or ≥26.5 µmol/l (≤48hrs)	<0.5ml/kg/hr x6 hrs
Injury	sCr ↑ x2.0 or GFR ↓ >50%	<0.5ml/kg/hr x12 hrs	**2**	sCr ↑ x2.0	<0.5ml/kg/hr x12 hrs
Failure	sCr ↑ x3.0 or GFR ↓ >75%	<0.3ml/kg/hr x24 hrs or Anuria x12 hrs	**3**	sCr ↑ x3.0 or sCr ≥4mg/dl (with acute rise ≥ 0.5mlg/dl)	<0.3ml/kg/hr x24 hrs or anuria x12 hrs
			N.B. If RRT started patients are considered to have met criteria for stage 3		

KDIGO Criteria 2012		
Stage	**sCr Criteria**	**Urine Output Criteria**
1	sCr ↑ x1.5 – 1.9 baseline or ≥26.5 µmol/l increase	UO <0.5ml/kg/hr 6 -12 hrs
2	sCr ↑ x2.0 – 2.9 baseline	UO <0.5ml/kg/hr for ≥12 hrs
3	sCr ↑ x3.0 or sCr ≥353.6 µmol/l or initiation of RRT or <18 yrs, decrease in eGFR <35ml/min	UO <0.3ml/kg/hr ≥24 hrs or Anuria for ≥ 12 hrs

N.B. AKI is defined as an increase in sCr by ≥26.5 µmol/l within 48 hours or ≥ 1.5x baseline known or presumed to have occurred within 7 days

Figure 1.3 The evolution of the KDIGO AKI criteria

Pictorial representation of the changes made during the evolution of ARF/AKI overtime

1.1.5 AKI: Epidemiology

Our understanding of the prevalence and outcomes of AKI was hampered by the lack of a concise definition. The publication of RIFLE, AKIN and KDIGO AKI criteria allowed for a more robust analysis of AKI epidemiology, which in turn transformed our understanding of the disease. Whichever diagnostic criteria for AKI are used, the incidence of AKI in the general population is believed to be around 2-12%[27-31], complicating 6-18% of all acute hospital admissions[28; 32; 29]. In the UK alone there are an estimated 500,000 cases of AKI annually[33].

Mortality in critically ill AKI patients is high: for community-acquired AKI (CA-AKI), between 19-26% [28; 34; 30; 35], for hospital-acquired AKI (HA-AKI) this increases to 30-43%[28; 34; 30; 36] and within the intensive care unit (ICU-AKI) setting 22-53% [37-41] [42-44]. My work in this field has demonstrated that AKI is a common finding in patients who present to the emergency department, with (ED-AKI) mortality reaching 24.4%, compared to 3.2% in the non-AKI cohort. By multivariable COX regression for survival analysis, ED-AKI significantly increased the odds of mortality, HR, 6.293; 95% CI, 1.887 to 20.790, p=0.003[45].

Economically, AKI inpatient care in NHS England is estimated to cost £1.02 billion per year, and £179 million annually in post-discharge costs[46]. At an inpatient level, a single hospital admission with AKI is estimated to cost £3,748- £5,065, rising to £8,404 in those whose kidneys fail and require renal replacement therapy (RRT) to prevent death[47; 48].

Following a diagnosis of AKI, three distinct outcomes are possible. The function can completely recover, partially recover with residual functional impairment to the kidney called chronic kidney disease (CKD) or decline unremittingly to end-stage renal disease (ESRD) and death. In the ED-AKI population, those who were discharged from hospital had a higher risk of CKD progression, new onset CKD (*de novo* CKD), long term dialysis, and death at 90 days[45]. These observations have been described in other AKI populations[49-51] and confirmed by meta-

analysis[52]. The close interconnection of AKI with CKD highlights the importance of CKD when framing the impact of AKI on the patient journey.

1.1.6 Chronic Kidney Disease (CKD)

CKD is a subtype of renal disease which describes a progressive loss in kidney function over a period of months or years. Epidemiology trials of AKI has demonstrated that AKI is an independent risk factor for *de novo* CKD[53; 54], progression of underlying CKD[55; 56], and ESRD requiring dialysis[57]. A meta-analysis of thirteen studies conducted by Coca et al. (2012) concluded that AKI increases the risk of both CKD and ESRD[58].

The clinical presentation of CKD is highly variable and is born from a combination of the underlying aetiology, rate of CKD progression, and the severity of kidney failure[7]. Historically, CKD diagnosis was made when patients experienced a combination of clinical symptoms including fatigue, anorexia, itching (pruritus), leg swelling (peripheral oedema), and shortness of breath (hypoxia). These clinical features reflect very advanced renal disease where the homeostasis of the kidney is inadequate, and the kidney has failed.

The advent of sCr as a surrogate marker of renal function facilitated the recognition that sub-clinical CKD exists, and that CKD is a spectrum of scaled disease. Although sCR allowed for early detection of CKD, there was no commonly accepted definition, and variable sCr cut-offs were used to define CKD[59-61]. Despite these limitations, a number of epidemiological studies and meta-analyses demonstrated that CKD is a progressive disease in which even small increases in sCr render the patient at an increased risk of cardiovascular disease[62; 63] and death[64; 60]. If left unchecked, renal function can progress to ESRD were the kidneys stop working. At the point of ESRD the options are either maximal conservative care, aimed at

improving the patient's quality of life but ultimately leading to death, or RRT in the form of dialysis or renal transplantation.

The recognition that smaller changes in sCr confer significant risk to the patient was an important milestone. In 1999 the National Kidney Foundation Kidney Disease Outcome Quality Initiative (NKF KDOQI) advisory board set the ambitious goal of defining CKD. NKF KDOQI used eGFR to classify those patients at greatest risk of renal decline by stages using the MDRD equation. Their landmark publication in 2002 defined CKD irrespective of underlying diagnosis, and arguably for the first time defined a common language to be used by the medical community[65]. In 2012 KDIGO refined CKD further, emphasizing the importance of albuminuria and subdividing CKD stage 3, into 3a and 3b, based upon evidence that the outcomes are different in these groups[66], Figure 1.4.

CURRENT CHRONIC KIDNEY DISEASE (CKD) NOMENCLATURE USED BY KDIGO

CKD is defined as abnormalities of kidney structure or function, present for >3 months, with implications for health and CKD is classified based on cause, GFR category, and albuminuria category (CGA).

Prognosis of CKD by GFR and albuminuria category

Prognosis of CKD by GFR and Albuminuria Categories: KDIGO 2012				Persistent albuminuria categories Description and range		
				A1	A2	A3
				Normal to mildly increased	Moderately increased	Severely increased
				<30 mg/g <3 mg/mmol	30-300 mg/g 3-30 mg/mmol	>300 mg/g >30 mg/mmol
GFR categories (ml/min/ 1.73 m²) Description and range	G1	Normal or high	≥90			
	G2	Mildly decreased	60-89			
	G3a	Mildly to moderately decreased	45-59			
	G3b	Moderately to severely decreased	30-44			
	G4	Severely decreased	15-29			
	G5	Kidney failure	<15			

Green: low risk (if no other markers of kidney disease, no CKD); Yellow: moderately increased risk; Orange: high risk; Red, very high risk.

Figure 1.4 KDIGO CKD criteria

Pictorial representation of the 5 stages of CKD based upon eGFR. Each stage can be further subclassified according to presence and level of albumin in the urine (albuminuria)

Image reproduced with permission of the rights holder, KDIGO: Kidney Disease: Improving Global Outcomes (KDIGO) CKD Work Group. KDIGO 2012 Clinical Practice Guideline for the Evaluation and Management of Chronic Kidney Disease[66]

1.1.7 CKD: Epidemiology

CKD can either remain indolent for many years or decline unremittingly over months to years. The progression of CKD to its most severe form, stage 5 (also called ESRD), necessitates invasive RRT or renal transplantation to circumvent death.

The global health care burden of CKD is increasing. In 2016 an estimated 275.9 million people were living with CKD, an increase of 30.4% (28.2 to 32.7%) from 2006[67]. The Global Burden of Disease Study (2016) estimated that 1.2 million deaths worldwide were directly related to CKD, an increase of 28.8% (25.5 to 31.4%) from 2006[68]. The increasing prevalence of CKD is largely attributed to the rise of diabetes and cardiovascular disease, both of which damage the filtration mechanism of the kidney leading to fibrosis and reduced renal function. In the UK, CKD is estimated to affect 14% of males and 13% of females[69]. Of these, the incidence of ESRD requiring RRT has increased to 120 per million population (pmp), reflecting 7,814 new patients in 2015[70], adding to the 61,256 adult patients already receiving RRT, prevalence 941 pmp[71].

Despite an increasing availability of RRT, it remains a poor substitute for native kidneys. The biological[72; 73], psychological[74; 75], and social impact[76] of RRT is significant. Furthermore the median survival of patients starting RRT in the UK is only 6 years in those aged between 55-64, and 3.5 years in those aged between 65-74[77]. The significant mortality and morbidity associated with CKD and ESRD has a profound impact on healthcare economics. Approximately 2% of the total budget in NHS England is spent on RRT, adding to an annual CKD NHS England expenditure of £1.64 billion[78]. The true financial cost of CKD on the NHS is likely significantly greater owing to the increased risk of cardiovascular disease, malignancy, and infection. As with all financial budgeting it fails to take into account lost employment, long-term social outcomes[79], stigma and the psychological impact[80-82] of CKD and RRT on the individual.

1.1.8 *In vivo* Models of AKI

AKI occurs in a variety of clinical settings resulting in a significant mortality and morbidity. Indeed, the impact of AKI is not short lived, and a single episode of AKI is a significant post-recovery risk factor for CKD and progression to ESRD. Although AKI has been clinically defined, successful strategies to ameliorate the condition are hampered by an incomplete understanding of the molecular mechanism underpinning the disease. Animal models are an important cornerstone in the investigation of the pathophysiology of AKI. Several *in vivo* models have been developed which are broadly categorised into septic, nephrotoxic and ischaemic.

1.1.8.1 Septic AKI Models

Sepsis is a life-threatening medical emergency were the body mounts a dysregulated immune response to infection resulting in tissue injury, organ failure and death[83]. *In vivo,* the most common model of septic-AKI is the endotoxin lipopolysaccharide (LPS) model. LPS is a membrane component of gram-negative bacteria and is a potent activator of systemic inflammation[84]. LPS can be injected into the surgical subject mimicking sepsis induced AKI. Although effective, LPS models have no microbial source for ongoing sepsis and instead models the acute inflammatory response to infection which differs from human septic-AKI[85]. Another model is Cecal Ligation and Puncture, where the bowel cecum is punctured allowing its contents to enter the abdomen inducing abdominal sepsis[84]. This method closely resembles sepsis in humans, however, the model is hampered by a lack of control over the degree of abdominal contamination, resulting in variable severities of sepsis and hampering experimental repeats[86].

1.1.8.2 Nephrotoxic AKI Models

The kidney plays a critical role in metabolism and clearance of drugs, meaning that minor increases in a drugs concentration outside the therapeutic range can induce cellular stress and direct toxicity to the kidney[87]. In animal models the principal xenobiotics used to study nephrotoxic-AKI are cisplatin and folic acid. Cisplatin is a chemotherapeutic drug used to treat a range of cancers[88]. However, cisplatin accumulates in the tubular epithelial cells resulting in DNA damage, mitochondrial dysfunction, and AKI[89]. The toxicity of cisplatin limits its use in humans, and on a population level is a rare cause of nephrotoxic-AKI[90]. Folic acid is a synthetic dietary supplement of folate, a vitamin found in foods. Folate is an essential nutrient for DNA replication, and its deficiency can cause anaemia and congenital abnormalities in the developing fetus[91]. However, high doses of folic acid cause significant tubular damage and interstial inflammation[92] making it an effective model of AKI *in vivo*[93]. Folic acid nephropathy is a rare cause of AKI in humans. It is often confined to individual cases of intentional overdose which limits its usefulness as a comparative model to AKI in humans.

1.1.8.3 Ischaemic AKI Models

A reduction in blood flow to the kidney, called ischaemia, is seen during infection and surgery. Ischaemia depletes the organ of oxygen and nutrients resulting in profound AKI[94]. To replicate this injury, *In vivo* models use a technique called Ischaemic Reperfusion Injury (IRI). This model uses clamps to temporarily occlude the vascular supply to the tissue (ischaemia) followed by a return in blood flow, and subsequent reoxygenation of the tissue (reperfusion). Kidney IRI is a common model of AKI *in vivo* and has several technical advantages. The severity of the ischaemic injury can be reduced or enhanced by controlling the duration of time of

vascular occlusion. As time is a measurable variable, replication of the model is simple. Furthermore, the IRI model can be applied to one kidney (unilateral IRI), both kidneys (bilateral IRI), and unilateral IRI with contralateral nephrectomy[95]. The unilateral model without nephrectomy is advantageous in studying renal fibrosis in CKD due to its low mortality. However, as the contralateral kidney is intact, measuring function by serum creatinine (sCr) is not possible[96]. In contrast, the unilateral model with contralateral nephrectomy allows measurements of sCr, but the non-nephrectomised kidney undergoes compensatory hypertrophy[97] which may influence scientific interpretation of results. The bilateral model is technically more challenging, but allows for sCr assessment and avoids the difficulties observed in the unilateral models[98]. In humans' AKI is commonly a result of hypovolaemia, hypotension, and circulator shock, resulting in bilateral renal IRI. As such, the bilateral IRI model closely mimics the physiological response to ischaemic AKI which is commonly seen in humans.

1.1.8.4 *In vivo* Models of AKI and Human AKI

Human AKI cohorts are a heterogenous group, with significant variation in age and comorbidities, e.g., diabetes[99], heart failure[100] and hypertension[101]. Indeed, comorbidities are a well-established risk factor for AKI[102; 103]. This heterogenicity introduces challenges when undertaking scientific research to model a disease. Although most animal models use healthy young subjects, several researchers have explored the influence of comorbidities like diabetes in animal models exposing the negative impact on AKI incidence and recovery[104]. It is well established that AKI is more common in elderly patients[45] and older rodents are more susceptible to IRI[105]. Interestingly, the incidence of AKI differs between sexes with male patients being more susceptible to AKI[106], an observation mirrored in animal models[107].

1.2 Ischaemic Reperfusion Injury (IRI)

Globally one of the commonest causes of AKI is IRI. Renal IRI is of particular scientific interest as it can occur in a variety of clinical settings which reduces blood flow to the kidney such as hypovolaemia from severe infection (septic shock), or cardiovascular collapse following a myocardial infarction. Similarly, patients undergoing cardiac surgery often experience profound shifts in vascular haemodynamics leading to hypotension and AKI in 36%[108]. In those patients undergoing organ transplantation the cold ischaemic time following organ retrieval, and reperfusion of the organ following transplantation into the recipient, invariably results in IRI[109-111]. Given the importance of renal IRI in multiple disease phenotypes, and the *in vivo* modelling advantage of bilateral IRI to measure functional injury (sCr), this thesis will explore AKI in the context of renal IRI.

1.2.1 Anatomy of Renal IRI

The kidney utilises approximately 10% of the body's total oxygen intake but receives a disproportionally large volume of the cardiac output (20-25%), filtering approximately 180 litres of blood daily in a normal adult male. This discrepancy can be explained by understanding the nephrons anatomy and appreciating its key role, to preferentially retain water. To allow this, the renal vasculature is constructed in a manner which allows rapid movement of solutes and water between the descending and ascending limbs of the convoluted tubules. However, this design permits oxygen to diffuse (shunt) readily from the arterial to the venous branches of the vasa recta. The countercurrent of blood flow between arteries and veins results in a low oxygen delivery to the deeper part to the kidney (medulla)[112]. In principle, this appears to be a design flaw. However, the nephron requires a limited blood flow in the medulla to enable

the Loop of Henle to create an osmotic gradient, thus facilitating salt and water homeostasis[113].

This knowledge of nephron anatomy enables us to appreciate why the tubules face a daily challenge. To create the intracellular-extracellular osmotic gradient within the proximal tubule, epithelial cells require a massive amount of energy in the form of Adenosine Triphosphate (ATP). ATP is generated from aerobic pathways and is used to drive sodium reabsorption via the enzyme Na^+/K^+-ATPase in the proximal tubules. In fact, around two thirds of the renal oxygen uptake is required by this transporter[114]. Even with this oxygen demand the vascular distribution around the nephron is such that the medulla operates at a dangerously low pO_2 of approximately 16 mmHg compared to the cortex value of around 50 mmHg[115]. Therefore, common medical conditions which reduce blood flow to the kidney can lead to significant medullary hypoxia and injury to the tissue.

1.2.2 Molecular Mechanisms of IRI

The molecular mechanisms underlying IRI are not yet completely understood. The pathogenesis of renal IRI can be broadly thought of in terms of its ischaemic and reperfusion phases. In brief, renal IRI results in gene expression and signal transduction changes, activation of inflammatory mediators culminating in endothelial dysfunction, functional dysregulation and adverse patient outcomes.

1.2.2.1 Ischaemia

The initial ischaemic phase of IRI is the result of reduced or absent renal blood flow, which reduces oxygen and nutrient delivery to the kidney. As oxygen levels reduce the

mitochondria, which are ATP-producing powerhouses, switch from aerobic to anaerobic metabolism, leading to lactate and hydrogen ion accumulation and acidification of the intracellular pH[116]. The cell attempts to maintain physiological pH by exchanging H^+ ions for Na^+ ions via the Na^+/H^+ exchanger. Initially, the increase in intracellular Na^+ is reduced by the Na^+/K^+-ATpase transporter, however, as ATP depletes the transporter inactivates and sodium exchange relies upon the Na^+/Ca^{2+} exchanger which utilises an electrochemical gradient to shift Na+ extracellularly in exchange for Ca^{2+}[117]. The net effect is transmembrane pump failures, increase in intracellular Ca^{2+} and Na^+, and intracellular acidosis[118].

The change in cellular environment destabilises the membranes of lysosomal organelles, resulting in hydrolytic enzyme release which in turn damages the cytoskeleton and cellular membrane. The hypercalcaemic intracellular environment triggers intracellular signalling cascades, including the proteolytic calpain pathway[119]. Calpains remain dormant in the acidotic environment but damage the cell as the pH normalises during reperfusion. Active calpains lead to proteolysis of cellular proteins including actin, degrading cytoskeletal integrity, as well as cleavage of the cell signalling molecule protein kinase C (PKC), thereby disrupting intracellular signalling[120].

Under oxidative stress aerobic respiration is paused, resulting in an accumulation of reduced coenzymes nicotinamide adenine dinucleotide phosphate (NADPH). During reperfusion the sudden introduction of NADPH exceeds the capacity of the respiratory chain to utilise electrons resulting in a net accumulation of reactive oxygen species (ROS)[121]. Furthermore, continued ischaemia triggers the breakdown of ATP to hypoxanthine which accumulates intracellularly[122]. The metabolism of hypoxanthine by xanthine oxidase requires oxygen which generates significant ROS during reperfusion[123]

Taken together, the hypercalcaemic environment of ischaemia stimulates the opening of the mitochondrial permeability transition pore (mPTP), a channel located on the mitochondrial membrane. This mPTP opening releases pro-apoptotic factor cytochrome c, which can induce cellular apoptosis[124].

1.2.2.2 Reperfusion

The reperfusion reoxygenation phase of IRI results in a complex orchestration of pH normalisation, ROS generation, Ca^{2+} movement and ATP production. The sudden influx in oxygen reactivates the electron transport chain generating ROS and restoration of protease activity. Intertwined in this process is a significant immune mediated inflammatory response mediated through cytokine and chemokine recruitment of inflammatory mediators.

The abrupt return of oxygen overloads the electron transport chain (ETC) at complex I, which generates ROS[125; 126]. The cellular re-oxygenation allows xanthine oxidase to metabolise hypoxanthine to xanthine, uric acid, and ROS[127]. Furthermore, the NADPH oxidase enzyme complex is upregulated during reperfusion, catalysing conversion of NADPH to ROS[128]. Thus ROS-mediated stress response causes direct damage to mitochondrial proteins, lipids and DNA, resulting in mitochondrial dysfunction and further ROS formation[129]. The destructive effect on the mitochondria disrupts ATP generation and exacerbates mitochondrial calcium accumulation. These processes initiate the opening of the mPTP pore ,which spans the inner and outer mitochondrial membrane, releasing pro-apoptotic factors cytochrome c and mitochondrial DNA (mtDNA) which together trigger cell death through apoptosis[130].

During reperfusion the intracellular pH normalises, and those proteases whose activity was inhibited by the acidotic environment of ischaemia are activated. The protease calpain is activated, which damages the cytoskeleton and the plasma membrane promoting apoptotic

cell death[131]. Those cells whose injury is severe can undergo cell death via necrosis or apoptosis.

1.2.3 Cell Death: Apoptosis

Apoptosis is a regulated event characterised by organised cell death that is triggered by cellular injury. The process can be activated by two pathways called the intrinsic (mitochondrial) pathway or the extrinsic (death receptor) pathway. Whichever pathway is involved, both result in an ordered process comprising of chromatin condensation, DNA fragmentation, cell shrinkage, membrane blebbing and loss of ECM adhesion.

The intrinsic pathway is triggered when intracellular death inducing signals activate a family of proteins which reside in the mitochondria and cytosol, called the B-cell Lymphoma 2 (Bcl-2) family[132]. The Bcl-2 protein family regulate the mitochondrial membrane permeability in a delicate balance between pro- and anti-apoptotic proteins of this family. During IRI, cytotoxic signals activate the pro-apoptotic proteins Bcl-2-associated X Protein (Bax) and Bcl-2 Homologous Antagonist Killer (Bak), which combine to form dimers that insert into the mitochondrial membrane forming a pore. Pore formation facilitates the release of cytochrome c and other pro-apoptotic proteins into the cytosol[133]. In turn, cytochrome c interacts with apoptotic peptidase activating factor (APAF-1), creating a protein complex called the apoptosome which in turn activates cysteinyl aspartic acid-protease 9 (caspase 9)[134].

The extrinsic pathway is initiated when the extracellular signalling ligands, tumour necrosis factor-α (TNF-α) or Fas ligand (FasL) bind to their corresponding death receptor (DR) TNF-receptor type 1 (TNFR1) and Fas respectively. DR signalling facilitates the death-induced signalling complex (DISC), which activates caspase 8[135].

Both the intrinsic and extrinsic pathway activation of caspases 9 and 8, respectively, initiate the activation of the executioner caspases (3, 6, 7, 10), resulting in proteolytic degradation of intracellular proteins[136; 137].

1.2.4 Cell Death: Necrosis

Necrosis is a form of cell death characterised by loss of membrane integrity as well as cytoplasmic and mitochondrial swelling, culminating in cell lysis and release of the intracellular contents[138]. The release of certain cellular components, referred to as damage associated molecular patterns (DAMP's) and including DNA, RNA, high mobility group box 1 (HMGB1) and heat-shock proteins, is immunostimulatory and activates innate and adaptive immunity[135].

Traditionally necrosis was thought to be an unregulated process, however, there is emerging evidence of a regulated subtype of necrosis in renal IRI, termed necroptosis[139]. The cytokine TNF-α, binds to endothelial cell TNFR1, eliciting signal to the TNF receptor-associated death domain (TRADD) which phosphorylates receptor-interacting protein kinase 1 (RIPK1), and subsequently RIPK3 is recruited. RIPK1 and RIPK3 then form a complex called the necrosome, which phosphorylates the mixed lineage kinase domain-like (MLKL) protein[140; 141]. MLKL then inserts into organelle and cellular membranes, forming pores via which DAMPs spill into the extracellular space, triggering proinflammatory responses and pinocytosis by macrophages.

1.2.5 Endothelial Dysfunction

IRI-induced endothelial cell injury upregulates the expression of chemotaxis molecules which trigger the adhesion and migration of leucocytes to the site of injury[139]. Endothelial

cells initially increase the expression of the adhesion transmembrane protein P-selectin on the intravascular surface of the cell, tethering leucocytes via the P-selectin ligand glycoprotein 1 (PSGL-1) on the leucocyte cell wall and facilitating leucocyte rolling to the sight of injury[142]. At the target location, leucocytes adhere to endothelial cells via binding of the leucocyte expressed β2-integrins or macrophage-1 antigen (MAC-1) to endothelial-expressed intracellular adhesion molecule-1 (ICAM-1). In turn, leucocyte transmigration to the intracellular compartment is achieved via binding of the platelet endothelial cell adhesion molecule-1 (PECAM-1) to the leucocyte[143].

Leucocytes adherent to the microvascular endothelium can block and prevent blood flow, leading to endothelial congestion prolonged ischaemia[144]. Activated leucocytes in the interstitium release pro-inflammatory cytokines, chemokines, proteases and ROS which accentuates the injury, creating a positive feedback loop of endothelial-leucocyte interaction and injury[145].

1.2.6 The Immune System

IRI triggers innate and adaptive immune responses in the kidney. The innate immune response is a rapid inflammatory defence mechanism activated by receptors that are responsive to molecules released by pathogens and injured tissue[146]. In contrast, the adaptive immune response is a slower response reliant upon antigen presentation to T and B cells[147].

1.2.6.1 Innate Immune Response

The innate immune response is activated when transmembrane pattern recognition receptors (PRR) recognise specific molecular patterns present on either a pathogen; called

pathogen-associated molecular patterns (PAMPs) or when cellular components are released from injured cells called DAMPs, e.g., DNA, RNA and HMGB1. In the context of IRI, cell death by necrosis triggers lysis of the cellular plasma membrane and release of intracellular DAMPs, which trigger the innate immune response[148; 149]. There are several different types of PRRs of which two have been demonstrated to be of particular importance to IRI; toll-like receptors (TLRs) a family of transmembrane receptors, and nucleotide-binding oligomerization domain-like receptors (NLRs) a family of intracellular PRRs.

TLRs are found on the cellular membrane of leucocytes, endothelial and tubular cells. Although thirteen TLRs have been described in humans and rodents, two, TLR2 and TLR4 appear to play a significant role in renal IRI[150]. Both TLR2 and TLR4 recognise several DAMPs and PAMP ligands. Both TLR2 and TLR4 recognise the DAMPs: HMGB1, HSP and S100 protein[151]. The PAMP, lipopolysaccharide (LPS) is a component of gram-negative bacteria and is a potent ligand of TLR4[152]. Gram-positive bacteria produce lipopeptides, which activate TLR2. In research the synthetic agonist PAM3 (Pam3Cys-Ser-(Lys)4) is a TLR2 agonist[153].

TLR activation by DAMPs is thought to activate the marrow differentiation factor 88 (MYD88) pathway, which facilitates the release of Nuclear Factor-Kappa B (NF-kB) from its inhibitor, enabling NF-kB translocation to the nucleus culminating in the transcription of genes encoding cytokines and chemokines including TNF-α, IL-6, and IL-1. An alternative, MYD88-independent pathway is posited to trigger mitochondrial transcription of interferon (IFN) via NF-kB[154; 155]. Indeed, TLR4 activation can trigger necrosis via necroptosis through a common pathway convergence of RIP3[156], (see 1.2.4 Cell Death: Necrosis). Activation of TLR4 on tubular epithelial cells promotes macrophage and neutrophil chemotaxis by increasing the expression of both macrophage inflammatory protein-2 (MIP-2) and monocyte

chemoattractant protein-1 (MCP-1, also known as CCL2), respectively[157]. Furthermore, TNF2 appears to regulate neutrophil chemotaxis via CXC motif chemokine ligand 1 (CXCL-1)[154].

Neutrophil recruitment in the kidney releases ROS, hydrolytic enzymes and cytokines, which together exacerbate renal injury and initiate further leucocyte recruitment[158]. Indeed, the physical process of neutrophil transmigration into the renal interstitium releases cytokines IL-4), IL-6, TNF-α and IFN-γ, which further stimulates the immune response[159].

Macrophages found in the renal interstitium are thought to originate from resident macrophage pools or from transformed blood-borne migratory monocytes which differentiate into macrophages and dendritic cells at the site of injury[160]. Although macrophages are classically defined as proinflammatory M1 or anti-inflammatory M2 subtypes, this classification is being redefined in current literature (see Huen et al. (2017)[161]. Monocyte recruitment is trigged by epithelial cell release of monocyte chemoattractant protein-1 (MCP-1) and chemokine ligand 1 (fractalkine, also known as CX3CL1). These ligands bind to the monocyte chemokine receptor CCR2 and CX3CR1 expressed on the surface of monocytes and activate migration[162].

At the site of injury, both macrophage and dendritic cells are activated by IFN- γ, DAMPs and ROS produced by injured cells via the PRRs, TLR2 and TLR4, located on the macrophage cell membrane. Intracellularly the PRRs, NOD1 and NOD2, which are part of NLR family of receptors, play an important role. Both, NOD1 and NOD2, ligands are bacterial peptidoglycans. NOD1 recognises γ-D-glutamyl-meso-diaminopimelic acid found in gram-negative bacteria and certain gram-positive bacteria. NOD2's ligand is muramyl dipeptide found in gram-negative and gram-positive bacteria[163]. However, both theses NLR receptors can respond to DAMPs[164] released during endoplasmic reticulum stress[165], and are important in renal IRI[166; 167] triggering release of proinflammatory cytokines IL-1, IL-6, IL-12 and TNF-α which further

stimulate the inflammatory response and promote tubular apoptosis. Activated macrophages produce ROS and metalloelastase enzymes which degrades extracellular matrix (ECM)[168; 167].

Dendritic cells (DC) are activated by DAMPs via TLRs and the complement system. Activated DCs secrete pro-inflammatory cytokines IL-12 and TNF-α as well as chemokine MCP-1, and present antigens to B- and T-cells, initiating the adaptive immune response after reperfusion[169].

Following IRI, DAMP-immunoglobulin complex formation and damaged cells activate all three **complement system** pathways: classical, alternative and lectin, which converge and activate the C3-convertase protease enzyme, which cleaves C3, to release C3a and C3b. C3b forms part of the C5 convertase protease, which cleaves C5 into C5a and C5b[170; 171]. Both C3a and C5a are pro-inflammatory peptides which promote leukocytes activation and chemotaxis via binding with C3a/C5a receptors on renal tubular epithelial cells and leucocytes[172; 173]. Downstream of the pathway C5b binds with C6-9 forming the membrane attack complex (MAC, also known as C5b-9), which deposits on the surface of tubular epithelial cells leading to cell lysis and death[174].

1.2.6.2 Adaptive Immune Response

The DAMPs released by stressed or dying cells are recognised by macrophage and DC PRRs, TLRs and NLRs. DAMPs are processed and presented on major histocompatibility complex Class-II (MHC-II) to CD4+ helper T-cells (Th)[148]. Upon activation Th differentiate into Th1, which produce IFN-γ, promoting activation of macrophages, recruitment of inflammatory cells and activation of inflammatory death pathways[175]. The interaction in IRI of other Th subtypes Th2 and Th17, is less clear, in IRI with some conflicting data, (see Dellepiane et al. (2020)[176]). During infection or injury, intracellular proteins are processed and presented on

MHC class 1 molecules. The peptide ligands presented on MHC class 1 molecules are recognised by CD8+ cytotoxic T-cells are involved in cellular defence against abnormal cells and intracellular pathogens. The role of cytotoxic T cells in IRI is less clear, and it has been reported that mice deficient in CD8+ T cells are not protected from renal IRI[177].

1.2.7 IRI Overview

From the above, the combination of ischaemia and reperfusion phases results in inflammatory cell trafficking and morphological and functional injury, as summarised in Figure 1.5. The complex interaction between these two phases of injury was elegantly summarised graphically by Bulkley et al. (1987), who introduced the concept of the sum of ischaemia and reperfusion injury being greater than their individual parts, as shown in Figure 1.6[178].

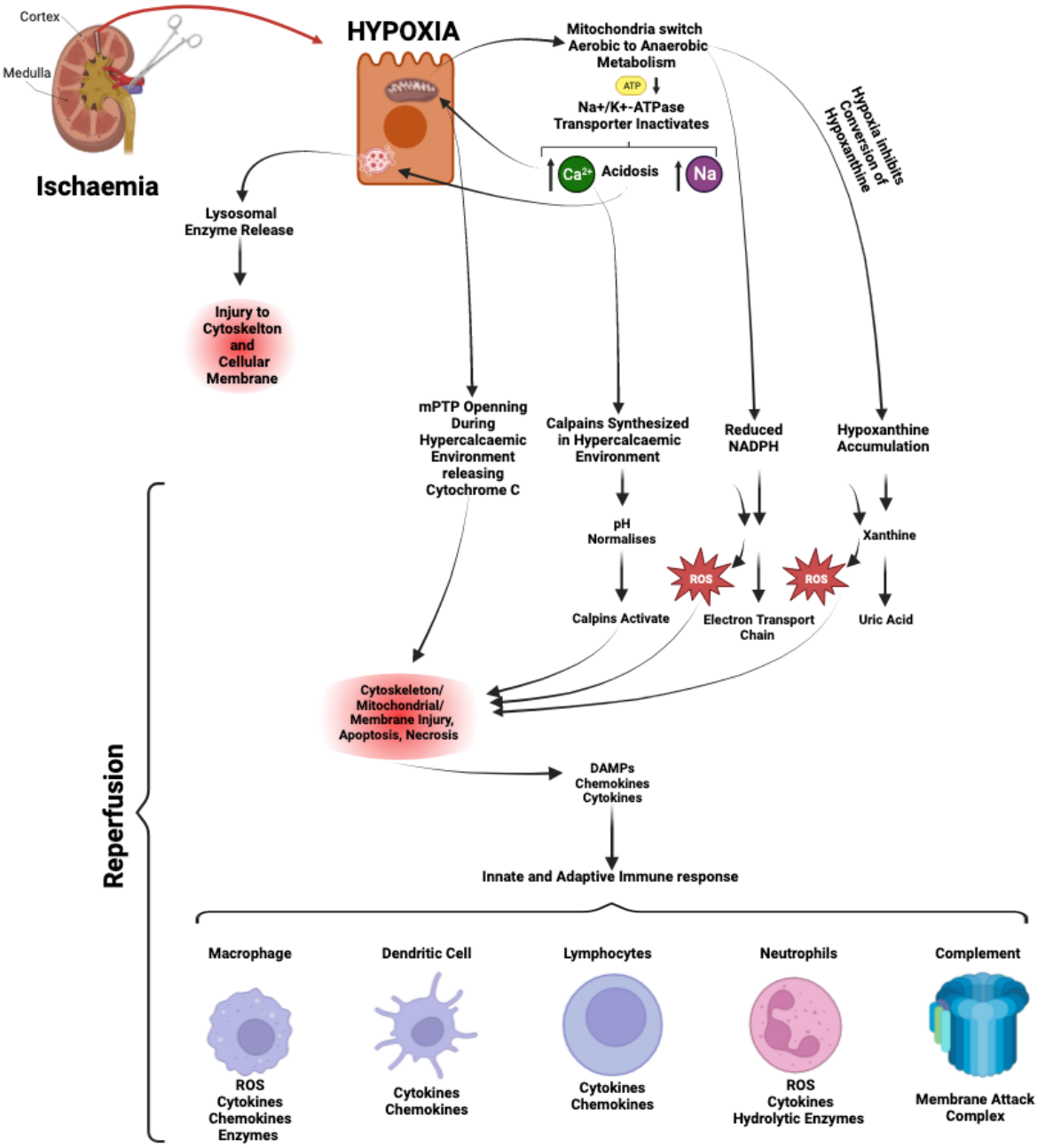

Figure 1.5 Molecular Mechanism of IRI

Pictorial representation of the molecular mechanism of renal IRI. The molecular process of renal IRI can be broadly thought of in terms of ischaemia followed by reperfusion. A detailed description of the pathways, chemokines and cytokines can be found in chapter 1.2.
Within the above figure abbreviations are as follows: Calcium (Ca^{2+}), Sodium (Na), Reactive Oxygen Species (ROS), Damage-Associated Molecular Patterns (DAMPs).
Figure created using Created with BioRender.com

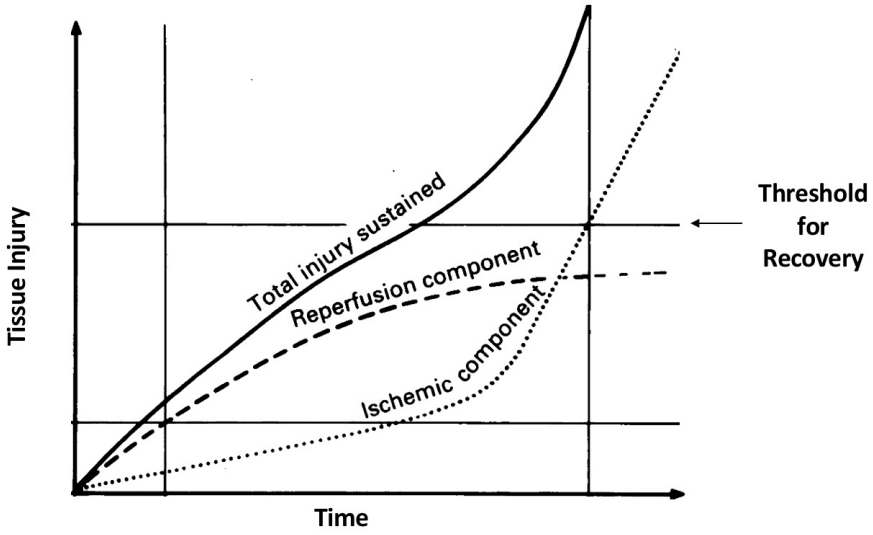

Figure 1.6 Ischaemia and Reperfusion Injury Threshold

The degree of injury sustained following a lethal ischaemic insult can be attributed to both the ischaemic insult and the reperfusion phase. The sum of the individual injury periods is thought to be greater than their individual components. The total injury can be appreciated graphically demonstrating the threshold of which sustained cellular injury occurs.
Figure is adapted from Bulkley et al. (1987)[170].

1.3 Interventions to Reduce IRI

IRI is a common mechanism underpinning AKI. In clinical practise methods to reduce the incidence of IRI can be broadly divided into preventative and reactive approaches. To date, both approaches have focused on optimisation of fluid status to improve renal blood flow (fluid hydration), removal of aggravating factors including non-steroidal anti-inflammatory drugs and treatment of the precipitant (e.g., sepsis).

To prevent IRI, two novel methods have emerged: the first uses ischaemic conditioning, the second targets a proposed molecular mechanism of IRI using pharmacological agents.

1.3.1 Ischaemic Conditioning

Ischaemic conditioning (IC) describes the contradictory observation that brief nonlethal periods of reduced blood flow to a tissue (ischaemia), followed by return of blood flow (reperfusion), offers some measure of protection to an organ from subsequent IRI.

The IC paradox was first described by Murry et al. (1986)[179]. These researchers had previously identified that the cumulative effects of repeated short periods of ischaemia with intermittent vascular reperfusion to the heart does not cause ATP loss or necrosis to the same extent as that seen with a single application of one period of ischaemia equivalent to the total time of these shorter bursts. Indeed, the authors identified that the rate of each ATP depletion was less with each subsequent ischaemic episode. The investigators postulated that the brief repetitive nonlethal ischaemia prior to IRI protected the myocardium from lethal myocardial ischaemia[180]. In brief, the group utilised IC prior to IRI in a dog model of myocardial infarction. Mongrel dogs were anaesthetised and mechanically ventilated. The heart was exposed, and the left circumflex coronary artery was isolated for ischaemic use. Subjects underwent 5

minutes of ischaemia followed by 5 minutes of reperfusion for four cycles, i.e., 5/5 x4 approach, immediately prior to 40 minutes of IRI. Animals were recovered and cardiac tissues harvested at 4 days. The group reported the infarct size reduced from 29.4% (IRI only) to 7.3% following IC[179].

This observation that IC can protect the heart from IRI was groundbreaking. Since 1986, IC has been successfully used to reduce IRI *in vivo* in the heart[181], kidneys[182], liver[183], in the pig[184], rabbit[185] and rat[186].

1.3.2 *In vivo* IC of the Kidney

The successful application of a prophylactic intervention to render the heart resistant to IRI was an extremely exciting observation. The high metabolic demand of the kidney and the relatively hypoxic conditions in which renal tissue routinely functions make the kidney particularly susceptible to IRI. What became clear in the early stages of renal IC research was, what worked in the myocardium would not transition easily to the kidney.

One of the first renal IC studies was reported by Islam et al. (1997), which failed to show a functional and histological improvement following unilateral kidney conditioning prior to IRI[187]. However, reductions in the time between IC and IRI, termed the "critical interval"[188], and small reductions in the ischaemic and reperfusion windows, were able to achieve functional and histological improvement[186]. A systematic review and meta-analysis of *in vivo* IC trials on the kidney by Wever et al. (2012) concluded that IC protected the kidney from IRI injury both functionally (reducing sCr relative to IRI) and histologically[189].

1.3.3 *In vivo* IC Protocols

In vivo, IC prior to IRI has been successfully achieved using several different protocols. The conditioning stimulus can be applied directly to the vasculature of the target organ undergoing IRI, a method called direct IC. Alternatively, IC can be applied to a different organ or tissue (e.g., the arm) to the organ undergoing IRI (e.g., the kidney), this procedure is called indirect IC.

The IC ischaemic/reperfusion time can differ and be applied either in brief repetitive cycles (pulsatile IC) or in a single short period of continuous sublethal ischaemia (continuous IC). Furthermore, the IC stimulus can be applied before the IRI event (ischaemic preconditioning, or IPC) or after, ischaemic postconditioning (I-POC), as shown in Figure 1.7.

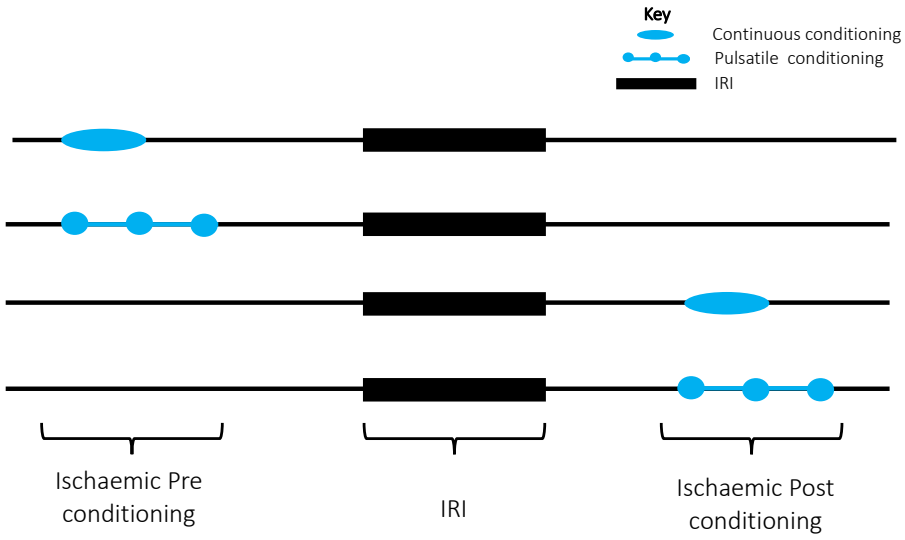

Figure 1.7 *In Vivo* Ischaemic Conditioning Protocols

Renal IRI *In-vivo*, it is a predefined injury brought about by temporary vascular occlusion of the renal pedicle rendering the organ ischaemic. Ischaemic preconditioning utilises shorter, sublethal periods of vascular occlusion before or after the IRI event. In the case of the kidney, the ischaemic conditioning stimuli can be either applied directly to the renal pedicle (direct IC), or remotely to another organ/tissue e.g. liver/lung/leg. The ischaemic conditioning protocol can differ in duration and can either be a short continuous application (continuous IC), or brief ischaemia followed by reperfusion for a predefined number of cycles (pulsatile IC). Finally, the IC stimulus can be either applied before IRI, called ischaemic preconditioning (IPC) or after IRI termed ischaemic postconditioning (I-POC)

Previous work at the host laboratory has systemically compared continuous and pulsatile IC protocols applied directly to the renal pedicle prior to IRI[190]. This work demonstrated that continuous direct IPC fails to reduce histological injury when applied directly to the renal vasculature[191], but a pulsatile method did[192]. The failure of direct continuous IPC to reduce injury has also been observed in a model of liver IRI[193]. By contrast, pulsatile IPC has yielded significant benefit in the kidney when applied before the injury[194; 195].

The cytoprotective effects of IC is not confined to local administration. Effective remote IC was achieved *in vivo* by occluding the vasculature of a single peripheral limb, or of the bilateral lower limbs[196; 197]. Wever et al. (2011) examined the effects of continuous and pulsatile remote IPC using the unilateral or bilateral limbs, concluding enhanced efficacy with bilateral, pulsatile-indirect IPC methods[198]. Furthermore, a different organ can be preconditioned to that undergoing IRI: e.g., heart IC and kidney IRI[199]. Finally, several groups have demonstrated efficacy with both IPC and I-POC approaches *in vivo*[200-202].

Of the IC methods described above, the potential to prevent IRI has made IPC an attractive approach for future research. Furthermore, the finding that remote IPC can confer protection may facilitate the transition of IPC to a minimally invasive approach in the clinical setting using peripheral sites such as the arm or leg.

1.3.4 Mechanisms of IPC

The precise mechanism by which IPC exerts its cytoprotective effect is unknown. It is hypothesised that both direct and indirect IPC exert their effects via the humoral immune response, anti-inflammatory signalling, and metabolic activity. Current understanding of the mechanism of preconditioning can be broadly divided into two phases, early and late: early

phase IPC protection is thought to be driven by intercellular mediators which culminate in mitochondrial change, while the late phase relies on gene expression changes.

1.3.4.1 Early phase IPC

The early phase of IPC is thought to be initiated by reperfusion. During this stage IC triggers the release of humoral trigger factors including adenosine[203], bradykinin and opioids[204] by endothelial, parenchymal, and inflammatory cells. These factors act as ligands that bind to the G-protein coupled receptors (GPCR) and elicit an intracellular ischaemic warning signal. GPCR activation activates the innate cellular anti-apoptotic pathway of survival first described by Hausenloy et al. (2004) and called the reperfusion injury salvage kinase (RISK) pathway[205].

The RISK pathway Involves several pro-survival cascades that trigger anti-apoptotic signals. These kinases activate the phosphatidylinositol-3-OH Kinase: PI3K–AKT pathway, and the extracellular signal-regulated kinase (ERK)1 (also known as p44)/ERK2 (also known as p42) pathway. Both these pathways have been implicated in cellular survival via IC. Both PI3K–Akt, and ERK1/2 cascades inhibit the pro-apoptotic protein, BCL2 associated agonist of cell death (BAD), through the phosphorylation and binding to 14-3-3 proteins, preventing mitochondrial activation and inhibition of BAD-induced cell death[206]. These kinase cascades further inhibit translocation to the mitochondria of the apoptosis regulator BCL2-associated X (BAX), thus preventing apoptosis via cytochrome C. PI3K–AKT activity results in phosphorylation of IKK-α, allowing the translocation of NF-kβ into the nucleus where it activates survival pathways. The P13K-AKT pathway also phosphorylates eNOS producing NO which inhibits the activation of the mitochondrial inner membrane protein, mPTP, whose activation results in mitochondrial rupture and release of the pro-apoptotic protein cytochrome c[205].

There is extensive evidence for the activation of the RISK pathway by renal IPC. Grenz et al. (2008) demonstrated that the beneficial effect of IPC was negated in mice where the A2B adenosine receptor (A2BAR) was knocked out, and that use of an A2BAR agonist prevented IRI injury[207]. Furthermore, the systemic administration of adenosine antagonists prior to IRI protects against IRI in the kidney, suggesting an important role for adenosine in renal IPC[208; 209]. The importance of the GPCR cell surface receptor family in mediating renal IPC was revealed by Lee et al. (2001), who demonstrated that both IPC and adenosine renal protection was lost when GPCRs were inhibited by pertussis toxin[210]. Further to the observation that GPCR signalling is important in IRI, Kakoki et al. (2007) investigated the effects of bradykinin inhibition in a knockout mouse model for bradykinin receptors B1 and B2, and concluded that bradykinin plays a protective role in IRI[211].

ERK1/2 cascade activation in IRI results in cellular resistance through the recruitment of anti-apoptotic pathways[212], while inhibition of this pathway progresses IRI[213]. Indeed, under IRI BAX undergoes conformational changes to facilitate translocation to the mitochondria, where it induces cytochrome c release via pore formation or via interaction with mPTP. IPC disrupts this pathway through the activation of ERK1/2, which inhibits BAX expression[182]. Indeed, targeting PKC using chelerythrine, inhibits the beneficial effect afforded by IPC[210]. It is posited that the P13K-AKT pathway activates PKC which in turn activates mitochondrial adenosine triphosphate-sensitive potassium channel mK(ATP) , inhibiting mPTP[201].

Other important possible mechanisms of IPC include the activation of natriuretic peptide receptor (NPR) by ANP/BNP. NPRs are abundantly expressed in renal vessels/podocytes and in the proximal tubule. These receptors act via the secondary messenger, cyclic guanosine monophosphate/protein kinase G (cGMP-PKG) pathway, to inhibit

mPTP activation in the mitochondria. NPR activates cGMP, which targets protein kinase G (PKG). PKG phosphorylates mitochondrial PKC, activating mk(ATP) and inhibiting mPTP[214]. The importance of atrial natriuretic peptide (ANP) in signal transduction has been shown by Chujo et al. (2010), and Tulafu et al. (2014), who demonstrated that the administration of ANP reduced IRI injury, and TNFα expression in the kidney[215; 216]. Downstream of NPR signalling, PKG levels are reduced following IRI, and overexpression of PKG using transgenic mice attenuated renal IRI injury[217]. Indeed, IPC signalling appears to have an important role in IRI attenuation via PKC[218].

Nitric oxide (NO) also has a role in IPC. NO is synthesised via three NO synthases: neuronal nitic oxide synthase (nNOS/NOS-1), inducible nitric oxide synthase (iNOS/NOS-2) and endothelial nitric oxide synthase (eNOS/NOS-3). Ogawa et al. (2001) demonstrated that a non-selective NO inhibitor N(G)-nitro-L-arginine methyl ester (L-NAME), reduced the protection afforded by IPC[219]. Similarly, selective knockout of iNOS in mice attenuated renal IRI[220], and eNOS knockout mice are resistant to IPC[221]. However, it is been posited that eNOS signalling induces the protective effects of IPC[222], possibly via phosphorylation of glycogen synthase kinase-3β (GSK-3β), which inhibits mPTP opening[223]. Furthermore, GSK-3β inhibition reduces BAX activation[224]. Thus, the downstream effector targets of NO activation act through the RISK and cGMP/PKC pathways to inhibit mPTP opening and preventing apoptosis.

1.3.4.2 Late phase IPC

Late phase IPC protection results from gene expression changes via differential regulation of transcription factors and subsequent protein synthesis. Indeed, several studies of renal IC have demonstrated the differential regulation of transcription factors including NF-

kB, hypoxia-inducible factor-1 alpha (HIF-1α) and synthesis of proteins including haem oxygenase 1 (HO-1) and heat shock proteins (HSPs) following IC.

Following IRI there is an activation of defence mechanisms against oxidative stress mediated through the oxidative stress-response transcription factor nuclear factor-erythroid factor 2–related factor (NRF2). Nezu et al. (2017) demonstrated that in mice knocked out for NRF2, IRI resulted in severe tubular injury in comparison with wild type (WT) mice, and the damage was ameliorated in hypomorphic kelch-like ECH-associated protein 1 (KEAP1), knockdown mice, which constitutively activate NRF2

[225]. Indeed, NRF2 activation is enhanced by IPC [226], and pre-treatment with NRF2 protected the kidney from IRI[227]. Activation of NRF2 induced the transcription of protective proteins like HO-1 and NADPH-quinone oxidoreductase-1 (NQO-1), which are increased following IPC[228].

The inflammatory response following IRI is well established with significant upregulation of pro-inflammatory cytokines TNF-α, IL-6 and IL-8[229]. Extensive research in this area has demonstrated that IPC is a potent inhibitor of TNF-α [207] and IL-6[199; 230]. Indeed, IRI can be attenuated when TNF-α is inhibited via siRNA gene silencing[231], while IL-6 knockout mice are resistant to IRI[232].

There is significant upregulation and expression of adhesion molecules ICAM-1 and P-selectin following IRI[232]. In concordance with this observation, ICAM-1 and P-selectin downregulation have been observed following IPC, perhaps as part of a preventative strategy to reduce immune cell migration[233]. Indeed, the inhibition of ICAM-1 using monoclonal antibodies reduces renal IRI[234].

In parallel to the above findings, IRI is a potent trigger for NF-κB expression. Studies testing the beneficial effects of IPC in the kidney have identified anti-inflammatory effects of

IPC through the downregulation of NF-κB[207; 229]. Indeed, the beneficial effects of NF-κB targeting have been validated using NF-κB inhibitors, which ameliorates renal IRI severity[235].

There is therefore a large body of evidence that IPC is not the result of a single mechanism but occurs via an immediate response to IPC and a delayed transcriptional effect. Whatever the stimulating signal of IPC, current thinking is that the underlying intracellular mediators and their downstream effector targets are thought to be the same[236]. A summary of the pathways involved in IPC is shown in Figure 1.8.

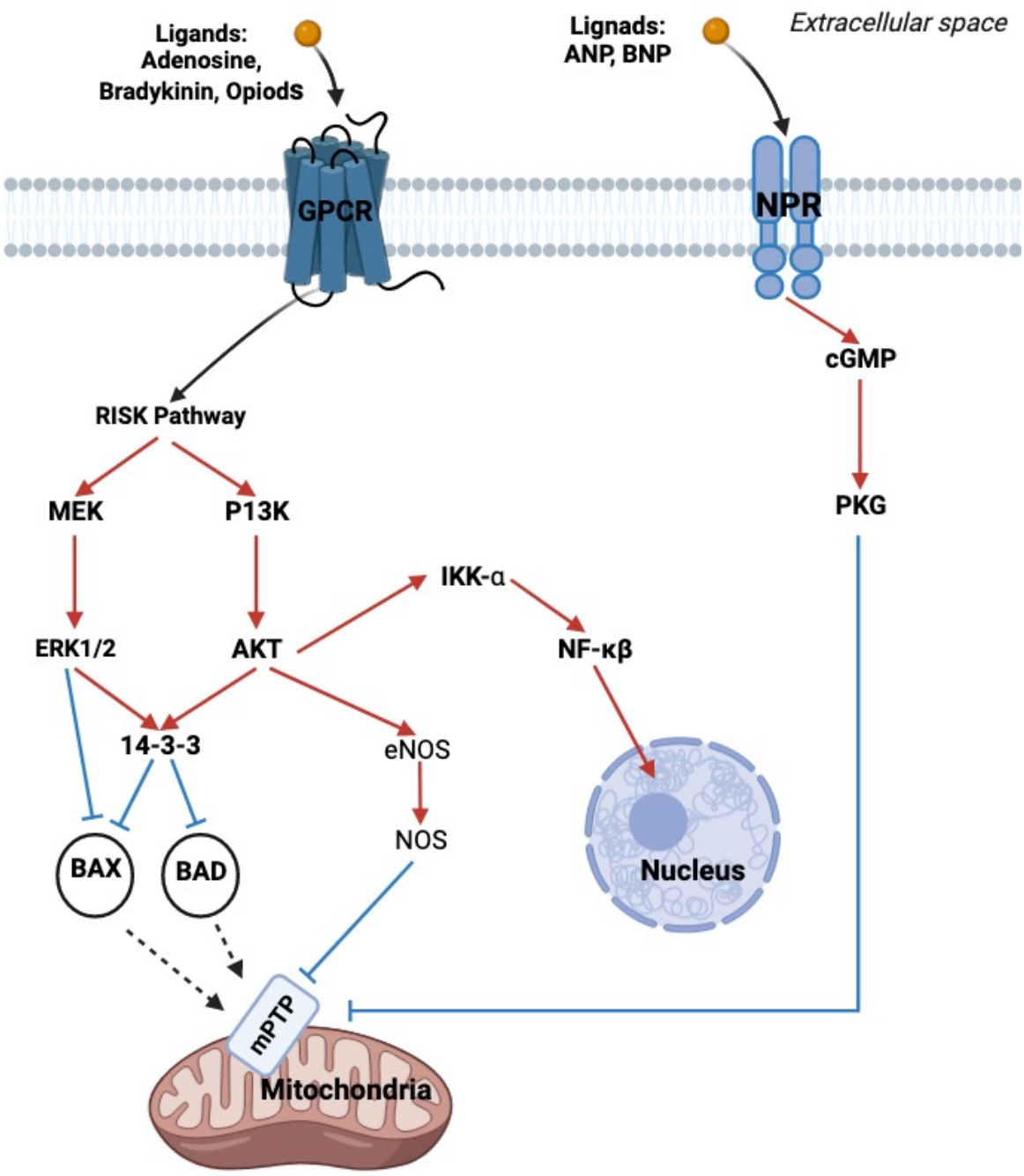

Figure 1.8 Molecular Mechanism of IPC

Pictorial representation of the molecular mechanism of renal IPC.. A detailed description of the pathways can be found in chapter 1.3.4.
Within the above figure abbreviations are as follows: G protein-coupled receptor (GPCR), Natriuretic Peptide Receptor (NPR), Atrial Natriuretic Peptide (ANP), B-type Natriuretic Peptide (BNP), Cyclic guanosine Monophosphate(cGMP) Protein Kinase G (PKG), Mitochondrial Permeability Transition Pore (mPTP), BCL2 Associated Agonist Of Cell Death (BAD), BCL2- associated X (BAX), Nitric Oxide Synthases (NOS), Endothelial Nitric Oxide Synthases (eNOS), Phosphatidylinositol 3-Kinase (PI3K), protein kinase B (AKT), Extracellular signal-regulated kinase (ERK 1 or 2), Mitogen-Activated Protein Kinase (MEK).
Blue line is inhibited, red line is activated. Dashed line is activated if inhibition upstream had not taken place.
Figure created using Created with BioRender.com

1.3.5 Clinical Applications of IPC

Although AKI has attracted significant research attention over the last 20-years, clinically there is still no agreed method to reduce the occurrence of AKI in high-risk individuals. To date, the most promising and widely investigated prophylactic intervention to prevent IRI *in vivo* is that of mechanical IPC[189]. Indeed, the potential clinical translation of IPC has huge therapeutic potential to prevent AKI in high-risk individuals.

IPC as a preventative strategy in humans to reduce the occurrence of AKI and prevent long-term renal sequelae is controversial. Several clinical trials in humans have been advantageous[237; 238], while others have demonstrated no benefit[239; 240]. Equally, some randomised controlled trials (RCT) have demonstrated efficacy[238; 241; 242], while others have not[243-245].

To date, PubMed lists 1,553 publications between July 1993 and July 2018 with the search terms i) isch(a)emic preconditioning, remote preconditioning, isch(a)emic postconditioning, remote preconditioning; ii) humans; and iii) English. Of these, 42 RCTs (39 trials in those ≥18 yrs of age, and 3 trials <18 yrs of age) contained a nephrological pathology as the primary or secondary outcomes. The characteristics of the trials are summarised in, Figure 1.9.

In total, 9,055 patients have been randomised across 42 trials. At an individual trial level, no firm consensuses can be drawn (Figure 1.9). Hausenloy et al. (2015) reported a large multi-centre RCT demonstrating a neutral impact of IPC on acute and chronic renal outcomes[244]. By contrast Zarbock et al. (2015)[238] and Deftereos et al. (2013)[246], showed a beneficial effect of IPC. Zarbock et al. (2017) followed-up their original trial patients post-discharge and demonstrated a lower incidence of CKD and requirement of RRT in the IPC group[247].

The challenges to understand if IPC has clinical potential have also been investigated in meta-analysis (MA). One recent MA of 26 RCTs investigated renal outcomes in patients undergoing cardiac and vascular interventions and reported reduced incidence in post-operative AKI[248], [p=0.01; RR 0.79 (95% CI 0.66-0.95)]. This observation has been supported by several other Mas[249-252]. However, other analyses have reported no improvement in AKI[253-255].

The above findings are further complicated by differences between the patient populations being studied. Some Mas have included RCTs where only patients undergoing cardiac and vascular surgery has shown benefit[248]. Other analyses have reported that mechanical IPC improves renal outcomes in those at risk of contrast-induced AKI (CI-AKI)[256; 257]. However, IPC does not appear to result in clinically meaningful outcomes in those undergoing renal transplant[258].

Study ID	Study Design				Renal Outcomes	
	Design	Group	N^0 enrolled	IPC Protocol	Acute (AKI)	CKD or RRT
Zhou 2018[242]	S.RCT	PCI	107	Arm IPC 5/5 (x4)	Improved sCr	RRT H_0
Cao 2017[259]	S.RCT	VS	63	Arm IPC 5/5 (x3)	H_0	N/A
Hou 2017[260]	S.RCT	LN	65	Arm IPC 5/5 (x3)	N/A	CKD Improved
Zarbock 2017[247]	M.RCT	CS	240	Arm IPC 5/5 (x3)	N/A	RRT & CKD less
Guerra 2017[261]	S.RCT	CS	45	Thigh IPC 5/5 (x2)	H_0	N/A
Kahlert 2017[240]	S.RCT	CS	100	Arm IPC 5/5 (x3)	H_0	N/A
Kim 2017[241]	S.RCT	CS	160	Arm IPC 5/5 (x4)	< AKI	N/A
Singh 2016[262]	S.RCT	PCI	102	Arm IPC 5/5 (x3)	H_0	N/A
Garcia 2016[263]	S.RCT	VS	201	Arm IPC 5/5 (x3)	H_0	N/A
Walsh 2016[264]	M. RCT	CS	258	Thigh 5/5 (x3)	H_0	N/A
Pinaud 2016[239]	S.RCT	VS	100	Arm IPC 5/5 (x3)	H_0	N/A
Meybohm 2015[245]	M.RCT	CS	1385	Arm IPC 5/5 (x4)	H_0	N/A
Hausenloy 2015[244]	M.RCT	CS	1612	Arm IPC 5/5 (x4)	H_0	CKD 12 mths H_0
Menting 2015[265]	M.RCT	RP	76	Arm IPC 5/5 (x4)	H_0	N/A
Zarbock 2015[238]	M.RCT	CS	240	Arm IPC 5/5 (x3)	< AKI & <RRT	N/A
Gallagher 2015[266]	S.RCT	CS	86	Arm IPC 5/5 (x3)	H_0	N/A
Candilio 2015[267]	S.RCT	CABG	178	Thigh vs Arm IPC 5/5 (x3)	H_0	N/A
Yamanaka 2015[268]	S.RCT	PCI	125	Arm IPC 5/5 (x3)	< AKI at 72 hrs	N/A
Hong 2014[243]	M.RCT	CS	1280	Arm IPC 5/5 (x4) x2	H_0	N/A
Savaj 2014[269]	S.RCT	PCI	96	Arm IPC 5/5 (x3)	< AKI at 48 hrs	N/A
Murphy 2014[270]	S.RCT	E-AAA	62	Arm IPC 5/5 (x3)	H_0	N/A
McCrindle 2014[271]	S.RCT	CS	339	Thigh IPC 5/5 (x3)	H_0	N/A
Lavi 2014[272]	S.RCT	E-PCI	360	Thigh vs Arm IPC 5/5 (x3)	H_0	N/A
Igarashi 2013[273]	S.RCT	PCI	60	Arm IPC 5/5 (x4)	<AKI	
Deftereos 2013[246]	S.RCT	PCI	255	C. IPC, 1/1 (x4)	< AKI	N/A
Chen 2013[274]	S.RCT	RT	60	Arm IPC 5/5 (x3)	H_0	N/A
Meybohm 2013[275]	S.RCT	CS	180	Arm IPC 5/5 (x4)	H_0	N/A
Luo 2013[276]	S.RCT	PCI	205	Arm IPC 5/5 (x3)	H_0	N/A
Er 2012[277]	S.RCT	PCI	100	Arm IPC 5/5 (x4)	< AKI	N/A
Young 2012[278]	S.RCT	CS	96	Arm IPC 5/5 (x3)	H_0	N/A
Hong 2012[279]	S.RCT	CABG	70	Arm IPC 5/5 (x4)	H_0	N/A
Kim 2012[280]	S.RCT	CS	54	Thigh IPC 10/5 (x4)	H_0	N/A

Pedersen 2012[281]	S.RCT	CS	105	Thigh IPC 5/5 (x4)	H_0	N/A
Zimmerman 2011[237]	S.RCT	CABG	120	Thigh IPC 5/5 (x3)	< AKI	N/A
Choi 2011[282]	S.RCT	CS	76	Thigh IPC 10/5 (x3)	H_0	N/A
Rahman 2010[283]	S.RCT	CS	162	Arm RIPC 5/5 (x3)	H_0	N/A
Venugopal 2010[284]	S.RCT	CABG	78	Arm RIPC 5/5 (x3)	< AKI	N/A
Walsh 2010[285]	S.RCT	AAA	40	I.IPC 10/10 (x2)	H_0	N/A
Walsh 2009[286]	S.RCT	EVAR	40	Thigh IPC 10/10 (x2)	H_0	N/A
Hoole 2009[287]	S.RCT	PCI	242	Arm RIPC 5/5 (x3)	H_0	N/A
Ali 2007[288]	S.RCT	AAA	82	I.IPC 10/10 (x2)	< AKI	N/A

Figure 1.9 Summary of IPC Randomised Controlled Trials Completed Between July 1993 and July 2018

The table demonstrates the trial study design, study population in question (group) and the number of enrolled participants. The IPC protocol used is briefly described alongside the principle renal outcomes.

S.RCT: single-centre RCT
M.RCT: multi-centre RCT
PCI: percutaneous cardiac intervention
VS: cardiac valve surgery
CS: cardiac surgery
CABG: coronary artery bypass graft
LN: laparoscopic nephrectomy
RP: radiological procedure
<RRT: reduced incidence of renal replacement therapy
E-AAA: elective abdominal aortic aneurysm surgery
EVAR: endovascular aneurysm repair
Arm IPC: IPC applied to the arm
Thigh IPC: IPC applied to the thigh
C.IPC : IPC applied to the heart
$H_{0:}$ no effect on AKI outcome
N/A: outcome not assessed
<AKI: Reduced incidence of AKI

1.3.6 Clinical Application of IPC: The Challenges

Although there is variation in the reported success of IPC in humans there is a broad agreement regarding the reasons behind these differences. A number of RCTs studied IPC in high-risk patient cohorts: people with diabetes and groups with multiple morbidities[262; 242], while others investigated patients traditionally thought of as low-risk: non-diabetic individuals and children[283; 284; 281]. The use of heterogenous populations fails to target at risk populations and risks being underpowered. Studies have further reported vast variation in AKI incidence which may be due to differing AKI definitions used: RIFLE[281], AKIN[237], KDIGO[244], sCr>25% baseline[283]. Furthermore, no universally agreed optimal IPC approach has been identified which has contributed to the heterogeneity of the IPC approaches used. Indeed, of the 42 RCTs described in Figure 1.4, there are twelve different IPC regimes.

The absence of standardised optima for IPC time-course and magnitude of ischemia required for successful IPC represent significant obstacles to the application of IPC in humans. Further confounders come from underpowered RCTs with highly heterogeneous populations with different levels of perioperative AKI in coronary artery bypass grafting (CABG), abdominal aortic aneurysm (AAA) and percutaneous coronary intervention (PCI) groups.

1.3.7 Chemical Preconditioning

An increasing body of evidence suggests that comorbidities can negatively influence the protective effects of IC. Diabetic rodents have been found to be resistant to IC in the kidney[289] and heart[290]. Indeed, in human clinical trials the beneficial effects of IC to reduce detrimental renal outcomes are ablated in diabetics[265; 262; 289]. Recently, the effects of IC in ageing kidneys have also been questioned. Jankauskas et al. (2017) compared the effects of IC

on renal outcome in young and old rats, demonstrating that elderly rats were resistant to IPC[291]. These observations are particularly germane as the patient group with the greatest risk of IRI, and which is therefore most likely to benefit from IC, is the elderly population with multiple comorbidities.

To address some of these difficulties, researchers have used pharmacological agents to activate individual pathways thought to be responsible for the IC effect via chemical preconditioning (CP). CP has obvious advantages, the potential for dose escalation plans for "IC resistant" cases, drug therapeutic monitoring of target effectors and the potential ease of administration makes CP an exciting and natural transition for IC.

Lee et al. (2000), were one of the first groups to use a chemical as a preconditioning agent in renal IRI. The researchers used adenosine, a potent A_1 adenosine receptor agonist, and a A_3 adenosine receptor antagonist. Both agents successfully protected the kidney from IRI, and the authors concluded that not all IC effects are mediated through one receptor[208]. The group went further and tested the effect of selective overexpression of adenosine A1 receptor (A_1Ars) mRNA and protein in a A_1Ars knockout mouse, both of which attenuated IRI [209]. Overall, this research revealed that numerous pathways are implicated in IRI, suggesting the possibility of multiple therapeutic targets.

Following the original work of Lee et al. (2000)[208], it has become increasingly clear that there may be many effector targets of IC. Chen et al. (2007) successfully demonstrated *in vivo* inhibition of NO abolished the protective effects of IPC and ozone (O_3) was able to confer protection from IRI thorough NO release[292], which is thought to stabilise the endoplasmic reticulum via HIF-1α[222]. Other researchers have used a screening approach. Wever et al. (2013), tested nine compounds whose target pathways were thought to be involved in IC and identified opioid signalling as another potential mediator of RIPC[293].

There have been limited attempts to utilise CP in human trials. The first randomised controlled trial in CP was conducted by Julier et al. (2003), who used the anaesthetic agent sevoflurane to precondition patients prior to CABG surgery. The study demonstrated improved renal function post-operatively, and the researchers concluded that that beneficial effect of sevoflurane IC may be mediated through the activation of PKC and increased formation of NO[294]. Ambrosi et al. (2016) used the potent antioxidant alpha-lipoic acid as a CP agent prior to kidney-pancreas transplantation, demonstrating improvement in inflammatory cytokines IL-6, IL-8 and TNF-α in the kidney-pancreas group, whose donor and recipient received pre-treatment, but failed to demonstrate an improvement in renal function. The authors posited that CP dose optimisation would observe more clinically meaningful results[295].

The extensive scientific research in the pathways involved in IC research has generated multiple potential targets which could be chemically augmented. As such, mimicking these pathways may be the next logical step in conditioning research.

1.4 Transcriptomics

Extensive research into the mechanism of IRI and IC has revealed a complex interplay between inflammatory mediators and signalling cascades in an array of cell types. It is therefore unlikely that there is a single molecular target responsible for the IRI phenotype, or the protection afforded by IC. This knowledge informs investigative approaches at the tissue and cellular level.

1.4.1 Gene Expression

Gene expression is a highly complex and ordered process. In brief, the DNA template is transcribed by the enzyme RNA polymerase in the cell nucleus, resulting in the formation of complimentary RNAs which can be divided broadly into coding and non-coding RNAs. Non-coding RNAs will not be addressed in this thesis, but excellent reviews are provided by Hombach et al. (2016)[296] and Liu et al. (2019)[297].

Protein coding RNAs are known as messenger RNAs (mRNAs), which undergo a series of editing steps via which the mature mRNA is prepared. The mRNA is transported from the nucleus to the ribosome where it is translated into a protein.

Differential regulation of mRNA transcripts has significant impact on the cellular and consequently organismal phenotype. Indeed, capturing the transcriptomic dynamics across multiple cell types and tissues provides valuable insights into the mechanism underpinning homeostasis and disease. In an attempt to identify the complex molecular processes leading to disease, current research aims to combine data from multiple investigative approaches via Omics[298].

1.4.2 Omics

Omics is a relatively new field of science that obtains a large volume of molecular information from tissues or cells in a single experiment. This comprehensive snapshot aims to link the molecular processes of the sample to the biological function or disease tested, known as the phenotype. Omics is a rapidly evolving research field that encompasses the measurement of many different biological molecules. Differing omics experiments include proteomics, which measures the protein signature of a sample; metabolomics, which analyses the metabolites; and transcriptomics, which studies the RNA transcripts of the sample[299].

Transcriptomics captures the gene expression cell fingerprint by profiling the samples RNA output. This technique facilitates the identification of genes that are switched on under conditions of interest. Accurate transcriptional profiling provides exciting opportunities to understand the transcriptional networks underpinning IRI and IPC[300]

RNA sequencing utilises a series of complex experimental steps to facilitate transcript identification. In brief, total RNA is extracted from tissue or cell samples. This RNA extract can then be depleted to remove specific abundant RNA species, such as ribosomal RNAs, and enrich for the mRNAs. The extract enriched in mRNAs then undergoes reverse transcription to the more stable complementary DNA (cDNA) which binds to the sequencing surface called the flow cell. Finally, fluorescent probes tagged to nucleotides bind to complementary nucleotides in the cDNA sequence. These fluorescent nucleotides are then monitored and interpreted by the sequencing software to deduce the cDNA nucleotide sequences. Each cDNA fragment sequence is termed a “read.” The reads are compared to the reference genome of the starting organism, e.g., rat, facilitating the qualitative and quantitative measurement of the original mRNA in the starting sample[301; 302].

1.4.3 IRI Transcriptional Profiling

Recent research has attempted to use transcriptome sequencing to describe the complex molecular events underpinning IRI. Giraud et al. (2018) used a porcine, donors deceased after circulatory death model of kidney transplantation to mimic the effects of ischaemia. These workers used a model of 60 minutes of warm ischaemia followed by either no cold storage, 6 hour cold storage or 24 hour cold storage. Using microarray technology, the authors revealed the impact of ischaemia on the whole transcriptome and found significant dysregulation in oxidative stress response, cell-cycle, and inflammation[303].

Park et al. (2020), studied the effects of IRI in five patients who were scheduled to have a total nephrectomy due to renal cell carcinoma. The researchers biopsied the kidney prior to removal, after 15 minutes of ischaemia and following 10 minutes of reperfusion. Samples were analysed by RNA sequencing and gene set analysis. The research demonstrated an enrichment of gene sets related to oxidative stress, and inflammation during ischaemia, and dysregulation of pathways linked to cellular function and proliferation during reperfusion[304].

In summary, it is evident that the transcriptional response to IRI is multifaceted, and that transcriptional profiling is a powerful method to move away from hypothesis driven to unbiased analysis. However, how the gene enrichment sets identified influence the disease phenotype is unknown.

1.4.2 Renal IPC Transcriptional Profiling

Understanding the molecular mechanisms that confers protection in renal IPC is important to facilitate the successful transition of IPC to the clinical setting. Correa-Costa et al. (2012) tested a 15 minute continuous IPC model prior to IRI and compared the IPC profile to

IRI. The study identified the downregulation of gene sets related to apoptosis, and an enrichment of biological functions related to DNA replication and the cell cycle[305].

Johnsen et al. (2020) used a sealed chamber to create a model of hypoxic preconditioning and compared this to caloric restriction preconditioning prior to IRI. This analysis found common genes and response pathways that overlapped between both preconditioning groups[306]. Nevertheless, the mechanisms via which IPC transcriptional response pathways compare to IRI is unknown.

1.5 Summary of Aims

IRI is a common cause of AKI in patients and is a danger to life. The pathophysiology of IRI is complex and born from an interplay between the renal endothelium, immune system, and intracellular pathways. IPC is a powerful technique to diminish IRI *in vivo*, but its transition to the clinical setting has failed. Multiple different IPC techniques have been used experimentally, and it is unknown if they share common molecular mechanisms. IPC optimisation in the clinical setting is challenging and pharmacological targeting of IPC response pathways may yield promising results.

Taken together, the objectives of this thesis were to:

1. Optimise IPC methodology in an existing rat model of IRI
2. Analyse the transcriptional signature of IRI and to elicit the response pathways activated by IPC
3. Investigate computational drug repurposing techniques to mirror the transcriptional response observed following IPC

Chapter 2

Methodology

2.1 *In vivo* Experiments

The host laboratory has a well-established *in vivo* model of bilateral renal IRI in the rat. The IRI technique was established by the Renal Transplant Consultant Mr Rafael Chavez (supervisor) and has been successfully refined by the PhD student, Mr Usman Khalid[190].

2.1.1 Surgical Subject

Genetically identical inbred male adult (8 to 12 weeks old) Lewis rats (LEW/Crl- Charles River Labourites, Inc.) weighing 220 to 260 grams were used in all *in vivo* experiments described in this thesis. Lewis rats have been well established as an excellent surgical candidate for *in vivo* surgical transplantation, inflammatory basic science and nonclinical drug discovery and development research. Characteristically, Lewis rats are robust *in vivo* candidates owing to their highly sociable, friendly, and easy to handle nature. These features allow for effective pre- and post-operative health status monitoring. The host animal research Establishment Licence holder, Cardiff University Joint Biological Services unity (JBIOS), has extensive experience housing this inbred line and were well suited to manage the animal husbandry.

2.1.2 Rodent Preparation

The Lewis rats were delivered a minimum of 7 days before the start of each experiment to allow for acclimatisation to their surroundings. Upon arrival the rats were checked by JBIOS staff to ensure health. Rodents were housed in tall (>30cm height), solid floored conventional cages to allow for full natural range of movement. Each cage had nesting material and toilet rolls for environmental enrichment. Rats were housed in groups of 2 or 4 for social welfare. The rat cages are lodged in the conventional holding room for rats which is lit with artificial

light (12-hour light/dark cycle) and kept at a temperature range of 20 to 22^{o}C. The rats had access to water, rat chow and sunflower seeds ad-libitum.

Twenty-four hours before surgery, the rats were moved to individual conventional cages and provided with buprenorphine enriched drinking water for pre-operative analgesia (200μg of buprenorphine dissolved in 500ml of drinking water), as recommended by the Named Animal Care and Welfare Officer (NAWCO), veterinary officer and approved as a regulated procedure in the project license.

Each rodent was assigned a unique identification number which linked to their biological sample. A logbook was kept for each animal detailing pre, intra and postoperative regulated procedures and monitoring outcomes. As per the local Standard Operating Procedures (SOP's) of JBIOS an identification card was placed on each cage to identify the rat to their responsible personal license holder, project license, date of entry to JBIOS, my personal contact details and any regulated procedure the animal had undergone. Any obtained samples were coded according to the rodents assigned unique identification number.

2.1.3 Preoperative Procedure

The experimental procedures were completed in accordance with the SOP's of JBIOS. The study experiments were carried out under the Home Office Project License PPL 30/3098 (protocol 1, 2 and 3) held by Mr Chavez, supervisor for this project. Mr Chavez and I completed a personal license. Following surgical training on the operative technique and achieving practical independence I completed all experimental procedures myself.

The operative theatre setup to be described was approved by the NAWCO, veterinary officer and completed in line with JBIOS SOPs of operative technique. All operative procedures

were completed in a designated procedure room away from the rat conventional holding room. All surgical procedures were completed using an aseptic technique.

The surgical field was prepared, and equipment set out. A surgical checklist was completed to ensure all equipment was available prior to surgery. Equipment required for each surgical step is outlined at each stage below.

2.1.4 Anaesthesia

Animals underwent gas-induced anaesthesia within an induction chamber using 5% isoflurane (IVAX Pharmaceuticals, UK). The 5% isoflurane was delivered via oxygen at 2 L/min and the rat was allowed to breath without mechanical ventilation until sedation was achieved. Sedation was typically achieved with 2-3 minutes. Following induction of anaesthesia, the rat was transferred from the induction chamber to a cork operating board which had been covered with a sterile drape (large dressing towel 715mm x 750mm: Ref 28517). The anaesthesia ventilator was located on the operating table for ease of access. A rodent facemask was placed around the rodent mouth and nose. Anaesthesia was delivered at a concentration of typically 2% isoflurane via 2 L/min oxygen. Concentration of isoflurane was augmented to achieve a heart rate, breathing pattern, and absent rear foot reflexes consistent with a surgical plane of anaesthesia.

2.2 Operative Procedure: IRI and Sham

The rats were maintained at a surgical plane using gaseous anaesthesia as described (2.1.3.1 Anaesthesia). The hair of the rat abdomen was shaved using a hair clipper (Contura Chrome AC 220-240V, UK, ref 523889400). The rodent limbs were retracted using rubber bands and the bands were pinned to the cork board. Sterile gloves and gown were put on. The skin was cleared using chlorhexidine spray. A sterile drape (large dressing towel 715mm x 750mm: Ref 28517) was placed across the abdomen and an overhead lamp was used to provide adequate lightening and heat to maintain the rodent body temperature. A midline 3cm laparotomy incision was made using a carbon steel 15-surgical blade (ref 0205 Swann Morton). The rectus sheath and peritoneum were opened using a McIndoe scissors and the abdominal wall was retracted using surgical retractors.

The bowel was mobilised and moved to the rodents right to expose the left kidney and renal pedicle. For those rats in the IRI group the left renal pedicle was lifted using a cotton tip applicator 15cm (Ref 88162) and an atraumatic vascular clamp was placed across the renal pedicle. Upon clamping of the renal pedicle, the kidney was visually inspected to confirm ischaemia which is characterised by the kidney colour shifting from a normal pink colour to a purple/grey colour. The bowel was then mobilised and moved to the rodent's left to expose the right kidney. The right kidney was then clamped and monitored in an identical manner to the left kidney. A saline soaked gauze was placed across the bowel to maintain hydration. Both vascular clamps were left to occlude the bilateral renal pedicles for 45 minutes.

Following 45 minutes of bilateral ischaemia both vascular clamps were removed, and the kidneys inspected for reperfusion, charactered by the return of a pink colour to the kidney. The saline-soaked gauze was removed. The laparotomy incision was closed in two planes using 4-0 vicryl suture. First, the muscle layer was closed, and the skin was then closed using a

continuous buried suture. The knots were buried deep to the skin to avoid the rat chewing the stitch. The skin was cleaned, and the isoflurane stopped. Oxygen delivery via the rodent facemask was continued at a rate of 2 L/min until the rat started to awaken. The cage was placed upon a heat mat and the rat was transferred to the cage. The rat was monitored during the recovery phase and once the rat started to move independently it was transferred to its holding room.

Those rats in the sham group underwent an identical procedure as described but in the absence of the application of the vascular clamps.

2.3 Operative Procedure: Mechanical Preconditioning

The rats were maintained at a surgical plane using gaseous anaesthesia as described (2.1.3.1 Anaesthesia). The rodent abdominal wall was prepared as described (2.2 Operative Procedure: IRI and Sham) and immediately prior to performing bilateral renal IRI, seven different methods of mechanical preconditioning were applied as described below (sections 2.3.1- 2.3.3) and pictorially represented in Figure 2.1.

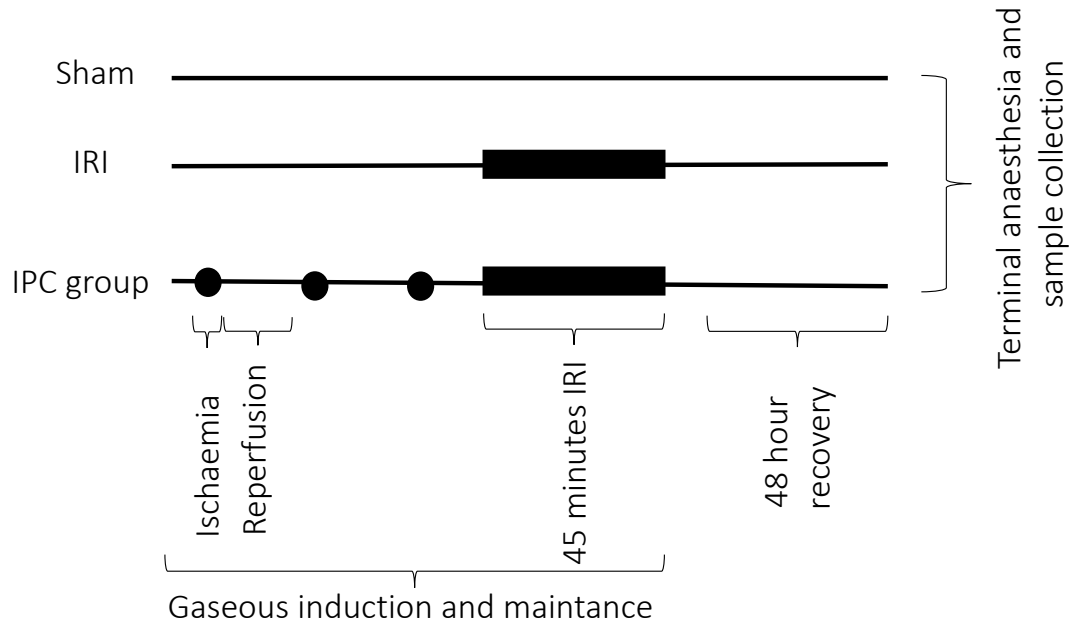

Figure 2.1 Operative Procedure: Mechanical Preconditioning

Male adult Lewis rats were randomly assigned to 7 different IPC groups. IPC intervention was applied prior to IRI in all groups.

2.3.1 Bilateral Direct IPC

The host laboratory has successfully tested several different methods of pulsatile Ischaemic Preconditioning (IPC) applied directly to the bilateral kidneys, concluding that the optimal technique is pulsatile IPC for 2-minutes ischaemia followed by 5-minutes reperfusion repeated for three cycles prior to IRI (direct-2/5[3]), (unpublished data). This methodology was

repeated as one of the investigated IPC techniques in this thesis. The technique is as follows. The bowel was mobilised and moved to the rodent's right to expose the left kidney and renal pedicle. The left renal pedicle was lifted using a cotton tip applicator 15cm (Ref 88162) and an atraumatic vascular clamp was placed across the renal pedicle. The bowel was then immediately moved to the rodent's left to expose the right kidney. The right kidney was then clamped and monitored in an identical manner to the left kidney. Both kidneys were visually inspected to confirm ischaemia which is characterised by the kidney moving from a normal pink colour to a purple/grey colour. Following 2 minutes of ischaemia both clamps were removed allowing reperfusion of the kidney for 5 minutes which was visually confirmed by return of pink colour to the bilateral kidneys. The ischaemia and reperfusion steps were repeated for 3 cycles. This technique is called IPC: direct-2/5^3.

2.3.2 Unilateral Direct IPC

The bowel was moved to the rodent's left to expose the right kidney and renal pedicle. The right renal pedicle was lifted using a cotton tip applicator 15cm (Ref 88162) and an atraumatic vascular clamp was placed across the renal pedicle. The kidney was visually inspected to confirm ischaemia which is characterised by the kidney moving from a normal pink colour to a purple/grey colour. Following 2 minutes of ischaemia the clamp was removed allowing reperfusion of the kidney for 5 minutes. Reperfusion was visually confirmed by return of pink colour to the kidney. The ischaemia and reperfusion steps were repeated for 3 cycles. This length of time of unilateral ischaemia was changed to test both 5 and 10 minutes of ischaemia. The three different experiments were called IPC: unilateral-2/5^3, unilateral-5/5^3 and unilateral-10/5^3.

2.3.3 Indirect IPC

The bowel was mobilised and overturned superiorly to allow excess to the retroperitoneal structures and aorta. The infrarenal aorta was dissected out using a cotton tip applicator 15cm (Ref 88162) and an atraumatic vascular clamp was placed across the infrarenal aorta. Confirmation of successful occlusion distal to the clamp was confirmed by absence of aortic pulsations and grey appearance of the bilateral hind feet of the rat. Following 2 minutes of ischaemia the clamp was removed allowing reperfusion of the bilateral hind limbs for 5 minutes. Reperfusion was visually confirmed by the return of distal aortic pulsations and pink appearance of the bilateral hind feet of the rat. The ischaemia and reperfusion steps were repeated for 3 cycles. This length of time of infrarenal ischaemia was changed to test both 5 and 10 minutes of ischaemia. The three different experiments were called IPC: indirect-2/5^3, indirect-5/5^3 and indirect-10/5^3.

Following successful IPC application as described above all rodents underwent bilateral renal IRI as described (2.2 Operative Procedure: IRI and Sham).

2.4 Operative Procedure: Chemical Preconditioning

The rats were maintained at a surgical plane using gaseous anaesthesia as described (2.1.3.1 Anaesthesia). The rodent abdominal wall was prepared as described (2.2 Operative Procedure: IRI and Sham) and immediately prior to performing bilateral renal IRI a chemical preconditioning agent was administered as described below.

A small midline 0.5 cm mini-laparotomy incision was made using a carbon steel 15-surgical blade (ref 0205 Swann Morton). The rectus sheath and peritoneum were opened using a McIndoe scissors allowing for direct visualisation in the abdominal cavity. At this point six

different chemical agents or one vehicle could be injected intraperitoneally as described below, Figure 2.2. The chemical agent used was diluted with 2ml of normal saline and injected under direct visualisation using a 5ml Luer Plastipak Syringe (ref 302187). The injected agent was left for 20 minutes to absorb, Figure 2.2.

Following the 20-minute absorption period the mini-laparotomy incision was extended to a 3cm laparotomy incision. Following successful administration of the chemical agent as described above all rodents underwent bilateral renal IRI as described (2.2 Operative Procedure: IRI and Sham).

Those rats assigned to the sham or IRI group in the chemical preconditioning experiment had 2ml of normal saline injected intraperitoneally instead of the chemical/vehicle agent in a manor identical to the described procedure above, Figure 2.2.

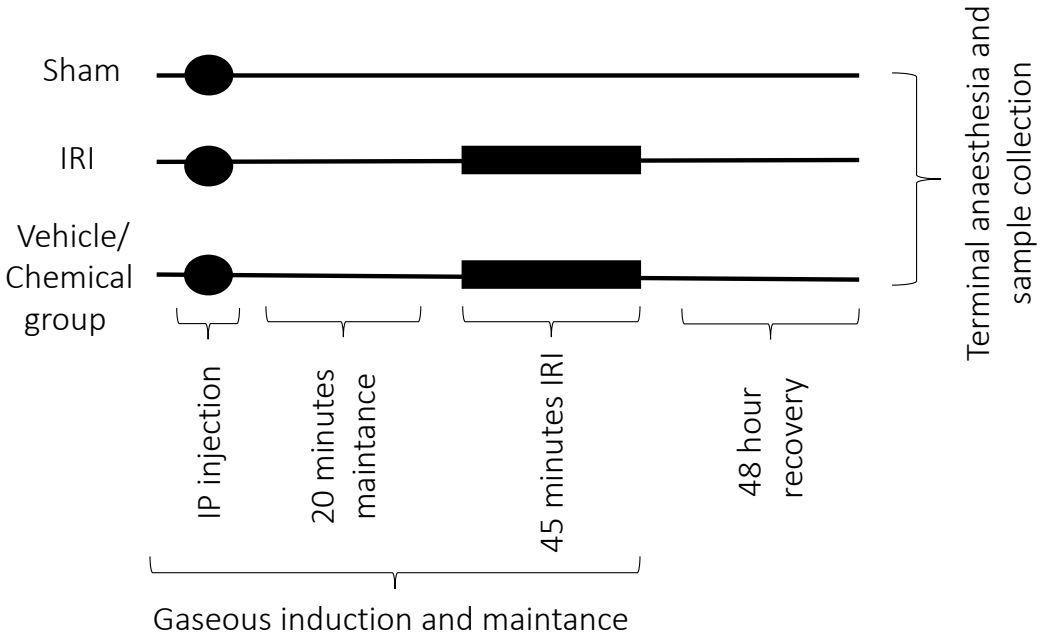

Figure 2.2 Operative Procedure: Chemical Preconditioning

Male adult Lewis rats were randomly assigned to 6 different chemical preconditioning groups. The chemical agent was dissolved in the vehicle and diluted in 2 ml of normal saline intervention was applied prior to IRI in all groups. Those rats in the IRI and Sham groups also received an IP injection of 2 ml normal saline.

2.5 Tail Tip Blood Sampling

Following rat anaesthesia and prior to shaving of the rodent abdominal hair a blood sample was collected from the tail tip of all animals undergoing a surgical procedure as described below. The tail tip was cleaned with chlorhexidine spray and left to dry. A small incision was made on the distal rat tail and the tail was hung off the surgical table. Drops of blood was collected under gravity to a maximal volume of 300μl in a MiniCollect Z Serum Sep 0.5ml blood collection tube (Ref 450473). The eppendorf of blood was inverted three times to facilitate mixture with the clot activator and allow separation of serum. The sample was transferred to the Biochemistry Laboratory at the University Hospital of Wales, Cardiff, for serum analysis.

Blood volume collection was calculated as per published guidance form The National Centre for the Replacement, Refinement and Reduction of Animals in Research (NC3RS). The blood volume taken during tail sampling is well below the recommended maximum blood volume of <10% of total blood volume: a 200g rat's approximate blood volume is 12.8ml, 10% of which is 1.28ml.

2.6 Postoperative Monitoring: Time 0 to 48 hours

Post-operatively, rats were housed in individual cages to allow for recovery. The decision to house rats individually was made in conjunction with the NAWCO, veterinary officer and approved within the project license based on risk that cohabiting animals may chew the abdominal stitching. Over the course of 48 hours rats were checked twice a day. Rats were monitored for signs of post-operative complications including pain, infection, bleeding, and wound dehiscence. Rats were provided with buprenorphine enriched drinking water for post-

operative analgesia (200μg of buprenorphine dissolved in 500ml of drinking water), as recommended by the NAWCO, veterinary officer and approved within the project license.

2.7 Sample Retrieval at 48 hours

At 48 hours post operatively, rats underwent further anaesthesia as described in section 2.1.3.1 Anaesthesia. The rat was maintained at a surgical plane using gaseous anaesthesia as described. The rodent limbs were retracted using rubber bands and the bands were pinned to the cork board. Sterile gloves and gown were put on. The skin was cleared using chlorhexidine spray. A sterile drape (large dressing towel 715mm x 750mm (Ref 28517) was placed across the abdomen. The stitches of the midline 3cm laparotomy incision were opened using a McIndoe scissors and the abdominal wall was retracted using surgical retractors.

Direct cardiac puncture was undertaken inferiorly through the diaphragm using a 21G hypodermic needle and 5ml Luer Plastipak Syringe (ref 302187). Extracted blood was decanted into MiniCollect Z Serum Sep 0.5ml blood collection tubes (Ref 450473) and inverted three times to facilitate mixture with the clot activator and allow separation of serum. The diaphragm was opened, and the cardiac vessels were transected resulting in animal death.

The bilateral kidneys were retrieved. Each kidney was cut longitudinally through the renal hilum. Half the kidney was placed in formalin and sent to histopathology for paraffin wax embedding, sectioning, and staining. The remaining half of each kidney was further cut to produce quarters. One quarter was placed in RNAlater Stabilization Solution (ThermoFisher Life Technologies Ltd) and a further one quarter was snap frozen in liquid nitrogen. Kidney samples were stored at -80 °C. Animal carcasses were placed in clinical waste bags and stored in the animal disposal freezer as per JBIOS SOP protocol.

2.8 Blood Serum Analysis

Extracted blood was decanted into MiniCollect Z Serum Sep 0.5ml blood collection tubes (Ref 450473). Samples were inverted three times to facilitate mixture with the clot activator and allow separation of serum. Samples were centrifuged at 4°C, 2000 rcf for 10 minutes and serum was extracted and analysed at the Biochemistry Laboratory, University Hospital of Wales, Cardiff, using an Abbott Architect c8000 analyser as per the hospital SOP.

2.9 Histology

Half of the rat kidney was transported in formalin to the Histology Department, University Hospital of Wales, Cardiff. The samples were embedded in paraffin, sectioned, and stained with haematoxylin and eosin (H&E) as per the hospitals SOP for sample preparation.

The kidney H&E sections were examined for evidence of histological renal IRI by an independent histopathologist (Dr Gilda Pino-Chavez). The histopathologist was blinded to the experimental design and group. The severity of renal IRI damage was graded according to a ranked scoring system; EGTI histology injury score[307]. This scoring method provided a ranking score based upon the degree of tubular, endothelial, glomerular, and tubular-interstial injury observed.

2.10 Tissue RNA Extraction

One quarter of a whole kidney, including renal, cortex and medulla, was homogenized in QIAzol lysis reagent at a ratio of 50mg of renal tissue to 700μL of QIAzol. Homogenization was achieved at approximately 5 minutes and endpoint defined as a visually uniform solution. Eppendorf's of 700μL of homogenate was decanted and frozen at -80 °C for storage or continued to the RNA extraction step.

RNA extraction was performed using a miRNeasy Mini Kit (Qiagen, Cat No./ID: 217004) column-based extraction method as per manufacture protocol. In summary, 700μL of QIAzol lysis reagent was left for 5 minutes at room temperature to achieve cell lysis. Chloroform (140μL) was added and shaken vigorously for 15 seconds and left at room temperature for three minutes to allow phase separation. The homogenate was centrifuged at 4°C for 20 minutes at 12,000g. Following centrifuge, the sample separated into three phases. The upper, clear aqueous phase containing RNA was extracted and placed in a new collection tube (approximately 300-350μL of volume). Ethanol 100%, 525 μl (1.5 x volume of aqueous phase) was mixed with the aqueous phase. Then, 700μL of sample was pipetted into the RNAeasy spin column and centrifugation was carried out for 30 seconds. Flow-through was discarded and the step repeated for any remaining sample. A volume of 700μL of Buffer RWT was added to the spin columns and centrifugation was carried out at 12,000g for 30 second. Flow-through was discarded. A volume of 500μL of Buffer RPE was added to the spin column and centrifugation was carried out at 12,000g for 30 second. Flow-through was discarded and a further 500μL of Buffer RPE was added to the spin column, after which centrifugation was carried out at 12,000g for 2 minutes. The collection tube containing the flow through was discarded, and the column was transferred to a new collection tube. A volume of 50μL of Rnase

free water was added to the column and centrifugation was carried out at 12,000g for 1 minute to elute the RNA. This first eluate was pipetted back into the spin column and centrifugation was carried out for a further 1 minute at 12,000g to elute the final RNA extract. Eluted RNA was frozen at -70°C for delayed downstream processing.

2.10.1 RNA Quantification, Purity, and Quality

Measurement of RNA concentration and purity was achieved using a Thermo Scientific NanoDrop 2000 spectrophotometer. Spectrophotometry was undertaken as per the manufacture's guidelines. In brief, the Nanodrop was configured to RNA analysis. The pedestal cover was lifted and both bottom and top pedestals were wiped using a lint free cloth. 1.2μL of nuclease-free water blank was pipetted onto the bottom pedestal, and "blank" was selected to normalise the reading. The blank solution was wiped away, 1.2μL of the RNA sample was pipetted onto the pedestal and "measure" was selected. The sample absorbance was measured at 230nm, 260nm and 280nm. The ratio of absorbance was calculated. A 260/280 ratio of >1.8 signified RNA of sufficient purity. The ratio of 260/230 of >1.8 signified a sample sufficiently free of impurities like phenol. The RNA was diluted in RNAase free water to a ratio of 1:3 and re-analysed using the Nanodrop if the RNA yield was >1000ng/μL.

RNA quality was assessed using an Agilent Technologies, Inc., 2100 Bioanalyzer with an RNA 6000 Nano chip. The analyser computed an RNA Integrity Number (RIN) which is a measure of RNA quality. Sufficient RNA quality for Next generation sequencing-RNA transcriptome, was defined as an RIN ≥8.0 as per The Wales Cancer Research Centre: Wales Gene Park (WGP), Cardiff University SOP.

2.10.2 Next Generation Sequencing (NGS)

The right kidneys from twenty-four adult male Lewis rats from four experimental groups were selected for total RNA next generation sequencing. The experimental groups comprised sham (n=6), 45-minute of bilateral Ischaemic Reperfusion Injury (IRI, n=6) and the Ischaemic Preconditioning (IPC) regimes of direct-IPC 2/5[3] (n=6) and indirect-IPC 2/5[3] (n=6). RNA was extracted and its quality analysed as described above.

Next Generation RNA Sequencing (NGS) was performed by WGP using the Illumina HiSeq 2500 platform with Total RNA sequencing Ribozero Gold chemistry. Each individual sample, termed a library, was labelled with a bar code (unique adaptor sequence) to facilitate indexing of individual transcripts to their respective starting library. All twenty-four RNA libraries were pooled and sequenced simultaneously across four lanes of one Illumina® flow cell (termed multiplexed) with the aim of achieving a sequencing depth of 60 million reads per library.

2.10.3 NGS: Raw Data Analysis

Raw data analysis was carried out using the bioinformatic pipeline constructed by Cardiff University Division of Infection and Immunity's Lead Bioinformatician, Dr Robert Andrews. Raw data files were received form WGP in an *in silico* text-based format for storing nucleotide sequences called FASTQ. The FASTQ files contain the individual RNA transcript sequence, corresponding unique adaptor sequence and the Phred quality score (probability of a base call being correct).

Each individual transcript was labelled with a unique adaptor sequence which links the transcript to their original starting sample (library). The transcripts were allocated to their

original library, called de-multiplexing. The adaptor sequence was then trimmed using Trimomatic [Ver 0.36], as per the standard user protocol leaving, the individual read.

To quantify the gene expression the individual reads (raw counts) were mapped to a single reference genome (*Rattus norvegicus* genome assembly: Rnar_6.0 [GCA_000001895.4]) using The Star (Spliced Transcripts Alignment to a Reference) RNA-Seq aligner. The Star RNA-Seq aligner computational assigns the individual nucleotide sequence read to the likely correct genomic loci. The Star aligner parameters were set to assign the individual reads to the reference genome in the following order.

1. Those reads which mapped to a single locus were assigned first.
2. If a read mapped to ≥2 loci, the mapping loci with the greatest alignment score (formula derived score which is computationally calculated by comparing the read to the reference genome amino acids and assigning a numerical value to predict the likelihood of the alignment being correct) was selected.
3. If a read mapped to ≥2 loci and the alignment score was identical, the mapping locus was assigned at random.

To quantify the differential gene expression changes between experimental groups the mapped raw count data was analysed using the program DESeq-2 (Ver. 1.14.1). DESeq-2 calculates the differential gene expression by performing an internal normalisation which aims to remove technical bias. The program aims to normalise for library size (sequencing depth) and library composition (adjust for overexpressed genes where the sequencing depth was preferentially used). To normalise the data DESeq-2 calculates a scaling factor for each library. In brief the scaling factor is calculated as follows:

1. Calculate the $\log_e$ of all genes using the read counts across every library
2. Calculate the mean of the $\log_e$ of each gene across samples (geometric mean)
3. Filter out and exclude all genes with a calculated geometric mean of -inf (i.e., had zero read count in one library)
4. Divide the geometric mean of a gene from the $\log_e$ value of that gene in a library to give a ratio for that library's gene
5. Calculate the median $\log_e$ ratio for each library
6. Convert the median $\log_e$ ratio to a number called the scaling factor
7. Divide original read count by the scaling factor

The final output of the DESeq-2 analysis computes the $\log_2$ fold change ($\log_2$FC) and corrected p values (adjusted as per Benjamini-Hochberg correction) for each mapped gene.

2.10.4 NGS: Data Quality Control

Following RNA sequencing, the raw sequence data quality was analysed using the FastQC (Ver. 0.11.5)[308] platform. The program aims to identify irregularities in the library material. A random sample of 10% of the raw data from each lane was analysed in the following steps as per the standard user protocol.

1. Quality of base call using the Phred score which computes the error probabilities of a base call
2. The guanine-cytosine (GC) content of each sequence was analysed relative to the theoretical GC content for differing sequencing lengths with the aim of detecting library

contamination by two adapter sequences which incorrectly ligated without an attached library sequence and amplified (adaptor dimers).

3. The raw data was finally tested for non-unique sequences in the dataset which could indicate a contaminant or a technical duplication. Failure criteria of a non-unique sequences of >50% of the total.

To test the effectiveness of Deseq-2 normalisation and investigate the distribution of the dataset and outliers Deseq-2 output was plotted as a histogram and compared to the histogram output observed for the raw count using the normalisation technique of Reads Per Kilobase of transcript per Million mapped reads (RPKM; normalises to consider gene length).

2.11 *In silico* Analysis: Ingenuity Pathway Analysis (IPA)

The *in silico* platform Ingenuity Pathway Analysis (IPA knowledge base Ver 2.3, Nov 2017) was used to analyse and investigate the biological content of the RNA sequencing data. IPA uses the expression profile of the dataset and applies algorithms to predict the molecular relationship between the dataset molecules and master regulators, pathways, biological functions, and diseases (IPA knowledge base Ver 2.3, Nov 2017).

Differentially expressed genes (DEGs) with a corrected p-value of $p < 0.05$ (-log [p-value] >1.3) and a $\log_2$FC ≤-1 and ≥1 was assigned as statistically significant.

To enable statistical analysis of the uploaded dataset, IPA requires a reference data set (defined as the complete universe of known transcripts) to be assigned. Following consultation with the IPA Advanced Genomics Support Unit, IPA Ingenuity Knowledge Base (genes only) was selected as the dataset reference to ensure that the number of DEGs compared to reference dataset was > 1:5.

To facilitate a blinded *in silico* analysis and allow the greatest level of freedom of interpretation, IPA was set to consider all data sources and no assignment of organ type was made.

2.12 Statistical Analysis

Statistical analysis was completed using GraphPad Prism Version 7 (San Diego, CA, USA). Data is presented as mean (± standard error of the mean) or median (range). Statistical tests included t-test, one-way ANOVA (Dunnett post-test), Mann-Whitney test or Kruskal-Wallis (Dunn's post-test) depending on whether a parametric or non-parametric test was required.

Volcano plots were completed using GraphPad Prism Version 7 (San Diego, CA, USA). Boxplots, Density plots and Principal Component Analysis were completed using DESeq-2 (Ver. 1.14.1). The RNA Sequencing quality control boxplots was completed using FastQC (Ver. 0.11.5). Bar charts and heatmaps were completed using IPA (knowledge base Ver 2.3, Nov 2017).

Statistical significance was annotated as: * $p<0.05$, **$p<0.01$, *** $p<0.001$ and **** $p<0.0001$.

Chapter 3

Ischaemic Preconditioning in a Bilateral Ischaemic Reperfusion Injury Rat Model

3.1 Introduction

The most common aetiology of AKI worldwide is Ischaemic Acute Tubular Necrosis (ATN) which is thought to cause 80-90% of AKI cases[309; 310]. ATN is a histological diagnosis that describes a disorganised appearance to the normal architecture of the renal tubules, impairing the filtration and excretory function of the kidney[311]. The injury is triggered by periods of reduced tissue oxygenation (ischaemia) followed by the restoration of blood circulation (reperfusion), called Ischaemia Reperfusion Injury (IRI). Both the ischaemic and reperfusion phases of IRI trigger inflammation, mitochondrial dysfunction and oxidative stress[312; 37; 313] resulting in renal tissue injury and culminating in reduced renal function and risk of death[314; 315]. Novel interventions have aimed to reduce the injury to a level which is compatible with renal tissue recovery. To date, the most promising strategy to alleviate IRI is Ischaemic Conditioning (IC). This approach aims to "train" the kidney to resist IRI through the use of brief, sub-lethal periods of ischaemia and reperfusion prior to the principal IRI event[316; 317].

A number of differing IC regimes have been used to protect the kidney in experimental models[189]. In these, the conditioning stimulus varies primarily in three domains: duration, time proximity to the IRI event and location. In brief, the conditioning stimulus has been applied as one continuous ischaemic period[318] or as multiple shorter ischaemic events (pulsatile)[317]. Furthermore, the conditioning stimulus can be applied immediately before, during, or after the IRI event[202], while conditioning has even been successfully applied minutes or days before IRI[319]. Although IC is classically applied directly to the vascular territory of the target organ, (e.g., renal pedicle); direct-IC, there is emerging evidence that IC can be applied to a distant tissue, (e.g., leg) to confer protection to the target organ, (e.g., kidney); indirect-IC[320].

In humans, randomised controlled trials require a predefined intervention which can be applied in a controlled environment immediately preceding an intervention which conveys an AKI risk[267; 321]. Thus, using a conditioning method applied directly before the intervention makes ischaemic preconditioning (IPC) an attractive approach. To address this, previous work completed at the host laboratory has successfully developed an *in vivo* model of IRI which injures both the right and left kidney simultaneously (bilateral IRI)[190]. The technique allows for serum creatinine (sCr) to be measured in a manner similar to that of humans. Furthermore, the host laboratory has successfully tested both a continuous[191] and pulsatile method of IPC applied directly to the kidney, concluding that the optimal technique is pulsatile IPC for 2 minutes ischaemia followed by 5 minutes reperfusion repeated for three cycles prior to IRI (direct-2/5^3)[190].

In clinical practise the potential application of direct-IPC is limited. The technique requires an operation to directly visualise the kidney artery and veins (renal pedicle) which are then used for the IPC procedure. With this in mind, the technical approach of direct-IPC as described would significantly limit its potential therapeutic application. Of interest, there is increasing data in differing tissue types to suggest that IPC protection can be applied to a distant tissue from the IRI with success[322; 197]; indirect-IPC.

Indeed, the notion that remote-IPC can confer protection to a distant organ has made indirect-IPC the favoured conditioning method in human trials. To date the data have been contentious, with large meta-analyses concluding both success[250] and failure[255]. Currently the optimal method for remote-IPC, and how this method compares to direct IPC *in vivo*, remain unknown.

The aim of this Chapter was to compare direct-IPC to indirect-IPC efficacy in reducing renal tissue injury *in vivo*. The previously optimised bilateral direct-IPC was performed, and was

compared to effects of unilateral renal IPC, in which direct protection to the preconditioned kidney may be combined with indirect effects on the contralateral kidney, and to hind limb preconditioning by distal aortic occlusion, a model of preconditioning applied to distant tissue. Effectiveness of preconditioning was evaluated by histological examination, and by sCr as a measure of excretory kidney function.

The experiments described in this Chapter aimed to:

1. Investigate unilateral-IPC as a method to ameliorate IRI
2. Investigate indirect-IPC as a method to ameliorate IRI
3. Identify the optimal IPC method to reduce renal IRI

3.2 Results

Sixty adult male Lewis rats underwent gaseous anaesthesia, tail vein blood sampling, midline laparotomy and allocation to one of eight experiential groups. The experimental groups comprised sham (n=12), 45 minutes of bilateral IRI (n=12) and six differing ischaemic preconditioning methods (total n=36) as described, (methodology; 2.3 Operative Procedure: Mechanical Preconditioning). Animals were recovered and allowed food and water as required. At 48 hours post-surgery, rodents were terminally anaesthetised, and blood and kidneys retrieved for analysis.

3.2.1 IRI

Twelve adult male Lewis rats were divided into two groups, sham (n=6) and IRI (n=6). Following gaseous anaesthesia and 45 minutes of sham or bilateral cross clamping of the renal pedicle (IRI), rodents were recovered, and samples collected at 48 hours as described, (methodology; 2.7 Sample Retrieval at 48 hours).

Sham and IRI animals were similar in pre-operative weight: 248.7 ±7.0 grams and 247 ±4.3 grams, respectively, p= 0.84. No differences were observed in pre-operative sCr between sham and IRI groups: 38.3 ±2.3 mmol/L versus 40.5 ± 4.8 mmol/L, p= 0.99; creatine kinase (CK): 780.9 ±59.0 IU/L vs 804.4 ±43.0 IU/L, p= 0.98; alanine transaminase (ALT): 59.3 ±1.4 IU/L vs 58.7 ±1.38 IU/L, p= 0.99 and lactate dehydrogenase (LDH): 1018 ± 91.7 IU/L and 1121 ± 72.6 IU/L, p= 0.83, respectively, as shown in Figure 3.1.

Post-operatively the sCr in the sham group was 32.2 ±0.17 mmol/L compared to 196.5 ±45.3 mmol/L in the IRI group, p= 0.0003. Post-operative ALT was 45.2 ±3.1 U/L in the sham group compared to 37.0 ±2.5 IU/L following IRI, p= 0.03. No statistically significant difference

was observed between the sham and IRI groups when comparing post-operative CK (720.4 ±49.0 IU/L vs 608.8 ±33.5 IU/L, p= 0.36) or LDH (778.2 ±111.2 IU/L vs 856 ±58.4 IU/L, p= 0.92), as shown in Figure 3.1.

The median (range) combined histological score in the sham operated kidney was 0 [0-1] compared to that of the IRI kidney of 20.5 [16-23], p=0.002. No difference in the total histology injury was demonstrated between the right and left kidneys within groups (sham, p>0.999; IRI, p= 0.567). Marked injury was demonstrated in all four sub compartments of the renal cortex and medulla. The endothelial compartment was well preserved in the sham group 0 [0], compared to the IRI score of 2 [1-2], p <0.0001. Similarly, the sham tubular compartment histological score was 0 [0] compared to the IRI score of 3.5 [3-4], p <0.0001. Preservation of the sham interstitial compartments was also observed 0 [0-1] compared to the IRI group of 3.5 [3-4)], p <0.0001. Within the glomerular compartment the sham group demonstrated no injury, 0 [0] while heightened injury was observed following IRI 2 [0-2], p= 0.0013, Figure 3.2. Examples of the differing histological features examined for during histology assessment are shown in Figures 3.3 and 3.4.

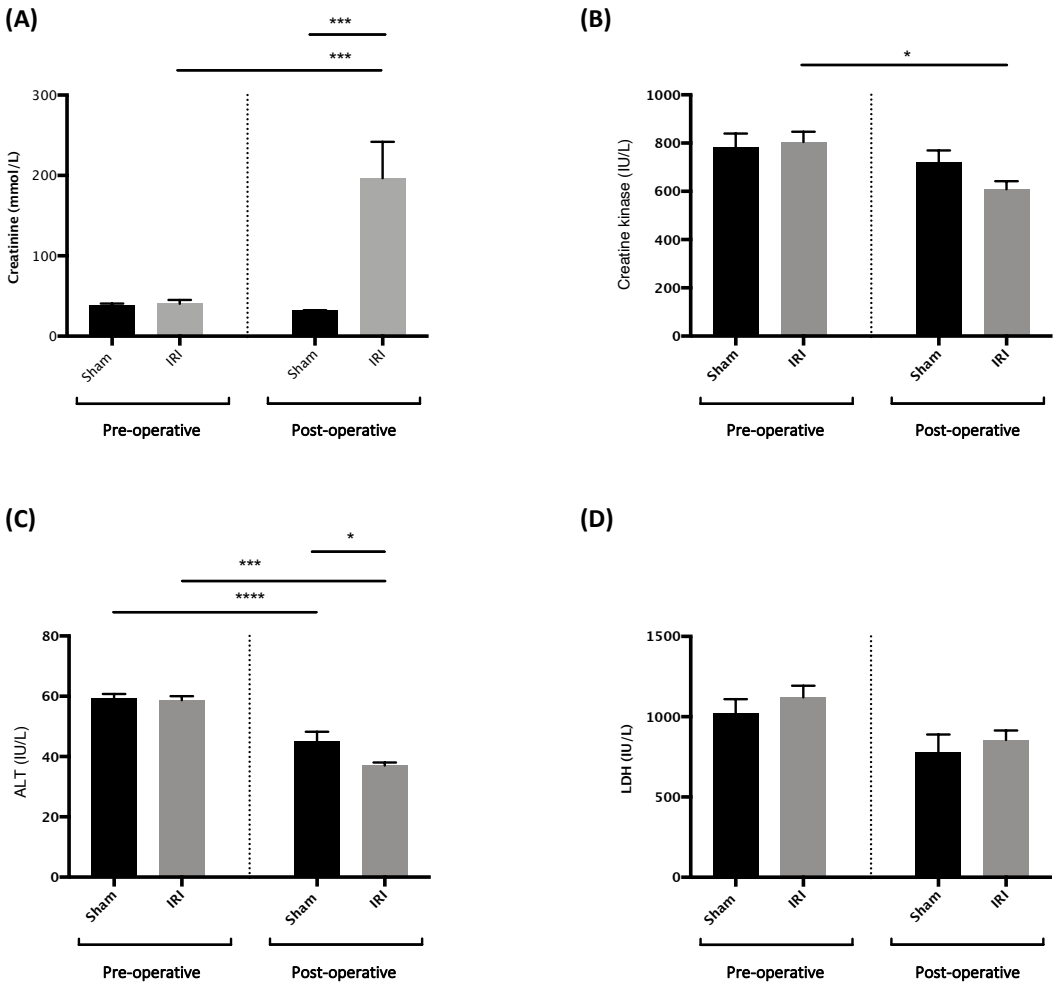

Figure 3.1 Effect of Ischaemia Reperfusion Injury (IRI) on Serum Creatinine, LDH, CK and ALT at 48 Hours

Pre-operative blood samples were collected from a lateral tail vein incision under general anaesthesia. Post-operatively blood was collected following direct cardiac puncture.

(A) Pre- and post-operative sCr blood results are plotted as mean ±SEM . A statistically significant difference was demonstrated between pre and post-operative IRI results (ANOVA with post-hoc Dunnett's multiple comparison, p=0.0005), similarly a statistically significant difference was shown between post-operative sham and IRI sCr results (ANOVA with post-hoc Dunnett's multiple comparison, p=0.0003) **(B)** Pre- and post-operative creatine kinase (CK) blood results are plotted as mean ±SEM. A statistically significant difference was demonstrated between pre- and post-operative CK IRI results (ANOVA with post-hoc Dunnett's multiple comparison, p=0.04). **(C)** Pre- and post-operative alanine aminotransferase (ALT) blood results are plotted as mean ±SEM. A statistically significant difference was demonstrated between pre- and post-operative IRI and sham results (ANOVA with post-hoc Dunnett's multiple comparison, p=0.002 and p<0.0001 respectively). **(D)** Pre- and post-operative lactate dehydrogenase (LDH) blood results are plotted as mean ±SEM. No statistically significant difference was demonstrated within or between experimental groups (ANOVA, p=0.06)

Numbers of animals in each group: sham (n=6) and IRI (n=6)
Statistical significance: * p<0.05, **p<0.01, *** p<0.001 and **** p<0.0001

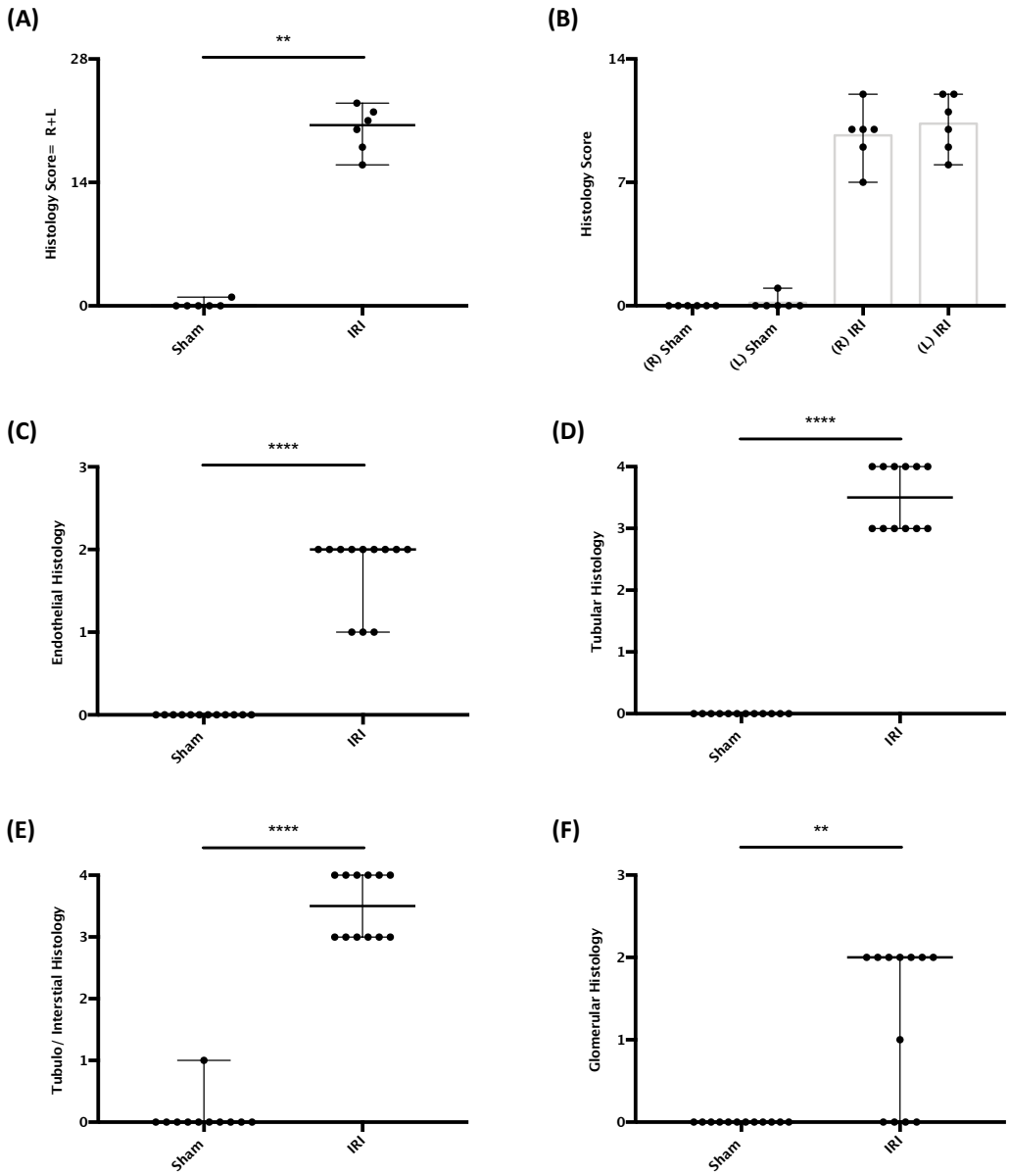

Figure 3.2 Effect of Ischaemia Reperfusion Injury (IRI) on Renal Histology at 48 Hours

48 hours post experimental procedure Renal tissue was blocked and stained with H&E and assessed using a comprehensive scoring system compromising of endothelial, glomerular, tubular and tubulo/interstitial (TI) damage (EGTI scoring). The EGTI scoring was plotted as median and range.

(A) Combining the EGTI scores of both kidneys histological damage confirmed a reduction in histological injury between the sham and IRI group (Mann-Whitney U test; p=0.002. (B) Comparing the right and left kidney within experimental groups demonstrated no significant difference between the differing kidneys (Mann-Whitney U test; Sham p >0.999 and IRI p=0.567). (C-F) A reduction in histological damage was observed within each histological compartment examined. Statistical results presented are p-values generated Mann-Whitney U test. Endothelial p <0.0001, tubular p <0.0001, TI compartments p <0.0001 and glomerular p= 0.0013

Numbers of animals in each group: sham (n=6) and IRI (n=6)
Statistical significance: * p<0.05, **p<0.01, *** p<0.001 and **** p<0.0001

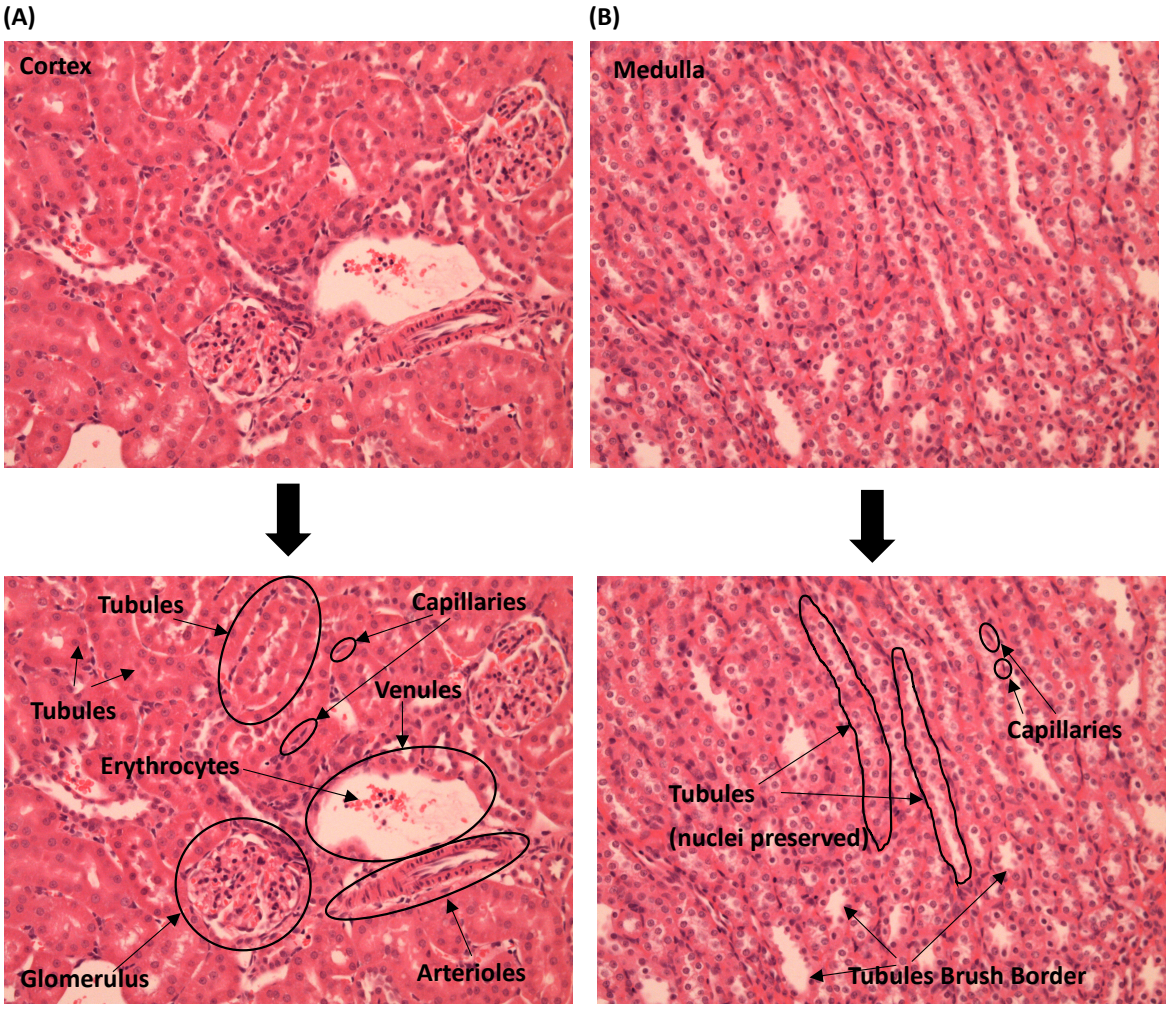

Figure 3.3 Sham Histological Images

At 48 hours post isoflurane anaesthesia animals were terminal anaesthetised and kidneys salvaged. Tissue was sectioned and H&E stained. Both the renal cortex and medulla was visualised. Image **(A)** and **(B)** are a 200x magnification of the renal cortex and medulla respectively. The images directly below each are an identical image with labelling. Both sections of the sham kidneys demonstrated normal histological architecture to include (but not limited to) normal glomerulus, tubules, arterioles, venules and capillaries. The tubular interstitium is the "scaffolding" cellular structure surrounding the renal tubules. Under normal conditions this structure is not pronounced and not readily visible. Similarly, the capillaries are located around the renal tubules. Their structure is not easily visible when normal. The small cell streaks circled above are the normal endothelial walls of the capillaries which can be seen in unremarkable renal histology.

Histology images displayed are photographic examples of the groups only. Individually they do not inform the final histology score displayed.

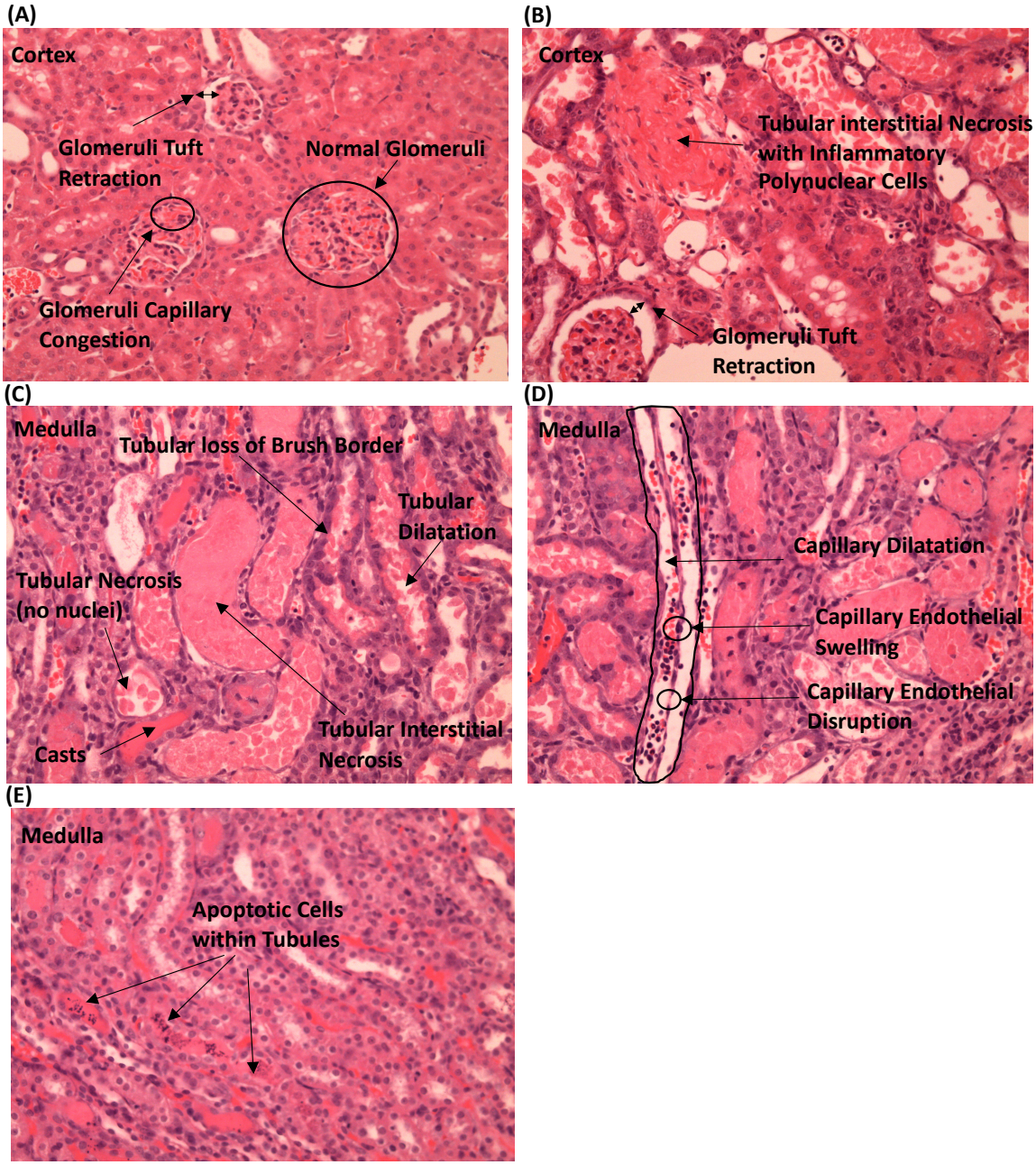

Figure 3.4 Ischaemia Reperfusion Injury (IRI) Histological Images

At 48 hours post isoflurane anaesthesia animals were terminally anaesthetised and kidneys salvaged. Tissue was sectioned and H&E stained. Both the renal cortex and medulla was visualised. All images presented are taken at 200x magnification. Significant histological damage was demonstrated in all four histological compartments. Glomerular injury was graded relative to observations of Bowman's capsule thickening, retraction of glomeruli tuft and evidence of glomeruli fibrosis, image **(A and B)**. Tubular injury was graded according to percentage of sections with brush border loss, cast formation and tubular necrosis, image **(B and C)**. Similarly, tubular interstitial (TI) injury was graded relative to coverage of TI inflammation and necrosis, image **(B and C)**. Finally, capillary endothelial injury was graded according to dilatation, cellular disruption and loss which can be seen in image **(D)**. Another feature seen following IRI (but not graded) was apoptosis within the renal tubules of the medulla, image **(E)**. Histology images displayed are photographic examples of the groups only. Individually they do not inform the final histology score displayed.

3.2.2 IPC

Forty-five minutes of bilateral cross clamping of the renal pedicle resulted in robust functional and histological injury at 48 hours in this experimental model. To test the optimal method of IPC to reduce the effects of IRI, three IPC approaches were tested: bilateral-direct (n=6), unilateral-direct (n=18) and indirect-aortic (n=12). In line with the principles of the three-Rs (replacement, refinement, reduction), a control group of sham (n=6) and IRI (n=6) were completed at the same time as the six different IPC groups. Animals were randomly allocated to the experimental groups and experimental approaches were performed concurrently. The three different IPC locations were then analysed separately with the aim of identifying the optimal protocol at each site.

3.2.2.1 Bilateral Direct-IPC

Eighteen adult male Lewis rats were divided into three groups: sham (n=6), IRI (n=6) and direct-IPC applied to the bilateral renal pedicle for 2 minutes ischaemia followed by 5 minutes reperfusion for three cycles followed by 45 minutes of bilateral IRI; (direct-2/5^3) (n=6).

Rodents were comparable in their pre-operative weight, Sham animals weighing 229.5 ±10.1 grams, IRI 235 ±7.9 grams and direct-2/5^3 group of 238.2 ±5.7 grams, p= 0.759. No difference was demonstrated in pre-operative creatinine results, sham 41.45 ±2.3 mmol/l, IRI 41.45 ±2.7 mmol/L and direct-2/5^3 of 34.5 ±2.3 mmol/L, p=0.07, Figure 3.5.

Post-operatively, rodents in the direct-2/5^3 group demonstrated significant reductions in post-operative sCr compared to the IRI group (37.9 ±2.3 mmol/L versus 65.7 ±4.9 mmol/L, respectively, p< 0.0001. Post-operative ALT and LDH was not differentially expressed between the post-operative groups, ANOVA p= 0.3993 and p= 0.7772, respectively, Figure 3.5.

Histologically, the direct-2/5^3 approach reduced the median (and range) total histological injury score from 18 [16-21] in the IRI group compared to 13 [9-16] in the direct-2/5^3 group, p= 0.0043. No statistically significant difference was demonstrated between the right and left kidney within groups: IRI p= 0.2316 and direct-2/5^3 p= 0.7944. The endothelial compartment injury score reduced from 2 [2-3] in the IRI group to 1 [1-2] in the direct-2/5^3 group (p= 0.0274). Similarly, the glomerular injury reduced from 1 [0-3] in the IRI group to 0 [0-1] in the direct-2/5^3 group, p=0.0003. No statistically significant differences were observed in histology score for tubular or interstitial compartments (p= 0.4791 and p= 0.1033, respectively), Figure 3.6. Representative histology images are provided in Figure 3.7.

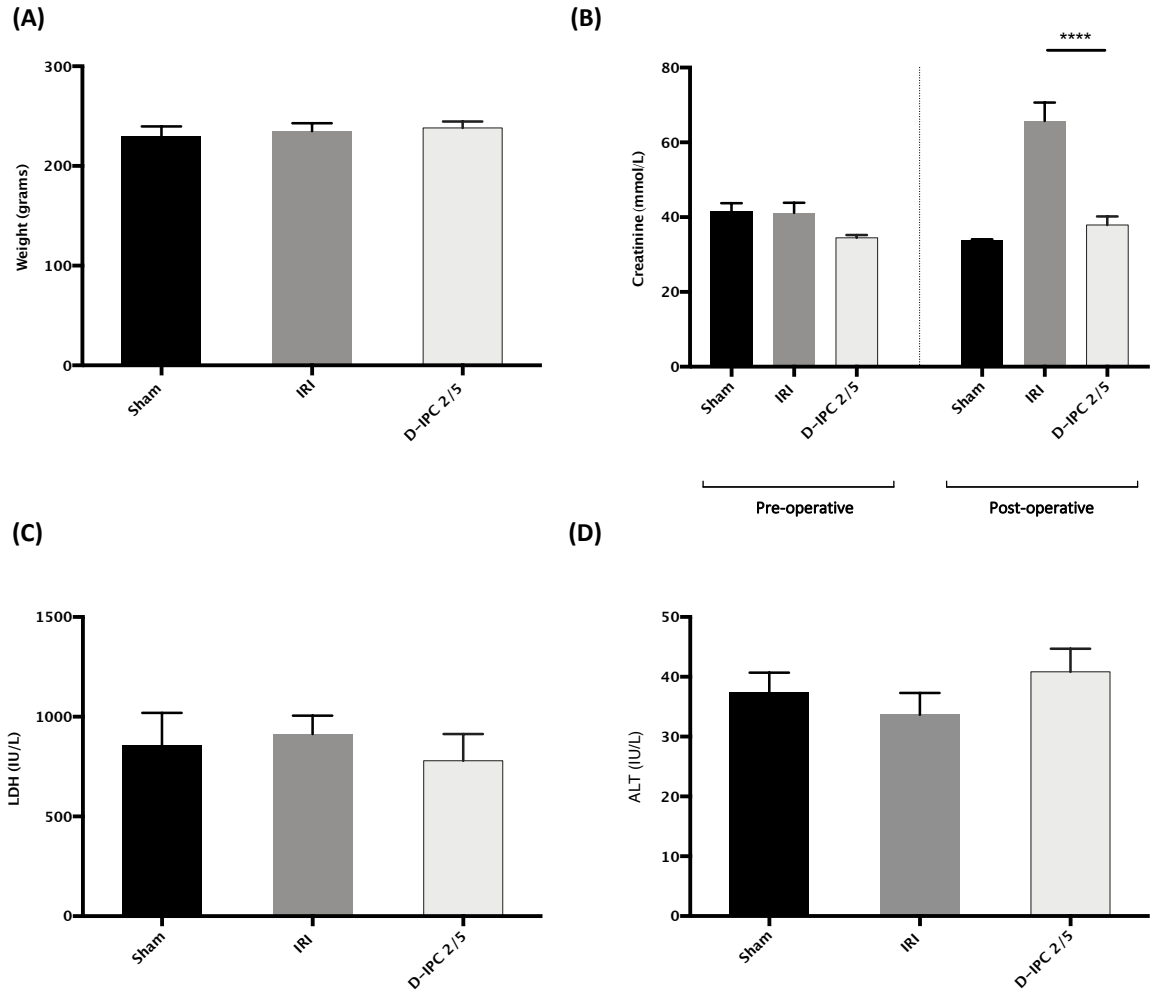

Figure 3.5 Effect of Direct-IPC 2/5 on Serum Creatinine, LDH and ALT at 48 Hours

Pre-operative blood samples were collected from a lateral tail vein incision under general anaesthesia. Post-operatively blood was collected following direct cardiac puncture.

(A) Pre-operatively the animals were weighed and results plotted as mean ±SEM. The rodents' weight were comparable across all experimental groups and no statistical difference was observed, ANOVA p= 0.759. (B) Pre- and post-operative sCr results are plotted as mean ±SEM . No statistical difference was demonstrated in pre-operative sCr between groups (ANOVA p=0.07). Post-operatively a statistical difference was shown between ischaemia reperfusion injury (IRI) and direct-IPC 2/5, ANOVA with post-hoc Dunnett's multiple comparison, $p<0.0001$. (C and D) LDH and ALT was measured at 48 hours and plotted as mean ±SEM, no statistical difference was found between groups, ANOVA p=0.7772 and p=0.3993 respectively

Numbers of animals in each group: sham (n=6), IRI (n=6) and direct-IPC 2/5 (n=6)
Statistical significance: * $p<0.05$, ** $p<0.01$, *** $p<0.001$ and **** $p<0.0001$
Direct-IPC is abbreviated to D-IPC and ischaemia reperfusion injury is abbreviated to IRI in the graphs

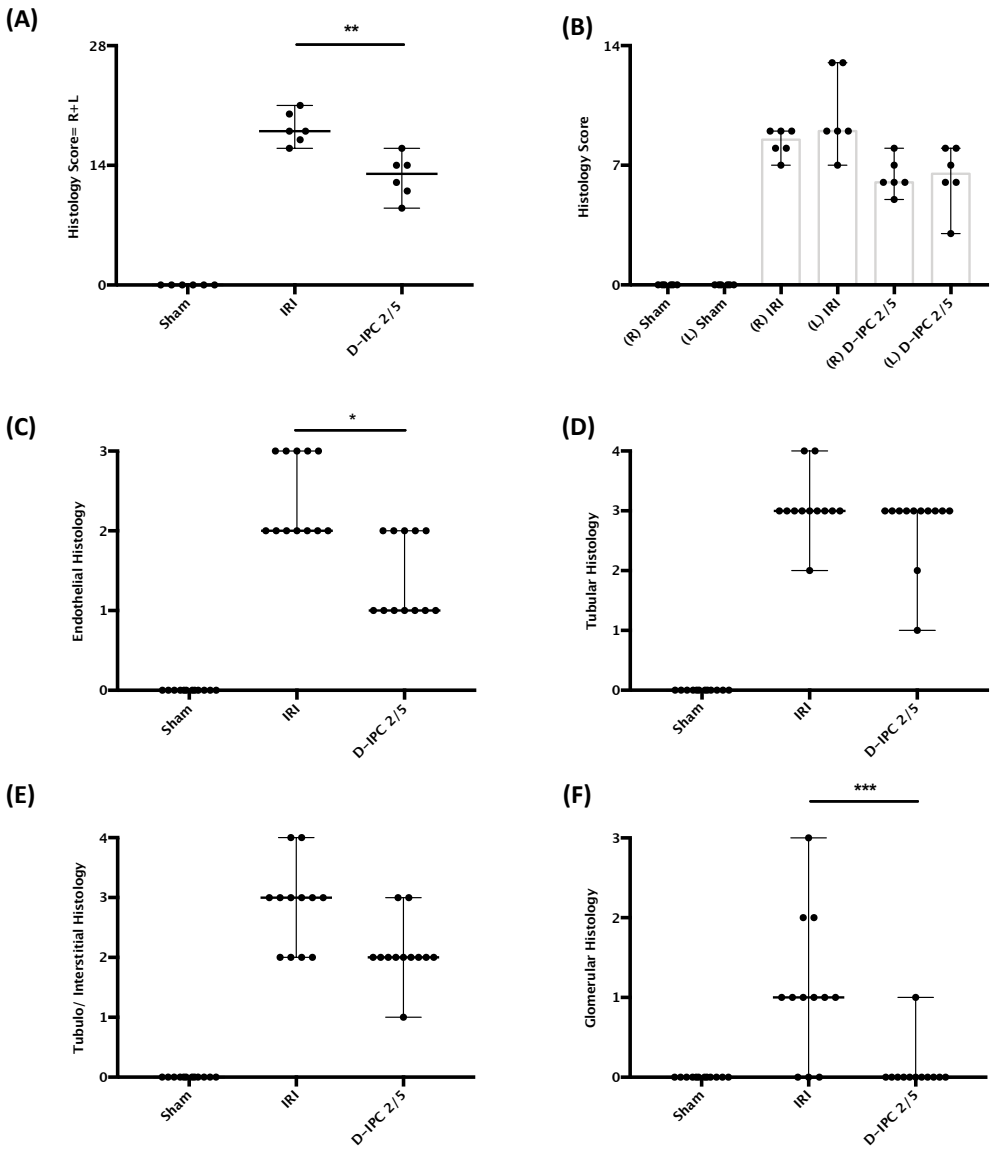

Figure 3.6 Effect of Direct-IPC 2/5 on Renal Histology at 48 Hours

At 48 hours post experimental procedure, renal tissue was blocked and stained with H&E and assessed using a comprehensive scoring system compromising of endothelial, glomerular, tubular and tubulo/interstitial (TI) damage (EGTI scoring). The EGTI scoring was plotted as median and range.
(A) Combing the EGTI scores of both kidneys, histological damage confirmed a reduction in histological injury between the ischaemia reperfusion injury (IRI) and direct-IPC 2/5 group, Mann-Whitney U test, p=0.0043. (B) Comparing the right and left kidney within experimental groups demonstrated no statistically significant difference , Mann-Whitney U test: IRI p=0.232 and direct-IPC 2/5 p=0.794. (C-F) A general reduction in histological damage was observed within each histological tissue area examined. Statistical results presented are p-values generated from Kruskal-Wallis test with Dunn's multiple comparisons. Of these, only the endothelial (post-hoc, p=0.0274) and glomerular compartment (post-hoc, p=0.0003) were statistically significant. Although the trend in histological injury reduced in the tubular and TI compartments this failed to be significant, p=0.4791 and p=0.1033, respectively.

Numbers of animals in each group: sham (n=6), IRI (n=6) and direct-IPC 2/5 (n=6)
Statistical significance: * p<0.05, **p<0.01, *** p<0.001 and **** p<0.0001
Direct-IPC is abbreviated to D-IPC in the graphs

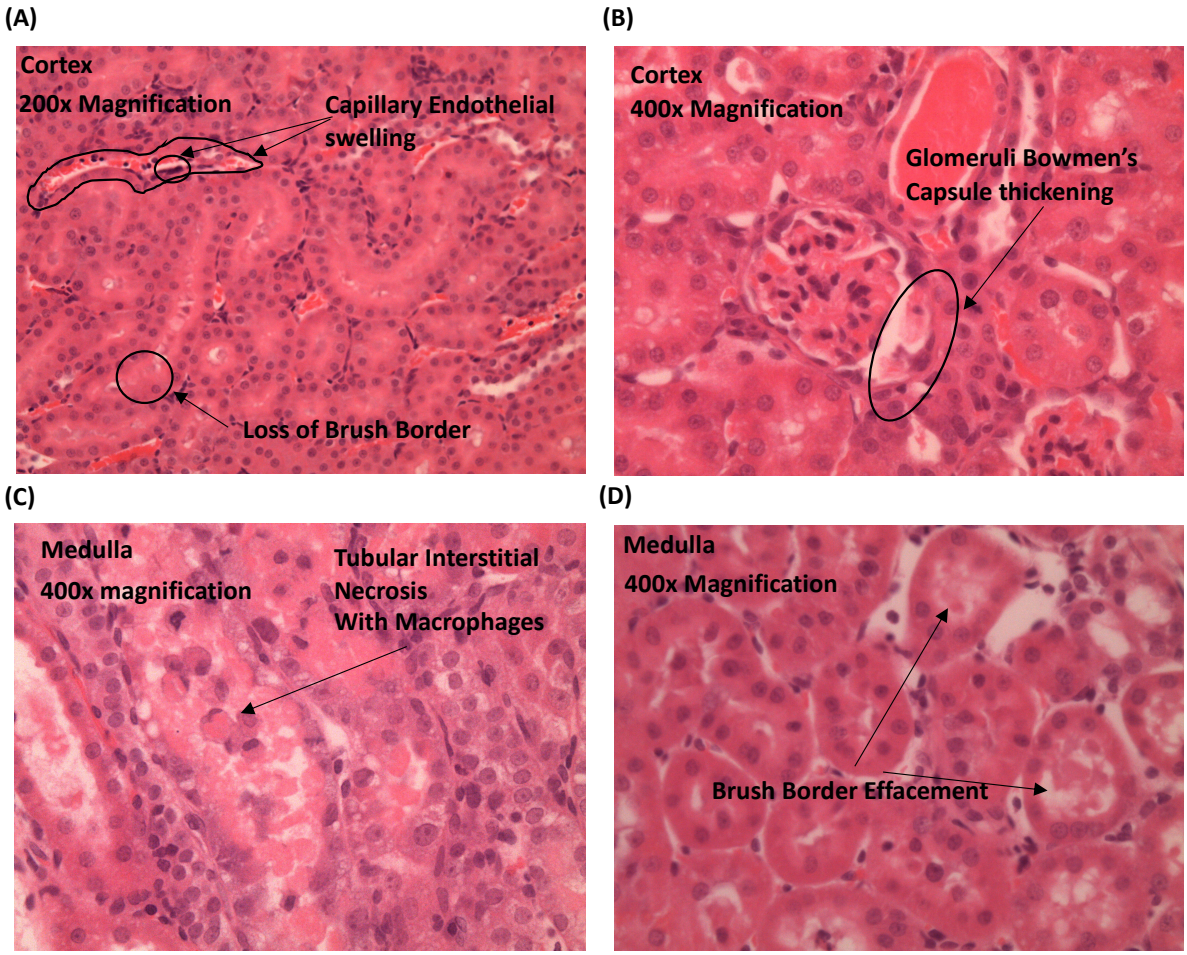

Figure 3.7 Direct-IPC 2/5 Histological Images

Following D-IPC a general trend in reduction in histological damage as scored by the EGTI scoring system was seen in all four compartments. Statistically significant reduction was only seen in the endothelial and glomerular compartments. Image **(A)** demonstrates the typical capillary injury observed in the endothelial compartment in the direct-IPC 2/5 group. The difference in capillary endothelial injury can be compared to the endothelial injury seen in the IRI group (figure 3.4, D). Image **(B)** displays the only evidence of glomerular injury seen (glomerular compartment) in the direct-IPC 2/5 group. This Bowmen's capsule thickening is subtle in comparison to the classical glomerular injury seen in the IRI group (figure 3.4, A). A non-significant trend towards a reduction in tubular interstitial damage was observed. Following IRI it was observed that tubular necrosis was often accompanied by tubular interstitial necrosis (figure 3.4, C). These appearances were not as pronounced following direct-IPC 2/5 and the observed tubular interstitial necrosis were often infiltrated by macrophages, **(C)**. Similarly the tubular damage was often more subtle with tubular brush border effacement compared to the often significant tubular necrosis and even apoptosis seen following IRI, (figure 3.4, C and E)

Histology images displayed are photographic examples of the groups only. Individually they do not inform the final histology score displayed.

3.2.2.2 Unilateral Direct-IPC

Eighteen male Lewis rats were divided into three groups, each group was allocated a different pulsatile IPC regime which was applied directly to unilateral renal pedicle prior to bilateral IRI. In the first group, IPC was applied to the right kidney for 2 minutes ischaemia followed by 5 minutes reperfusion for three cycles prior to 45 minutes of bilateral IRI (unilateral-2/5^3), n=6. The second and third group utilised unilateral-5/5^3 and unilateral-10/5^3 approaches, (n=6 each group). Experimental groups were compared to the control groups of sham (n=6) and IRI (n=6).

Pre-operatively rodents were similar in weight, sham 229.5 ±10.1 grams, IRI 235.2 ±7.9 grams, unilateral-2/5^3 254.0 ±5.7 grams, unilateral-5/5^3 249.1 ±6.8 grams, unilateral-10/5^3 252.3 ±4.7 grams, p= 0.0878. Similarly, pre-operative sCr was comparable across all groups, sham 41.5 ±2.3 mmol/L, IRI 41.5 ±2.7 mmol/L, unilateral-2/5^3 37.8 ±1.7 mmol/L, unilateral-5/5^3 41.2 ±2.3 mmol/L and unilateral-10/5^3 42.4 ±4.7 mmol/L p=0.8327, Figure 3.8.

Post-operatively the sCr in the IRI group was 65.73 ±4.9 mmol/L. The use of unilateral direct IPC prior to IRI statistically reduced sCr in the unilateral-2/5^3 group to 52.33 ±1.2 mmol/L, p=0.0103, and the unilateral 5/5^3 group to 41.17 ±2.2 mmol/L, p=0.0006. The mean creatinine following the unilateral-10/5^3 approach was 57.27 ±3.0 mmol/L not significantly different from IRI, p=0.1474. No significant difference was found in the post-operative ALT (sham 37.3 ±3.4 IU/L, IRI 33.7 ±3.7 IU/L, unilateral-2/5^3 35.3 ±4.9 IU/L, unilateral-5/5^3 33.0 ±3.4 IU/L and unilateral-10/5^3 35.2 ±1.6 IU/L, p= 0.9213) or LDH (sham 856.5 ±163.1 IU/L, IRI 913.3 ±92.0 IU/L, unilateral-2/5^3 833 ±66.6 IU/L, unilateral-5/5^3 574.7 ±88.0 U/L and unilateral-10/5^3 804.2 ±104.0 IU/L, p= 0.2437), Figure 3.8.

The combined median (and range) histology score for each group was sham 0 [0], IRI 18 [16-21], unilateral-2/5^3 20 [15-22], unilateral-5/5^3 17.5 [14-23] and unilateral-10/5^3 21 [16-

24], no significant difference was demonstrated between IPC groups, p> 0.9999. Similarly, there was no significant difference between the right and left kidney histology score within the unilateral-2/5^3 (p= 0.4069), unilateral-5/5^3 (p=0.2338) and unilateral-10/5^3 (p=0.6017) groups. Across the four histology compartments, no significant difference was demonstrated between any of the unilateral-IPC groups and that of IRI, (*tubulointerstitial*: unilateral-2/5^3 p> 0.9999, unilateral-5/5^3 p> 0.9999 and unilateral-10/5^3 p=0.7480; *glomerular*: unilateral-2/5^3 p= 0.7165, unilateral-5/5^3 p=0.4125 and unilateral-10/5^3 p>0.9999, *Endothelial*; unilateral-2/5^3 p>0.9999, unilateral-5/5^3 p= 0.5867 and unilateral-10/5^3 p=0.5867; and *tubular*: unilateral-2/5^3 p=0.8857, unilateral-5/5^3 p> 0.9999 and unilateral-10/5^3 p= 0.1677), Figure 3.9.

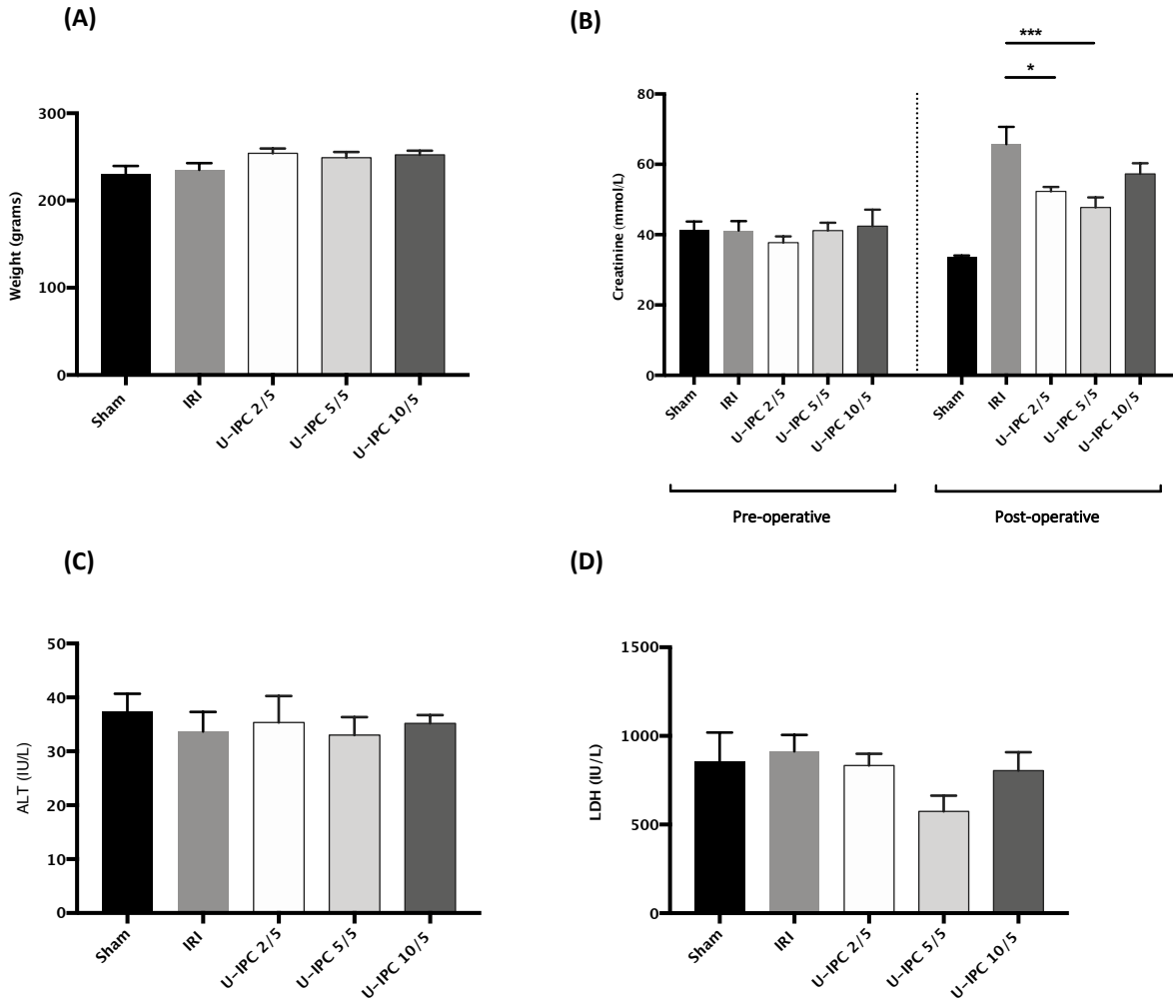

Figure 3.8 Effect of Unilateral-IPC 2/5, 5/5 and 10/5 on Serum Creatinine, LDH and ALT at 48 Hours

Pre-operative blood samples were collected from a lateral tail vein incision under general anaesthesia. Post operatively blood was collected following direct cardiac puncture.

(A) Pre-operative rodent's weights are plotted as mean ±SEM. The rodent's weights were comparable across all experimental groups, ANOVA p= 0.0878. (B) Pre-operatively sCr, results are plotted as mean ±SEM . No significant difference in sCr was demonstrated pre-operatively, ANOVA p=0.8327. Post-operatively, sCr results are plotted as mean ±SEM. A statistically significant difference was shown between ischaemia reperfusion injury (IRI) versus unilateral-IPC 2/5, ANOVA with post-hoc Dunnett's multiple comparison $p<0.001$ and IRI versus unilateral-IPC 5/5, ANOVA with post-hoc Dunnett's multiple comparison, $p<0.0006$. No significant difference was demonstrated between IRI versus unilateral-IPC 10/5, ANOVA with post-hoc Dunnett's multiple comparison, $p=0.1474$. (C and D) LDH and Alt was measured at 48 hours and plotted as mean ±SEM, no statistically significant difference was found between all groups, ANOVA $p=0.2437$ and $p=0.9213$ respectively.

Numbers of animals in each group: sham (n=6), IRI (n=6) and unilateral-IPC (n=6 in each subgroup)
Statistical significance: * $p<0.05$, ** $p<0.01$, *** $p<0.001$ and **** $p<0.0001$
Unilateral-IPC is abbreviated to U-IPC in the graphs

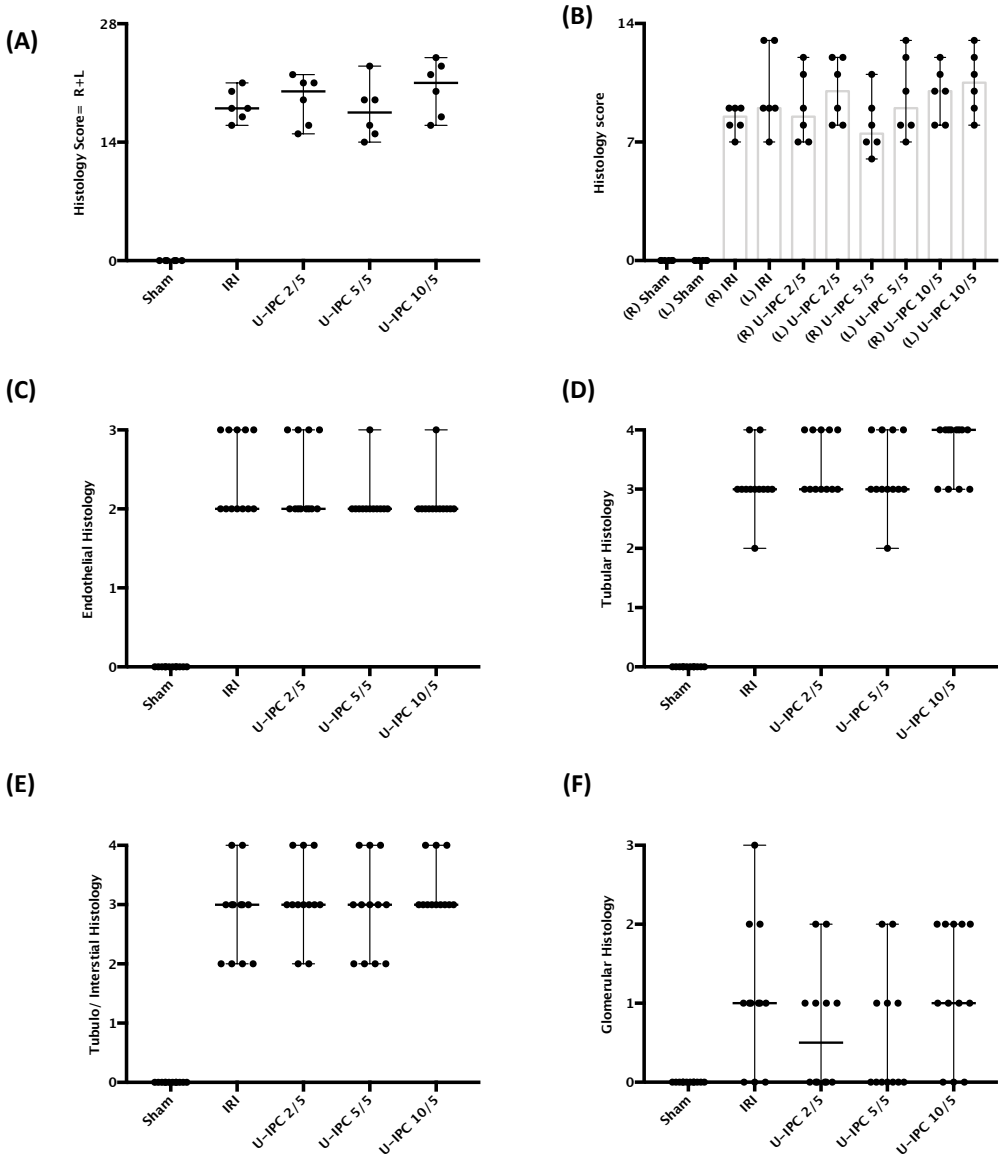

Figure 3.9 Effect of Unilateral-IPC 2/5, 5/5 and 10/5 on Renal Histology at 48 Hours

At 48 hours post experimental procedure renal tissue was blocked and stained with H&E and assessed using a comprehensive scoring system compromising of endothelial, glomerular, tubular and tubulo/interstitial (TI) damage (EGTI scoring). The EGTI scoring was plotted as median and range.

(A) Combining the EGTI scores of both kidneys no difference was demonstrated between each experimental group, Kruskal-Wallis p>0.99. **(B)** Comparing the right and left kidney within experimental groups demonstrated no statistically significant difference, Mann-Whitney U test; unilateral-IPC 2/5 p=0.407 and unilateral-IPC 5/5 p=0.234 and unilateral-IPC 10/5 p=0.602. **(C-F)** No significant reduction in injury was demonstrated across each of the 4 histological compartments.

Numbers of animals in each group: sham (n=6), IRI (n=6) and U-IPC (n=6, within each subgroup)
Statistical significance: * p<0.05, **p<0.01, *** p<0.001 and **** p<0.0001
Unilateral-IPC is abbreviated to U-IPC and ischaemia reperfusion injury is abbreviated to IRI in the graphs

3.2.2.3 Indirect-IPC

Twelve male Lewis rats were divided into two groups, each group was allocated a differing pulsatile IPC regime applied directly to the infra-renal aorta prior to bilateral IRI. In the first group, IPC was applied to the infra-renal aorta for 2 minutes ischaemia followed by 5 minutes reperfusion for three cycles prior to 45 minutes of bilateral IRI (indirect-2/5^3 approach), n=6. The second indirect IPC protocol was an indirect-5/5^3 approach, n=6, and an indirect-10/5^3 approach. The indirect-10/5^3 approach was abandoned in line with the principles of the three-Rs (replacement, refinement, reduction), (see Chapter 3 Discussion).

Pre-operatively animals were similar in weight to sham; 229.5 ±10.1 grams, IRI; 235 ±7.9 grams, indirect-2/5^3; 241.3 ±3.58 grams and indirect-5/5^3; 239.5 ±3.7 grams, p=0.6106. No statistically significant difference was demonstrated between groups for their pre-operative sCr: sham; 41.5 ±2.3 mmol/L, IRI; 41.5 ±2.7 mmol/L, indirect-2/5^3; 39.0 ±3.2 mmol/L and indirect-5/5^3; 36.4 ±1.56 mmol/L, p=0.4738, Figure 3.10.

Post-operatively IRI increased sCr to 65.73 ±4.9 mmol/L. Following IPC, the post-operative sCr was significantly reduced in both the indirect-2/5^3; 40.4 ±1.47 mmol/L (p<0.0001) and indirect-5/5^3; 43.9 ±1.9 mmol/L groups (p<0.0001). Post-operatively the CK, in the IRI group was 212.4 ±13.9 IU/L, this increased significantly to 565.5 ±50.3 IU/L in the direct-2/5^3 group, (p<0.0001) and 631.8 ±46.3 IU/L in the direct-5/5^3 group, p<0.0001. Serum LDH was not significantly increased in any of the experimental groups (sham; 856.5 ±163.1 IU/L, IRI; 913.3 ±92.0 IU/L, indirect-2/5^3; 745.7 ±109.6 IU/L and indirect-5/5^3; 836.0 ±126.9 IU/L, p=0.8200), Figure 3.10.

The median (and range) total histological score was reduced following the indirect-2/5^3 approach to 15.5 [12-18] compared to the IRI score of 18 [16-21], p=0.0159. The total indirect-5/5^3 approach of 16.0 [16-19] failed to reach statistical significance, p=0.2928. When

comparing the right and left kidneys, no intra-group significant variation was seen in the indirect-2/5^3 and indirect-5/5^3 approach, (p=0.8593 and p=0.7273, respectively). Of the four histological sub-compartments examined, only a reduction in histological injury in the glomerular compartment was statistically significant for both the indirect-2/5^3 (0 [0-1], p=0.0027) and indirect-5/5^3 (0 [0-2], p=0.0144) approach compared to the IRI group (1 [1-3]). Tubular histology score was 3 [2-4] after IRI compared to 3 [2-3] following indirect-2/5^3 (p=0.7772) and 3 [0] in the indirect-5/5^3 group, (p>0.9999). Similar results were seen in the tubulo/interstitial compartment with IRI resulting a median score of 3 [2-4], compared to 3 [2-3] following indirect-2/5^3, p>0.9999 and 3 [0-3] in the indirect-5/5^3 approach, p>0.9999. The endothelial compartment did not demonstrate a significant reduction in histological injury following IRI: 2 [3-2] compared to indirect-2/5^3; 2 [1-2], p=0.1615 and indirect-5/5^3; 2 [2], p=0.2758, Figure 3.11.

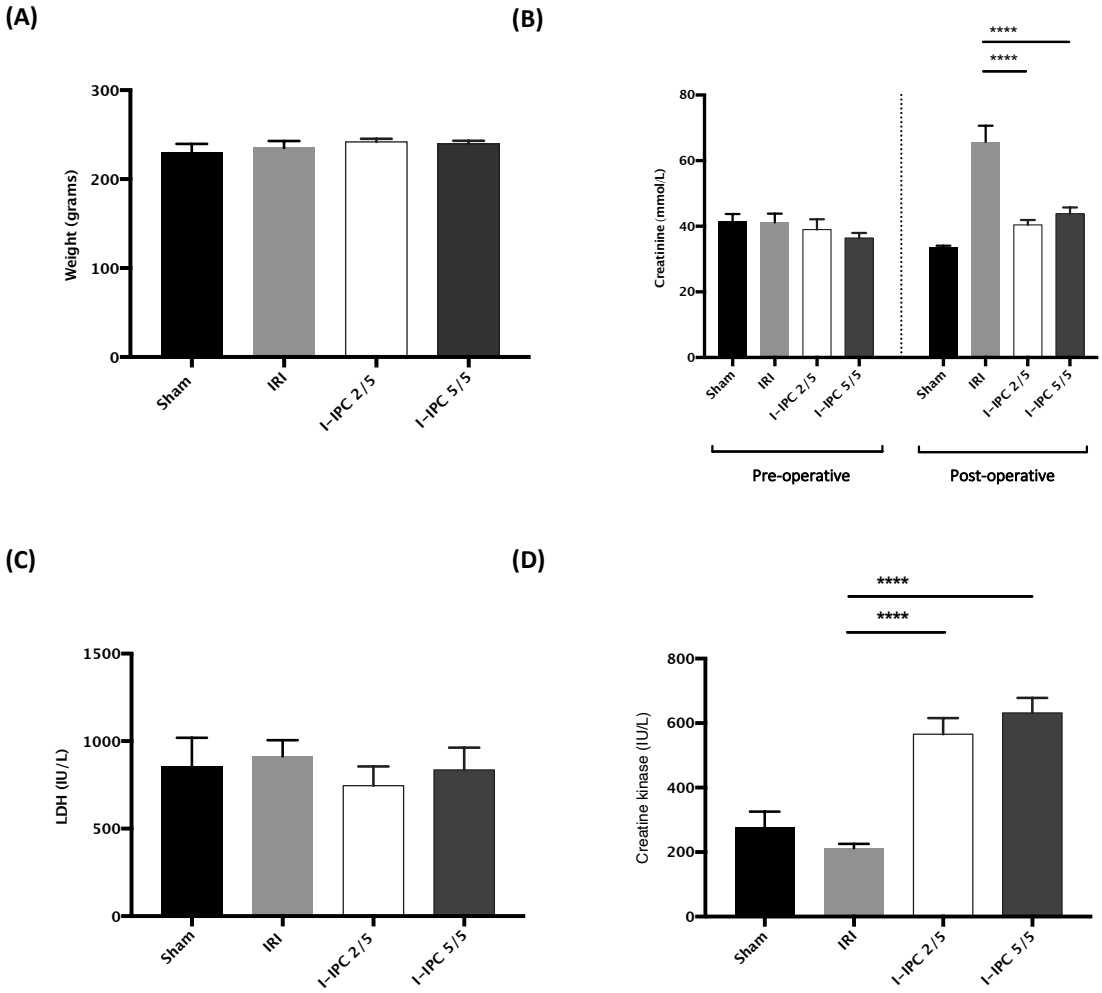

Figure 3.10 Effect of Indirect-IPC 2/5 and 5/5 on Serum Creatinine, LDH and CK at 48 Hours

Pre-operative blood samples were collected from a lateral tail vein incision under general anaesthesia. Post-operatively blood was collected following direct cardiac puncture.

(A) Pre-operative rodent's weights are plotted as mean ±SEM. The rodent's weights were comparable across all experimental group and no significant difference was demonstrated, ANOVA p= 0.6106. **(B)** Pre-operative sCr results are plotted as mean ±SEM . No significant difference was demonstrated pre-operatively between groups, ANOVA p=0.4738. Post-operatively a significant difference was shown in sCr results between ischaemia reperfusion injury (IRI) versus indirect-IPC 2/5, ANOVA with post-hoc Dunnett's multiple comparison, $p<0.0001$ and IRI versus indirect-IPC 5/5, ANOVA with post-hoc Dunnett's multiple comparison, $p<0.0001$. **(C)** LDH was measured at 48 hours and plotted as mean ±SEM, no significant difference was found between groups, ANOVA p=0.82. **(D)** Creatine kinase (CK) was measured at 48 hours and plotted as mean ±SEM. Following both indirect-IPC 2/5 and 5/5 a significant increase in CK was demonstrated post-operatively compared to that of IRI, ANOVA with post-hoc Dunnett's multiple comparison, $p<0.0001$ for both groups.

Numbers of animals in each group: sham (n=6), IRI (n=6) and indirect-IPC (n=6,within each subgroup)
Statistical significance: * $p<0.05$, ** $p<0.01$, *** $p<0.001$ and **** $p<0.0001$
Indirect-IPC is abbreviated to I-IPC in the graphs

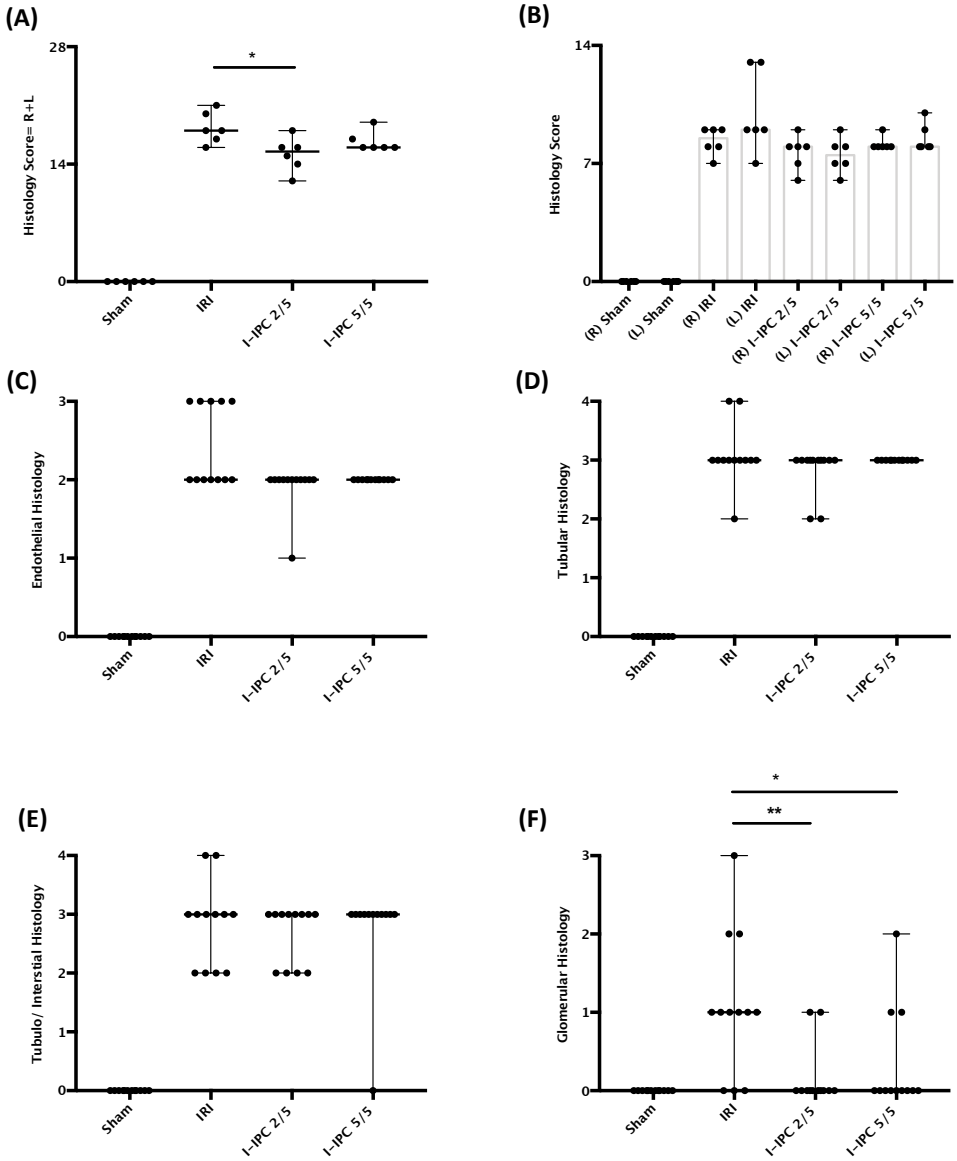

Figure 3.11 Effect of Indirect-IPC 2/5 and 5/5 on Renal Histology at 48 Hours

48 hours post experimental procedure Renal tissue was blocked and stained with H&E and assessed using a comprehensive scoring system compromising of endothelial, glomerular, tubular and tubulo/interstitial (TI) damage (EGTI scoring). The EGTI scoring was plotted as median and range.
(A) Combining the EGTI scores of both kidneys demonstrated a significant reduction in histological injury in the indirect-IPC 2/5 approach, Kruskal-Wallis, Dunn's multiple comparisons, p=0.0159. **(B)** Comparing the right and left kidney within experimental groups demonstrated no significant difference, Mann-Whitney U test; indirect 2/5 approach p=0.8593 and indirect 5/5 approach 0.7273. **(C-E)** No significant reduction in injury was demonstrated across each of the histological compartments of endothelial, tubular and tubulointerstitial compartment. **(F)** Indirect 2/5 and indirect 5/5 approach significantly improved the glomerular histological injury compared to IRI, Kruskal-Wallis, Dunn's multiple comparisons p=0.0027 and p=0.0144, respectively.

Numbers of animals in each group: sham (n=6), IRI (n=6) and indirect-IPC (n=6, within each subgroup)
Statistical significance: * p<0.05, **p<0.01, *** p<0.001 and **** p<0.0001
Indirect-IPC is abbreviated to I-IPC and ischaemia reperfusion injury is abbreviated to IRI in the graphs

3.3 Discussion

3.3.1 IRI

The experimental work in this chapter has shown that temporary occlusion of the bilateral renal pedicles to be technically achievable, non-lethal and recoverable technique to induce kidney injury in the rat. The bilateral model of IRI in this chapter induced by 45 minutes of reversable vascular occlusion resulted in robust renal injury as measured by sCr. Importantly, at 48 hours the IRI model used in this chapter resulted in significant symmetrical histological injury which was observed across the endothelial, tubular, interstial and glomerular compartments.

The IRI model used in this chapter supports the conclusions of prior research that temporary occlusion of the renal pedicle results in significant functional and histological damage[323]. Other researchers have utilised a number of IRI models, including a) occlusion of the bilateral renal vessels, b) occluding a unilateral kidney and leaving the other kidney untouched (UIRI) or c) unilaterally occluding kidney vasculature and performing a contralateral nephrectomy, (UIRI/N).

Both UIRI and UIRI/N are thought to be technically easier then bilateral IRI, and reduce potential differences between clamp pressures, ischaemic time and experimental variability[324]. Indeed, previous UIRI/N work has successfully demonstrated that 45 minutes of ischaemia achieves optimal functional injury while reducing mortality[325]. However, controversy remains regarding the effect of a contralateral nephrectomy on the remaining kidney subjected to ischaemia. Evidence suggests that the remaining ischaemic kidney has less severe reductions in sCr and preservation of the remaining kidney's epithelial structure,[326] possibly through increased perfusion of the renal medulla and alleviation of pro-inflammatory

responses[327]. Furthermore, studies have suggested that UIRI results in compensatory changes in the contralateral kidney. Jang et al. (2012) demonstrated that unilateral IRI induces hypertrophy and ROS formation in the contralateral kidney,[328] while Fatemikia et al. (2016) showed that following 2 hours of unilateral ischaemia and 24 hours reperfusion, the contralateral kidney demonstrated oxidative stress and increased renal blood flow[329]. Kato et al. (2014) demonstrated that, following unilateral renal IRI, the contralateral kidney exhibits an exaggerated profibrotic response[96]. Indeed, this Chapter confirms that under gaseous anaesthesia, bilateral occlusion of the renal pedicle for 45 minutes induces significant increases in sCr and histological injury which are reproducible, statistically relevant, and importantly, non-lethal.

In prior research the most frequently used histological scoring system for renal IRI *in vivo* uses the Jablonski criteria[325; 189]. Although commonly used, this scoring system only assesses the renal tubular injury and fails to address other histological changes seen in humans. The most appropriate comparison to *in vivo* IRI is the deceased donor renal transplant[330]. Almost 65% of renal donations are from deceased patients[331] and owing to the complex logistics of patient matching, organ retrieval, transport and surgical coordination a large proportion of these kidneys spend over 16 hours in ischaemic cold storage[332]. Histologically this period of ischaemia leads to a complex array of tubular, endothelial and glomerular injury[333]. To further our understanding of the histological effects of IRI *in vivo* this Chapter presented the histological injury using the EGTI scoring system, which defines renal IRI in terms of four compartments: endothelial, tubular, glomerular and tubulointerstial[307]. Using the experimental technique described, the injury observed following bilateral IRI was found to be similar in both kidneys. Furthermore, in this chapter bilateral IRI for 45 minutes achieved histological injury similar to that seen in humans[333], building on the premise that, *in vivo*, IRI

is not confined to the renal tubules but is actually a complex injury seen across the renal cortex and medulla.

3.3.2 Direct and Unilateral-IPC

In humans, the bench-to-bedside transition of renal conditioning has had successes[288; 268] and failures[244; 245]. A number of meta-analyses of human trials have concluded that preconditioning may have merit,[249; 248] but its application is hampered by incomplete consensus on the optimal methodology[334] and variation in experimental approach. The experimental design in this Chapter addressed some of these issues by extending the reperfusion window post-IRI to 48 hours to align with the current AKI diagnostic criteria in humans[26].

To further explore the optimal IPC regime *in vivo* and align with human research, this Chapter also investigated the transition of a direct IPC approach to a more favourable minimally invasive approach using a number of differing techniques. The work described successfully demonstrated that brief cyclical periods of IPC applied directly to both kidneys prior to IRI reduced loss of function and histological damage evident 48 hours after subsequent IRI. Other groups have reached similar conclusions, demonstrating that cyclical bilateral IPC can reduce the histological and functional injury of the kidney at 6 hours[182]. The data presented in this Chapter agrees with previous publications, albeit in research which has used a short reperfusion window post IRI of 24 hours, that cyclical periods of IPC that are short in duration compared to longer ischaemic periods has a greater propensity to reduce renal injury[186].

The work presented in this Chapter also tested whether unilateral IPC confers ischaemic tolerance to the contralateral kidney. The phenomenon of transference has been

studied in other organs. Schumacher et al. (2014) demonstrated that brief unilateral brain ischemia can induce resistance to a prolonged bilateral IRI[335]. This observation in the brain has been supported[336] and contradicted[337] by others as well as being successfully applied in other tissue types, for example the testes[338]. The data presented here demonstrated that unilateral pulsatile preconditioning applied directly to the renal pedicle prior to bilateral IRI reduced sCr at 48 hours. However, no difference in histological injury was observed between the ipsilateral or contralateral histology scores in preconditioned animals when compared to IRI.

Such disparate effects of IPC on sCr and histology have previously been reported[323]. It is well established that sCr does not always correlate with histological findings. Brown et al (2023) who tested the longitudinal effects of renal IRI in rats, found that post-operative sCr normalised at day 7, while acute histological injury normalised by day 14[339]. In humans, Moledina et al (2017), found that the histological findings of acute tubular injury in deceased kidney donors had poor diagnostic performance with sCr, and 49% of donors with severe tubular injury on histology did not have AKI as measured by sCr[340].Furthermore, Parekh et al (2013) demonstrated that minimal histological changes are observed following renal IRI when the renal biopsy is performed 5 minutes after reperfusion in patients undergoing a nephrectomy despite observing an increase in sCr[341]. Interestingly the discrepancy between histology and sCr has also been observed in the early stages of AKI-sepsis and in CKD. Santoriello et al (2020) investigated the correlation between renal histology in post-mortem patients with AKI-sepsis finding that 71% of patients with stage 2 or 3 AKI had only mild acute tubular necrosis[342], a finding mirrored in an *in vivo* severe AKI-sepsis model[343]. The concordance between histological changes in the kidney and CKD is similarly poor. Trevisani et al (2021) demonstrated that 40% of patient with stage 3 CKD defined using eGFR had minimal

histological changes[344]. The disparate correlation of sCr with renal histology and the delayed recovery of renal histology when compared to sCr may be a result of residual functional nephron compensation. Importantly, unlike sCr, histological changes in the kidney have not been shown to correlate with patient outcomes which may be a result of AKI being an incompletely defined disease process.

The benefits of indirect-IPC as described in this Chapter contrasts with other research by Park et al. (2001), who tested the effects of delayed continuous preconditioning 15-days before IRI in the mouse. The group found that unilateral conditioning was able to reduce IRI in the ipsilateral kidney but not the contralateral kidney, concluding that the local effect of conditioning is likely responsible for the protection[345]. The differing experimental outcome in the work presented here may be due to the pulsatile IPC technique used and the conditioning stimulus being applied immediately prior to the IRI. Previous work in the host laboratory and others have demonstrated that continuous-IPC[191] compared to pulsatile-IPC[198; 193] has reduced effectiveness. In addition, other published data suggests that acute IPC is superior to delayed preconditioning[316] and I hypothesise that the benefits of transferred ischaemic tolerance may be lost as the window to IRI is extended.

3.3.3 Indirect-IPC

To conclude the experimental transition to an indirect-IPC approach, the bilateral hind limbs were tested as the IPC target. The work in this Chapter successfully employed cross clamping of the infra-renal aorta to deliver pulsatile bilateral hind limb IPC. Functionally and histologically, the optimal methodology identified was the indirect-2/5^3 approach. The experiment was designed as a dose escalation technique, and as described in the methodology, the indirect-10/5^3 approach was abandoned as animals displayed features suggestive of

circulatory distress during the indirect-5/5^3 approach: reduced isoflurane requirement, dusky appearance to the feet and prolonged recovery period. Therefore, due to concern for animal welfare and in line with the three Rs (Reduction, Refinement and Replacement) the indirect-10/5^3 approach was abandoned. The finding that extended aortic cross clamping increases the complexity of surgery is not surprising. In humans, it is well established that extended aortic cross clamping during vascular surgery leads to the accumulation of ischaemic metabolites and upon release the increase in peripheral vascular resistance causes significant haemodynamic instability[346]. This Chapter demonstrated increasing CK as the indirect-IPC ischaemic time increased, alluding to the significant ischaemic insult achieved through bilateral hind-limb ischaemia.

Previous research into indirect conditioning has used the ischaemic model of UIRI/N. Wever et al. (2011) tested both a continuous and pulsatile remote conditioning model using both the unilateral and bilateral hind-limb-based procedures. While this work used only a single pulsatile approach of indirect-4/4^3 and a UIRI/N model, the authors concluded that a bilateral pulsatile approach was the optimal method[198]. In support of these findings both Jiang et al. (2015) and Hussain et al. (2016) used a UIRI/N model in conjunction with a unilateral hind limb conditioning demonstrating efficacy[202; 197]. Other groups have supported the biological relevance of a pulsatile conditioning by demonstrating that a continuous indirect conditioning for 15 minutes prior to IRI failed to achieve benefit[347]. The work presented in this Chapter adds to this research through the support that in a bilateral model of IRI, indirect IPC of the bilateral peripheral limbs using brief repetitive periods of ischaemia can successfully achieve ischaemic tolerance and improve functional and histological parameters to a degree comparable to that of the established model of direct-IPC.

The principal findings of this Chapter are:

1. Bilateral IRI applied directly to the renal pedicle is a non-fatal and reliable method to induce renal injury in the rat at 48 hours. The injury leads to a robust increase in sCr and histological damage. The experimental method of bilateral IRI leads to a comparable histological injury to both the right and left kidney with no statistically significant difference demonstrated. Histologically, the injury is established in all four cellular compartments leading to robust endothelial, tubular, glomerular and tubulointerstial damage.
2. Pulsatile bilateral preconditioning applied directly to the renal pedicle (direct-2/5^3) prior to IRI is a safe and effective technique. The method improved functional and histological injury to the kidneys at 48 hours.
3. Pulsatile unilateral preconditioning applied directly to the right renal pedicle prior to IRI was also a safe experimental technique. Post-operatively both unilateral-2/5^3 and unilateral-5/5^3 approaches improved sCr at 48 hours. Histologically, all three unilateral-IPC techniques failed to demonstrate histological improvement at 48 hours.
4. Pulsatile indirect preconditioning applied to the infra-renal aorta prior to IRI was shown to be technically achievable. At 48 hours, Indirect-IPC significantly improved sCr in both the indirect-2/5^3 and indirect-2/5^3 approach. Histologically only the 2 indirect-2/5^3 approach significantly reduced the total histological injury of the kidney. Both indirect-IPC techniques significantly increased CK at 48 hours.

3.4 Concluding Remarks

The work presented in this Chapter demonstrates effective kidney protection following ischaemic preconditioning in a rat model of bilateral IRI. Similar protective benefit, and optimal conditions, were demonstrated following direct and indirect IPC. In both cases, the optimal IPC approach was 2 minute ischaemia followed by 5 minute reperfusion, for 3 cycles. However, significant questions remain over the mechanisms by which the kidney is protected from subsequent ischemic damage by IPC.

Chapter 4

RNA Sequencing and Ingenuity Pathway Analysis:

Ischaemia Reperfusion Injury and

Ischaemic Preconditioning Comparative Analysis

4.1 Introduction

In the previous Chapter, the use of IPC was investigated to minimise the damage caused by renal IRI. Six different mechanical pulsatile IPC protocols were tested to explore the optimal intervention. Of these, two methods improved functional outcomes as measured by sCr and histological injury at 48 hours. The first method utilised direct-IPC applied to the bilateral renal pedicle for two minutes ischaemia followed by five minutes reperfusion repeated for three iterations: direct-IPC $2/5^3$. The second protocol employed pulsatile IPC to the infra-renal aorta, simulating bilateral hand limb IPC for two minutes ischaemia followed by five minutes reperfusion repeated for three iterations: indirect-IPC $2/5^3$. Both techniques were shown to be technically achievable, non-fatal and effective methods to reduce IRI.

A large number of molecular and immunological pathways contribute to the complex pathophysiology of renal IRI[313]. It is therefore plausible that the IRI phenotype is not the result of a single cellular cascade, but that injury is born from multiple cellular responses, as discussed previously (Chapter 1.2.2, Molecular Mechanisms of IRI). In concordance with this, no single molecular trigger for IPC has been identified and researchers have similarly posited that IPC triggers a cascade of mechanisms which interact synergistically to ameliorate IRI (see also Chapter 1.3.4, Mechanisms of IPC).

It is therefore logical to consider the pathophysiology and response pathways in IRI and IPC research in the context of whole tissue. The advent of RNA analysis techniques such as microarray analysis and next-generation RNA-sequencing (NGS) facilitate acquisition of transcriptional signatures of samples to elucidate the molecular mechanisms underlying the disease state. There techniques generate large, highly complex datasets from which drawing conclusions requires care[348]. To simplify the data output, researchers first group lists of genes into their functional categories called “bins,” which can represent a specific biological process

(e.g., cell cycle), or the number of genes in each pathway (e.g., 10 genes in cell cycle pathway). This technique is called gene set analysis (GSA) and the commonest bioinformatic pipeline for these analyses has been the public repositories, gene ontology (GO) and the Kyoto encyclopaedia of genes and genomes (KEGG).

Yoshida et al. (2002)[349] and Supavekin et al. (2003)[350] used microarray technology to reveal differentially expressed genes (DEGs) in renal IRI. The authors grouped 18 and 247 DEGs, respectively, following renal IRI, identifying an enrichment of molecules which functionally relate to apoptosis, growth/proliferation, cytoskeleton, and signal transduction. Further work by Kim et al. (2011), introduced a more complex microarray GO bioinformatics pipeline to construct and visually demonstrate the network connections between associated genes in an IRI mouse model, concluding that there was overlap between multiple functional categories including inflammation and apoptosis[351]. Research into the transcriptional signature of IPC has been limited. GSA analysis of microarray data from IPC kidneys have demonstrated enrichment of transcripts related to stress, apoptosis, and protein metabolism, but how these functions relate to IRI is unknown [305].

The traditional GSA bioinformatic pipeline is unordered and fails to describe the genes in the context of a complex interaction of molecules in which gene expression may lead to downstream functional changes due to molecular interactions and posttranscriptional modifications. GSA further fails to allow robust comparisons across multiple differing experimental groups or conditions. One recently developed approach to sequencing analysis uses a bioinformatic approach: pathway analysis (PA). PA computationally builds connections between the molecular phenotype and disease based upon the DEGs of the dataset and their predicted upstream regulators.

To date, the precise pathophysiology of renal IRI and the response pathways of IPC are poorly understood, and studies have often been limited to selection of molecules and pathways of interest. Furthermore, no studies have attempted to describe the IPC response pathways or compared the response pathways to IPC in direct and indirect models. To address this paucity of data, this Chapter describes an unbiased transcriptional approach carried out by generating RNA-sequencing data and analysing the output data in a bioinformatic pipeline to investigate the functional changes and molecular interactions following IRI and IPC. The work presented in this Chapter used PA to explore the transcriptional signatures of IRI and IPC in the context of the underlying mechanisms that govern these phenotypes.

The experiments described in this Chapter aimed to:

1. Describe the changes in gene expression profile in the kidney following IRI
2. Explore the response pathways of the kidney to direct-IPC $2/5^3$ and indirect-IPC $2/5^3$
3. Evaluate potential differences and similarities in differentially regulated pathways following IPC.

4.2 Results

The right kidneys from twenty-four, adult male, Lewis rats from four experimental groups were selected for total RNA next generation sequencing. The experimental groups comprised sham (n=6), 45 minutes of bilateral IRI (n=6) and the optimal IPC regimes of direct-IPC $2/5^3$ (n=6) and indirect-IPC $2/5^3$ (n=6).

4.2.1 Total RNA NGS

Using the miRNeasy mini-Kit (Qiagen, Cat No.ID: 217004), total RNA was extracted from the right kidney of twenty-four rats from four experimental groups (n=6 per group): sham, IRI, direct-IPC $2/5^3$ and indirect-IPC $2/5^3$. Next Generation RNA Sequencing (NGS) was performed by The Wales Cancer Research Centre/ Wales Gene Park (WGP) using the Illumina HiSeq 2500 platform with Total RNA sequencing Ribozero Gold chemistry. Each individual sample, termed a library, was labelled with a bar code (a unique adaptor sequence) to facilitate indexing of individual transcripts to their respective starting library. All twenty-four RNA libraries were pooled and sequenced simultaneously across four lanes of one Illumina® flow cell (termed multiplexed). Each individual RNA transcript fragment (called a read) was sequenced and the inferred base pairs corresponding to that transcript collected. The sequencing aimed to achieve a sequencing depth of 60 million reads per library. Following sequencing, a mean paired end sequencing depth of 354.7 million reads (range: 211.9 million to 404.7 million reads) per lane (four lanes in total) was achieved, equating to a mean sequencing depth of 59.4 million reads per library, and therefore achieving the pre-set desired sequencing depth.

Raw data analysis was carried out using the bioinformatic pipeline constructed by Dr Robert Andrews, a Cardiff University Bioinformatician. Raw data files were received from WGP

in an *in silico* text-based format for storing nucleotide sequences called FASTQ. FASTQ files contain the individual RNA transcript sequences, corresponding adaptor sequences and the Phred quality score (probability of a base call being correct). The reads were allocated to their starting library (de-multiplexed), and the adaptor sequences were trimmed using Trimomatic [Ver 0.36], leaving the individual read. To quantify the gene expression the individual reads were mapped to a single reference genome (*Rattus norvegicus* genome assembly: Rnar_6.0 [GCA_000001895.4]) using the program, Star RNA-Seq aligner. Star RNA-Seq aligner computationally assigns reads to their correct genomic loci thus: reads mapping to a single locus were assigned first; if a read mapped to ≥2 loci, the mapping locus with the highest alignment score was selected (thus formula-derived score was calculated by comparing the read to the reference genome nucleotides and assigning a numerical value to predict the likelihood of the alignment being correct); if a read mapped to ≥2 loci and the alignment score was identical, the mapping locus was assigned at random. In total, the sequenced reads mapped to 16,780 unique genes.

To quantify DEGs between experimental groups, the mapped raw count data were analysed using the program DESeq-2 (Ver. 1.14.1). DESeq-2 calculates differential gene expression by performing an internal normalisation that corrects for library size and RNA composition. The final output of the analysis computes the $\log_2$ fold change ($\log_2$FC), and corrected p values, adjusted as per Benjamini-Hochberg correction, for each mapped gene. This analysis pipeline summary and output described in the above text is shown in Figure 4.1.

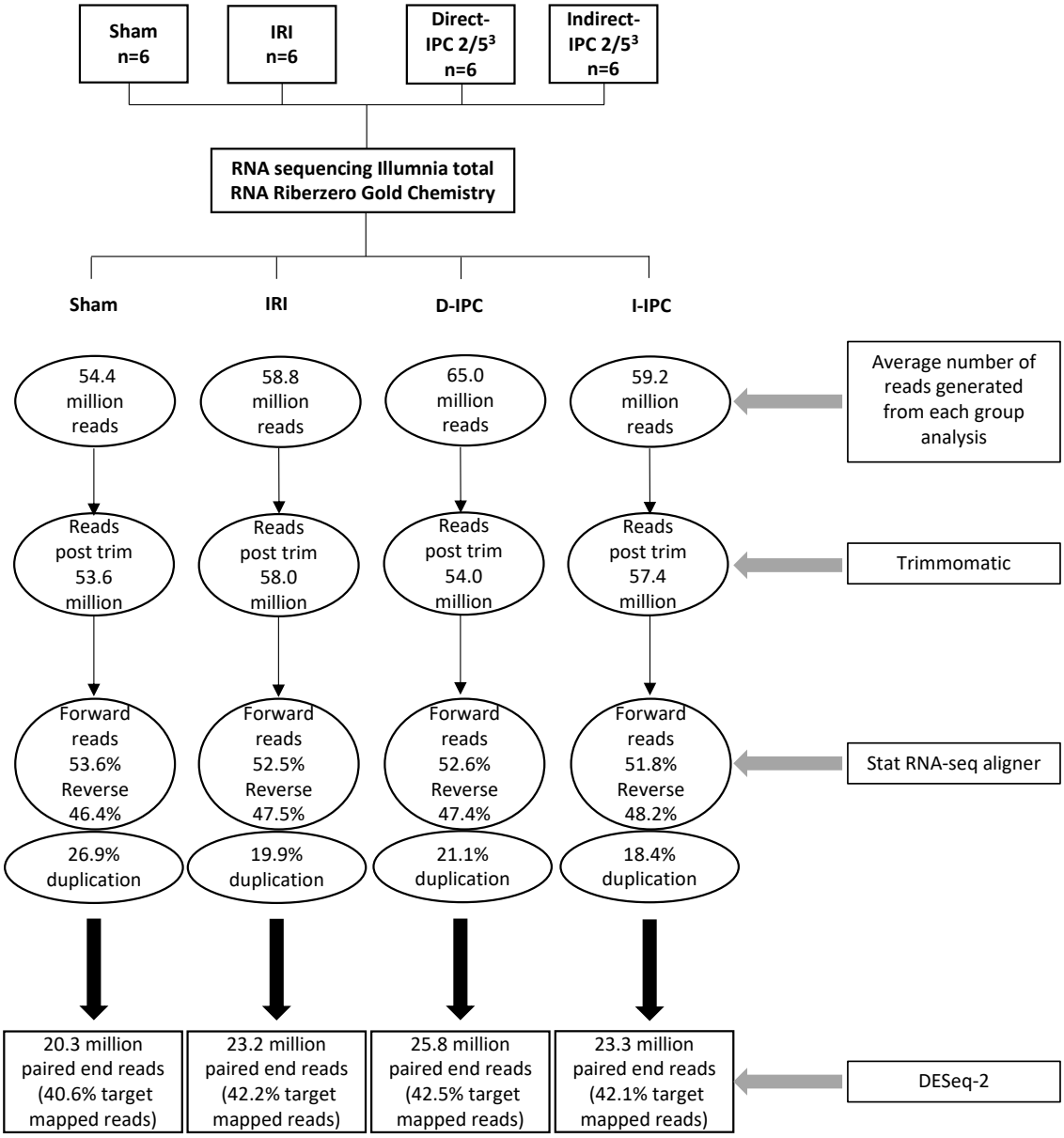

Figure 4.1 Next Generation Sequencing: Total RNA Sequencing Pipeline

On average a sequencing depth of 30 million pair end reads was achieved. Reads were trimmed using Trimomatic (Ver 0.36) and mapped using Star RNA-seq aligner (Ver 2.0) to a single reference genome, Ensembl *Rattus norvegicus*_6.0 (Ver. 87.6) as described in methodology. Following mapping the raw count data was uploaded to Deseq-2 (Ver.1.14.1) and corrected p-values and Log 2 Fold changes were calculated for each transcript.

Numbers of RNA extracted kidneys (biological repeats) in each experimental group: sham (n=6), IRI (n=6), direct-IPC $2/5^3$(n=6) and indirect-IPC $2/5^3$ (n=6).

4.2.1.1 NGS: Sample and Data Quality Analysis

Before proceeding to sequencing analysis, the sequencing experiment and the raw bioinformatic data was analysed to confirm quality. In all, three quality control stages were employed: first, the quality of the RNA sample entering sequencing was tested; next, the quality of the sequencing was analysed; finally, the bioinformatic differential gene analysis quality (DESeq-2 normalised data) was reviewed.

Following total RNA extraction, the quality of RNA extracted from each kidney was analysed on an Agilent 2100 Bioanalyzer (Agilent Technologies, Inc.) using the Assay Class-Eukaryote Total RNA Nano (Ver 2.0, Agilent Technologies, Inc.). The mean RNA integrity number (RIN) value was 9.7 (range: 8.7 to 10). The Illumina NGS platform recommends that RNA with a RIN value of ≥8 is sufficient for RNA-sequencing. All samples exceeded this RIN score. The electropherogram summary is displayed in Figure 4.2.

Following RNA-sequencing, the raw sequencing data quality was analysed using the FastQC (Ver. 0.11.5)[308] platform. Firstly, to test for sequencing irregularities originating from the starting library material, a random sample of 10% of the raw data from each sample lane was analysed using FastQC. Samples were initially assessed for the quality of each base call using the Phred score, which logarithmically linked to error probabilities where Phred = 30 equates to a base call accuracy of 99.9% and visualised as a box plot. All samples demonstrated a Phred score for each base call of >30 corresponding to a very good quality (failure equates to Phred <20), an example of a typical Phred score box plot from this analysis can be seen in Figure 4.2Bi. The guanine-cytosine (GC) content of each sequence was analysed relative to the theoretical GC content for different sequencing lengths to detect library contamination by adaptor sequences which may ligate without an attached library sequence and amplified (adaptor dimers). The libraries tested demonstrated excellent overlap with the theoretical GC

distribution, and all were significantly above the predefined failure criteria of the sum of the deviations from the normal distribution of >30% (e.g., Figure 4.2Bii). The raw data was finally tested for non-unique sequences in the dataset, to detect contaminants or technical duplicates. This analysis confirmed that all datasets were significantly above the predefined failure criteria of a non-unique sequences of >50% of the total. Figure 4.2Biii is an example of the analysis demonstrating that 87.46% of the sequences remain if de-duplicated.

Finally, Deseq-2 employed a complex quashing algorithm to normalise data to correct for differences in individual library size and composition. In brief, Deseq-2 normalised data internally through a method of $\log_e$ transforming fold changes; averaging the geometric mean to remove dataset extremes due to exclusion of negative infinity, thereby aiming to identify housekeeper expression; dividing average log value from $\log_e$ counts; calculating the sample median; converting median to $\log_e$ (scaling factor) and dividing the original read counts by the scaling factor. The Deseq-2 output was plotted as a histogram and compared to the histogram output observed for the raw count using the normalisation technique of reads per kilobase of transcript per million mapped reads (RPKM), which normalised data taking gene length into account. The above analysis confirmed that normalisation did not significantly change the distribution of the dataset and no outliers were observed (Figure 4.2C).

(A) Experimental Group RIN Values

Sham	IRI	Indirect-IPC 2/5[3]	Direct-IPC 2/5[3]
9.4	9.1	9.9	9.8
8.7	10	9.8	9.9
9.3	10	9.9	9.8
9.4	9.8	9.9	10
9.3	10	9.9	10
9.1	10	9.9	10

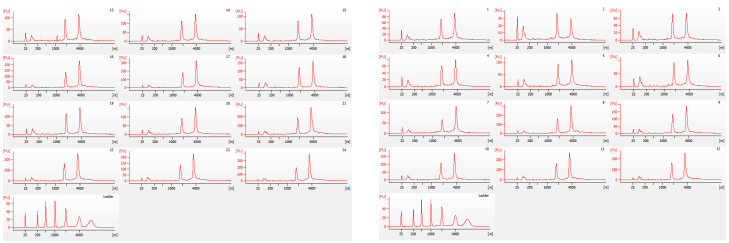

(B)

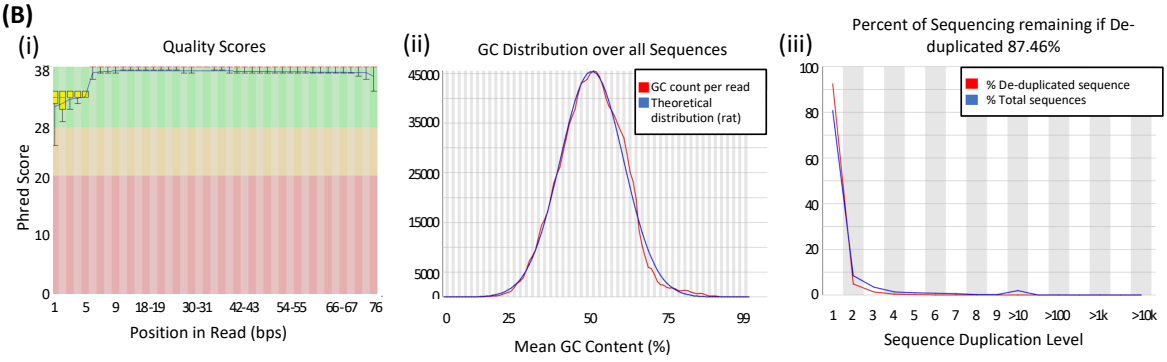

(C)

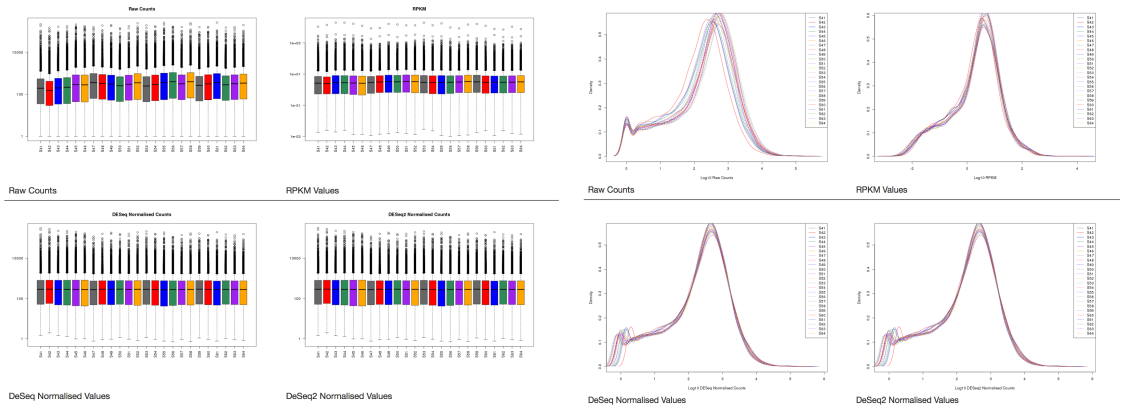

Figure 4.2 Next Generation Sequencing Sample and Data Quality Analysis (QC)

(A) Individually extracted RNA samples were tested for sample quality. All samples achieved a RIN value of >8.5. **(B, i-iii)** All samples passed QC thresholds. QC was completed on 10% of the raw data from each sample lane using the bioinformatics program FastQc (Ver 0.11.5). All samples passed sequencing length distributions, duplicate sequences and adaptor sequencing content. **(B, i)** Per base sequence quality plot demonstrates the quality of each base call using phred scores. The central red lines in the box plots represent median values and the blue line represents mean quality. Failure donates those with a median score <20. All median scores passed sequence quality. **(B, ii)** Per sequence GC content was visulised to measure the GC content across the length of each sequence. Blue represents a modelled normal distribution with the central peak representing the GC content of the underlying genome. Distribution is as expected. **(B, iii)** Duplicate sequences plot were examined for evidence of PCR over amplification. The library demonstrated low duplication, with the majority of the library originating from sequences which only occurred once, (pass is defined as duplication >50%). All samples passed sequencing length distributions, duplicate sequences and adaptor sequencing content. **(C)** The data was uploaded to DESeq-2 and boxplots and density plots were generated to visualise the distribution of data pre- and post-normalisation. Data outliers would appear as boxplots and histograms which visually differed to other samples. The visulised raw data, RPKM values and DeSeq2 normalised values were all as expected with no significant outliers.

4.2.1.2 NGS: Differentially Expressed Genes and Sample Clustering

In total, the transcripts sequenced mapped to 16,780 unique genes identified in the *Rattus norvegicus* genome (total genes in the genome 39,373). To identify DEGs, Deseq-2 was used to compare the differences between two sample groups. Significant DEGs were defined as those with a $\log_2$FC of ≥1 or ≤-1 and a corrected p-value of p≤0.05.

Comparing IRI to sham identified 1,667 upregulated and 1,029 down regulated transcripts (total n=2,696). Comparing indirect-IPC to sham there were 1,307 upregulated and 718 downregulated DEGs (total n=2,025). Following direct-IPC the number of DEGs differentially regulated relative to sham reduced to 894 upregulated and 166 downregulated (total, n=1,060), as shown in Figure 4.3.

To explore the variation between individual samples (libraries) and the experimental groups (sham, IRI, direct-IPC, indirect-IPC) the distance matrix model principal component analysis (PCA) was calculated using DESeq-2 transformed data. PCA is an unsupervised method to reduce the complexity of a dataset and reveal the high-level structure of that dataset. Expression profiles of all 16,780 unique genes in all twenty-four samples were included. The PCA plot demonstrated that samples from the same group clustered appropriately. Furthermore, the sample with the greatest variance is sham and IRI, and direct-IPC and indirect-IPC groups cluster between the extremes of the controls (Figure 4.4A).

To further explore the variation of the datasets, all DEGs which were differentially expressed between any two-group comparisons were collected and the Fragments Per Kilobase of transcript per Million mapped reads (FPKM; fold change normalised relative to sequencing lane and gene length) values were extracted from DESeq-2. In all, 2,826 differentially expressed transcripts were identified. Differential transcript expression data were then biclustered using spearman rank correlation, and clustered using average linkage.

In concordance with the PCA plot (Figure 4.4A), both a heatmap and column dendrogram clustering methods grouped the preconditioning groups together between the opposite experimental poles of IRI and sham, Figure 4.4B and 4.4C. Both preconditioning groups demonstrate clear distinction from the controls of sham and IRI. Within the PCA plot, heatmap and column dendrogram there is overlap between the two preconditioning groups. The preconditioning group cross over may exist due to several reasons. The cross over may suggest there is no clear distinction between the preconditioning groups due to similar transcriptional characteristics. The cross over may occur due to subgroups within the preconditioning groups. These observed subgroups may be due to a variability within each group inherent to *In vivo* experiments, or be a result of enhanced preconditioning in one individual sample compared to another.

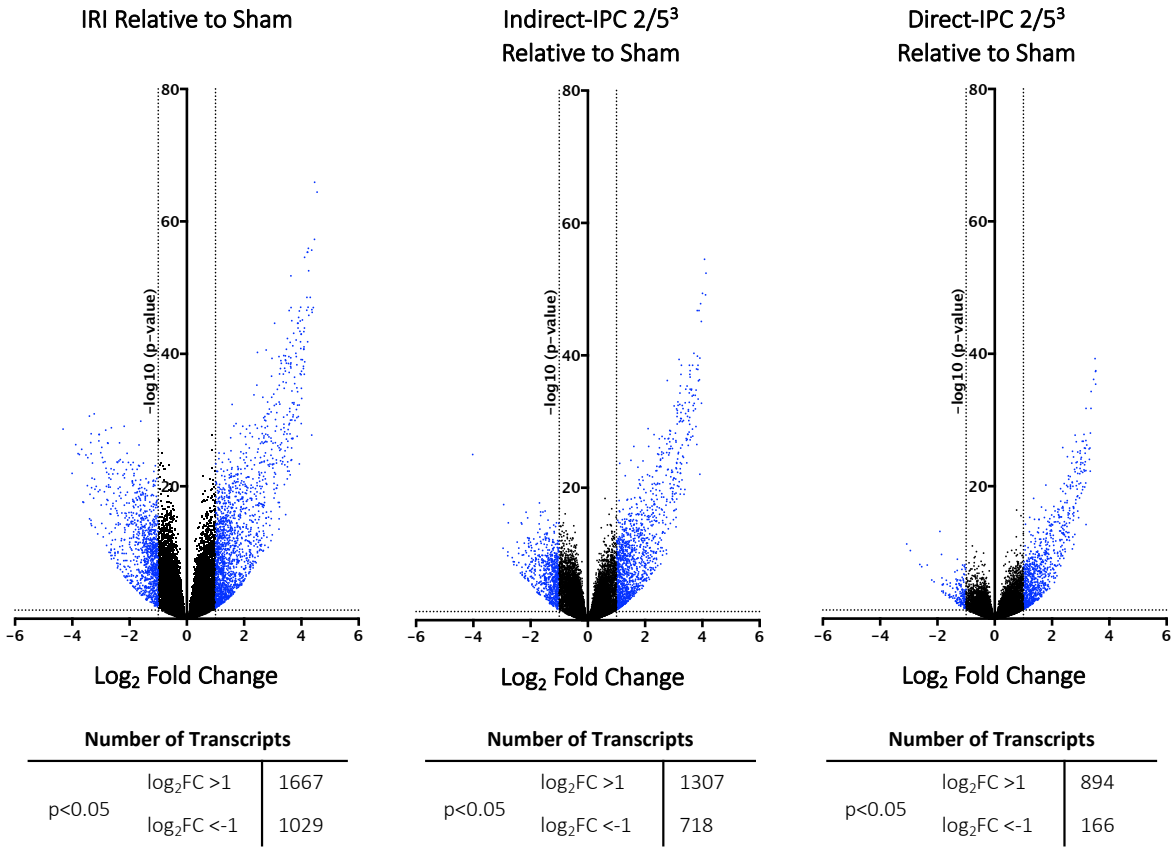

Figure 4.3 Next Generation Sequencing: Volcano Plots

Differential gene expression was computed relative to the background expression universe of sham. Volcano plots of the experimental groups IRI, indirect-IPC 2/5^3 and direct-IPC 2/5^3 was generated to visualise significant transcripts. Clear differences in the number of significant transcripts (IRI= 2696, Indirect-IPC 2/5^3 = 2025 and Direct-IPC 2/5^3 = 1060) within each experimental group was seen. Significant transcripts are coloured blue for ease of reference, x-axis dotted line represents dataset significance cut off of p=0.05 and y-axis dotted line log_2FC of <-1 and >1 .

Numbers of RNA extracted kidneys (biological repeats) in each experimental group: sham (n=6), IRI (n=6), direct-IPC 2/5^3 (n=6) and indirect-IPC 2/5^3 (n=6). Significant transcripts defined as DESeq-2 calculated p<0.05 and log_2FC <-1 or >1.

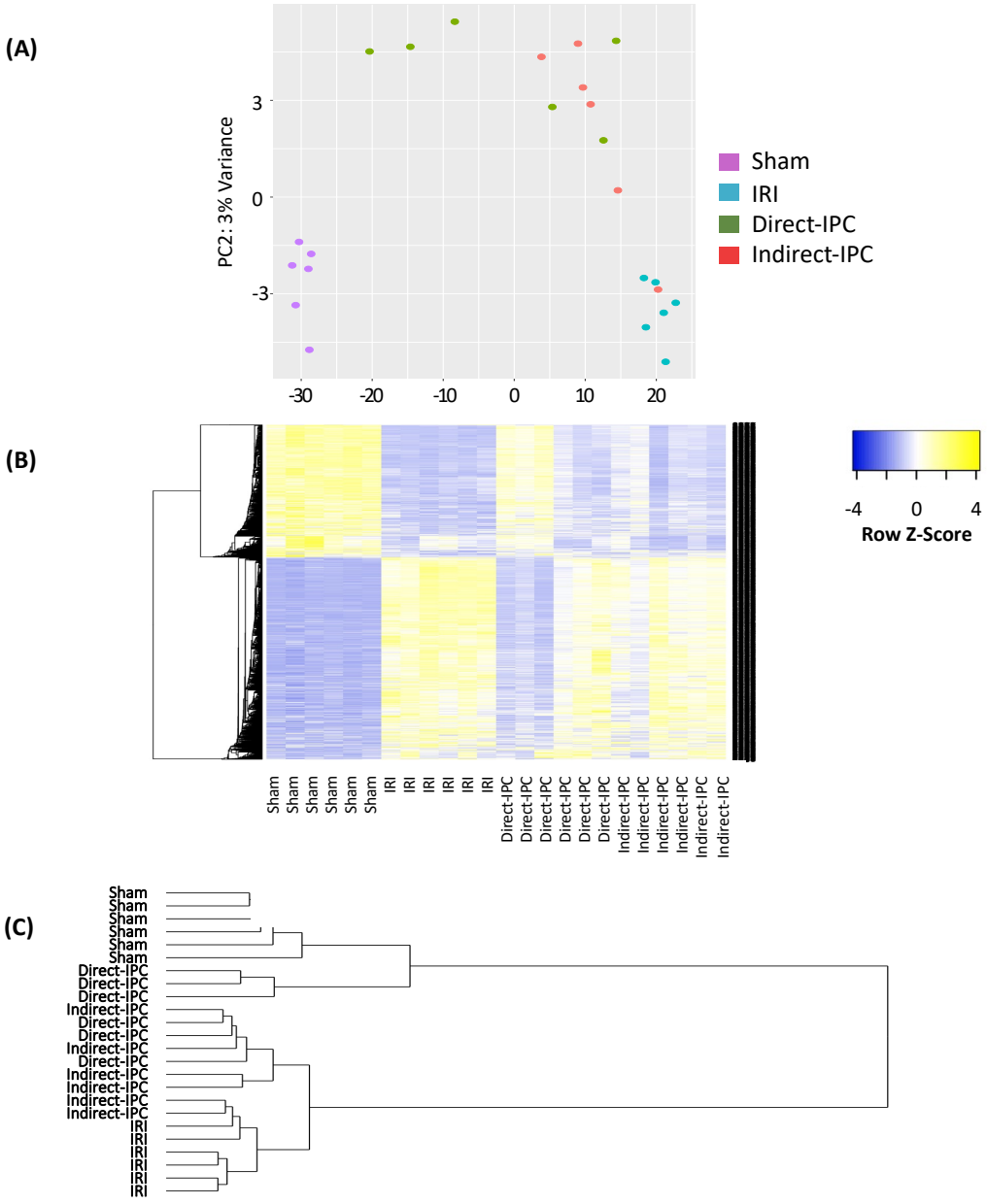

Figure 4.4 Next Generation Sequencing: Sample Clustering and Visualisation

(A) Principle component analysis (PCA) was computed using the standard operational calculation within DESeq-2. The PCA plot was mapped to explore the variation within the dataset and grouped into the two principle components that account for the greatest variation within the dataset. **(B and C)** DESeq-2 was used to calculate the differential transcript expression of all possible RNA-library experimental comparisons (e.g. IRI versus sham, total comparisons n=16). The data was interrogated to identify all differentially expressed transcripts with $\log_2$FC <-1 or >1 and an adjusted p<0.05. In total 2,826 transcripts were compiled and FPKM data for each library was extracted. Transcript data was clustered using Heatmapper (Spearman's rank correlation and clustered using average linkage). The column dendrogram was formatted to unbiased biclustering.

Numbers of RNA extracted kidneys (biological repeats) in each experimental group: sham (n=6), IRI (n=6), direct-IPC (n=6) and indirect-IPC (n=6)

4.2.2 Ingenuity Pathway Analysis (IPA): IRI

The *in silico* platform, Ingenuity Pathway Analysis (IPA) was used to analyse the RNA sequencing data. IPA used the gene expression profiles of the dataset and applied statistical algorithms to predict the molecular relationships between the dataset molecules and master regulators, pathways, biological functions, and diseases.

To test the biological responses of IRI, the differential gene analysis of 16,780 mapped transcripts was completed between the experimental groups of IRI and sham (Deseq-2). The $\log_2$FC and corrected p values of theses transcripts were downloaded to Microsoft Excel and uploaded to IPA. Of the 16,780 mapped transcripts, IPA knowledge base (Ver 2.3, Nov 2017) contained mapping IDs for 14,789 transcripts (unmapped 2,057). DEGs in the IRI verses sham group were defined as a corrected $p<0.05$ (-log [p-value] >1.3) and $\log_2$FC ≤-1 and ≥1. Of the 14,789 IPA recognised transcript IDs, a total of 2,358 transcripts met the above significance criteria (IPA recommended target 200 to 3,000), of which 1,506 were upregulated and 852 downregulated.

To enable statistical analysis of the uploaded dataset, IPA required a reference data set, defined as the complete universe of known transcripts, to be assigned. The IPA Ingenuity Knowledge Base (genes only) was selected as the reference dataset. To facilitate a blinded *in silico* analysis and allow the greatest level of freedom of interpretation, IPA was set to consider all data sources and no assignment of organ type was made. The IPA comparison analysis termed "Core Analysis" was completed to analyse the DEGs between the IRI and sham experimental groups, and the workflow is shown in Figure 4.5.

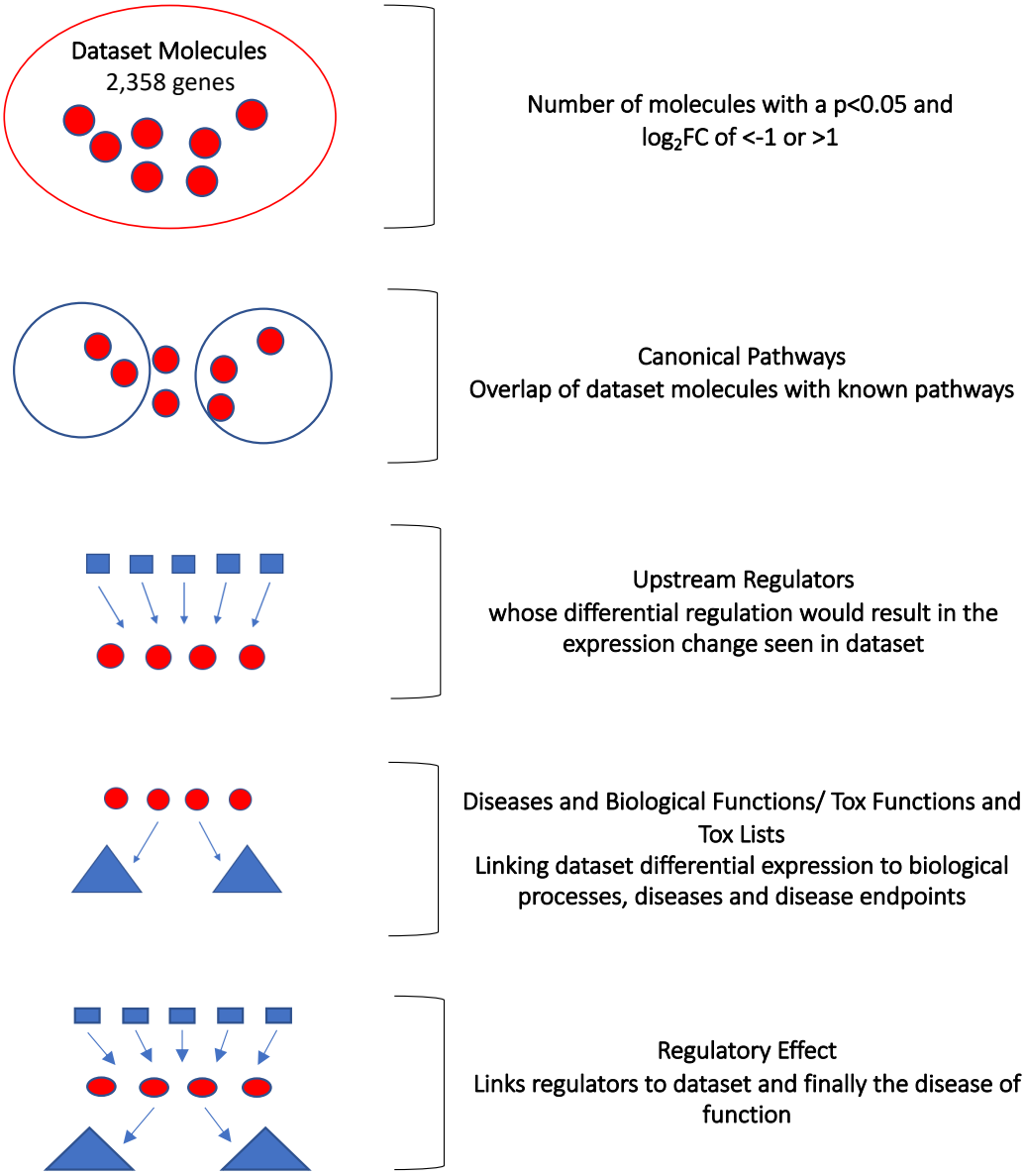

Figure 4.5 Ingenuity Pathway Analysis: Core Analysis Work Flow

Functional enrichment analysis was completed using the omics analysis platform Ingenuity Pathway Analysis (IPA). The sham experimental group was used as the background expression universe and all experimental comparisons were made relative to this data set. IPA knowledge base (Ver 2.3, Nov 2017) was used as the reference total gene universe. In brief, 16,780 transcripts were uploaded to IPA of which 14,789 had mapping IDs contained within IPA. Applying a significance cut off criteria of $p<0.05$ and $\log_2$FC of <-1 or >1 a total of 2,358 transcripts mapped, 852 downregulated and 1,506 upregulated. These transcripts were uploaded to the IPA Core Analysis which linked the dataset's gene expression profiles to known signalling/metabolic pathways **(canonical pathways)**, regulators whose differential expression may influence large numbers of dataset transcripts **(upstream regulators)**, disease or biological functions **(diseases and biological functions/ tox functions and tox lists)** and finally IPA analysis linked the upstream regulators to the dataset molecules and the downstream phenotype **(regulatory effects)**.

4.2.2.1 IPA: Summary Overview of the Core Analysis

Following completion of the IPA Core Analysis the summary page was inspected, providing a high-level overview of IPA's interpretation of the dataset phenotype. IPA displays the output as an ontology tree with the highest description being the "Function Tab", followed by the "Super Categories", then the "High-level functions" and finally Ontology (or annotations). IPA's knowledge base curate's organ toxicities and critical biological processes within two Function Tabs called Tox Functions and Tox Lists, respectively. The Tox Functions divide organ toxicities into the high-level super categories of Cardiotoxicity, Hepatotoxicity, Nephrotoxicity, Clinical Chemistry and Haematology. Under the function tab of Tox Lists, IPA groups pre-defined gene sets that functionally cluster to describe a critical biological process following a xenobiotic insult.

The Tox Function analysis ranked the super category of Nephrotoxicity as the principal phenotype of the dataset. Within this category, the high-level functional interpretation of the dataset was: Renal Damage (p=2.68E-01 - 8.06E-26), Renal Tubule Injury (p=1.92E-01 - 8.06E-26), Renal Necrosis/Cell Death (p=2.68E-01 - 2.03E-10), Glomerular Injury (p=4.13E-01 - 8.25E-08) and Renal Fibrosis (p=2.74E-01 - 1.66E-06). The analysis further described the principal ranked Tox Lists of the dataset as Acute Renal Failure Panel (Rat) (p=1.32E-27) and Renal Proximal Tubule Toxicity Biomarker Panel (Rat) (p=5.06E-15).

4.2.2.2 IPA: Canonical Pathways

IPA knowledge base contained information on 554 metabolic and signalling pathways which are collectively called canonical pathways. Of these pathways, the dataset molecules significantly overlapped (overlap value of $p<0.05$ [-log=1.3], range –log p value 1.3 to 11.2) with 136 pathways, of which 40% [54/136] were metabolic pathways and 60% [82/136] signalling pathways. Individual pathways were mapped manually to their principal functional category and grouped, revealing an enrichment of signalling pathways linked to cellular stress/ injury, repair and apoptosis, as shown in Figure 4.6.

To aid interpretation of the canonical pathways, IPA mapped the expression profile of the dataset molecules to the pathways and predicts the likely activation state (activation state defined as a z-score >2 or inhibition z-score <-2). The canonical pathways were filtered to reveal those pathways predicted to be most significant. The significance was defined as those with an overlap -log p value of >1.3 and z-score <-2 or >2. In total twenty-two pathways (19 upregulated and 3 downregulated) fulfilled these selection criteria, as shown in Figure 4.7A further 12 pathways were predicted to be involved in the dataset with an overlap -log p value of >1.3, but were constructed in a manner that no activity prediction could be made (see Appendix 1).

Of the twenty-two identified pathways, five were linked to inflammatory cytokine activation, of which the predicted pathway directional activation supported a pro-inflammatory phenotype: Acute Phase Response Signalling (p=7.8E-04, z= 3.13), LPS/IL-1 Mediated Inhibition of RXR Function (p=4.89E-05, z= 2.18), Ceramide Signalling (p=0.02, z=2.50) and Neuroinflammation Signalling Pathway (p= 0.02, z=2.54).

The inflammatory phenotype was further corroborated by the differential regulation of signalling pathways linked to pro-inflammatory cells (n=6): GP6 Signalling Pathway (p=7.24E-

06, z=4.49), Leucocyte Extravasation Signalling (p=2.04E-03, z= 3.53), TREM1 Signalling (p=6.91E-03, z= 2.84) and Fcy Receptor-mediated Phagocytosis in Macrophages and Monocytes (p=0.04, z=2.84), Tec Kinase Signalling (p=0.03, z=3.71) and Production of Nitric Oxide and Reactive Oxygen Species in Macrophages (p=0.03, z=2.50).

Several dataset molecules further linked to pathway's whose differential regulation is linked to Extracellular Matrix Signalling (ESM): Actin Cytoskeleton Signalling (p=0.01, z=3.4), Integrin Signalling (p=0.03, z=3.16) and ILK Signalling (p=2.29E-03, z=2.92). Furthermore, there was an enrichment of pathways related to Rho Cytoskeletal Signalling (n=5); RhoA Signalling (p=0.04, z=3.30), Regulation of Actin-based Motility by Rho (p=0.02, z=3.00), Signalling by Rho Family GTPases (p=2.40E-03, z=4.00), RhoGDI Signalling (p=0.02, z=2.71) and Agrin Interactions at Neuromuscular Junction (p=7.8E-03, z=2.31).

The dataset molecules were predicted to be significantly linked to pathways linked to DNA damage: Colorectal Metastasis Signalling (p=0.04, z= 2.48), as well as checkpoint pathways linked to DNA repair: Role of BRCA1 in DNA Damage Response (p=5.90E-07, z=2.18) and one linked to the pathway Cardiac Beta-adrenergic Signalling (p=0.04, z= -2.32).

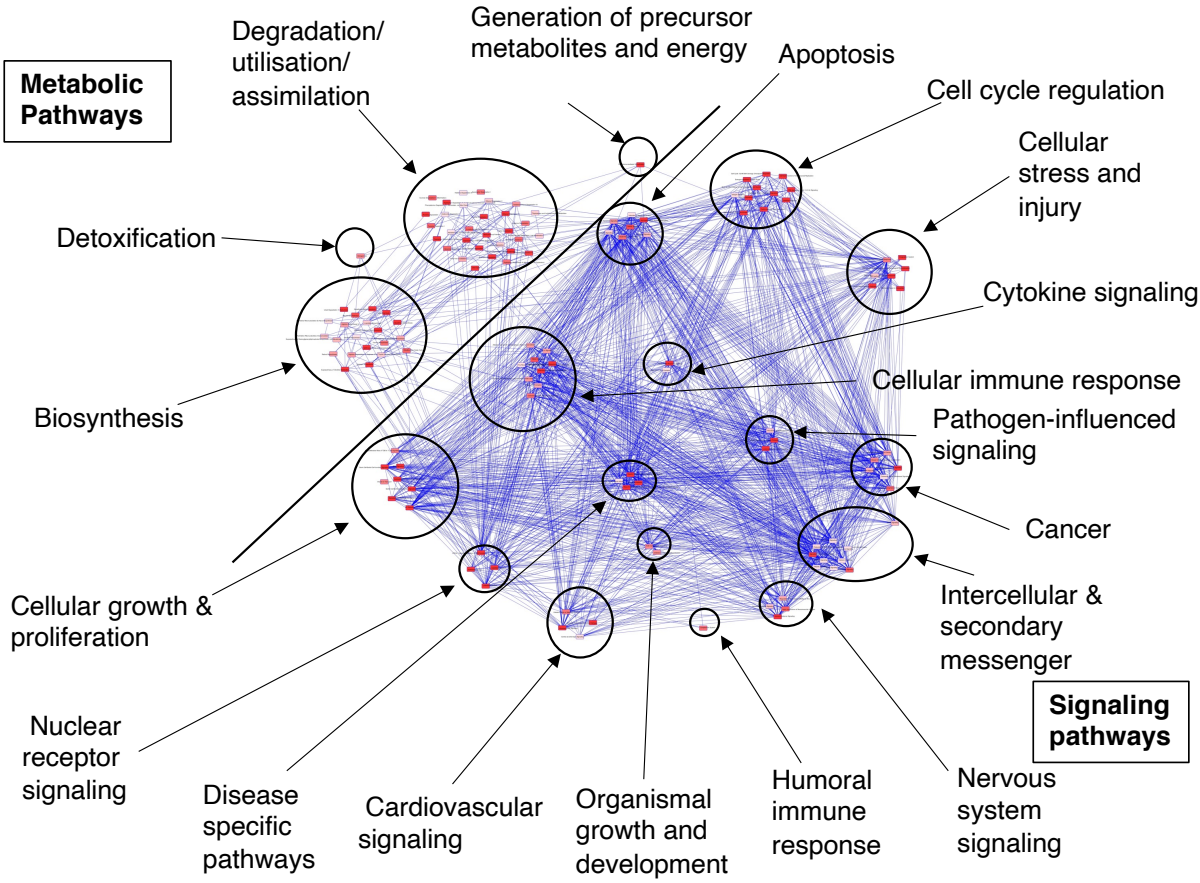

Figure 4.6 Ingenuity Pathway Analysis: Signalling Pathways of the IRI Dataset

IPA canonical pathways were examined for signalling pathways which are predicted to be associated with the dataset. Of the 554 known canonical pathways, 136 pathways had a calculated overlap of $p<0.05$.

Of these significant pathways, 40% (54/136) mapped to a metabolic pathway and 60% (82/136) to a signalling pathway. Statistical calculations across the 136 pathways corresponded to a -log p value (range 1.3 to 9.7), Ratio (0.134 to 1.0), Z-score (-2.711 to 4.49).

The above image is a pictorial representation of the 136 canonical pathways with a $p<0.05$ when grouped by functional categories. Each individual red box (node) represents a pathway. In summary, 9 pathways had molecules which solely mapped to that pathway and did not link to another pathway (orphan pathway), the remaining 127 pathways contained molecules which mapped to >1 pathway.

Pathways which bridge >1 functional description are placed in the functional group in which it exerts its dominant effect. Connecting blue line represents ≥1 connection between two pathways.

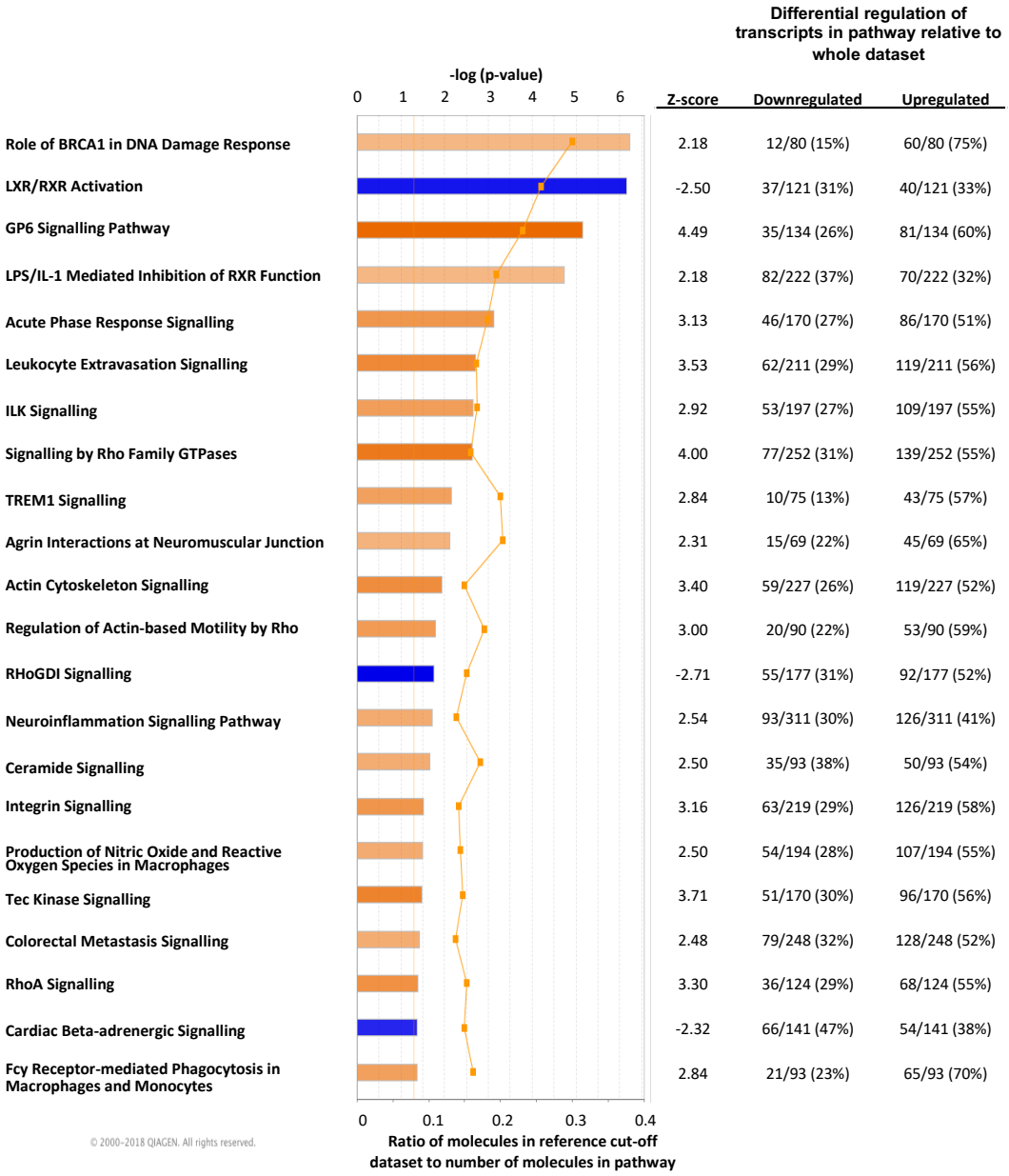

Figure 4.7 Ingenuity Pathway Analysis: Signalling Pathways of the IRI Dataset

IPA canonical pathways were examined for signalling pathways which are predicted to be associated with the dataset. IPA links the dataset molecules to 554 canonical pathways. The pathways were filtered for those with a p<0.05 (-log (p-value) = 1.3) and an activation z score of >2 or<-2. Of the 554 known canonical pathways twenty-two fulfilled selection criteria, of which 19 were upregulated and 3 downregulated. The above figure ranks those pathways by p-value as an indication of confidence in the functional grouping. The bar chart is coloured blue for inhibition and orange for activation (according to z-score). The ratio of DEGs within the dataset relative to the total number of molecules within a pathway is shown by the orange dot and line. The exact z-score is recorded to the right of the graph. The number of molecules upregulated and downregulated within the dataset is shown in the far right two columns.

4.2.2.3 IPA: Upstream Regulators

IPA also computed links between the DEGs dataset molecules and upstream regulators whose differential regulation provided an explanation for the downstream DEGs of the dataset molecules. Filtering upstream regulators with a predicted significance of $p<0.05$ and a z-score of >2 or <2 identified 480 unique upstream regulators (358 activated and 122 inhibited, see Appendix 2) whose differential regulation would statistically overlap with the dataset DEGs.

To aid visualisation of the data, the upstream regulators were ranked by p value and the principal forty ranked regulators are displayed in Figure 4.8 (p value 4.41E-46 to 1.55E-14, z-score 9.211 to -7.644). The top ranked regulators demonstrated an enrichment of regulatory proteins functionally grouped to Cellular Transcription (Regulator and Receptors), Growth Factors, Kinases, Cytokines, and Membrane/Nuclear Receptors. These forty-differentially regulated upstream regulators were predicted to target 1,193 unique DEGs within the dataset (Figure 4.8).

Upstream Regulator	Name	Molecule Type	Activation State	P-value	Z-score	Number of Dataset Molecules Targeted
TGFB1	transforming growth factor beta 1	growth factor	Activated	4.41E-46	8.338	373
ERBB2	erb-b2 receptor tyrosine kinase 2	kinase	Activated	2.09E-43	7.224	208
CDKN1A	cyclin dependent kinase inhibitor 1A	kinase	Inhibited	3.44E-41	-3.231	99
CSF2	colony stimulating factor 2	cytokine	Activated	2.58E-36	9.085	143
TNF	tumour necrosis factor	cytokine	Activated	1.1E-34	9.211	343
IL1B	interleukin 1 beta	cytokine	Activated	1.65E-29	7.845	202
Vegf	vascular endothelial growth factor	group	Activated	1.75E-28	7.311	138
IL6	interleukin 6	cytokine	Activated	2.81E-27	6.419	173
HGF	hepatocyte growth factor	growth factor	Activated	1.03E-26	7.035	133
CDKN2A	cyclin dependent kinase inhibitor 2A	transcription regulator	Inhibited	2.33E-24	-3.945	93
CCND1	cyclin D1	transcription regulator	Activated	4.78E-24	6.028	100
RABL6	RAB, member RAS oncogene family like 6	other	Activated	7.06E-24	5.692	40
TBX2	T-box 2	transcription regulator	Activated	1.71E-23	4.848	43
let-7	microRNA let-7	microrna	Inhibited	1.9E-23	-7.644	72
HRAS	HRas proto-oncogene, GTPase	enzyme	Activated	2.56E-22	3.131	141
SP1	Sp1 transcription factor	transcription regulator	Activated	1.44E-21	3.17	133
PDGF BB	Platelet-derived growth factor	complex	Activated	4.94E-21	5.421	93
IKBKB	inhibitor of nuclear factor kappa B kinase subunit beta	kinase	Activated	7.74E-21	4.296	85
IFNG	interferon gamma	cytokine	Activated	1.7E-19	6.787	240
MYC	MYC proto-oncogene	transcription regulator	Activated	2.2E-19	2.348	208
E2f	E2F transcription factor	group	Activated	1.03E-18	4.184	50
SMARCA4	SWI/SNF related, matrix associated, actin dependent regulator of chromatin, subfamily a, member 4	transcription regulator	Activated	2.35E-18	3.735	134
EGFR	epidermal growth factor receptor	kinase	Activated	2.47E-18	4.035	101
FOXM1	forkhead box M1	transcription regulator	Activated	2.83E-18	5.594	51
Alpha catenin	Alpha catenin	group	Inhibited	7.52E-18	-5.861	48
NFKBIA	NFKB inhibitor alpha	transcription regulator	Activated	1.35E-17	3.077	106
PTGER2	prostaglandin E receptor 2	g-protein coupled receptor	Activated	2.15E-17	5.453	44
EP400	E1A binding protein p400	other	Activated	2.9E-17	4.353	27
E2F1	E2F transcription factor 1	transcription regulator	Activated	1.36E-16	4.876	112
ESR1	estrogen receptor 1	ligand-dependent nuclear receptor	Activated	1.38E-16	2.21	227
TCF3	transcription factor 3	transcription regulator	Inhibited	1.6E-16	-2.144	86
CTNNB1	catenin beta 1	transcription regulator	Activated	2.13E-16	3.442	152
IL4	interleukin 4	cytokine	Activated	6.72E-16	4.619	166
Cg	Conjoined gene	complex	Activated	8.74E-16	4.457	89
RB1	RB transcriptional corepressor 1	transcription regulator	Inhibited	1.59E-15	-5.149	93
E2F3	E2F transcription factor 3	transcription regulator	Activated	3.26E-15	3.738	56
MITF	melanogenesis associated transcription factor	transcription regulator	Activated	3.61E-15	6.149	67
IL10RA	interleukin 10 receptor subunit alpha	transmembrane receptor	Inhibited	8.81E-15	-2.986	79
NFkB (complex)	NFkB (complex)	complex	Activated	1.39E-14	6.639	128
JUN	Jun proto-oncogene, AP-1 transcription factor subunit	transcription regulator	Activated	1.55E-14	3.593	101

Figure 4.8 Ingenuity Pathway Analysis: Upstream Regulators of the IRI Dataset

IPA upstream regulator analysis linked the dataset molecules whose differential regulation can be linked to a single regulator. Predictions were made on the basis of known transcript differential regulation in the IPA knowledge base. Analysis of the overlap between genes in the dataset and known transcriptionally regulated targets generated the p values shown. The activation z-score was calculated to predict the activation state of the regulator. In total 480 regulators with a $p<0.05$ and a z-score of >2 or <-2 were predicted (358 activated and 122 inhibited). Upstream regulators were ranked by p value and the top 40 upstream regulators are displayed.

4.2.2.4 IPA: Disease and Biological Functions

To identify key biological and cellular processes, IPA correlated the DEGs of the dataset to 84,770 curated gene expression lists that linked to specific cellular processes termed annotations. The annotations were further grouped into 90-high level functions, which in turn converged into three super category domains: Disease and Disorders, Molecular and Cellular Functions, and Physiological System Development and Function.

The statistically significant annotations ($p<0.05$ and a z-score of >2 or <-2) were filtered, revealing 134 annotations (121 upregulated and 13 downregulated) which grouped to 37 high-level functions . Visualising the dataset from the vantage point of the high-level functions and ranking by activation state (z-score) demonstrated significant groupings of annotations related to Inflammation, Cellular Movement, Immune Cell Trafficking, Cell-to-Cell Signalling and Cellular Function (Figure 4.9A). In concordance with this observation, ranking the high-level functions by p value revealed the principal high-level functions significant to: Cell Death and Survival (seven annotations, p= 1.03E-31 to 1.63E-09), Cellular Movement (forty-six annotations, p= 6.87E-29 to 9.83E-09), Cell Cycle (four annotations, p = 2.15E-22 to 2.74E-14), Figure 4.9B. Tissue Morphology (seven annotations, p=1.17E-28 to 8.66E-10), Immune Cell Trafficking (twenty-nine annotations, p=3.10E-22 to 9.83E-09) and Organismal Survival (two annotations, p=1.13E-20 to 5.41E-18), as shown in Figure 4.9C.

The 134 significant functional annotations contained within the Disease and Biological Functions Analysis (121 upregulated and 13 downregulated) were ranked by z-score, and the principal 30 upregulated and 10 downregulated are visualised in Figure 4.10. The DEGs in the dataset linked significantly to annotations linked to a molecular signal of cell survival (p=1.62E-13, Z=7.599), reduction in apoptosis (p=3.04E-24, Z=-3.082) and cell death (p=1.03E-31, Z=-2.405). The DEGs further linked to annotations consistent with inflammatory recruitment,

evidenced through a molecular signal of cell movement (p=6.87E-29, Z=7.18), migration of cells (p=8.17E-29 Z=6.946) and immune cell trafficking; cell movement of leucocytes (p=1.49E-17, p=5.244) and cell movement of phagocytes (p=1.86E-15, p=5.261), Figure 4.10.

Figure 4.9 Ingenuity Pathway Analysis: Disease and Biological Functions – High-Level Functions

(A) IPA Disease and Biological Functions was viewed as a TreeMap (hierarchical heatmap) to provide a high-level overview of the dataset. Orange coloured boxes represent activation, blue boxes inhibition: z-score increases with darker colour and the larger the area covered the greater the corresponding p value.

IPA functional annotations were filtered to consider only those with $p<0.05$ and a z-score of >2 or <-2. In total 134 annotations fulfilled this criteria (121 upregulated and 13 downregulated). These annotations grouped into 37 major functional families. Eleven functional families grouped into the category of Molecular and Cellular Function **(B)** and thirteen within the category of Physiological System Development and Function **(C).** Each grouping was ranked relative to the greatest overlap p-value. The remainder of the annotations link to the category of disease and function which are addressed in more detail in Figure 4.11: Tox Functions.

High Level Functions	Annotations	P-value	Z-score	Number Molecules
Cell Death and Survival	Cell survival	1.62E-13	7.599	326
	Cell viability	7.58E-13	7.319	308
	Cell viability of tumour cell lines	1.63E-09	7.222	201
	Cell death	1.03E-31	-2.405	751
	Apoptosis	3.04E-24	-3.082	584
Cell-To-Cell Signalling and Interaction	Interaction of tumour cell lines	2.18E-18	5.063	124
	Binding of tumour cell lines	1.76E-17	4.963	119
	Interaction of blood cells	9.05E-15	4.786	120
	Adhesion of blood cells	2.4E-17	4.77	115
Cell-To-Cell Signalling and Interaction, Cellular Movement	Recruitment of cells	7.94E-15	4.716	105
Cell-To-Cell Signalling and Interaction, Cellular Movement, Haematological System Development and Function, Immune Cell Trafficking	Recruitment of leukocytes	1.09E-15	4.793	99
Cell-To-Cell Signalling and Interaction, Haematological System Development and Function	Interaction of leukocytes	3.84E-14	4.789	109
Cellular Development, Cellular Growth and Proliferation	Cell proliferation of tumour cell lines	1.46E-14	4.95	365
Cellular Movement	Cell movement	6.87E-29	7.18	529
	Migration of cells	8.17E-29	6.946	481
	Cell movement of tumour cell lines	1.03E-12	5.888	224
	Cell movement of blood cells	6.65E-23	5.716	248
	Migration of blood cells	1.75E-22	5.618	245
	Migration of tumour cell lines	1.75E-09	5.375	179
	Homing of blood cells	1.53E-10	5.012	100
	Chemotaxis of blood cells	5.16E-09	4.927	91
	Invasion of cells	1.58E-15	4.916	230
Cellular Movement, Haematological System Development and Function, Immune Cell Trafficking	Cell movement of mononuclear leukocytes	1.69E-09	5.747	117
	Cell movement of leukocytes	1.49E-17	5.244	209
	Migration of mononuclear leukocytes	1.02E-09	5.226	97
	Homing of leukocytes	1.02E-09	5.086	97
	Cell movement of lymphocytes	2.51E-09	4.978	101
	Lymphocyte migration	1.61E-09	4.76	91
Cellular Movement, Haematological System Development and Function, Immune Cell Trafficking, Inflammatory Response	Cell movement of phagocytes	1.86E-15	5.261	155
	Chemotaxis of leukocytes	9.83E-09	4.927	90
Cellular Movement, Immune Cell Trafficking	Leukocyte migration	3.1E-22	5.6	244
Connective Tissue Disorders, Hereditary Disorder, Organismal Injury and Abnormalities	Hereditary connective tissue disorder	5.59E-12	-3.396	133
Haematological Disease, Immunological Disease	Lymphoproliferative disorder	1.11E-14	-2.352	391
Infectious Diseases	Parasitic Infection	1.13E-10	-2.678	55
	Infection of mammalia	5.46E-17	-3.13	102
Molecular Transport	Transport of ion	1.25E-14	-2.008	126
	Transport of cation	3.11E-11	-2.465	97
Organismal Survival	Morbidity or mortality	1.13E-20	-7.963	536
	Organismal death	5.41E-18	-8.175	518

Figure 4.10 Ingenuity Pathway Analysis: Diseases and Biological Functions - Top Ranked Annotations

The top ranked functional annotations of the dataset ($p<0.05$ and a z-score of >2 or <-2) were filtered. In total 134 functional annotations (121 activated and 13 inhibited) fulfilled this significance inclusion criteria. The significant functional annotations were ranked by z-score and the top 30 upregulated and 10 downregulated are visualised. For each functional annotation the major function family linked to the annotation is presented along with the overlap p value, z-score and the total number of molecules contained within the uploaded dataset which supports this prediction.

The principal biological functions linked to the annotations of Cell Survival, Cell-to-Cell Signalling and Cellular Movement. In concordance with this observation IPA linked the dataset molecules to a downregulatory state of Organismal Death, Morbidity and Mortality and Apoptosis. Taken together the biological functions predicted to be functional altered within the dataset were linked to Cellular Injury and Inflammatory Cell Recruitment. Furthermore, the tissue displayed differential transcript expression favouring an injury recovery phase.

4.2.2.5 IPA: Tox Functions and Tox Lists

IPA Tox Functions used the gene expression dataset to link to Clinical Pathology Endpoints under the super categories of Cardiotoxicity, Hepatotoxicity, Nephrotoxicity, and assays: Clinical Chemistry and Haematology. The principal aim of this analysis was to image the predicted phenotype endpoint of the dataset. In the case of the IRI relative to sham dataset, the aim was to examine for IRI clinical endpoints.

IPA knowledge base tested the transcript data against 2,385 clinical pathology endpoints (annotations), which converged into 101 high-level functions and four super categories. Ranking those functions by p value demonstrated an enrichment of DEGs significant to the high-level function of Renal Damage: top ranked annotations were Proximal Tubular Toxicity (p=8.06E-26, containing 50 DEGs) and Renal Tubule Injury - Nephrotoxicity (p-1.05 E-25, containing 51 DEGs) (see Figure 4.11).

Of the 50 DEGs in the Proximal Tubular Injury Function, 23 were upregulated and 27 downregulated. These DEGs linked to five canonical pathways: LXR/RXR Activation, Acute Phase Response Signalling, GP6 Signalling Pathway, Hepatic Fibrosis and LPS/IL-1 Mediated Inhibition of RXR Function, A (see Appendix 3).

IPA knowledge base further grouped pre-defined gene sets that were functionally grouped to describe a critical biological process that results from a xenobiotic insult. In total 38 Tox Lists achieved a $p<0.05$. The top ranked (p-value) Tox Lists linked to the biological process observed in the dataset is Acute Renal Failure Panel (Rat) p=1.00 E-27, Renal Proximal Tubule Toxicity Biomarker Panel (Rat) p=4.00 E-15 and Renal Necrosis/Cell Death p=2.51 E-12 are shown in Figure 4.12.

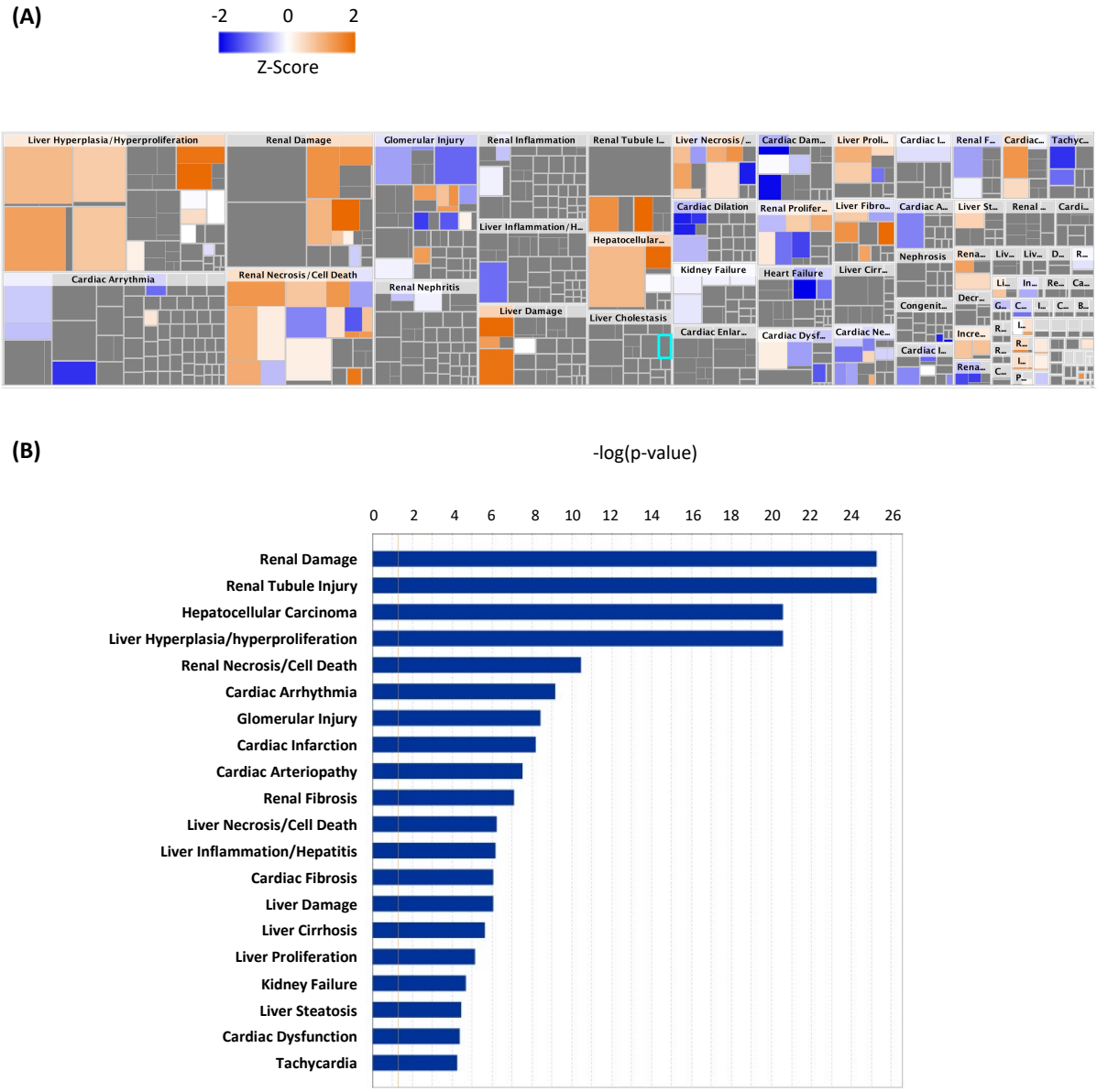

Figure 4.11 Ingenuity Pathway Analysis: Tox Functions

IPA Tox Functions used the gene expression dataset to link to Clinical Pathology Endpoints, thereby imaging the predicted endpoint resulting from the altered transcript profile. In the case of the IRI relative to sham dataset the aim is to examine for clinical end points of the IRI. In total IPA knowledge base tests the transcript data against 2,385 clinical pathology endpoints which converge into four supercategories; cardiotoxicity, hepatotoxicity, nephrotoxicity and Assays: *clinical chemistry and haematology*.

IPA Tox Functions was viewed as a TreeMap (hierarchical heatmap) were the major boxes represents a category of related functions clustered together, image **(A)**. Orange coloured boxes represent activation, blue boxes inhibition: z-score increases with darker colour. The larger the area cover the greater the corresponding p value.

The high - level functions were ranked by p-value and the top 20 are graphically displayed **(B)** The principle predicted tox function exhibited by the IRI dataset was that of the high level function of Renal Damage. The top ranked tox function annotation contained within the high level function of Renal Damage was that of Renal Proximal Tubular Toxicity p=5.24E-26, which contains 50 dataset molecules.

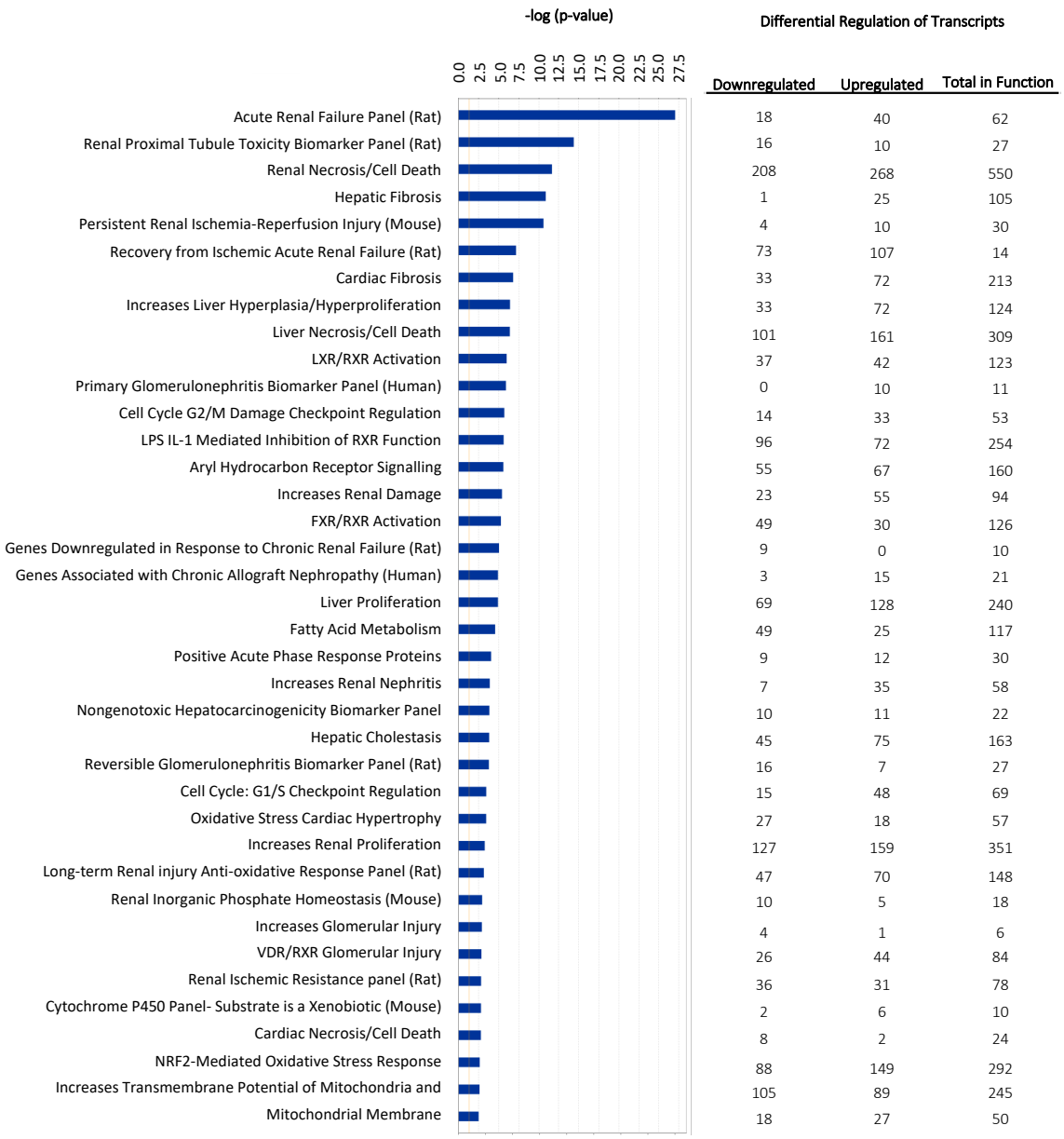

	Differential Regulation of Transcripts		
	Downregulated	Upregulated	Total in Function
Acute Renal Failure Panel (Rat)	18	40	62
Renal Proximal Tubule Toxicity Biomarker Panel (Rat)	16	10	27
Renal Necrosis/Cell Death	208	268	550
Hepatic Fibrosis	1	25	105
Persistent Renal Ischemia-Reperfusion Injury (Mouse)	4	10	30
Recovery from Ischemic Acute Renal Failure (Rat)	73	107	14
Cardiac Fibrosis	33	72	213
Increases Liver Hyperplasia/Hyperproliferation	33	72	124
Liver Necrosis/Cell Death	101	161	309
LXR/RXR Activation	37	42	123
Primary Glomerulonephritis Biomarker Panel (Human)	0	10	11
Cell Cycle G2/M Damage Checkpoint Regulation	14	33	53
LPS IL-1 Mediated Inhibition of RXR Function	96	72	254
Aryl Hydrocarbon Receptor Signalling	55	67	160
Increases Renal Damage	23	55	94
FXR/RXR Activation	49	30	126
Genes Downregulated in Response to Chronic Renal Failure (Rat)	9	0	10
Genes Associated with Chronic Allograft Nephropathy (Human)	3	15	21
Liver Proliferation	69	128	240
Fatty Acid Metabolism	49	25	117
Positive Acute Phase Response Proteins	9	12	30
Increases Renal Nephritis	7	35	58
Nongenotoxic Hepatocarcinogenicity Biomarker Panel	10	11	22
Hepatic Cholestasis	45	75	163
Reversible Glomerulonephritis Biomarker Panel (Rat)	16	7	27
Cell Cycle: G1/S Checkpoint Regulation	15	48	69
Oxidative Stress Cardiac Hypertrophy	27	18	57
Increases Renal Proliferation	127	159	351
Long-term Renal injury Anti-oxidative Response Panel (Rat)	47	70	148
Renal Inorganic Phosphate Homeostasis (Mouse)	10	5	18
Increases Glomerular Injury	4	1	6
VDR/RXR Glomerular Injury	26	44	84
Renal Ischemic Resistance panel (Rat)	36	31	78
Cytochrome P450 Panel- Substrate is a Xenobiotic (Mouse)	2	6	10
Cardiac Necrosis/Cell Death	8	2	24
NRF2-Mediated Oxidative Stress Response	88	149	292
Increases Transmembrane Potential of Mitochondria and	105	89	245
Mitochondrial Membrane	18	27	50

Figure 4.12 Ingenuity Pathway Analysis: Tox Lists of the IRI Dataset

IPA Tox lists described critical biological processes resulting from a xenobiotic insult. The analysis predicted toxicity outcomes from treatment interventions.

The plot demonstrates the toxicities ranked by p value and grouped according to biological function and/or organ. Filtering for those with a corrected $p<0.05$ identified 38 significant tox lists. The total number of transcripts within IPAs knowledge database which are grouped to form each tox list are displayed in the table column under the heading: total in function. The number of upregulated or downregulated significant DEGs within the dataset which were used to make the prediction are listed under upregulated and downregulated. The top 5 principal lists predicted were, Acute Renal Failure Panel (Rat) p=9.3 E-28, Renal Proximal Tubule Toxicity Biomarker (Rat) 4.26 E-15, Renal Necrosis/Cell Death 2.24 E-12, Hepatic Fibrosis 1.34 E-11 and Persistent Renal Ischemia-Reperfusion Injury (Mouse) 2.57 E-11.

4.2.2.6 IPA : Regulatory Effects Network

The Regulator Effect Network (REN) built connections between the activation or inhibition of the predicted upstream regulators, the downstream target molecules in the data set, and finally the disease or biological function. This analysis predicted the most statistically significant findings, in an ordered fashion, to identify regulators influencing the dataset which explained the dataset phenotype.

IPA required a limited number of regulators and phenotypes to be considered for the analysis. Therefore, the Regulatory Effects algorithm was limited to Genes, RNA, Proteins as regulators ($p<0.01$, $z>2$ or <-2 and maximum n=10), and phenotypes linked to Molecular and Cellular Function, and Disease and Biological Function: Renal Disease ($p<0.01$ and $z>2$ or <-2). The principal significant networks ranked by the consistency score (an arbitrary score which ranked the statistical significance of the prediction) was viewed.

The top ranked network predicted to be the principal network leading to the Molecular and Cellular Phenotype of the dataset was viewed, (consistency score 35.4, range 35.4 to -6.5), Figure 4.13. In total, IPA predicts that the network has 8 regulators, which targets 30 dataset molecules, regulating four diseases and functions. In total 44% (14/32) of the regulator to disease/function relationships are known in the IPA knowledge base and the remainder are computational novel predictions, Figure 4.13.

To further explore the regulatory network described in, Figure 4.13, the principal canonical pathways predicted to be significantly regulated by the network was overlaid, Figure 4.14. This demonstrated a significant shared molecule overlap between the network and the canonical pathways of: Agranulocyte Adhesion and Diapedesis (n=13), Granulocyte Adhesion and Diapedesis (n=12), TREMI signalling (n=9), Hepatic fibrosis and Hepatic Stellate Cell Activation (n=7) and the Role of Macrophages, Fibroblasts and Endothelial Cells in Rheumatoid

Arthritis (n=10). Taken together IPA was probed to explore the principal disease and function ranked by p-value linked to the network exposing the connection to Inflammatory Responses, p= 4.55 E-44.

The top ranked network predicted to be the principal network leading to the biological function; renal disease of the dataset was viewed, (consistency score 6.5, range 6.5 to -23.7). The top ranked disease phenotype of the dataset was predicted to be Injury of the Renal Tuble. In all, 10 upstream regulators target 7 principal dataset molecules leading to the disease phonotype, Figure 4.15.

The network leading to Injury of the Renal Tubule was overlaid with the top ranked signalling pathways predicted to be differentially activated in a manner consistent with the DEGs and network. The network formed pathway connections with; Acute Phase Response Signalling, Role of macrophages, Fibroblasts and Endothelial Cells in Rheumatoid Arthritis, Production of Nitric Oxide and Reactive Oxygen Species in Macrophages, LPS/IL-1 Mediated Inhibition of RXR Function and Hepatic Fibrosis/Hepatic Stellate Cell Activation, Figure 4.16A. The regulatory network was finally overlaid with the top ranked (p-value) functional annotation predicted to be most significant in the network, Recruitment of Phagocytes, p= 6.09 E-27, Figure 4.16B.

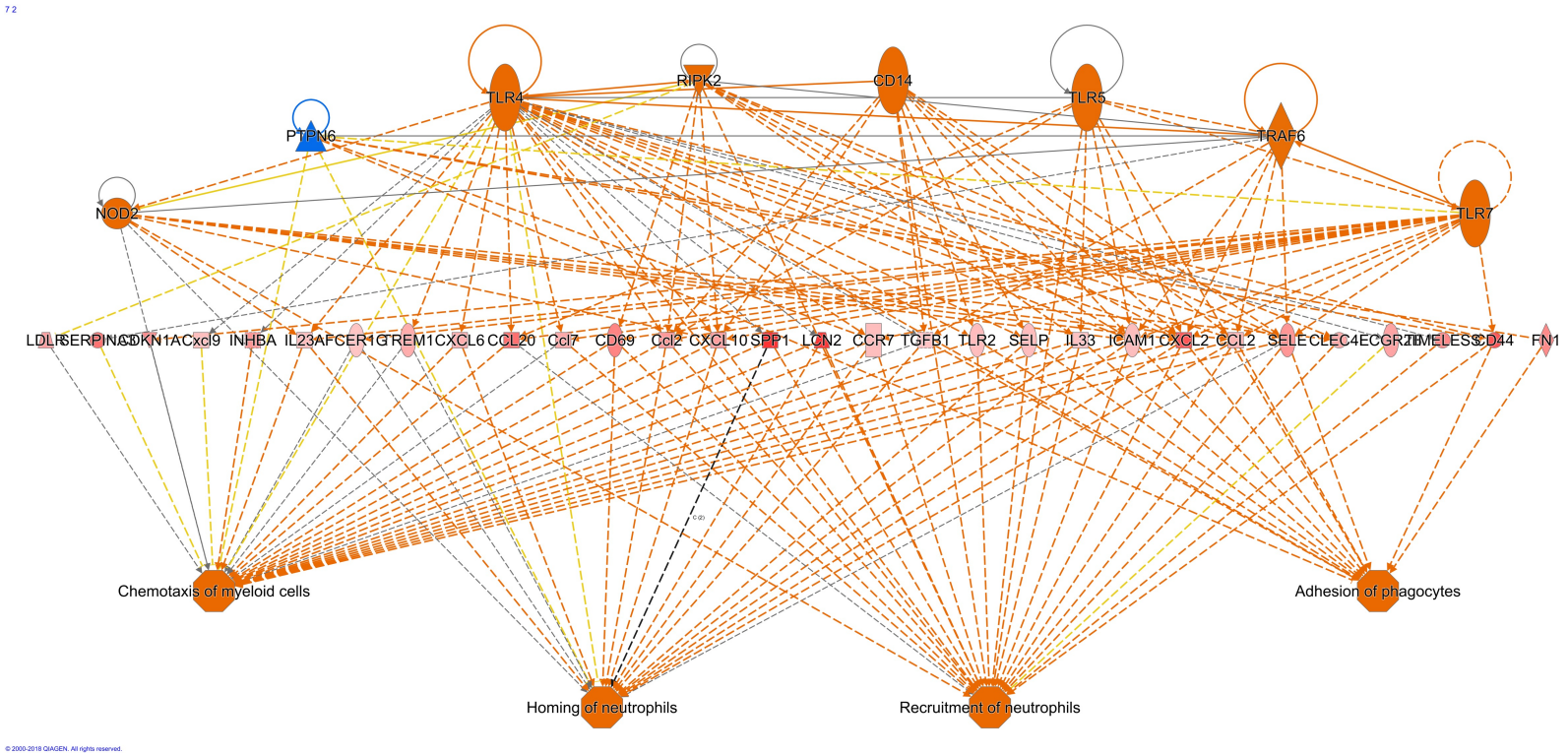

Figure 4.13 Ingenuity Pathway Analysis: Regulatory Effect Analysis

IPA: Regulatory Effect Analysis linked the analysis outputs of the upstream regulators, dataset molecules and the disease or biological function. The analysis predicted the most statistically significant findings in an ordered fashion to identify regulators influencing the dataset which explained the dataset phenotype. The IPA regulatory effect analysis output was ranked by the consistency score, an arbitrary score which aims to rank the statistical significance of the prediction. The top ranked network (consistency score 35.4, range 35.4 to -6.5) was viewed. In total IPA predicts that the network has 8 regulators (CD14, NOD2, PTPN6, RIPK2, TLR4, TLR5, TLR7, TRAF6), which targets 30 dataset molecules (CCL2, Ccl2, CCL20, Ccl7, CCR7, CD44, CD69, CDKN1A, CLEC4E, CXCL10, CXCL2, CXCL6, Cxcl9, FCER1G, FCGR2B, FN1, ICAM1, IL23A, IL33, INHBA, LCN2, LDLR, SELE, SELP, SERPINA3, SPP1, TGFB1, TIMELESS, TLR2, TREM1) which are predicted to influence four diseases and functions. In total 44% (14/32) of the regulator to disease/function relationships are known in the IPA knowledge base.

IPA required a limited number of regulators and phenotypes to be considered for the analysis. Therefore, the Regulatory Effects algorithm was limited to Genes, RNA, Proteins as regulators (only considering those with a $p<0.01$, $z>2$ or <-2) to a maximum of 8 diseases and functions (only considering those with a $p<0.01$, $z>2$ or <-2) linked to Molecular and Cellular Function. Node and connecting lines coloured red or orange denotes activation and blue/green inhibition. Those connecting lines which are dashed represents an indirect link and solid colouring direct. Those lines coloured yellow describe regulators whose activation state is in the opposite direction to what is seen downstream.

(A)

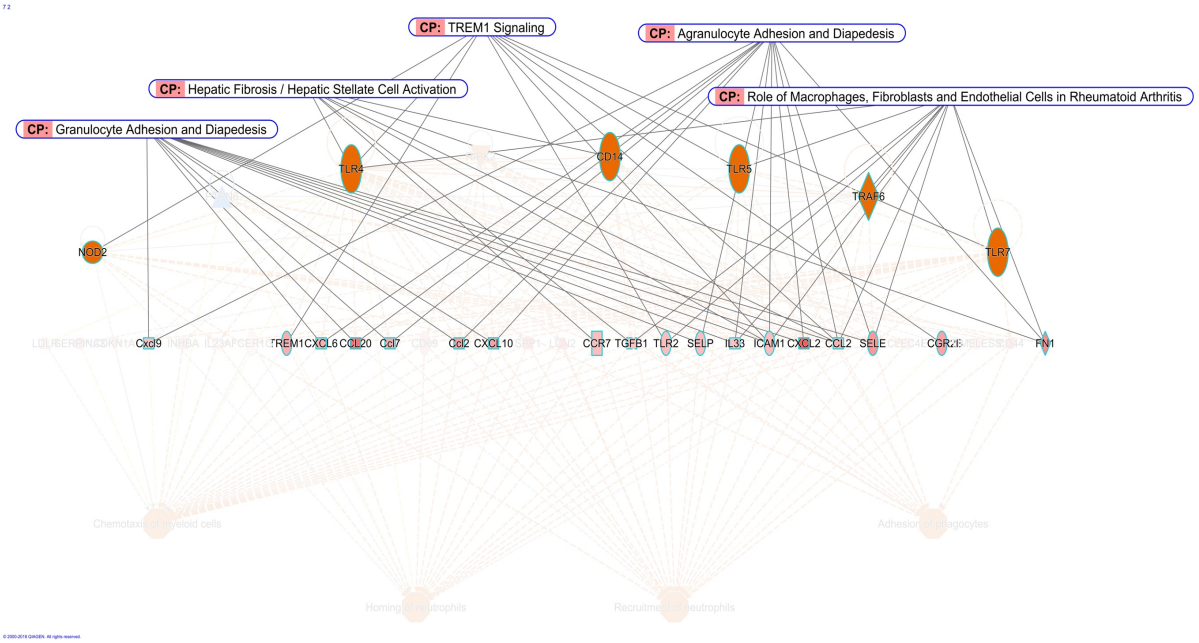

(B)

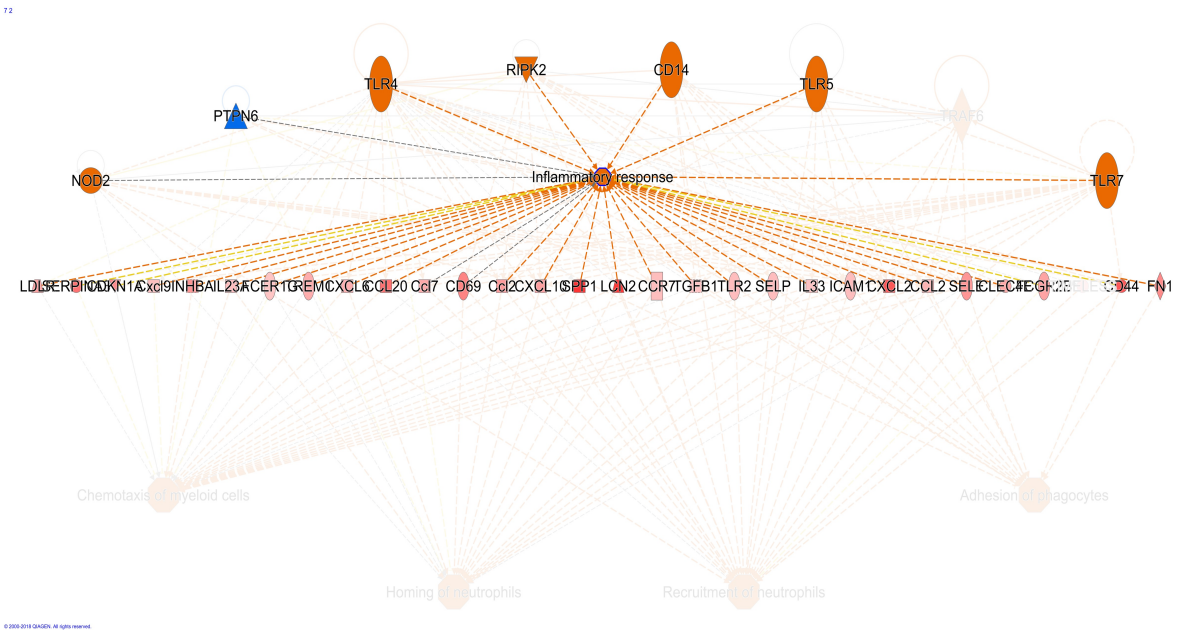

Figure 4.14 Ingenuity Pathway Analysis: Regulatory Effect Analysis

(A) The top ranked (p value) canonical signalling pathways with shared molecules with the pathway were overlaid, image. To further explore the networks relationship with phenotype the top ranked disease and function linked to the principal regulatory effect network was overlaid. **(B)** The principal function linked to Inflammatory Responses (p= 4.55 E-44).

To allow for ease of visualisation those molecules which demonstrate concordance with the network and the pathways and principle function are highlighted. Those not participating in the function are faded out . Node and connecting lines coloured red or orange denotes activation and blue/green inhibition. Those connecting lines which are dashed represents an indirect link and solid colouring direct. Those lines coloured yellow describe regulators whose activation state is in the opposite direction to what is seen downstream.

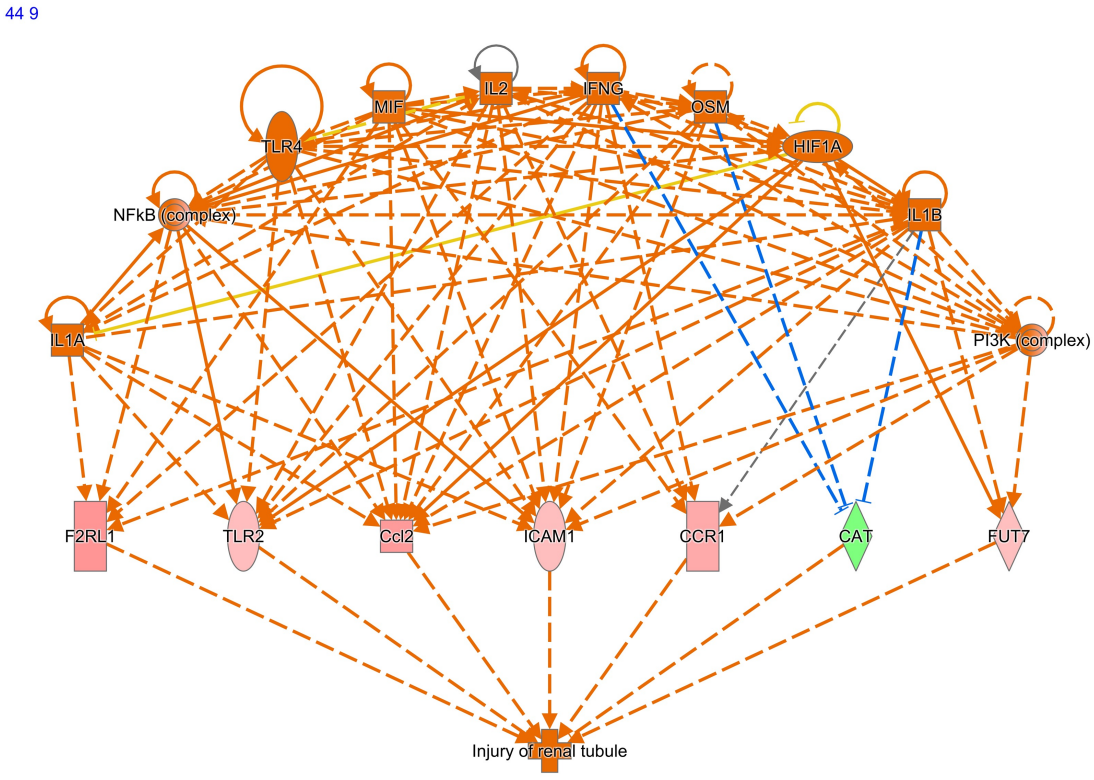

Figure 4.15 Ingenuity Pathway Analysis: Regulatory Effect Analysis

IPA: Regulatory Effect Analysis was tested for upstream regulators and dataset molecules which link to the top ranked disease or function related to renal disease.

The top ranked network by consistency score is presented above. The network depicts the connections between the upstream regulators, the dataset molecules and finally the phenotype of Injury of Renal Tubule.

Node and connecting lines coloured red or orange denotes activation and blue/green inhibition. Those connecting lines which are dashed represents an indirect link and solid colouring direct. Those lines coloured yellow describe regulators whose activation state found in the dataset is in the opposite direction to what is seen downstream.

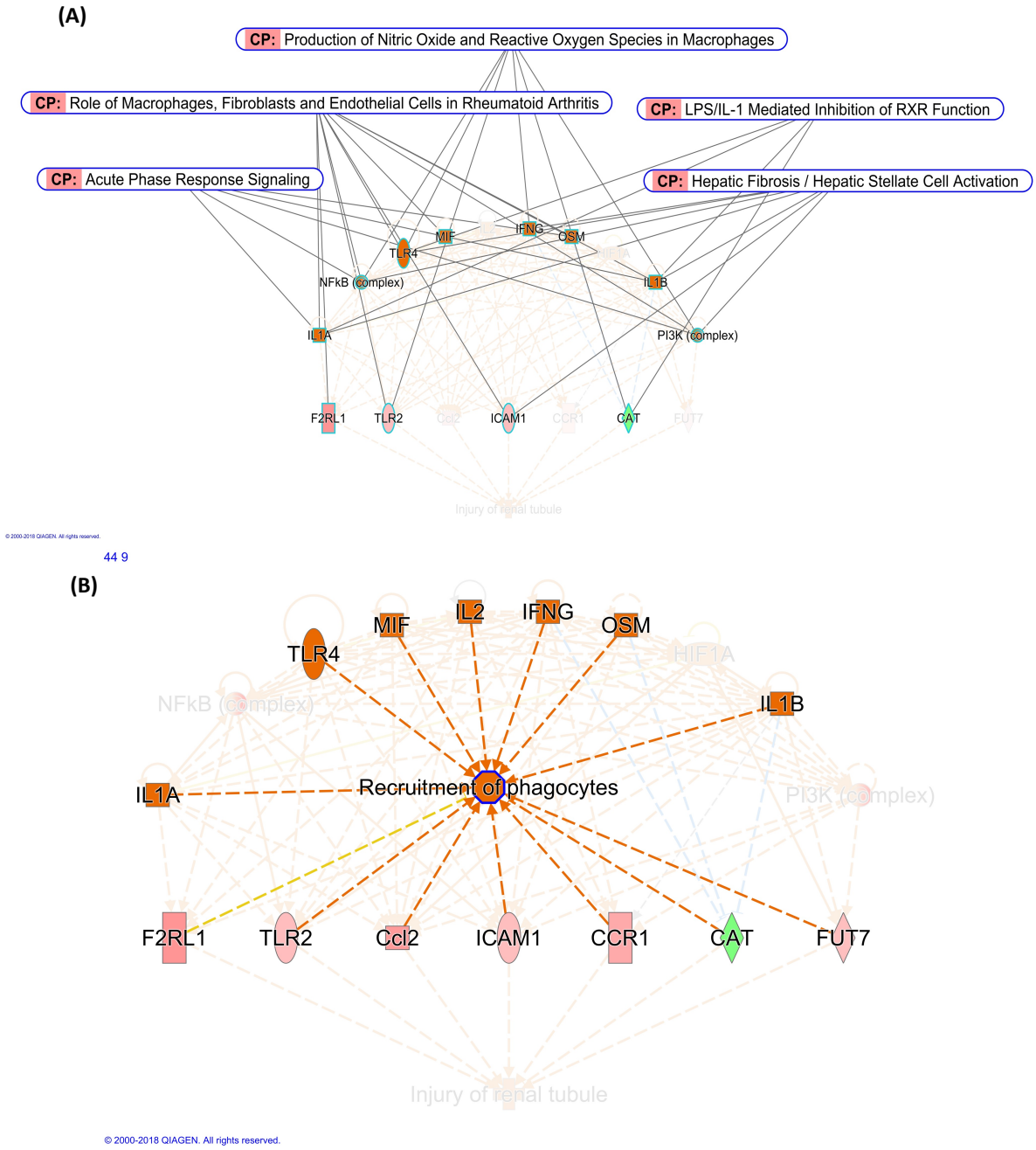

Figure 4.16 Ingenuity Pathway Analysis: Regulatory Effect Analysis

(A) The top ranked IPA Regulatory Effect Analysis network linked to Renal Injury or Disease was visualised with the top ranked canonical signalling pathways significant to the network overlapped.

(B) The top ranked IPA annotation of Recruitment of Phagocytes (p=6.09 E-27) linked to the molecules of the network. To allow for ease of visualisation those molecules which demonstrated concordance with the network and the principal function are highlighted (n=16) and those not participating in the function are faded.

Node and connecting lines coloured red or orange denotes activation and blue/green inhibition. Those connecting lines which are dashed represents an indirect link and solid colouring direct. Those lines coloured yellow describe regulators whose activation state is in the opposite direction to what is seen downstream.

4.2.3 IPA: IPC Comparative Analysis

To test the biological differences and similarities between IRI and IPC groups, direct-IPC 2/5[3] and indirect-IPC 2/5[3], differential gene expression analysis of 16,780 mapped transcripts was completed relative to the control group sham. Statistically significant DEGs were defined as those which with a $p<0.05$ (-log [p-value] >1.3) and log2FC ≤-1 and ≥1.

The total number of DEGs (relative to sham) identified in the IRI group was 2,696 (1,667 upregulated and 1,029 downregulated), in the indirect-IPC group was 2,025 (1,307 upregulated and 718 downregulated) and in the direct-IPC group was 1,060 (894 upregulated and 166 downregulated). The datasets were uploaded to IPA, and all three Core Analyses were completed as described in Chapter 4.2.2 Ingenuity Pathway Analysis: Ischaemia Reperfusion Injury.

To facilitate comparison across experimental groups, each Core Analysis was compared to identify similarities, differences and trends using the IPA comparative analysis platform. The workflow used for this comparison is described in Figure 4.17.

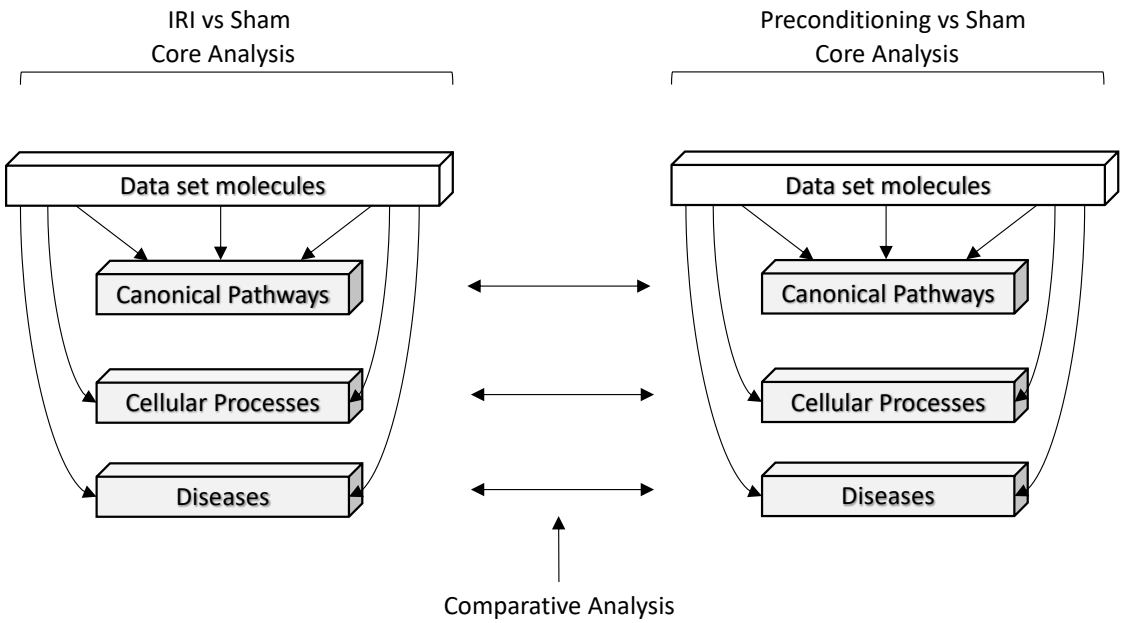

Figure 4.17 Ingenuity Pathway Analysis: Comparative Analysis

Three Core Analysis were completed comparing IRI, direct-IPC 2/5[3] and indirect-IPC 2/5[3] relative to the background expression universe of sham. Identical significance cut-off criteria of $p<0.05$ and $\log_2 FC >1$ or <-1 were used for each Core Analysis. Similarly, the IPA knowledge base was used as the reference dataset.

The reference IPA knowledge base was used as the complete universe utilising all molecules associated with disease, functions, pathways or list annotations to be considered for statistical calculations. The comparative analysis aimed to describe the response pathways differentially activated following intervention.

4.2.3.1 IPA: Comparative Analysis - Canonical Pathways

To explore the differences and similarities between IRI and the preconditioning groups the canonical signalling pathways which were statistically significant (p value <0.05 [-log=1.3] and z-score <-2 or >2) within each individual core analysis were collated and compared across the groups. In the IRI core analysis twenty-two signalling pathways met the significance criteria (19 upregulated and 3 downregulated), of which sixteen were unique to IRI. In the indirect-IPC analysis nine pathways fulfilled the significance criteria (9 upregulated), of which three were unique to indirect-IPC. In the direct-IPC analysis, four pathways were significant (4 upregulated), of which two were unique to direct-IPC. In total, across the three core analyses twenty-seven unique pathways were identified, Figure 4.18.

A trend towards a reduction in activation state (z-score) of pathways related to Inflammatory Cytokine Activation was observed in both the indirect-IPC and direct-IPC groups compared to IRI. In the IRI analysis both LPS/IL-1 Medicated Inhibition of RXR Function (p= 1.86E-05, z= 2.18) and Ceramide Signalling (p=0.02, z= 2.50) were predicted to be activated following IRI and non-significant to both indirect-IPC and direct-IPC. The observed activation of IRI Pro-inflammatory Response pathways; Leucocyte Extravasation Signalling (p= 2.0E-03, z= 3.53), Fcy Receptor-mediated Phagocytosis in Macrophages and Monocytes (p= 0.04, z= 2.84), Tec Kinase Signalling (p= 0.03, z= 3.71) and Production of Nitric Oxide and Reactive Oxygen Species in Macrophages (0.03 z= 2.50) were non-significant in both preconditioning groups. The trend towards a reduction in inflammatory activation was seen in the Acute Phase Response Signalling pathways evidenced by a reduction in the ratio of DEGs (IRI= 0.18, indirect-IPC= 0.15 and direct-IPC 0.09) and z-score (IRI 3.13, indirect-IPC=2.52 and direct-IPC=2.50) in both preconditioning groups.

IPC was further seen to negate the activation of response pathways linked to extracellular matrix signalling. In total three pathways were activated following IRI but were not significant in the IPC groups; Actin Cytoskeleton Signalling (p= 0.01, z=3.53), Integrin Signalling (p= 0.03, z=3.16) and ILK Signalling (p= 2.29E-03, z=2.92).

Three pathways were predicted to be uniquely upregulated following indirect-IPC: Role of IL-17F in Allergic Inflammatory Airway Diseases (p=0.04, DEGs= 0.16 and Z=2.24), p38 MAPK signalling (p=0.05, DEGs=0.12 and Z=3.05) and 14-3-3-mediated Signalling (p=0.03, DEGs 0.12 and Z=2.65). Two pathways were predicted to be uniquely activated in the direct-IPC analysis: Oestrogen-mediated S-phase Entry (p=4.68E-06, DEGs= 0.31, Z= 2.12) and VDR/RXR Activation (p=0.01, DEGs= 0.10, Z= 2.24).

	IRI			Indirect-IPC			Direct-IPC		
	-log (p-value)	Ratio	Z-score	-log (p-value)	Ratio	Z-score	-log (p-value)	Ratio	Z-score
Role of BRCA1 in DNA Damage Response	6.23	0.30	2.18	4.35	0.21	2.14	/	/	/
LXR/RXR Activation	6.15	0.26	-2.50	/	/	/	/	/	/
Oestrogen-mediated S-phase Entry	/	/	/	/	/	/	5.32	0.31	2.12
GP6 Signalling Pathway	5.14	0.23	4.49	4.09	0.17	4.80	3.57	0.11	3.87
LPS/IL-1 Mediated Inhibition of RXR Function	4.73	0.19	2.18	/	/	/	/	/	/
Acute Phase Response Signalling	3.12	0.18	3.13	3.30	0.15	2.52	2.93	0.09	2.50
VDR/RXR Activation	/	/	/	/	/	/	1.93	0.10	2.24
Leukocyte Extravasation Signalling	2.69	0.17	3.53	/	/	/	/	/	/
ILK Signalling	2.64	0.17	2.92	/	/	/	/	/	/
Signalling by Rho Family GTPases	2.62	0.16	4.00	1.39	0.10	3.41	/	/	/
TREM1 Signalling	2.16	0.20	2.84	2.60	0.17	2.50	/	/	/
Agrin Interactions at Neuromuscular Junction	2.11	0.20	2.31	/	/	/	/	/	/
Actin Cytoskeleton Signalling	1.94	0.15	3.53	/	/	/	/	/	/
Regulation of Actin-based Motility by Rho	1.78	0.18	3.00	/	/	/	/	/	/
RhoGDI Signalling	1.74	0.15	-2.71	/	/	/	/	/	/
Neuroinflammation Signalling Pathway	1.72	0.14	2.54	1.39	0.10	2.50	/	/	/
Ceramide Signalling	1.65	0.17	2.50	/	/	/	/	/	/
Integrin Signalling	1.50	0.14	3.16	/	/	/	/	/	/
Production of Nitric Oxide and Reactive Oxygen Species in Macrophages	1.50	0.14	2.50	/	/	/	/	/	/
Tec Kinase Signalling	1.48	0.15	3.71	/	/	/	/	/	/
Colorectal Cancer Metastasis Signalling	1.42	0.14	2.48	/	/	/	/	/	/
Cardiac β-adrenergic Signalling	1.40	0.15	-2.32	/	/	/	/	/	/
RhoA Signalling	1.39	0.15	3.15	/	/	/	/	/	/
Fcγ Receptor-mediated Phagocytosis in Macrophages and Monocytes	1.36	0.16	2.84	/	/	/	/	/	/
Role of IL-17F in Allergic Inflammatory Airway Diseases	/	/	/	1.39	0.16	2.24	/	/	/
p38 MAPK Signalling	/	/	/	1.31	0.12	3.05	/	/	/
14-3-3-mediated Signalling	/	/	/	1.58	0.12	2.65	/	/	/

Figure 4.18 Ingenuity Pathway Analysis: Comparative Analysis - Signalling Pathways

Three core analyses were uploaded to IPA comparative analysis and the signalling canonical pathways were compared across the three experimental groups. Pathways were filtered for those with a p value <0.05 [-log=1.3] and z-score <-2 or >2 in one or more of the groups (n=27 unique pathways). The above table contains the calculated –log p value for ease of visual comparison, the ratio of DEGs relative to the total number of known molecules contained within the pathway and the calculated z-score for each pathway. Positive z-scores donate those predicted to be activated and negative those inhibited. Those pathways which did not achieve statistical significance are represented by a forward slash (/).

4.2.3.2 IPA: Comparative Analysis - Disease and Functions

To identify key biological and cellular processes, IPA correlated dataset DEGs to 84,770 curated gene expression lists linked to specific cellular processes termed annotations. The annotations were further grouped into 90 high-level functions that converged into three super category domains termed: Disease and Disorders, Molecular and Cellular Functions, and Physiological System Development and Function.

Statistically significant annotations ($p<0.05$ and a z-score of >2 or <-2) were filtered revealing 134 annotations in the IRI group (121 upregulated and 13 downregulated), 96 in the indirect-IPC group (13 downregulated and 83 upregulated) and 118 in the direct-IPC group (16 downregulated and 102 upregulated). Across all three groups, 192 unique annotations were identified, which grouped into thirty-one families. Seventeen of these families were from the super category of Physiological System Development and Function, and fourteen from the super category of Molecular and Cellular Function (see Figure 4.19).

Across both IPC groups there was a trend towards a reduction in significance (p value) associated with the top ranked annotations linked to the high-level function of Cell Death/Survival (IRI; p=1.03E-31, indirect-IPC; p=2.92E-27, direct-IPC; p=1.29E-20) and Cellular Movement (IRI; p=6.87E-29, indirect-IPC; p=1.86E-20, direct-IPC; p=1.95E-19). Both IPC groups further demonstrated a trend towards an increased significance of the annotations linked to Cell Cycle (IRI; p=2.15E-22, indirect-IPC; p=4.34E-24, direct-IPC; p=6.68E-30) and DNA Replication, Recombination and Repair (IRI; p=2.03E-21, indirect-IPC; p=1.3E-23, direct-IPC; p=6.68E-30). Both IPC groups had an enrichment of annotations related to the high-level function of Free Radical Scavenging (indirect-IPC; p=3.15E-08 and direct-IPC; p=6.37E-07). The high-level functions contained within the super category of Physiological System Development and Function demonstrated further trends towards reductions in significance associated with

Tissue Morphology (IRI; p=1.17E-28, indirect-IPC; p=3.63E-23, direct-IPC; p=7.01E-14), immune cell trafficking (IRI; p=3.1E-22, indirect-IPC; p=3.29E-16, direct-IPC; p=5.92E-13) and Organismal Survival (IRI; p=6.73E-22, indirect-IPC; p=1.08E-18, direct-IPC; p=9.43E-17), as shown in Figure 4.19A,B.

A total of 192 unique functional annotations were identified. For each annotation the IPA statistical outputs of p value, z-score, and number of molecules were collated and ranked by z-score. The top ten ranked annotations from each potential experimental comparison were tabulated. The IPC groups demonstrated differential regulation of several annotations relative to IRI. Both indirect-IPC (p= 7.37E-25, z= -2.15) and direct-IPC (p= 5.20 E-18, z= -2.17) were predicted to inhibit the annotation of Necrosis and activate the annotations linked to Proliferation of Epithelial Cells; indirect-IPC, p=3.29 E-10, z= 2.84 and direct-IPC, p= 5.10 E-07, z= 2.71 (see Figure 4.20).

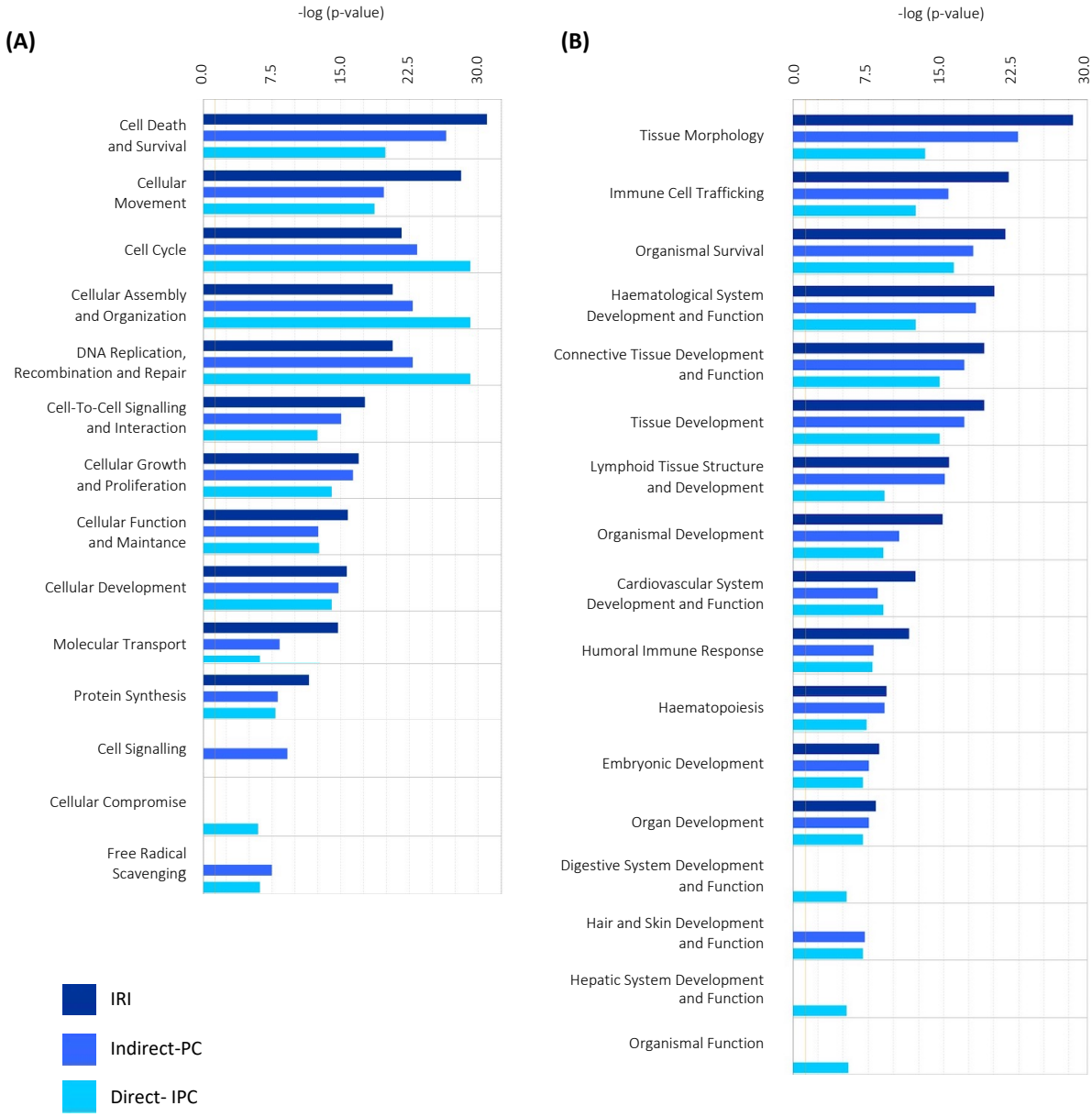

Figure 4.19 Ingenuity Pathway Analysis: Comparative Analysis - Disease and Functions

IPA functional annotations were filtered to consider only those with p<0.05 and a z-score of >2 or <-2 which grouped into the two super category domains of Molecular and Cellular Functions, and Physiological System Development and Function. A total of 192 unique annotations fulfilled these criteria across the three Core Analyses. These annotations grouped into 31 major functional families (high-level functions). **(A)** Fourteen functional families grouped into the category of Molecular and Cellular Function and **(B)** seventeen within the category of Physiological System Development and Function. The high level functions were ranked relative to the greatest overlap p value observed within the contained annotations. The remainder of the annotations link to the category of disease and function which are addressed in more detail in Figure 4.21: Tox Functions.

	IRI			IIPC			DIPC		
	p-value	z-score	Nº molecules	p-value	z-score	Nº molecules	p-value	z-score	Nº molecules
Cell viability of tumor cell lines	1.63E-09	7.22	201	7.08E-09	6.48	152	/	/	/
Cell movement of mononuclear leukocytes	1.69E-09	5.75	117	/	/	/	/	/	/
Migration of blood cells	1.75E-22	5.62	245	1.79E-16	4.69	177	/	/	/
Migration of mononuclear leukocytes	1.02E-09	5.23	97	/	/	/	/	/	/
Homing of leukocytes	1.02E-09	5.09	97	/	/	/	/	/	/
Homing of blood cells	1.53E-10	5.01	100	/	/	/	/	/	/
Cell movement of lymphocytes	2.51E-09	4.98	101	/	/	/	/	/	/
Homing of cells	1.22E-12	4.67	149	/	/	/	2.8E-08	3.37	67
Chemotaxis	1.11E-11	4.60	140	/	/	/	9.7E-08	3.51	63
Recruitment of myeloid cells	1.43E-13	3.91	83	2.26E-11	3.09	63	/	/	/
Cell death of immune cells	3.04E-11	2.63	155	8.95E-09	2.01	113	/	/	/
Advanced stage tumour	7.02E-23	2.29	270	2.57E-23	3.25	214	/	/	/
Occlusion of artery	/	/	/	/	/	/	2.5E-09	3.26	66
Glioma	/	/	/	2.61E-08	2.27	165	/	/	/
Vaso-occlusion	/	/	/	/	/	/	2.5E-10	3.26	70
Advanced lung cancer	/	/	/	2.8E-09	2.41	54	3.7E-10	2.22	39
Proliferation of epithelial cells	/	/	/	3.29E-10	2.84	97	5.1E-07	2.71	56
Vasculogenesis	/	/	/	/	/	/	1.1E-09	3.33	88
Cell death of tumour cell lines	/	/	/	5.84E-18	-2.08	279	/	/	/
Hematologic cancer	/	/	/	1.28E-14	-2.01	406	/	/	/
Necrosis	/	/	/	7.37E-25	-2.15	451	5.2E-18	-2.17	262
Lymphoreticular neoplasm	/	/	/	5.74E-13	-2.08	394	/	/	/
Lymphocytic neoplasm	4.81E-15	-2.00	382	8.44E-15	-2.59	291	2.1E-08	-2.07	159
Neoplasia of leukocytes	6.45E-15	-2.00	384	1.4E-14	-2.59	292	2.2E-08	-2.07	160
Lymphoma	6.15E-13	-2.00	361	1.1E-12	-2.59	274	6.3E-07	-2.07	148
Transport of ion	1.25E-14	-2.01	126	/	/	/	/	/	/
Skin tumour	2.64E-22	-2.01	1168	1.86E-13	-1.04	823	/	/	/
Development of respiratory system tumour	1.39E-13	-2.25	270	/	/	/	/	/	/
Development of lung tumour	2.1E-13	-2.44	269	/	/	/	4.3E-10	-2.01	122
Transport of cation	3.11E-11	-2.47	97	/	/	/	/	/	/
Parasitic Infection	1.13E-10	-2.68	55	/	/	/	/	/	/
Infection of mammalia	5.46E-17	-3.13	102	/	/	/	6.5E-13	-2.59	52
Hereditary connective tissue disorder	5.59E-12	-3.40	133	4.78E-08	-2.77	93	/	/	/
Cell death of sarcoma cell lines	/	/	/	/	/	/	6.7E-08	-2.45	33
Quantity of mitotic spindle	/	/	/	/	/	/	7E-08	-2.18	9
Congenital malformation of genitourinary system	/	/	/	/	/	/	3.9E-07	-2.45	47
Invasion of breast cancer cell lines	/	/	/	/	/	/	4.6E-07	3.33	38
Apoptosis of cervical cancer cell lines	/	/	/	/	/	/	8E-07	-2.50	37
Cell movement of breast cancer cell lines	/	/	/	/	/	/	9.8E-07	3.25	40
Bleeding	/	/	/	/	/	/	1.1E-06	-4.50	49
Migration of breast cancer cell lines	/	/	/	/	/	/	1.6E-06	3.49	35
Visceral metastasis	/	/	/	4.52E-09	2.37	44	6.3E-08	2.24	29
Development of sarcoma	/	/	/	5.53E-08	-2.36	57	8.5E-07	-2.01	36
Tensile strength of skin	/	/	/	8.57E-08	3.11	11	/	/	/
Cytokinesis	/	/	/	9.87E-08	3.63	40	2.4E-08	3.18	29
Checkpoint control	/	/	/	3.23E-09	2.15	28	/	/	/

Figure 4.20 Ingenuity Pathway Analysis: Comparative Analysis - Differences between Disease and Biological Functions

The functional annotations contained within each of the IRI, indirect-IPC and direct-IPC core analyses were filtered to identify the annotations with a $p<0.05$ and a z-score of >2 or <-2. The total number significant annotations was IRI, 133; indirect-IPC, 96; and direct-IPC, 119. A total of 46 unique annotations were collated. The annotations were compared across all possible group comparisons (n=9). The top ranked annotations with the greatest z-score difference between them were collated from each possible group comparisons (to a maximum of 10).

The p value, z-score and total number of molecules within each group's dataset linking to the annotation data are displayed in the above table. Those annotations which did not fulfil the cut-off for significance are represented by a forward slash (/).

4.2.3.3 IPA: Tox Functions and Tox Lists

IPA Tox Functions used the gene expression dataset to link to Clinical Pathology endpoints and predict phenotype conferred by the differentially expressed mRNA transcripts profiles. The high-level functions contained within the tox functions were ranked by p value and the principal 10 ranked tox functions were tabulated (Figure 4.21A). The top ranked function was Renal Damage. Following IRI, the significance associated and number of DEGs contained within the function of Renal Damage (p=5.42E-26, DEGs=94) were reduced in the indirect-IPC group (p=1.82E-23, DEGs= 77) and further reduced following direct-IPC (p=3.19E-09, DEGs=38).

Expanding the annotations within the high-level function of Renal Damage revealed differential activation state (z-score) of the functional annotations following IPC compared to that of IRI (Figure 4.21B). The differential activation of annotations was more significant in the direct-IPC group than the indirect-IPC group. The top ranked differences between annotations were that of a reduction in the activation state of the annotation of Injury of Renal Tubule and a shift towards favourable inhibition of the annotation representing Apoptosis of Tubular Cells. Further shifts in activation states of significant annotations was predicted in those representing Failure of the Kidney, Cell Death of Renal Tubular Epithelial Cells and Necrosis of Renal Tubule.

IPA knowledge base further grouped pre-defined gene sets that functionally grouped to describe a critical biological process that results from a xenobiotic insult. The top ten ranked (p-value) Tox List linked to the biological process observed in the dataset is that of Acute Renal Failure Panel (Rat), Renal Proximal Tubule Toxicity Biomarker Panel (Rat) and Renal Necrosis/Cell Death (Figure 4.22). The statistical significance and number of DEGs contained within each list is reduced following IPC, but more pronounced following direct-IPC. Within the gene set of Acute Renal Failure Panel (Rat), IRI linked to 42 genes (p=1.0E-27;

DEGs:panel=0.68). In the indirect-IPC group, the significance reduced (p=5.01E-23; DEGs=34; DEGs:panel=0.55) and further still in the direct-IPC group (p=1.25E-20, DEGs=26; DEGs:panel=0.42). The genes making up this panel and the change in their expression levels is shown in Appendix 4. An identical pattern of reduced statistical significance and number of significant DEGs associated with the Tox List was observed in Renal Proximal Tubule Toxicity Biomarker Panel, IRI (p=4.0E-15, DEGs=20); indirect-IPC (p=1.3E-13, DEGs=17) and direct-IPC (p=5.4E-04, DEGs=6) and Renal Necrosis/Cell Death, IRI (p=2.5E-12, DEGs=109); indirect-IPC (p=4.0E-11, DEGs=84) and direct-IPC (p=4.0E-03, DEGs=35).

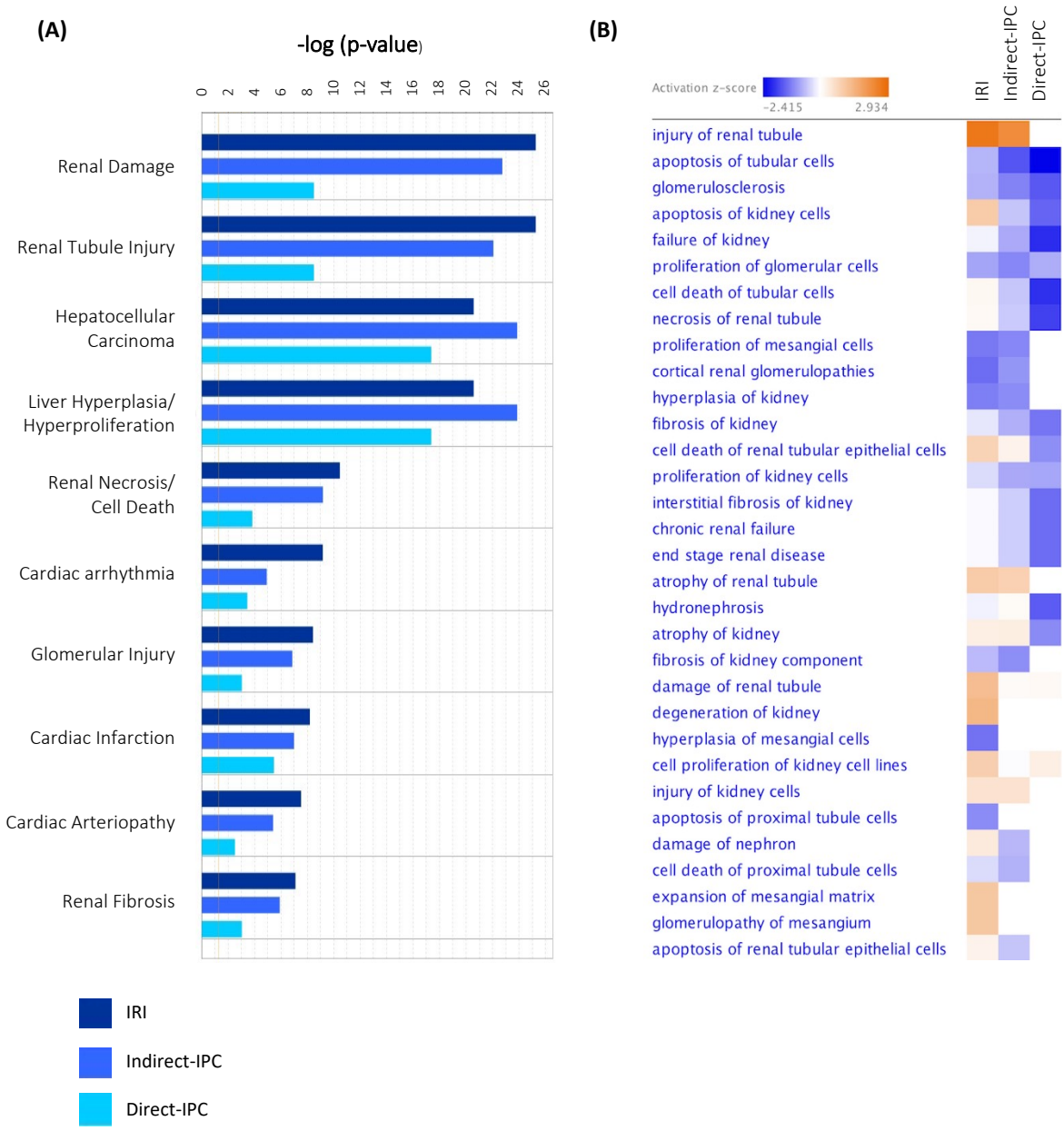

Figure 4.21 Ingenuity Pathway Analysis: Comparative Analysis - Tox Functions

(A) The top ten high-level functions ranked by p value of the IRI dataset are presented graphically. **(B)** The annotations which were used to rank the top ranked high-level function of renal damage are displayed. The annotations contained within the high level function of renal damage are displayed as a coloured z-score. The darker the blue the greater the negative z-score and the darker the orange the greater the positive z-score.

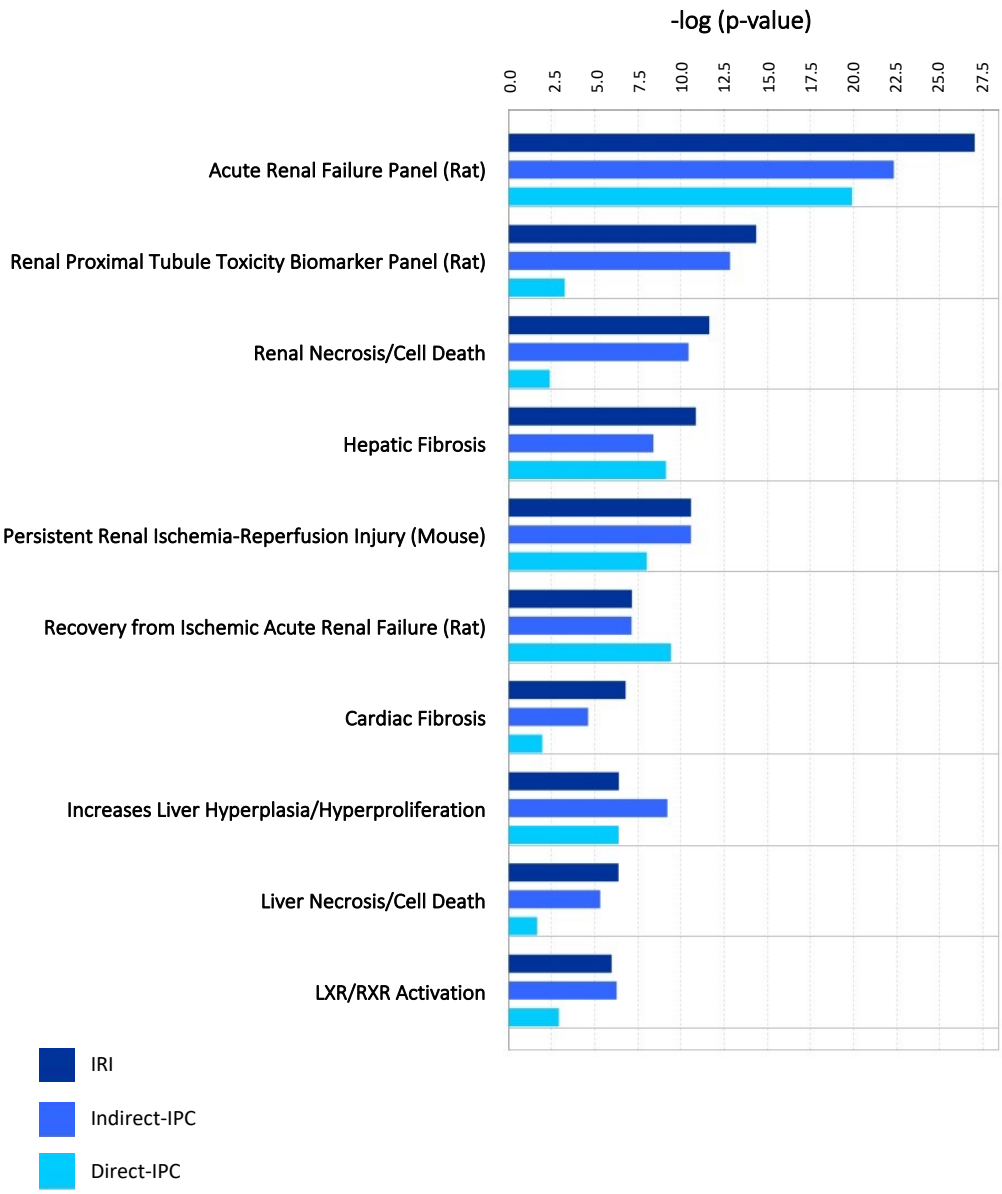

Figure 4.22 Ingenuity Pathway Analysis: Comparative Analysis - Tox Lists of the IRI Dataset

IPA Tox Lists are pre-defined gene sets that are functionally grouped and describe critical biological processes that result from a xenobiotic insult. The analysis predicted toxicity outcomes from a treatment interventions.

The plot demonstrates the Tox Lists ranked by p value and grouped according to biological function and/or organ. Filtering for those with a corrected $p<0.05$ in more than one group, the top ten ranked tox lists are graphically represented above and displayed in p-value rank order.

4.3 Discussion

4.3.1 Transcriptional response to IRI

Many complex molecular and immunological pathways contribute to the pathophysiology of IRI, but how their pathways synergise to confer the injury phenotype remains uncharacterised. In this Chapter, IRI response pathways were compared to sham using a blinded, unbiased analysis, to identify the transcriptomic fingerprint of renal IRI. Pathway analysis revealed an enrichment of DEGs linked to cytokines, nuclear signalling, ECM and cytoskeleton, and immune response. This discussion will explore these areas in the context of the literature, and discuss the principal renal phenotype: injury of the renal tubule.

4.3.1.1 Cytokines

Pathway analysis of the IRI dataset identified a significant cytokine response and upregulation of pro-inflammatory cytokines IL-1β, TGFβ1, TNFα, IL-6, IFN-γ, and granulocyte-macrophage colony-stimulating factor (GM-CSF). In concordance with this cytokine signal, the signalling pathways TREM1 and Tec Kinase were significantly dysregulated following IRI. TREM1 signalling is important to the amplification of TLR4 signalling and production of pro-inflammatory cytokines[352]. However, inhibiting TREM1 signalling in renal IRI reduces cytokine production but does not prevent renal injury[353], which may suggest that synergistic pathways promote injury. Interestingly, the Tec kinase signalling family are a group of five nonreceptor tyrosine kinases thought to be key components in intracellular signalling of cytokines: TEC, BMX, BTK, ITK and TXK[354]. Tec family signalling has been implicated in ischaemic cardiac signalling[355], proinflammatory macrophage function in diabetic nephropathy[356], and a recent study in sepsis induced AKI reported that Tec inhibition alleviates AKI by augmenting

TLR4/MyD88/NFκB signalling pathway[357]. How these signalling pathways synergise in IRI is unknown, and future inhibition of their pathways may benefit from dual targeting.

4.3.1.2 Nuclear Signalling

Pathway analysis revealed a significant dysregulation of retinoid nuclear pathways. The retinoid X receptor (RXR)/liver X receptor (LXR) pathway was inhibited by IRI. It is unknown if LXR activation improves IRI injury[358], but Yang et al. (2015) showed that LXR agonists ameliorates inflammatory response in a cisplatin-induced AKI model[359], possibly through inhibition of NFκB[360]. Moreover, IRI activates the LPS/IL-1-mediated inhibition of retinoid protective X factor (RXR) pathway, which reduces transcription of the antioxidant enzymes catalase (CAT) and superoxide dismutase (SOD), propagating ROS injury. Oxidative stress is a significant factor in the pathogenesis of renal IRI[361; 362] and other organs[363]. Indeed, the xanthine oxidase inhibitor allopurinol can inhibit ROS formation and ameliorate renal IRI[364], but the ROS scavenger N-acetyl cysteine has failed to prevent contrast-induced nephropathy in human trials[365]. It is therefore possible that in renal IRI the differential regulation of retinoid pathways is beyond ROS, and its importance lie within transcriptional regulation[358]. Therefore, the direct targeting of LXR and RXR using agonists may have a role in renal IRI which has not been described.

4.3.1.3 ECM and Cytoskeleton

Pathway analysis of the dataset revealed an enrichment of ECM and cytoskeleton signalling pathways following IRI. Indeed, integrin, ILK and Rho signalling was upregulated by IRI, suggesting the importance of intermediate signalling pathways in ECM and cytoskeleton

cross talk following IRI. The role of ECM/cytoskeletal signalling in transmission of structural stress, cell migration and the maladaptive repair process in CKD is well established[366-368]. Interestingly, there is emerging evidence of the role of ECM/cytoskeleton and their intermediate signalling pathways in AKI. McCurley et al. (2017) demonstrated that blocking integrin attenuates IRI by modulating vascular leak[369]. Surprisingly, Cano-Penalver et al. (2016) demonstrated ILK-depletion protects from cisplatin-induced AKI in mice[370] and Prakash et al. (2008) reduced IRI injury through Rho inhibition[371]. The role of the ECM and cytoskeleton in fibrosis is well established, but their dysregulation in acute IRI and targeting as a preventative AKI approach may be of profound benefit.

4.3.1.4 Immune Response

IRI generated a significant inflammatory response evidenced by pathway activation of Leukocyte Extravasation, Agranulocyte Adhesion and Diapedesis, and Fcy Receptor-mediated Phagocytes in Macrophages and Monocytes pathways in IRI. Indeed, the top ranked REN of the dataset was comprised of functions related to leucocyte trafficking which connected to eight principal regulators of the phenotype: NOD2, PTPN6, TLR4, TLR5, TLR7, RIPK2, CD14 and TNF receptor-associated factor 6 (TRAF6) (see Figure 4.13). Other researchers in renal IRI transcriptomics have reported the importance of PRRs, NOD2 and TLR4 in renal IRI[372] and the network analysis in this Chapter corroborated their role in leucocyte trafficking and cytokine dysregulation in renal IRI. The network further revealed the importance of TRAF6 networking with TLR4, which activates NF-κB[373] via the TLR4/MyD88 signalling cascade[374]. TRAF6 targeting has recently been a focus of interest in analysis of septic models of AKI[375] and renal IRI[376].

The role of TLR5 and TLR7 in renal IRI, and their crosstalk with TLR4, is an interesting finding in the analysis in this Chapter. TLR5 is expressed on epithelial and immune cells[377], and its natural ligand is the bacterial structural protein, flagellin, which triggers the innate immune response[378]. Recently TLR5 has been implicated in lupus nephritis[379] and diabetic nephropathy[380], possibly acting via a MYD88-dependent pathway. Fukuzama et al. (2011) first described that the administration of TLR5 agonists, prior to IRI, improved sCr and inhibited neutrophil infiltration of the kidney[381]. These researchers' findings suggests that activation of TLR5 protective factors may be confined to its administration prior to IRI in a manner like IPC. In contrast, TLR7 is expressed on the membrane of endosomes, e.g., lysosomes and endoplasmic reticulum[382], and recognises ligands of single-stranded RNA from viruses[383]. TLR7 importance in renal disease has recently been identified. Huang et al (2017) demonstrated that TLR7 is increased following IRI and enhances the expression of pro-inflammatory cytokines in IRI[384], while TLR7 inhibition attenuates IRI injury in diabetic rats[385]. Recently it has been shown that in mice models of kidney fibrosis, TLR7 KO mice demonstrated reduced inflammation and immune cell infiltration[386]. The finding that both TLR5 and TLR7 feature as principal regulators of an injury phenotype in IRI has not been described. Furthermore, their exact roles have not been described fully in renal IRI, where they may act via cross talk with TLR4[387; 388].

The transcriptomic analysis was carried out on whole kidney tissue, therefore proportions of the transcriptional inflammatory fingerprint will be contributed by renal tissue, resident, and trafficked leucocytes. While IPA has computationally linked the transcriptional profile to leucocyte trafficking and not to another cellular pathway, is not possible from the data to assign DEGs to renal tissue and/or trafficked leucocytes. Going forward, this could be investigated further by cell sorting and single cell sequencing to differentiate which DEG is

related to which cell subtype(s), adding granular detail to findings from analyses exploring IRI in the context of the whole tissue and the complex interaction between cell types.

4.3.1.5 Renal Tubule Injury Network

The transcriptional fingerprint in this work has alluded to the complex interplay of many molecular processes to confer the renal IRI phenotype. To connect these processes, the REN computational analysis identified ten upstream regulators; IL-1α, NF-κB, TLR4, macrophage migration inhibitory factor (MIF), IL-2, IFNG, oncostatin-M (OSM), HIF-1A, IL-1β and PI3K, directly or indirectly targeted F2RL1, TLR2, CCL2, ICAM-1, C-C chemokine receptor type 1 (CCR1), CAT and Fucosyltransferase type 7 (FUT7), which are predicted to network together to result in the Injury of the Renal Tuble phenotype (see Figure 4.15).

Pre-clinical work in IL-1α/β KO mice demonstrated reduced acute tubular necrosis following IRI histologically[389] and the use of an IL-1 receptor antagonist reduced inflammation, apoptosis, and leucocyte infiltration in renal IRI *in vivo*[389]. A recent phase 2 clinical trial of an anti-IL-1β monoclonal antibody gevokizumab in diabetic kidney disease was designed, but withdrawn due to funding constraints[390] and may be an interesting drug to test in AKI given the importance of IL-1 to Renal Tubule Injury. It is well established that the PRRs, TLR2 and TLR4 are important in IRI. Both TLR2[391] and TLR4[392] knockout mice are resistant to IRI, while the inhibition of TRL2[393] and TLR4[394] can ameliorate IRI through the inhibition of cytokine transcription and synthesis of selectin ligands required for leucocyte trafficking[395]. The network revealed interesting novel molecules which are important in renal leucocyte trafficking. Indeed, inhibition of the enzyme FUT-7, which is required for the synthesis of selectin ligands, attenuates monocyte adhesion[393] and is under intense research in cancer therapy due to its potential to regulate tumour cell invasion[396]. Interestingly, the chemokine

CCR1 has been shown to increase leucocyte recruitment, but in a recent study which tested both a mouse CCR1 knockout and pre-treatment with CCR1 antagonist BX471, demonstrated that CCR1 promotes the accumulation of macrophages and neutrophils in IRI, but failed to attenuate the injury leading the authors to postulate that CCR1 alone is not sufficient to stop IRI[397]. The simultaneous targeting of multiple regulators at once may prove therefore more effective.

The network activation of upstream regulators MIF and P13K is noteworthy. MIF is released by injured epithelial cells and binds to the CD74 transmembrane receptor activating pro-survival pathways possibly through P13K-Akt signalling[398]. Indeed, Li et al. (2019), recently demonstrated that MIF knockout mice are protected from renal IRI[399], and targeting MIF ablates cisplatin-induced AKI[400]. It has been suggested that P13K signalling via the RISK pathway may have an important role in IPC. However, P13K is a diverse enzyme family grouped into 3 classes. P13Kγ class 1 may have an inflammatory component which triggers leucocyte recruitment and cytokine release exacerbating IRI[401], while other studies have alluded to the protective effect of P13K activation[402; 403]. Determining the role of MIF signalling and differing P13K class activation may provide a greater depth of understanding in the pathophysiology of IRI.

4.3.2 Response Pathways of IPC

To date, the transcriptional response pathways of IPC in two different mechanical IPC techniques have not been described. Phenotypically, both indirect and direct-IPC were seen to reduce pathological endpoints of renal damage and renal tubular injury. Indeed, the functional annotations of apoptosis of kidney cells, and cell death of renal tubular epithelial cells were inhibited by IPC. IPC further attenuated the functional phenotypes of Necrosis of the Renal

Tubule and Interstial Fibrous of the Kidney. In concordance with the functional and histological findings in Chapter 3, direct-IPC was found to inhibit the IRI response pathways to a greater extent.

IRI was shown to activate functions related to the Cell Movement of Mononuclear Leucocytes and Homing of Leucocytes. Indeed, successful leucocyte trafficking requires multiple complex molecular processes that include, intracellular signalling of injury, cytokine expression and ECM/cytoskeletal signalling. Both IPC techniques quashed integrin receptor ILK and actin signalling, and prevented the activation of leucocyte extravasation signalling which was shown to be critical to the IRI transcriptional phenotype. Indeed, leucocyte trafficking following renal reperfusion is an important hallmark of IRI[404], and prevention of leucocyte chemotaxis by ICAM-1 inhibition[405] or macrophages migration by inhibition of CCR2[406] has been shown to improve postischaemic renal function. Both direct- and indirect-IPC suppressed biological functions related to migration of mononuclear leucocytes. Investigative work in renal transplantation has demonstrated the benefit of leucocyte depletion in improving function following reperfusion[407], but does not completely prevent injury adding weight to the multifaceted molecular approach that IPC affords protection

Interestingly, both IPC groups were predicted to prevent the dysregulation of retinoid metabolic response pathways which were found in the IRI analysis. Indeed, IRI was shown to significantly downregulate the expression of antioxidant enzymes CAT, and SOD, through the inhibition of the nuclear RXR function. Indeed, LPS/IL-1-Mediated Inhibition of RXR Function and LXR/RXR Activation pathways were normalised by IPC. Antioxidant inhibition is well established in IRI[408], while remote- [409] and direct-IPC increase antioxidant formation[410]. Johnsen et al. (2020) carried out RNA sequencing analysis in caloric restriction and hypoxic preconditioning in renal IRI, and demonstrated a significant mitochondrial signature which

they contributed to ROS defence[306]. However, the true role of RXR normalisation by preconditioning may lie in transcriptional regulation of IL-1β and TNF-α[411].The analysis in this Chapter of two different IPC methods concurs with Johnsen et al. (2020) that IPC shares common response pathways which may be shared by other preconditioning strategies[306].

Although both IPC groups demonstrated shared response pathways there were some differences. Direct-IPC was predicted to activate the Vitamin D Receptor (VDR)/RXR pathway, which has been shown to be involved in transcriptional regulation of immune function. Interestingly, VDR agonists can attenuate progression of diabetic nephropathy[412] and renal IRI[413], possibly through the regulation of oxidative[414] and inflammatory pathways[415]. Indirect-IPC uniquely activated 14-3-3-mediated signalling, which has been shown to be important in diverse roles such as renal tubular epithelial repair in CKD[416] and programmed cell death[417]. In IPC, 14-3-3 appears to be important in protection from ischemic stroke[418]. The role of these pathways in renal IPC has not been described, and their differential activation in direct- vs indirect-IPC is an interesting area for future research.

Comparative analysis of indirect- and direct-IPC has shown similar transcriptomic and network effects which strongly support their common mechanisms of action. Indeed, this analysis has demonstrated multiple different mechanisms via which IPC may benefit the kidney, including the prevention of leukocyte trafficking, reducing cellular necrosis, and activating the proliferation of epithelial cells. Interestingly, there were differences between direct- and indirect-IPC which will be interesting targets for future research. In summary, this work has defined a transcriptional signature of the protected kidney in reference to IRI and revealed the transcriptional response pathways of IPC.

The principal findings of this Chapter are:

1. The experiments described in Chapter 3 have generated an in-depth, high-quality bulk RNA sequencing dataset. Bioinformatic analysis demonstrated clustering of replicates by experimental groups and predicted magnitude of injury in accordance with what was observed histologically and functionally.
2. Unbiased pathway analysis can successfully infer the starting experimental phenotype. Computational analysis of the IRI dataset has revealed several upstream regulators that directly and indirectly influence the dataset molecules to lead to the dataset top ranked phenotype of injury of the renal tubule.
3. Transcriptionally, IPC ameliorates renal damage by reducing proinflammatory response pathways resulting from IRI. IPC inhibits both the necrosis of the renal tubule and cell death of tubular cells. In concordance with observations in Chapter 3, direct-2/5[3] IPC inhibits IRI response pathways more effectively than indirect-2/5[3] IPC.

4.4 Concluding Remarks

The work presented in this Chapter has characterised the IRI transcriptional fingerprint and response pathways conferred by IPC. The transcriptional analysis has revealed multiple regulators involved in the injury phenotype of the IRI dataset. Indeed, the IPC response pathways have been shown to reduce the IRI phenotype.

While the individual targeting of each upstream regulator may have the potential to ameliorate IRI, the sum of their synergistic targeting may be of greater benefit. The work undertaken in Chapter 5 will utilise genomic data and computational *in silico* analysis to hypothesise drugs with "genomic anti-similarity," to the IRI phenotype. Furthermore, Chapter

5 will aim to compare the transcriptional targets of candidate drugs to the expression profile of IPC.

Chapter 5

Computational Prediction of Drug Repurposing Targets

5.1 Introduction

In the previous Chapters, bilateral IRI was found to be a reliable and non-fatal method to induce renal injury in the rat kidney. Using an RNA-sequencing-based unbiased transcriptional approach, a total of 2,696 DEGs were identified in comparison to sham animals. IPA transcriptome pathway analysis revealed a post-IRI phenotype of nephrotoxicity and renal tubule injury originating from a complex network of functional annotations related to leucocyte trafficking, cytokines, and ECM and cytoskeletal signalling.

To explore the therapeutic potential of IPC to ameliorate IRI, six different protocols were tested. Of these, pulsatile direct- and indirect-IPC had the greatest therapeutic potential to reduce IRI. Transcriptional analysis showed that indirect- and direct IPC reduced the number of DEGs relative to sham (2,025 and 1,060, respectively). IPA of the RNA sequencing dataset identified response pathways of direct- and indirect-IPC to IRI: both IPC methods reduced the critical pathological endpoints of renal damage and renal tubular injury. Indeed, the work presented in this thesis supports the hypothesis that IPC works across multiple networks to exert its therapeutic effect, and that both direct- and indirect-IPC share common response pathways to prevent renal injury.

To date, the therapeutic application of IPC in humans has been hampered by the heterogeneity of the populations analysed, and current research suggests the therapeutic effect of IPC may be negated in people with diabetes[419; 289], the elderly population[291] and males[194]. One alternative to mechanical IPC is the use of a pharmacological agent that can mimic the effects of this process, and which can be dose-adjusted to meet patient needs.

Traditional research into therapeutic targets for disease relies upon an in-depth knowledge of a singular biological mechanism. This traditional method of drug discovery is arduous, taking on average 15 years and costing over $1.3 billion to research, develop and

bring a new drug to market[420]. There is significant evidence that several established drugs may be beneficial in other disease states. The successful recycling of drugs, termed "drug repurposing," has been highly effective in such cases as sildenafil which was originally identified to treat angina, but is now successfully used in erectile dysfunction, pulmonary arterial hypertension and digital ulcers[421].

Researchers in the field of drug repurposing have posited that comparing diseased genome (e.g., cancer cells) to drug genome, (e.g., non-cancer cells treated with a drug) and ranking the degree of "genomic anti-similarity," may yield novel drug candidates for disease treatment [422; 423]. The successful application of this method was accomplished by Dudley et al. (2011), who investigated novel therapeutic options for inflammatory bowel disease (IBD) by comparting the genomic signature of IBD to that of an array of drugs. The computational work and rodent model validated Topiramate, a drug used as an anticonvulsant in epilepsy as a novel therapeutic option for IBD[424]. Similar work by Sirota et al. (2011) demonstrated the effectiveness of computational genomic analysis to identify novel therapeutic indications for the established drug compound Cimetidine (a stomach acid suppressant) for the treatment of lung adenocarcinoma[425].

The work undertaken in this final Chapter utilised genomic data and computational analysis to identify drugs that shared "genomic anti-similarity," to the disease process of IRI. Furthermore, this work compared the transcriptional targets of candidate drugs to the expression profile of IPC with the aim of identifying novel agents which could be investigated further for therapeutic application.

The sets of experiments described in this Chapter aimed to:

1. Identify *in silico* chemicals predicted to oppose the transcriptional signature of IRI: drug repurposing
2. Quantify the levels of evidence that the chemicals identified in 1. had the potential to reverse the injury phenotype in concordance with the transcriptional signal of IPC: candidate drug concordance
3. Test candidate agents *in vivo*

5.2 Results

Data from IPA *in silico* analysis was used for computational prediction of compounds that would act as upstream regulators to influence the downstream dataset and attenuate the IRI phenotype. To test concordance with the IPC response pathways, the effects of the predicted upstream regulator compound and phenotype targets were compared *in silico*. Of the two IPC methods tested in this thesis, functional, histological, and transcriptional reduction of IRI effects was greatest with direct-IPC and this was therefore used as the comparison for compound transcriptional targets.

5.2.1 Computational Drug Repurposing Workflow

The IPA *in silico* platform was used to build connections between the dataset molecules, predicted upstream regulators and their downstream disease or biological phenotype, using an algorithm called the regulatory effect network (REN). The REN can be grown to identify compounds with known transcriptional targets opposite to those in the IRI transcriptional signature, "anti-correlation," and would therefore be predicted to reduce the effects of IRI. At the time of use for this study, the IPA knowledge base contained the known transcriptional targets of 2,000 compounds.

The initial aim of the workflow was to identify compounds predicted to elicit the opposite activation or inhibition states of the DEGs following IRI, in concordance with the predicted phenotype of the dataset. To build a computational prediction of compounds of interest, the REN algorithm was set to predict compounds whose absence as an upstream regulator would mirror the above dataset expression changes and the downstream phenotype. The algorithm was set to examine compounds as a regulator of function with a significance cut

off as p<0.001 and z score >2 or <-2. The phenotype of the dataset was set to include no limit on the number of phenotypes with a significance of p<0.001 and z= >2 or <-2, Figure 5.1.

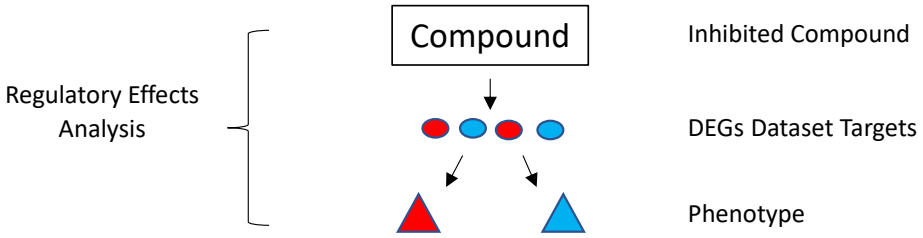

Figure 5.1 Computational Drug Repurposing Workflow: Compound Identification

The core analysis undertaken between IRI and Sham was investigated for compounds from the IPA knowledge base predicted to reverse the dataset expression and attenuate injury phenotype.

The IPA REN algorithm was set to identify upstream regulator compounds with significance as a regulator of function of p<0.001 and z score >2 or <-2. Functions of the dataset were set to include no limit to the number of phenotypes and consider only those with a p<0.001 and z score >2 or <-2 significant.

5.2.2 Computational Drug Repurposing: Compound Identification

The REN algorithm was set to identify connections between compounds from the IPA knowledge base, dataset molecules and phenotype. The compound networks predicted to be significant were ranked by consistency score (correlation) and examined to consider those with a score >5 (positive correlation) or <-5 (anti-correlation).

Twenty-seven compounds were predicted to have a positive consistency score and a directional expression with respect to the IRI dataset that was mirrored by its predicted genomic signature. A positive score indicates that the compound shares an expression signal similar to the IRI dataset suggesting that the compound may share a common transcriptional fingerprint and phenotype to that of IRI, Figure 5.2. Of these, the top seven ranked compunds by consistency score was Escherichia coli lipopolysaccharide (16.837), Ni2+ (10.583),

Salmonella minnesota R595 lipopolysaccharides (10.000), Ionomycin (9.807), 2-bromoethylamine (7.778), fenamic acid (7.778) and gentamicin C (7.778) which are well established induces of AKI. A full list of the upstream regulators predicted to be targeted by these twenty-seven compounds is shown in Figure 5.3.

A further seven compounds were computational predicted to have an anti-correlation to the IRI signature, with consistency score ranking of: pyrrolidine dithiocarbamate (14.711), AG490 (11.068), pirfenidone (8.165), U0126 (8.033), SP600125 (6.822), Diphenyleneiodonium (6.633) and Sn50 peptide (5.292) (Figure 5.2). IPA was used to identify the number of upstream regulator targets for each compound. For example, pirfenidone was predicted to exert a directional expression change on six upstream regulators resulting in a functional change of Cell Proliferation of Tumour Cell Lines, Invasion of Cells, Leukocyte Migration, Migration of Tumour Cell Lines, Quantity of Cells, and Recruitment of Blood Cells. A complete breakdown of the number of upstream regulators and functional targets of each chemical is described Figure 5.4. The upstream regulators predicted to be targeted by the anti-correlation compounds to the IRI signature is explored further in section, 5.2.3 Computational Drug Repurposing Workflow- IPC Comparison, and Appendix 5-16.

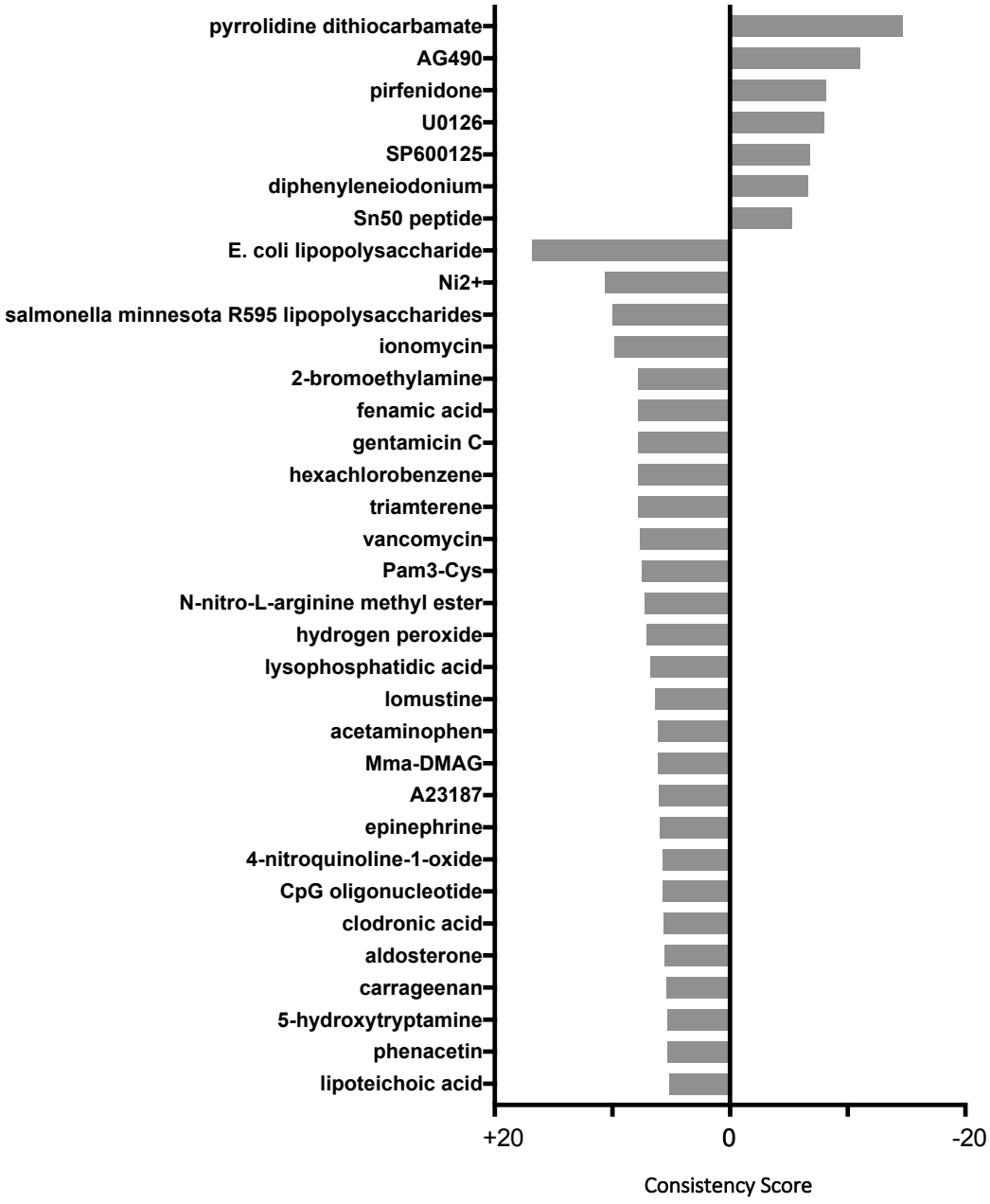

Figure 5.2 Computational Drug Repurposing: Compound Prediction

The networks ranked by consistency score are displaced. Those compounds with a +ve consistency score are computationally predicted to be consistent with the DEGs of the dataset and phenotype (+ve range 16.837 – 5.196). Those with a negative consistency score are those compounds which if administered in the experiment would differentially regulate the DEGs and phenotype in a manor apposed to the observed state (-ve range 14.711 – 5.292).

Regulators	Consistency Score	Target Molecules in Dataset
E. coli lipopolysaccharide	16.837	CCL2, Ccl2, CCR7, CD80, CXCL10, CXCL2, CXCL6, ICAM1, IL23A, S100A8, S100A9, SELE, TGFB1, TREM1
Ni2+	10.583	ANGPTL4, CCL2, CCL20, CSF1, CXCL2, CXCL6, ICAM1
Salmonella minnesota R595 lipopolysaccharides	10	AXL, CCL2, Ccl2, CCL20, CEBPD, CXCL10, CXCL2, CXCL6, EGR1, FOS, FOSL1, ICAM1, NFKB2, SERPINE1, SOCS3, TLR2
Ionomycin	9.807	AHNAK, BCL2A1, BDNF, BTK, CASP3, CD69, CLDN4, CXCL10, DNMT1, EGR1, FOS, ICAM1, ITGAL, ITPR3, KCNN4, LDLR, MYC, NFIL3, POU2AF1, SPP1, TGFB1, TLR2
2-bromoethylamine	7.778	ANXA1, CD14, CD44, LCN2, LGALS3, MRC1, MYC, VIM
Fenamic acid	7.778	ANXA1, CD14, CD44, LCN2, LGALS3, MRC1, MYC, VIM
Gentamicin C	7.778	ANXA1, CD14, CD44, LCN2, LGALS3, MRC1, MYC, VIM
Hexachlorobenzene	7.778	ANXA1, CD14, CD44, LCN2, LGALS3, MRC1, MYC, VIM
Triamterene	7.778	ANXA1, CD14, CD44, LCN2, LGALS3, MRC1, MYC, VIM
Vancomycin	7.667	ANXA1, CAT, CD14, CD44, LCN2, LGALS3, MRC1, MYC, VIM
Pam3-Cys	7.488	CCL2, Ccl2, CD14, CD69, CXCL10, CXCL2, IL1RL1, IL1RN, SELE, SELP, SERPINE1, TLR2, TNC
N-nitro-L-arginine methyl ester	7.273	CCL2, Ccl2, CSF1, CXCL2, FN1, ICAM1, SELE, SERPINE1, TGFB1, TLR2
Hydrogen peroxide	7.089	AGT, ANXA2, CCL2, Ccl2, CD80, CDKN1A, COL1A1, CSF1, CSF3R, CXCL6, ELN, F2RL1, FAS, FN1, FOS, ICAM1, LCN2, LDLR, MYC, NFIL3, PLAUR, SERPINE1, SPP1
Lysophosphatidic acid	6.791	ACTA2, CCL2, Ccl2, CSF1, CXCL10, CXCL2, EGR1, FOS, ICAM1, KLF5, LIF, MYC, PLAUR, SCARB1, SERPINE1, SNAI1, VIM
lomustine	6.332	ANXA1, ANXA2, CD14, CD44, LCN2, LGALS3, MYC, RBM3, TGIF1, TIMP1, VIM
Acetaminophen	6.25	BIRC5, CASP3, CCNB1, CCNE1, CD44, CDK1, CDK6, CDKN1A, EGR1, FN1, IGFBP3, MMP2, MYC, PLAUR, SNAI1, VIM
Mma-DMAG	6.124	CCL2, CCR7, CD44, CXCL10, CXCL2, ICAM1
A23187	6.01	ATF3, CD80, EGR1, FN1, FOS, ICAM1, MYC, TLR2
Epinephrine	6	IL23A, IL33, SELL, TLR5
4-nitroquinoline-1-oxide	5.692	AURKA, AURKB, CCNA2, CCNB1, CCNB2, CCNE1, CDK1, CDK6, CDKN1A, EGR1
CpG oligonucleotide	5.692	CCR1, CXCL10, CXCL2, FAS, ICAM1, IL23A, IL33, SDC1, SERPINE1, TLR2
Clodronic acid	5.657	CXCL10, ICAM1, MFGE8, MRC1, MSR1, SELE, SELP, TGFB1
Aldosterone	5.59	ACTA1, AGT, BDNF, CCL2, Ccl2, COL1A1, ELN, FN1, FOS, HAS2, ICAM1, LOX, mir-21, MMP2, PIK3CD, PLAUR, PROCR, SERPINE1, SPP1, TGFB1
Carrageenan	5.427	Ccl2, CXCL2, EGR1, EGR2, F2RL1, FOS, FOSB, FOSL1, FOSL2, ICAM1, SELP
5-hydroxytryptamine	5.303	CCL2, FOS, ICAM1, MYC, SERPINE1, STAB1, TGFB1, TNFRSF1A
Phenacetin	5.292	ANXA1, CD44, LCN2, LGALS3, MRC1, MYC, VIM
Lipoteichoic acid	5.196	CD14, CXCL10, TLR2

Figure 5.3 Computational Drug Repurposing: Compounds with a Positive Consistency Score

In total twenty-seven compunds were predicted to have a positive consistency score. These compounds were predicted by the REN algorithm to have a mirrored genomic signature to the directional expression change of the IRI dataset. A full list of the upstream regulators predicted to be targeted by the compound are displayed.

Compound Agent	Consistency Score	Number of Transcriptional Targets			Functions
		IPA Knowledge Base	IRI dataset	Upstream regulator targets in network	
Pyrrolidine Dithiocarbamate	14.711	148	99	24	Atherosclerosis Cell movement of mononuclear leukocytes Cell movement of Tumour Cell Lines Chemotaxis Inflammatory Response Quantity of Lymphoid Cells Aggregation of Cells
AG490	11.068	141	91	13	Activation of Myeloid Cells Adhesion of Blood Cells Binding of Leucocytes Recruitment of Leucocytes Failure of Heart Quantity of metal
Pirfenidone	8.165	25	16	6	Cell Proliferation of Tumour Cell Lines Invasion of Cells Leukocyte Migration Migration of tumour cell lines Quantity of Cells Recruitment of Blood Cells
U0126	8.033	671	466	30	Chemotaxis of Myeloid Cells Migration of Phagocytes Recruitment of Blood Cells
SP600125	6.822	321	320	22	Adhesion of Tumour Cell Lines Differentiation of Bone Extravasation
Diphenyleneiodonium	6.633	129	79	11	Activation of Blood Cells Cell Movement of Myeloid Cells Cellular Infiltration by Phagocytes
Sn50	5.292	75	54	10	Recruitment of phagocytes Recruitment of myeloid cells Failure of Heart

Figure 5.4 Computational Drug Repurposing

Seven compounds were predicted to have a negative consistency score (negative correlation) when computationally compared to the IRI dataset. The total number of transcriptional targets known to IPA knowledge base is presented alongside the number of transcriptional targets found within the IRI dataset. These targets form a network to involve a number of upstream regulators. The compound downstream regulators and the eventual phenotype targets are presented.

5.2.3 Computational Drug Repurposing Workflow- IPC Comparison

To test concordance of the predicted compounds (n=7, Figure 5.2) to ameliorate the dataset molecule targets and downstream phenotype in a manner consistent with the response pathway signature of the direct-IPC dataset, the predicted upstream regulators of the network and the downstream network functions were collated and compared to the core analysis observations of the direct-IPC dataset as per the workflow in Figure 5.5.

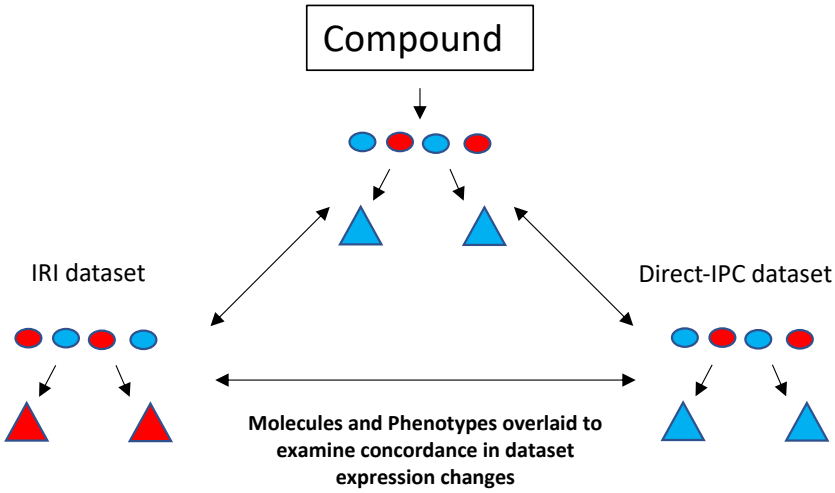

Figure 5.5 Computational Drug Repurposing Workflow: IPC Comparison

The top ranked compound networks with a negative consistency score (n=7) were selected and the compound was activated using the IPA Molecule Activity Predictor. The changes predicted following introduction of the compound on the downstream dataset and phenotype was compared to the IRI and direct-IPC core analysis.

Using pirfenidone as an example of this workflow, IPA predicted a total of six upstream regulator targets. The differential regulation of these upstream regulators would result in functional changes to the IRI phenotype in an anti-correlative manor, opposed to the IRI transcriptional signature, (Figure 5.6). Figure 5.6A displays the computational effects of not administering pirfenidone on the IRI DEGs and the downstream injury phenotype of the IRI

dataset. In Figure 5.6B pirfenidone was “activated” and the computational downstream effects of its administration on the upstream regulators and function are displayed.

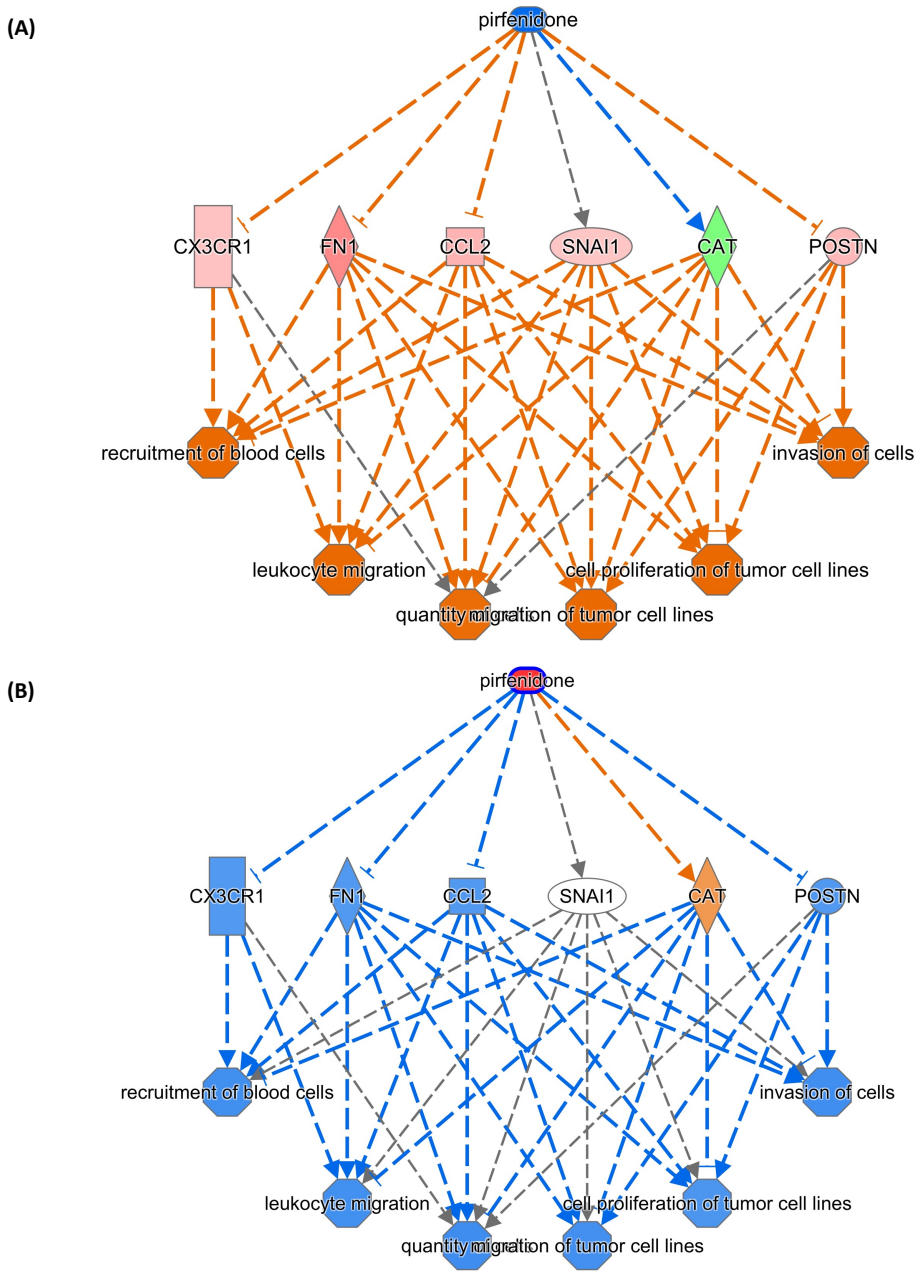

Figure 5.6 Pirfenidone Targets in the IRI Dataset

The Regulatory Effects Network algorithm was set to examine for connections between known compounds (contained in IPA knowledge base), the dataset molecules and finally the phenotype. The compound pirfenidone was predicted to demonstrate a high consistency of 8.165, connecting to 6 upstream regulators which in term target 6 downstream functions. Image **(A)** demonstrates the anti-correlation between pirfenidone and the IRI dataset. Image **(B)** demonstrates the activation of pirfenidone (coloured red) and hypothesized regulator effect and function.

Node key
Compound: blue (not administered), red (administered)
Upstream regulator: red and orange (activated), blue and green (inhibited)
Function: orange (activated), blue (inhibited)

Pirfenidone was predicted to target six upstream regulators, including inhibition of CX3CR1, FN1 and CCL2, all three of these molecules were predicted to be inhibited by direct-IPC. Following IRI, CAT was predicted to be inhibited and non-significant in direct-IPC, but pirfenidone was predicted to activate CAT expression. SNAl1 expression was upregulated following IRI and non- significant in direct-IPC. Pirfenidone was predicted to target this regulator in a manner which could not be predicted by IPA, but computationally appeared significant to the inhibitory effect on IRI. POSTN was predicted to be activated by direct-IPC but inhibited by pirfenidone. Therefore, pirfenidone demonstrated a positive correlation with the direct-IPC signature in 66.7% (4/6) of the upstream regulators (Figure 5.7A).

The function targets of pirfenidone were collated and compared to the activation or inhibition state of the corresponding functions in the IRI and direct-IPC core analysis using IPA comparison analysis. The directional activation of the functions was compared across the groups using the z-score. i.e., computational rank to predict the directionality of the function. Pirfenidone was predicted to differentially regulate six functions, and inhibition of these functions demonstrated concordance with direct-IPC response pathways in, 83.3% (5/6) of these functions (Figure 5.7B).

All seven compounds predicted to demonstrate anti-correlation to the IRI transcriptional signature were compared using the workflow described in Figure 5.5 (see Appendix 5-16). The concordance of these compounds to differentially regulate their target upstream regulators and functions in a reflective manor to the direct-IPC response signature and pathways is displayed in Figure 5.8.

(A)

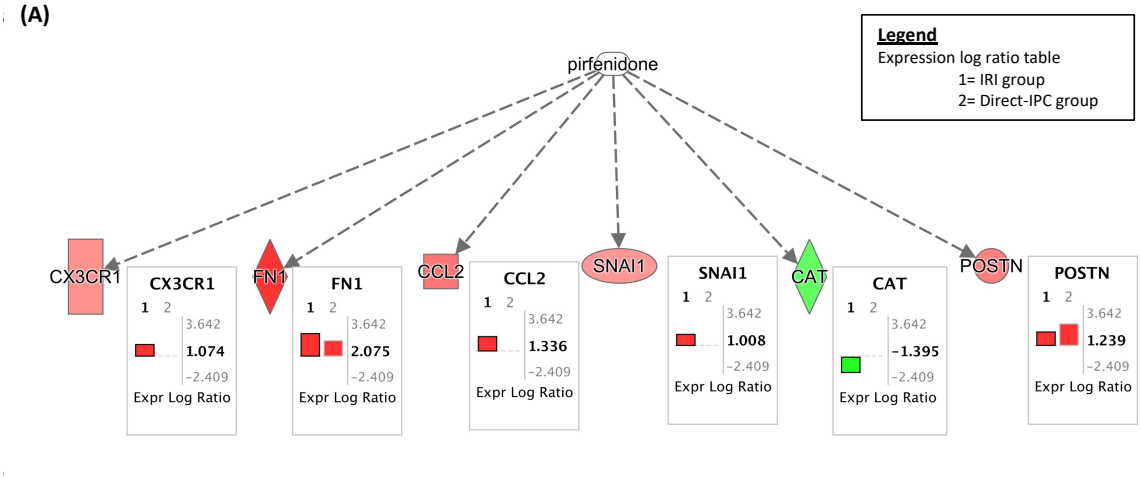

(B)

Diseases/Toxicity/Bio Functions	Z-score		Direction of Chemical Prediction
Pirfenidone	IRI	D-IPC	
Cell proliferation of tumor cell lines	4.9	4.5	Inhibition
Invasion of cells	5.0	4.7	Inhibition
Leukocyte migration	5.7	4.0	Inhibition
Migration of tumor cell lines	5.4	5.0	Inhibition
Quantity of cells	2.2	3.4	Inhibition
Recruitment of blood cells	4.8	3.4	Inhibition

Figure 5.7 Pirfenidone IPC Transcriptional Comparison

(A) Those upstream regulators predicted to be targeted by Pirfenidone in the IRI dataset are displayed. The log_2FC of each upstream regulator in the IRI and direct-IPC datasets are displayed relative to sham. In total Pirfenidone is predicted to inhibit CX3CR1, FN1 and CCL2 in line with expression change seen following direct-IPC. CAT is further predicted to be inhibited following IRI and non-significant following IPC in concordance with Pirfenidone. IPA is unable to predict the effect of Pirfenidone on SNAL1. Pirfenidone computationally inhibits POSTN which is hypothesized to inhibit the injury phenotype. POSTN inhibition by Pirfenidone is opposite to the activation state seen in the direct-IPC dataset.
(B) The downstream directional change of the function of the network was further examined for concordance with the direct-IPC. Pirfenidone was predicted to inhibit all 6 functions of the network. Direct-IPC shared concordance with Pirfenidone functional changes in 5 of the 6 functions.

Chemical Compound	Upstream Regulator	Network Functions
	% (node directionality/ total nodes)	% (node directionality/ total nodes)
Pyrrolidine Dithiocarbamate	91.7 (22/24)	85.7 (6/7)
SP600125	90.9 (20/22)	100 (3/3)
Diphenyleneiodonium	90.9 (10/11)	100 (3/3)
U0126	86.7 (26/30)	100 (3/3)
Pirfenidone	66.7 (4/6)	83.3(5/6)
AG490	76.9 (10/13)	83.3 (5/6)
Sn50	70.0 (7/10)	66.6 (2/3)

Figure 5.8 Computational Drug Repurposing Workflow: Concordance Of Compounds to Direct-Ischemic-Preconditioning

IPA Regulatory Effects Analysis algorithm was filtered to test for compound agents which IPA computationally hypothesises would reverse the molecule expression change and phenotype seen following IRI. Compounds were examined for evidence of target molecule and phenotype consistency relative to the directional expression change of the direct-IPC dataset. The ratio of upstream regulator molecules and phenotypes (network functions) which demonstrated consistency were computed and displayed.

5.2.4 Drug Repurposing *In vivo*

The computational compound predictions which are hypothesised to inhibit the IRI phenotype were tested *in vivo*. Of the seven compunds identified from the computational analysis of sequencing data, Sn50 peptide was excluded from further analysis since Sn50 and pyrrolidine dithiocarbamate (PDTC) were known to be NF-$_k$B inhibitors, and PDTC performed better *in silico* (Figure 5.7). Therefore, in keeping with the principles of the National Centre for the Replacement, Refinement, and Reduction of Animals in Research, Sn50 peptide was not included in the *in vivo* analysis.

5.2.4.1 Drug Repurposing *In vivo*: Methodology

Thirty-six adult male Lewis rats underwent gaseous anaesthesia, intra-peritoneal (IP) injection of group defined fluid, midline laparotomy and allocation to one of nine experimental groups. The experimental groups comprised sham (n=6), 45 minutes of bilateral IRI (n=6), vehicle (DMSO) (n=6) and six different chemical preconditioning methods using the selected compunds (total, n=18). Animals were recovered and allowed food and water as required. At 48 hours post-surgery, rodents were terminally anaesthetised, and blood and kidneys were retrieved for analysis, as shown in the experimental flow diagram in Figure 5.9.

The selection of DMSO as vehicle was made to support chemical solubility. The vehicle was diluted with 2.5 ml of 0.9% sodium chloride to achieve a 3.4% concentration. Both sham and IRI groups received 2.5ml of 0.9% sodium chloride IP. All compounds were diluted using DMSO and 0.9% sodium chloride to achieve a volume of 2.5 ml and vehicle concentration of 3.4%. Based on a comprehensive literature search (Figure 5.10), compounds were used at the following IP dosages: Pyrrolidine Dithiocarbamate (PDTC 100 mg/kg), AG490 (10 mg/kg),

Pirfenidone (100 mg/kg), U0126 (10 mg/kg), SP600125 (15 mg/kg) and Diphenyleneiodonium (DPI 1.5 mg/kg), (see Chapter 2.4, Operative Procedure: Chemical Preconditioning).

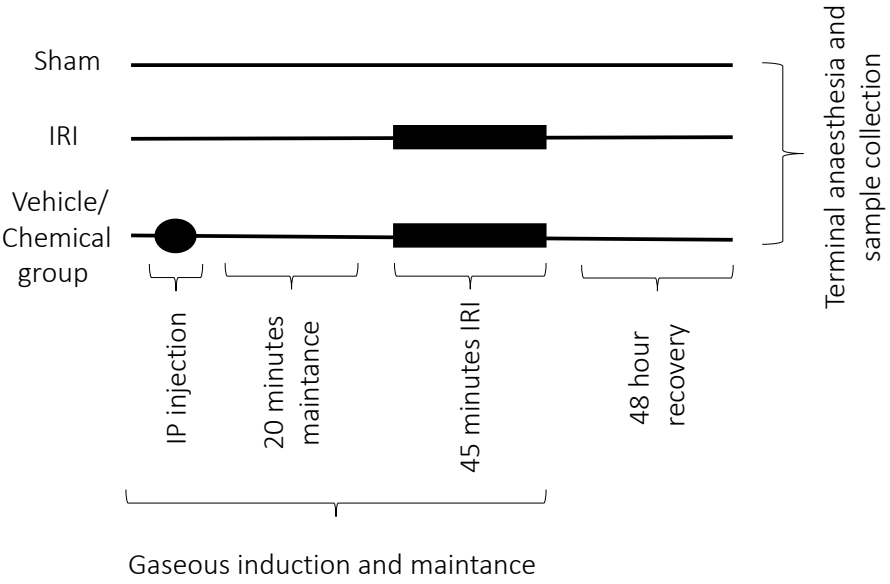

Figure 5.9 *In vivo* Chemical Preconditioning Model

Male adult Lewis rats were randomly allocated to nine experimental groups. Following gaseous anaesthetic induction and maintance the midline mini-laparotomy incision was made and under direct vision the IP fluid (fluid injected determined by pre defined experimental group) was injected into the peritoneal cavity. The incision was closed and the rat was maintained under gaseous maintance for a total of 20 minutes. The laparotomy was extended and either sham operation or bilateral renal pedicle cross clamping was administered for 45 minutes. Following 45 minutes of IRI or sham the bilateral clips were removed and the abdominal cavity inspected for complications. The midline laparotomy incision was closed in two plains and the rodent was moved to the recovery station. Animals were allowed food and water as required. At 48-hours post-surgery rodents were terminally anaesthetised and blood and kidneys retrieved for analysis.

Compound	Dosage	Literature references
Pyrrolidine Dithiocarbamate	100mg/kg	[426-436]
AG490	10mg/kg	[437-440]
Pirfenidone	100mg/kg	[441-444]
U0126	10mg/kg	[445-447]
SP600125	15mg/kg	[448-451]
Diphenyleneiodonium	1.5mg/kg	[452-455]

Figure 5.10 *In vivo* Compound Preconditioning: Dosages

A literature search was completed for all six compounds to be tested *in vivo*. Information was collated regarding route of administration, dosage and reported side effects, morbidity and mortality. Selected dosage was chosen with the aim of avoidance of adverse events in the animals.

5.2.4.2 Drug Repurposing *In vivo*: Results

Thirty-six male adult Lewis rats were divided into the nine experimental groups described above. No difference in pre-operative sCr (46.4 ± 2.0 mmol/L, p= 0.74,) or animal weight (246.2 grams, p= 0.95,) was observed across the groups.

As shown in Figure 5.11, post-operative sCr in the sham group was 32.6 ± 0.4 mmol/L compared to 142.8 ± 31.0 mmol/L in the IRI group, and 178.2 ± 29.5 mmol/L in the DMSO group. No statistically significant difference was seen between the DMSO and IRI group (p=0.77). In the compound-treated groups, sCr was significantly reduced compared to DMSO, in the pirfenidone group (sCr 39.2 ± 3.0 mmol/L, p= 0.003), PDTC group, (sCr 39.6 ± 2.0 mmol/L, p=0.003) and the U0126 group (sCr 77.6 ± 18.8 mmol/L, p= 0.05). No statistically significant difference was seen in the other chemical preconditioning groups: SP600125 (sCr 80.1 ± 16.4 mmol/L, p= 0.053); AG490 (sCr 86.0 ± 23.1 mmol/L, p= 0.08) and the DPI group (sCr 96.6 ± 17.6 mmol/L, p= 0.14).

Post-operative alanine aminotransferase (ALT) was similar between the sham and DMSO groups, 46.5 ±2.4 U/L and 43.0 ± 4.1 U/L respectively, p=0.99. No difference between DMSO and IRI (34.0 ±3.4 U/L p=0.46), U0126 (39.3 ± 4.6 U/L, p=0.99), SP600125 (39.7 ± 1.8 U/L, p=0.99), pirfenidone (44.0 ± 4.5 U/L, p=0.99), PDTC (35.0 ± 6.5 U/L, p=0.78) and AG490 (54.7 ± 10.0 U/L, p= 0.39) was observed. The DPI group demonstrated an increased ALT relative to DMSO (62.0 ± 3.8 U/L, p=0.04) (Figure 5.11).

Post-operative lactate dehydrogenase (LDH) was not statistically different across all experimental groups (p=0.56): Sham (555.5 ± 135.7 U/L), IRI (400.7 ± 116.3 U/L), DMSO (541.5 ± 73.56 U/L), U0126 (488.7 ± 118.5 U/L), SP600125 (370.0 ± 144.6 U/L), pirfenidone (497.7 ± 145.6 U/L), PDTC (220.0 ± 101.7 U/L), AG490 (286.0 ± 133.3 U/L) and DPI (367.7 ± 27.49 U/L) (Figure 5.11).

As shown in Figure 5.12, the combined median (and range) histological score in the sham operated kidney was 1 [0-2] compared to the DMSO kidney of 24 [18-26] (p=0.009). No statistically significant difference was demonstrated between the DMSO combined histology score (24 [18-26]) and all chemical preconditioning groups: U0126 (24 [18-26], p= 0.99), SP600125 (25 [20-25], p= 0.99), pirfenidone (22 [14-22], p= 0.99), PDTC (23 [22-23], p= 0.99), AG490 25 [22-26], p= 0.99) and DPI 24 [20-25], p= 0.99).

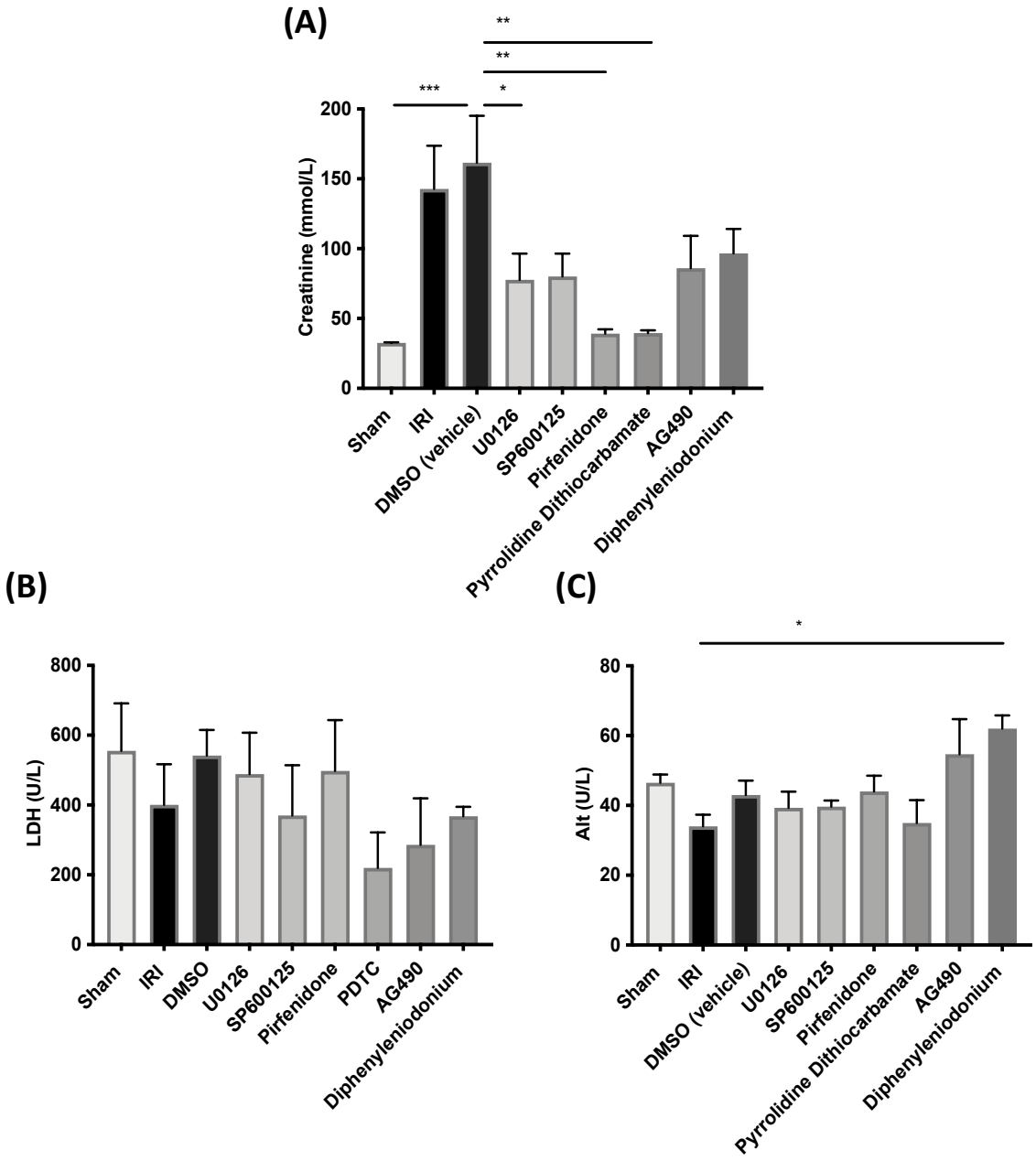

Figure 5.11 *In vivo* Validation of Computational Drug Repurposing Post Operative Biochemistry

Post operatively blood was collected following direct cardiac puncture.

(A) Post-operative sCr blood results are plotted as mean ±SEM . A statistically significant difference was demonstrated between DMSO versus the pirfenidone group (sCr 39.2 ± 3.0 mmol/L, p= 0.003), PDTC group, (sCr 39.6 ± 2.0 mmol/L, p=0.003) and the U0126 group (sCr 77.6 ± 18.8 mmol/L, p= 0.05). (B) Post-operative lactate dehydrogenase (LDH) was statistically no different across all experimental groups, p=0.56. (C) Post-operative alanine aminotransferase (ALT) was similar between the sham and DMSO group, 46.5 ± 2.4 U/L and 34.0 ± 3.4 U/L respectively, p=0.98. The DPI group demonstrated an increased Alt relative to DMSO (62.0 ± 3.8 U/L, p=0.04)

Statistics completed using ANOVA with post-hoc Dunnett's multiple comparison
Statistical significance: * p<0.05, **p<0.01, *** p<0.001 and **** p<0.0001

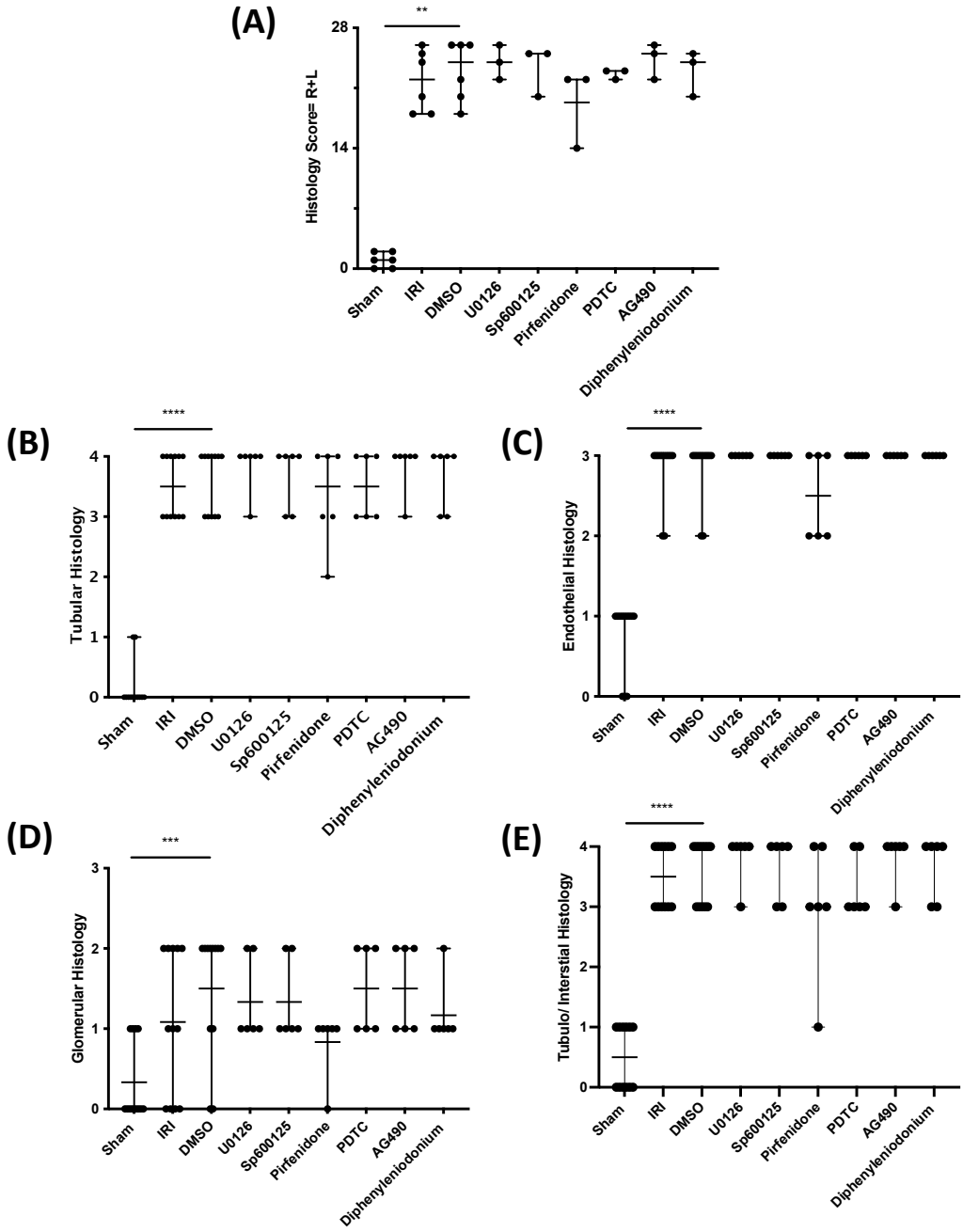

Figure 5.12 *In vivo* Validation of Computational Drug Repurposing Post operative Histology

48 hours post experimental procedure renal tissue was blocked and stained with H&E and assessed using a comprehensive scoring system compromising of Endothelial, Glomerular, Tubular and Tubule/Interstitial (TI) cell damage. The EGTI scoring was plotted as median and range.

(A) Combing the EGTI scores of both kidneys histological damage confirmed no statistically significant difference between the DMSO group and the compound agents tested . (B-D) No statistically significant difference was demonstrated within each histological compartment.

Statistics completed using Kruskal-Wallis test and Dunn's multiple comparison
Statistical significance: * $p<0.05$, ** $p<0.01$, *** $p<0.001$ and **** $p<0.0001$

5.4 Discussion

5.4.1 Drug Repurposing

The current failure rate of clinical trials to deliver a novel therapies to routine clinical practise is 90%[456], with many failing to demonstrate efficacy and safety[457]. The financial burden of pharmaceutical research has rendered stagnation in novel drug development, and innovative approaches are required to drive advancement. Drug repurposing is a highly successful strategy that seeks to use drugs already approved for use in one field of medicine in other medical fields. The repurposing of Dapagliflozin, a highly effective treatment for type two diabetes[458], to treat CKD[459] and heart failure[460] was ground-breaking ,and has undoubtably revolutionised the treatment of these diseases.

Traditional drug repurposing uses hypothesis generation, mechanistic assessment, preclinical study and finally evaluation in clinical trials. In contrast, a new method called computational drug repurposing, uses experimental results, such as gene expression data, and *in silico* analysis to identify candidate drugs for treatment of disease[461]. The technique can use the known gene expression of a disease and computationally compare it to the gene expression of drugs in a process, called signature matching[462]. The technique was first described by Dudley et al. (2012), who compared the gene expression of inflammatory bowel disease to the gene expression of drug compounds to infer anti-correlated disease-drug relationships hypothesised to reverse the disease transcriptional profile. The group validated a single candidate drug, Topiramate, *in vivo,* inferring a novel therapeutic benefit[424].

The work presented in this Chapter used a more complex pathway-based mapping which not only inferred candidate drugs, but also described the possible mechanism of action, and the phenotype target of the drug prediction. Furthermore, the work-compared the drug

predictions to the transcriptional response pathways of a known ameliorator of renal IRI, IPC. These data describe a computational workflow using IPA that successfully identified candidate drug for repurposing. Furthermore, candidate compounds were tested for validation *in vivo* to confirm the *in silico* analysis predictions.

5.4.2 Computational Analysis *and In vivo* Confirmation

Computational analysis of the IRI dataset identified seven drugs predicted to exhibit a transcriptional pattern opposite to IRI, and a further twenty-seven whose transcriptional fingerprint was in concordance with the IRI injury. As expected, those drugs with a positive correlation that would be predicted to mirror the transcriptional effect of IRI are known inducers of AKI including LPS[463], gentamicin[464] and vancomycin[465]. The endotoxin LPS is found on the outer membrane of *E.coli* and *Salmonella* bacteria. In the kidney LPS is an important cause of septic-AKI, as it induces cellular injury via TLR4 signalling[466; 467]. The analysis in this chapter demonstrates that *Salmonella* and *E.coli* LPS share common upstream regulator targets to those shown in the IRI transcriptional analysis. Indeed, LPS in the *E.coli* and *Salmonella* analysis, upregulates the chemokines: CCL2 and CXCL-1, and the cell adhesion molecule ICAM-1, resulting in the infiltration of phagocytes to the site of injury which has been shown to be critical in IRI pathogenesis[323; 468]. Indeed, this injury phenotype was corroborated by the computational significance of ionomycin which is used to increase intracellular calcium concentrations inhibiting mitochondrial function[469]. Ionomycin's network targets include caspase-3 which has been shown to trigger cell death in proximal tubular epithelial cells [470; 131] in a manner consistent with IRI[136]. Interestingly, known pharmacological agents which can cause human AKI: gentamicin, vancomycin, and the organic compound fenamic acid (found in the drug mefenamic acid) were ranked highly in the analysis. These pharmacological agents

targeted common upstream regulators: CD14 and CD44. The cluster of differentiation protein 14; CD14, is a co-receptor for TLR signalling and its ligands include PAMPs (LPS) and DAMPs (HSP70)[471]. CD14 is a potent inducer of inflammation in the innate immune response[472]. It has been suggested that CD14 may be an important target to prevent ischaemia in donor organs[473]. In concordance with this observation, the cell surface glycoprotein CD44 which serves as an adhesion molecule mediating cell migration[474] has been shown to be important in renal IRI[475], and its deficiency in CD44 KO mice impairs pro-inflammatory cytokines and leucocyte recruitment[476]. The identification of compounds which share concordance with the IRI transcriptional signature in this chapter supports that the computational workflow successfully identifies the principal injury response which strengthens and validates the analysis methodology. This chapter has identified common regulatory pathways in multiple differing induces of AKI and demonstrated that their shared phenotype is the innate immune response.

Analysis i*n silico* identified seven drugs that had a negative correlation with IRI and therefore had potential to ameliorate IRI. In total, six drugs which shared common transcript and biological targets with that of the response pathways seen in IPC were tested *in vivo*, all of which improved renal function at 48 hours. Of these six drugs, all have been used in other *in vivo* models of AKI with success: PDTC[426; 477], SP600125[448; 450], DPI[454], U0126[445; 212], AG490[437; 439] and pirfenidone[478]. Importantly all drugs were predicted to inhibit stages and processes involved in the recruitment and activation of the innate immune response. DPI, is a potent NADPH oxidase inhibitor which reduces ROS formation in IRI[479]. Indeed, NADPH oxidase is an important mediator of phagocyte to endothelium adhesion in LPS- mediated renal injury, via VCAM-1[480]. Pathway analysis of DPI predicted the inhibition of adhesion molecules: L-selectin, ICAM-1 and the monocyte chemoattractant CCL2 (MCP-1), and the

downstream phenotype; cellular infiltration by phagocytes. Consistent with this observation, SP600125, an inhibitor of JNK a member of the MAPK family suppresses the inflammatory response[449]. In this chapter, SP600125 inhibits cell adhesion through multiple upstream regulators: SELE, ICAM-1 and SELP, which have been shown by other groups to be upregulated in IRI[481] and essential in LPS mediated nephritis[482]. PDTC is a potent inhibitor of IκB phosphorylation, which prevents NF- κB translocation to the nucleus, inhibiting cytokines [483]. PDTC was shown to inhibit chemotaxis molecules: CXCL2, CXCL6, CXCL9 and CXCL10. In humans CXCL9 is increased in the serum of patients with acute rejection of the kidney, and higher levels of CXCL6 pre kidney transplant was predictive of future acute rejection[484]. Recently, Canney et al (2023), has demonstrated CXCL9 may serve as an effective biomarker in AKI induced by acute tubulointerstitial nephritis[485] but its role in renal IRI represents a paucity of data. U0126 acts by inhibiting the kinase activity of MEK 1/2. Indeed, U0126 attenuates cisplatin-induced AKI[486] and renal IR *in vivo*[445] by preventing ERK1/2 activation. Computationally U0126 targets upstream regulators CCL2, ICAM-1, CXCL10 whose differential regulation inhibits chemotaxis of phagocytes. AG490 a JAK kinase inhibitor inhibits the JAK/STAT signalling pathway to prevent signal transduction from cytokine receptors to the nucleus[487]. The analysis showed the importance of CCL2 and ICAM-1 inhibition in reducing the recruitment and activation of phagocytes, a finding which has been observed in other models of ischaemia [488; 440]. All five of these compounds target similar upstream regulators whose downstream phenotype is the innate immune response. These common regulatory pathways share similarities to the compounds that has a positive correlation to the IRI signature. Together the analysis in this chapter suggests shared targets of chemokines and adhesion molecules in different models of AKI.

Interestingly, the sixth drug, pirfenidone, was shown to be opposed to the transcriptional signature of IRI and achieved the greatest improvement in renal function *in vivo*. Pirfenidone is of significant interest as it is already licensed in the UK as an oral antifibrotic to treat pulmonary fibrosis, making it an excellent candidate for drug repurposing. One group has used pirfenidone pre-treatment prior to 20 minutes of bilateral renal IRI in the rat. Lima-Posada et al.(2019), successfully demonstrated that oral pirfenidone can reduce tubular injury and creatinine clearance at 24-hours[478]. The work presented in this chapter utilised a more severe IRI model (45-minutes of ischaemia), and extended the time to sample retrieval to 48-hours. By extending to 48-hours, this chapter has mirrored the current human-AKI diagnostic criteria: sCR rise within 48 hours[18], and enhances our understanding of the potential importance of pirfenidone in AKI. However, the exact mechanism of action of pirfenidone is not fully understood, but it is thought to inhibit the pro-fibrotic cytokines TNF-α and TGF-β[489]. As an antifibrotic compound pirfenidone has particularly interested basic science research workers in heart failure[490], liver fibrosis[491] and CKD[492; 493]. Indeed, pirfenidone has recently been used in clinical trials to treat myocardial fibrosis [494], advanced liver fibrosis[495] and diabetic nephropathy[493].

5.4.3 Pirfenidone Pathway Analysis

Pathway analysis of pirfenidone identified six key transcriptional targets: CX3CR1, FN1, CCL2, SNAI1, CAT and POSTIN. Two of these regulators, fibronectin (FN1); an ECM glycoprotein, and periostin (POSTIN), a non-structural ECM protein, have traditionally been thought of as profibrotic[496; 497] and are inhibited by pirfenidone[498; 499]. Interestingly, recent single-cell RNA sequencing data studies on AKI have shown that fibronectin appears early in AKI[500], and its inhibition reduces immune cell infiltration of leucocytes[368]. The RNA

sequencing work in Chapter 5 corroborated the finding that fibronectin is expressed early in AKI, which has also been confirmed by other groups[501]. Furthermore, blocking periostin in a rhabdomyolysis-induced AKI mice model has recently been shown by Muratsu et al. (2022) to reduce MCP-1, TNF-α and IL-6, possibly though NF-κB pathways and resulting in reduced tubular injury[502]. These traditional CKD fibrosis markers may thus have important roles in the pathogenesis of AKI, and their function may be mediated via inflammatory cell signalling.

The finding that pirfenidone inhibits the IRI network via fibrosis transcripts is further evidenced by pirfenidone networking with SNAI1. Cellular injury activates matrix producing cells resulting in excessive ECM deposition and fibrosis[503]. One of the proposed sources of ECM-producing cells is thought to be through epithelial-mesenchymal transition (EMT)[504]. Indeed, SNAI1 is produced in tubular cells during injury and is a potent transcriptional regulator and promotor of EMT in fibrosis[505]. However, there is increasing evidence that SNAI1 may have a critical role in AKI pathogenesis. Recent work by Grande et al. (2015), has demonstrated that the activation of SNAI1 in epithelial cells triggers a partial EMT response which sustains inflammation in a folic acid AKI model[506]. Work by Tang et al. (2021), has consolidated the importance of SNAI1 in AKI, demonstrating that targeted SNAI1 using RNA interference therapy delivered directly to the renal tubules, alleviates IRI[507].

Aside from the anti-fibrotic targets of pirfenidone, the network revealed antioxidant and anti-inflammatory targets. It is well established that pirfenidone has antioxidant properties and its use can ameliorate CAT and SOD suppression following hypoxia[508; 509]. In a CKD kidney model, pirfenidone has been shown to stabilise the mitochondria through the enhancement of SOD and reduction in oxidative stress[510], however, no pre-clinical research has confirmed the benefit of pirfenidone regulation of antioxidants in AKI.

The network target on leucocyte trafficking by pirfenidone is of particular interest. The network chemokine MCP-1 has been shown to be a key regulator of monocyte recruitment to the kidney after IRI[468]. Indeed, its expression is so pronounced that it has been proposed as a biomarker of AKI[511]. Interestingly, leucocyte infiltration in a 5/6 nephrectomised rat model of CKD can be attenuated by pirfenidone through its inhibition of MCP-1[512], a finding which has been confirmed in a mouse lung transplant model[513]. Sharawy et al. (2020), also demonstrated that in a gentamicin-AKI model, pirfenidone inhibits pro-inflammatory cytokines and MCP-1 mitigating macrophage infiltration[514]. In concordance with this observation the chemokine receptor CX3CR1, which is abundantly expressed on monocytes, can be inhibited by pirfenidone in an acute hypoxic model of placental injury[515]. Indeed, acute IRI models which block CX3CR1 on macrophages decrease macrophage trafficking, preventing injury[516; 517]. Pirfenidone is therefore predicted to target regulators which function in ECM structure, oxidative stress, and leukocyte trafficking.

The principal findings of this Chapter are:

1. Drug repurposing by pathway-based analysis is an effective method to infer novel drug targets for future pre-clinical testing
2. Pirfenidone may serve as a novel treatment for IRI-induced AKI. Future pre-clinical work to explore its therapeutic potential is required

5.5 Concluding Remarks

Computational drug repurposing using pathway-based analysis is an effective method to identify target drugs of interest for future pre-clinical assessment. The *in silico* technique described in this Chapter allows investigation of the mechanisms of drug action in novel diseases. Indeed, the findings of this Chapter have alluded to novel targets to prevent renal IRI. Interestingly, pirfenidone was shown to target multiple transcripts which have been extensively investigated in renal fibrosis. It is therefore likely that there is overlap between AKI and CKD, and that the transition from one to the other involves previously defined fibrotic markers which may have critical roles in the acute setting of AKI. The role of fibrotic markers and EMT regulators in AKI promises to be an interesting future field of research.

Chapter 6

General Discussion

The principal aim of this thesis was to study methods to reduce ischaemia reperfusion injury (IRI) of the kidney. Renal IRI is one of the most common causes of acute kidney injury (AKI) in hospital[35; 41; 45]. Patients diagnosed with AKI are at increased risk of in-hospital mortality, while those surviving to discharge are subjected to long term sequelae, which include, de-novo CKD, progressive underlying CKD, ESRD and early death[518; 519]. To date, the corner stone of AKI management is reactive, relying upon recognition and intervention. This strategy is failing patients. Novel tactics to prevent AKI have used ischaemic preconditioning (IPC) as a preventative approach to render the kidney resistant to IRI. To date, the successful application of IPC in humans has had limited success, largely due to a lack of detailed mechanistic understanding of IRI and IPC. An alternative to mechanical IPC is the use of pharmacological agents to activate individual pathways thought to be responsible for the IPC effect, a method called chemical preconditioning (CP).

Based upon this knowledge, this thesis first aimed to explore the optimal method of IPC *in vivo*. Given the ongoing need to describe the mechanism of IRI and IPC the second aim of this thesis was to describe the RNA-transcriptional fingerprint of IRI and the renal response pathways to IPC. Finally, this thesis aimed to utilise genomic data and in silico pathway-based mapping analysis to infer candidate drugs to ameliorate renal IRI.

The host laboratory had developed a robust *in vivo* model of bilateral IRI in the rat and had previously concluded that pulsatile IPC applied directly to the bilateral kidneys prior to IRI could reduce injury[190]. Although this direct method of IPC was effective, it is highly invasive, and has limited therapeutic potential in clinical practise. Therefore, the experiments in Chapter 3 aimed first to characterise the extent of the renal injury induced by bilateral IRI, and secondly, test the effectiveness of remote IPC in ameliorating renal IRI.

The work presented in Chapter 3 demonstrated a robust and reproducible model of bilateral IRI in the rat. Importantly, the model was survivable to 48 hours, and allowed for an accurate measure of the degree of renal dysfunction, evidenced by robust changes in serum creatinine (sCr) and histological injury. To test the effectiveness of IPC to ameliorate IRI, the experimental work in Chapter 3 used an ischaemic dose escalation protocol which aimed to optimise the IPC intervention. In total, six different IPC regimes in one model of direct-IPC, and two different models of remote-IPC were tested. The results demonstrated the effectiveness of direct-IPC $2/5^3$ and bilateral hind limb remote-IPC $2/5^3$ in ameliorating IRI in the kidney.

The experimental work completed in Chapter 3 confirmed that bilateral IRI is an effective model of AKI in the rat. Furthermore, two methods of IPC, one local and one remote, were able to protect the kidney from IRI and reduce functional and histological markers of injury. The next objective of this thesis was to describe the RNA-transcriptional fingerprint of IRI and the renal response pathways to IPC. The whole kidney from the experimental groups of sham, IRI, direct-IPC and indirect-IPC were selected for total RNA next generation sequencing (NGS). The RNA sequencing data was analysed using Ingenuity Pathway Analysis (IPA). This analysis demonstrated a unique transcriptional fingerprint of IRI characterised by cytokine dysregulation, nuclear signalling, extracellular matrix/cytoskeleton signalling and leukocyte trafficking. The transcriptional signature of IRI was reduced in both IPC groups. Interestingly, both direct- and indirect-IPC shared common response pathways. This strongly supports the hypothesis that IPC works across multiple networks to ameliorate IRI, and that both direct- and indirect-IPC share common mechanisms of action.

The work presented in Chapter 4 has revealed the complex transcriptional signature of renal IRI and the response pathways of IPC. To date the application of IPC in humans has had limited success. One alternative to mechanical IPC is chemical IPC which uses a pharmacological agent to target a molecule thought significant in renal IRI pathogenesis. The work undertaken in Chapter 5 uses the genomic data from Chapter 4 and *in silico* analysis to identify candidate drugs that share "genomic anti-similarity" to the transcriptional signature of IRI. In total seven drugs demonstrated genomic anti-correlation to the IRI transcriptional profile. The transcriptional target of each drug was individually compared to the transcriptional signature of the direct-IPC dataset to explore the similarities and differences shared. Six drugs which was predicted to be inhibitory of the IRI signature was validated i*n vivo*. All drugs were shown to inhibit renal injury as measured by sCr.

In summary, the work presented in this thesis has demonstrated the transcriptional injury signature of IRI in the rat kidney. The work has further confirmed that the beneficial effect of IPC is multifaceted, targeting several response pathways to inhibit renal IRI. Furthermore, the data presented in this thesis indicates that there are shared mechanisms between direct- and indirect-IPC. Interestingly, pirfenidone was found to be a highly effective drug to prevent renal IRI. Pirfenidone is already licensed in the UK as an oral antifibrotic to treat pulmonary fibrosis making it an excellent drug candidate for future investigation in renal IRI. Pirfenidone may serve as a novel agent to prevent IRI and future work is required to explore its therapeutic potential.

6.1 Future Work

The transition of the remote IPC model described in this thesis to a minimally invasive IPC technique is the logical next step. A future model of minimally invasive remote IPC may utilise a torniquet which could be applied to the unilateral or bilateral hind limbs of the rat to simulate indirect IPC. The challenge of this future model is anatomical. The large muscles of the rat thigh lie in close proximity to the hip joint. As such, external compression of the leg may miss a large proportion of the rat thigh muscle. To overcome this, researchers may directly visualise the femoral artery in the groin and clamp the artery under direct visualisation. This experiment would use an ischaemic dose escalation protocol and utilise both unilateral and bilateral femoral clamping.

During *in silico* Regulatory Effects Network (REN) analysis it became clear that IRI shared a similar transcriptional profile to that of other injury models of the kidney. Indeed, the top ranked network for concordance with IRI was that of LPS-Induced Acute Kidney Injury (Chapter 5, Figure 5.2). This is an interesting observation as this may suggest that although there is a diverse pool of insults which lead to AKI there may be a common pathway leading to the injury. Future research could investigate the differences and similarities between different models of AKI using NGS and *in silico* analysis. This work could aim to investigate common response pathways between these models with the objective of identifying a common pathway for pharmacological manipulation.

Computational drug analysis and *in vivo* confirmation identified six candidate drugs to reduce IRI. The IRI model described in this thesis is one of many causes of AKI. Future work could validate each of these chemicals in several differing models of AKI.

The finding that pirfenidone computational ameliorated IRI and demonstrates efficacy *in vivo* is an exciting observation. Pirfenidone is licensed in the UK as an oral medication to

treat pulmonary fibrosis. In humans pirfenidone is rapidly absorbed after oral administration reaching peak concentrations within 1 hour and cleared from plasma within 2.5 hours[520]. Pirfenidone's metabolism is predominantly by the liver cytochrome P450 pathway and approximately 80% of pirfenidone is excreted in the urine[521]. Pharmacokinetic evaluation of pirfenidone in healthy rats have demonstrated high concentrations of the drug in the kidney[522]. To explore the therapeutic potential of pirfenidone to ameliorate renal IRI future research should aim to perform a drug dose-response curve for pirfenidone in renal IRI *in vivo*. Pirfenidone *in vivo* models may further include the administration of pirfenidone prior to IRI as a once only dose compared to a pirfenidone dose given prior to and following the IRI event. In this thesis pirfenidone was administered intraperitoneally to the rat. A logical transition of this model would be to use oral pirfenidone administered via gavage to ensure ingestion. Future clinical trial work in humans may test the hypothesis that a single dose of oral pirfenidone prior to a risk factor for IRI (e.g., Cardiac Surgery) may augment the incidence of AKI.

Finally, a natural progression of this IRI model is to convert the procedure to a CKD protocol. It would be interesting to establish if 45 minutes of bilateral IRI is sufficient to induce CKD at 28 days. Pathway analysis of pirfenidone alluded to targeting of traditional transcripts linked to CKD. It would be interesting to establish if pirfenidone could prevent AKI to CKD transition.

6.2. Overall Conclusions

In summary, the work presented in this thesis demonstrates that remote IPC is both technically achievable and is a highly effective method to reduce renal IRI in the rat. The thesis successfully described the IRI transcriptional signature and the renal response pathway to IPC. In the final Chapter the thesis draws upon the proceeding work in this thesis to present a novel approach to drug repurposing using transcriptomic analysis to drive experimental design.

References

1. Zhuo, J. L. and Li, X. C. 2013. Proximal nephron. *Compr Physiol* 3(3), pp. 1079-1123.

2. Danziger, J. and Zeidel, M. L. 2015. Osmotic Homeostasis. *Clinical Journal of the American Society of Nephrology* 10(5), pp. 852-862.

3. Preuss, H. G. 1993. Basics of renal anatomy and physiology. *Clin Lab Med* 13(1), pp. 1-11.

4. Wallace, M. A. 1998. Anatomy and physiology of the kidney. *Aorn j* 68(5), pp. 800, 803-816, 819-820; quiz 821-804.

5. Chaya Gopalan Ph.D., F., Erik Kirk Ph.D. 2022. *Biology of Cardiovascular and Metabolic Diseases*.

6. Robson, L. 2014. The kidney--an organ of critical importance in physiology. *J Physiol* 592(18), pp. 3953-3954.

7. Inker, L. A. et al. 2014. KDOQI US commentary on the 2012 KDIGO clinical practice guideline for the evaluation and management of CKD. *Am J Kidney Dis* 63(5), pp. 713-735.

8. Organization, W. H. 2020. *The top 10 causes of death* [Online]. WHO. Available at: https://www.who.int/news-room/fact-sheets/detail/the-top-10-causes-of-death [Accessed: 16/03/2023].

9. 1831. Reports of Medical Cases, Selected with a View of Illustrating the Symptoms and Cure of Diseases, by a Reference to Morbid Anatomy. *Med Chir Rev* 15(30), pp. 289-330.

10. F, D. 1888. *Acute Bright's Disease*. The Medical Record.

11. James Tyson, S. D., Deorge Edmund 1904. *A treatise on Bright's disease and diabetes : with especial reference to pathology and therapeutics*. Philadelphia: P. Blakiston's Son & Co., p. 407.

12. Eknoyan, G. 2002. Emergence of the concept of acute renal failure. *Am J Nephrol* 22(2-3), pp. 225-230.

13. Peitzman, S. J. 1989. From dropsy to Bright's disease to end-stage renal disease. *Milbank Q* 67 Suppl 1, pp. 16-32.

14. HW, S. 1951. *The Kidney. Structure and Function in Health and Disease*. New York Oxford University Press.

15. Swann, R. C. and Merrill, J. P. 1953. The clinical course of acute renal failure. *Medicine (Baltimore)* 32(2), pp. 215-292.

16. Ferguson, M. A. and Waikar, S. S. 2012. Established and emerging markers of kidney function. *Clin Chem* 58(4), pp. 680-689.

17. Shannon, J. A. and Smith, H. W. 1935. THE EXCRETION OF INULIN, XYLOSE AND UREA BY NORMAL AND PHLORIZINIZED MAN. *J Clin Invest* 14(4), pp. 393-401.

18. 2012. Kidney Disease: Improving Global Outcomes (KDIGO) Acute Kidney Injury Work Group. KDIGO Clinical Practice Guideline for Acute Kidney Injury. *Kidney International* 2, pp. 1-138.

19. Cockcroft, D. W. and Gault, M. H. 1976. Prediction of creatinine clearance from serum creatinine. *Nephron* 16(1), pp. 31-41.

20. Levey, A. S. et al. 1999. A more accurate method to estimate glomerular filtration rate from serum creatinine: a new prediction equation. Modification of Diet in Renal Disease Study Group. *Ann Intern Med* 130(6), pp. 461-470.

21. Kellum, J. A. et al. 2002. Developing a consensus classification system for acute renal failure. *Curr Opin Crit Care* 8(6), pp. 509-514.

22. Anderson, R. J. et al. 2000. Mild renal failure is associated with adverse outcome after cardiac valve surgery. *Am J Kidney Dis* 35(6), pp. 1127-1134.

23. Lassnigg, A. et al. 2004. Minimal changes of serum creatinine predict prognosis in patients after cardiothoracic surgery: a prospective cohort study. *J Am Soc Nephrol* 15(6), pp. 1597-1605.

24. Schrier, R. W. 2010. ARF, AKI, or ATN? *Nat Rev Nephrol* 6(3), p. 125.

25. Bellomo, R. et al. 2004. Acute renal failure - definition, outcome measures, animal models, fluid therapy and information technology needs: the Second International Consensus Conference of the Acute Dialysis Quality Initiative (ADQI) Group. *Crit Care* 8(4), pp. R204-212.

26. Khwaja, A. 2012. KDIGO clinical practice guidelines for acute kidney injury. *Nephron Clin Pract* 120(4), pp. c179-184.

27. Fujii, T. et al. 2014. Validation of the Kidney Disease Improving Global Outcomes criteria for AKI and comparison of three criteria in hospitalized patients. *Clin J Am Soc Nephrol* 9(5), pp. 848-854.

28. Wonnacott, A. et al. 2014. Epidemiology and outcomes in community-acquired versus hospital-acquired AKI. *Clin J Am Soc Nephrol* 9(6), pp. 1007-1014.

29. Xu, X. et al. 2015. Epidemiology and Clinical Correlates of AKI in Chinese Hospitalized Adults. *Clin J Am Soc Nephrol* 10(9), pp. 1510-1518.

30. Hsu, C. N. et al. 2016. Incidence, Outcomes, and Risk Factors of Community-Acquired and Hospital-Acquired Acute Kidney Injury: A Retrospective Cohort Study. *Medicine (Baltimore)* 95(19), p. e3674.

31. Nie, S. et al. 2017. Risk factors of prognosis after acute kidney injury in hospitalized patients. *Front Med* 11(3), pp. 393-402.

32. Zeng, X. et al. 2014. Incidence, outcomes, and comparisons across definitions of AKI in hospitalized individuals. *Clin J Am Soc Nephrol* 9(1), pp. 12-20.

33. Associaion, T. R. 2018. *Acute kidney injury (AKI) in England – a report on the nationwide collection of AKI warning test scores from 2018* [Online]. Available at: [Accessed: 25th Feb].

34. Holmes, J. et al. 2016. Acute Kidney Injury in the Era of the AKI E-Alert. *Clin J Am Soc Nephrol* 11(12), pp. 2123-2131.

35. Holmes, J. et al. 2017. Acute kidney injury electronic alerts in primary care - findings from a large population cohort. *Qjm* 110(9), pp. 577-582.

36. Jurawan, N. et al. 2017. Hospital acquired Acute Kidney Injury is associated with increased mortality but not increased readmission rates in a UK acute hospital. *BMC Nephrol* 18(1), p. 317.

37. Odutayo, A. et al. 2012. Epidemiology of acute kidney injury in Canadian critical care units: a prospective cohort study. *Can J Anaesth* 59(10), pp. 934-942.

38. Hoste, E. A. et al. 2015. Epidemiology of acute kidney injury in critically ill patients: the multinational AKI-EPI study. *Intensive Care Med* 41(8), pp. 1411-1423.

39. Abd ElHafeez, S. et al. 2017. Risk, Predictors, and Outcomes of Acute Kidney Injury in Patients Admitted to Intensive Care Units in Egypt. *Sci Rep* 7(1), p. 17163.

40. Fuhrman, D. Y. et al. 2018. Acute kidney injury epidemiology, risk factors, and outcomes in critically ill patients 16-25 years of age treated in an adult intensive care unit. *Ann Intensive Care* 8(1), p. 26.

41. Holmes, J. et al. 2018. Utility of electronic AKI alerts in intensive care: A national multicentre cohort study. *J Crit Care* 44, pp. 185-190.

42. Bagshaw, S. M. et al. 2008. A comparison of the RIFLE and AKIN criteria for acute kidney injury in critically ill patients. *Nephrol Dial Transplant* 23(5), pp. 1569-1574.

43. Lopes, J. A. et al. 2008. Acute kidney injury in intensive care unit patients: a comparison between the RIFLE and the Acute Kidney Injury Network classifications. *Crit Care* 12(4), p. R110.

44. Koeze, J. et al. 2017. Incidence, timing and outcome of AKI in critically ill patients varies with the definition used and the addition of urine output criteria. *BMC Nephrol* 18(1), p. 70.

45. Foxwell, D. A. et al. 2019. Epidemiology of emergency department acute kidney injury. *Nephrology (Carlton)*.

46. Kerr, M. et al. 2014. The economic impact of acute kidney injury in England. *Nephrol Dial Transplant* 29(7), pp. 1362-1368.

47. Kolhe, N. V. et al. 2014. The reimbursement and cost of acute kidney injury: a UK hospital perspective. *Nephron Clin Pract* 126(1), pp. 51-56.

48. Selby, N. M. et al. 2021. Randomized Controlled Trial Evidence of Cost-Effectiveness of a Multifaceted AKI Intervention Approach. *Kidney Int Rep* 6(3), pp. 636-644.

49. Hsu, C. Y. et al. 2009. Nonrecovery of kidney function and death after acute on chronic renal failure. *Clin J Am Soc Nephrol* 4(5), pp. 891-898.

50. Bucaloiu, I. D. et al. 2012. Increased risk of death and de novo chronic kidney disease following reversible acute kidney injury. *Kidney Int* 81(5), pp. 477-485.

51. Soto, K. et al. 2016. The risk of chronic kidney disease and mortality are increased after community-acquired acute kidney injury. *Kidney Int* 90(5), pp. 1090-1099.

52. Coca, S. G. et al. 2012. Chronic kidney disease after acute kidney injury: a systematic review and meta-analysis. *Kidney Int* 81(5), pp. 442-448.

53. Schiffl, H. et al. 2012. Long-term outcomes of survivors of ICU acute kidney injury requiring renal replacement therapy: a 10-year prospective cohort study. *Clin Kidney J* 5(4), pp. 297-302.

54. Horne, K. L. et al. 2017. Three-year outcomes after acute kidney injury: results of a prospective parallel group cohort study. *BMJ Open* 7(3), p. e015316.

55. Thakar, C. V. et al. 2011. Acute kidney injury episodes and chronic kidney disease risk in diabetes mellitus. *Clin J Am Soc Nephrol* 6(11), pp. 2567-2572.

56. Sawhney, S. et al. 2017. Post-discharge kidney function is associated with subsequent ten-year renal progression risk among survivors of acute kidney injury. *Kidney Int*.

57. Wald, R. et al. 2012. Risk of chronic dialysis and death following acute kidney injury. *Am J Med* 125(6), pp. 585-593.

58. Coca, S. G. et al. 2012. Chronic kidney disease after acute kidney injury: a systematic review and meta-analysis. *Kidney international* 81(5), pp. 442-448.

59. Jones, C. A. et al. 1998. Serum creatinine levels in the US population: third National Health and Nutrition Examination Survey. *Am J Kidney Dis* 32(6), pp. 992-999.

60. Culleton, B. F. et al. 1999. Cardiovascular disease and mortality in a community-based cohort with mild renal insufficiency. *Kidney Int* 56(6), pp. 2214-2219.

61. Nissenson, A. R. et al. 2001. Prevalence and characteristics of individuals with chronic kidney disease in a large health maintenance organization. *Am J Kidney Dis* 37(6), pp. 1177-1183.

62. Levin, A. et al. 2001. Cardiovascular disease in patients with chronic kidney disease: getting to the heart of the matter. *Am J Kidney Dis* 38(6), pp. 1398-1407.

63. Mann, J. F. et al. 2001. Renal insufficiency as a predictor of cardiovascular outcomes and the impact of ramipril: the HOPE randomized trial. *Ann Intern Med* 134(8), pp. 629-636.

64. Fried, L. P. et al. 1998. Risk factors for 5-year mortality in older adults: the Cardiovascular Health Study. *Jama* 279(8), pp. 585-592.

65. 2002. K/DOQI clinical practice guidelines for chronic kidney disease: evaluation, classification, and stratification. *Am J Kidney Dis* 39(2 Suppl 1), pp. S1-266.

66. Stevens, P. E. and Levin, A. 2013. Evaluation and management of chronic kidney disease: synopsis of the kidney disease: improving global outcomes 2012 clinical practice guideline. *Ann Intern Med* 158(11), pp. 825-830.

67. 2017. Global, regional, and national incidence, prevalence, and years lived with disability for 328 diseases and injuries for 195 countries, 1990-2016: a systematic analysis for the Global Burden of Disease Study 2016. *Lancet* 390(10100), pp. 1211-1259.

68. 2017. Global, regional, and national age-sex specific mortality for 264 causes of death, 1980-2016: a systematic analysis for the Global Burden of Disease Study 2016. *Lancet* 390(10100), pp. 1151-1210.

69. Roderick, P. et al. 2011. Prevalence of chronic kidney disease in England: Findings from the 2009 Health Survey for England. *Journal of Epidemiology and Community Health* 65(Suppl 2), pp. A12-A12.

70. Gilg, J. et al. 2017. UK Renal Registry 19th Annual Report: Chapter 1 UK RRT Adult Incidence in 2015: National and Centre-specific Analyses. *Nephron* 137 Suppl 1, pp. 11-44.

71. MacNeill, S. J. and Ford, D. 2017. UK Renal Registry 19th Annual Report: Chapter 2 UK Renal Replacement Therapy Prevalence in 2015: National and Centre-specific Analyses. *Nephron* 137 Suppl 1, pp. 45-72.

72. Parfrey, P. S. and Foley, R. N. 1999. The clinical epidemiology of cardiac disease in chronic renal failure. *J Am Soc Nephrol* 10(7), pp. 1606-1615.

73. Cheung, C. Y. et al. 2016. Cancer Incidence and Mortality in Chronic Dialysis Population: A Multicenter Cohort Study. *Am J Nephrol* 43(3), pp. 153-159.

74. Belayev, L. Y. et al. 2015. Longitudinal associations of depressive symptoms and pain with quality of life in patients receiving chronic hemodialysis. *Hemodial Int* 19(2), pp. 216-224.

75. Al-Nashri, F. and Almutary, H. 2022. Impact of anxiety and depression on the quality of life of haemodialysis patients. *J Clin Nurs* 31(1-2), pp. 220-230.

76. Juergensen, E. et al. 2006. Hemodialysis and peritoneal dialysis: patients' assessment of their satisfaction with therapy and the impact of the therapy on their lives. *Clin J Am Soc Nephrol* 1(6), pp. 1191-1196.

77. Methven, S. et al. 2017. UK Renal Registry 19th Annual Report: Chapter 5 Survival and Causes of Death in UK Adult Patients on Renal Replacement Therapy in 2015: National and Centre-specific Analyses. *Nephron* 137 Suppl 1, pp. 117-150.

78. Kerr, M. et al. 2012. Estimating the financial cost of chronic kidney disease to the NHS in England. *Nephrol Dial Transplant* 27 Suppl 3, pp. iii73-80.

79. Tjaden, L. A. et al. 2016. Impact of Renal Replacement Therapy in Childhood on Long-Term Socioprofessional Outcomes: A 30-year Follow-Up Study. *J Pediatr* 171, pp. 189-195.e181-182.

80. McClellan, W. M. et al. 2010. Physical and psychological burden of chronic kidney disease among older adults. *Am J Nephrol* 31(4), pp. 309-317.

81. Vasilopoulou, C. et al. 2015. The Impact of Anxiety and Depression on the Quality of Life of Hemodialysis Patients. *Glob J Health Sci* 8(1), pp. 45-55.

82. Rebollo Rubio, A. et al. 2017. Depression, anxiety and health-related quality of life amongst patients who are starting dialysis treatment. *J Ren Care* 43(2), pp. 73-82.

83. Cecconi, M. et al. 2018. Sepsis and septic shock. *Lancet* 392(10141), pp. 75-87.

84. Doi, K. et al. 2009. Animal models of sepsis and sepsis-induced kidney injury. *J Clin Invest* 119(10), pp. 2868-2878.

85. Remick, D. G. and Ward, P. A. 2005. Evaluation of endotoxin models for the study of sepsis. *Shock* 24 Suppl 1, pp. 7-11.

86. Drechsler, S. and Osuchowski, M. 2021. Cecal Ligation and Puncture. *Methods Mol Biol* 2321, pp. 1-8.

87. Perazella, M. A. 2018. Pharmacology behind Common Drug Nephrotoxicities. *Clin J Am Soc Nephrol* 13(12), pp. 1897-1908.

88. Zhang, J. et al. 2021. Cisplatin chemotherapy and renal function. *Adv Cancer Res* 152, pp. 305-327.

89. Santos, N. A. et al. 2007. Cisplatin-induced nephrotoxicity is associated with oxidative stress, redox state unbalance, impairment of energetic metabolism and apoptosis in rat kidney mitochondria. *Arch Toxicol* 81(7), pp. 495-504.

90. Alasdair R. Irvine, D. v. B., Rawan Shekhani, Rosalinde Masereeuw,. 2021. A systematic review of in vitro models of drug-induced kidney injury. *Current Opinion in Toxicology* 27, pp. 18-26.

91. Greenberg, J. A. et al. 2011. Folic Acid supplementation and pregnancy: more than just neural tube defect prevention. *Rev Obstet Gynecol* 4(2), pp. 52-59.

92. Yan, L. J. 2021. Folic acid-induced animal model of kidney disease. *Animal Model Exp Med* 4(4), pp. 329-342.

93. He, S. et al. 2013. EGFR activity is required for renal tubular cell dedifferentiation and proliferation in a murine model of folic acid-induced acute kidney injury. *Am J Physiol Renal Physiol* 304(4), pp. F356-366.

94. Makris, K. and Spanou, L. 2016. Acute Kidney Injury: Definition, Pathophysiology and Clinical Phenotypes. *Clin Biochem Rev* 37(2), pp. 85-98.

95. Shiva, N. et al. 2020. Renal ischemia/reperfusion injury: An insight on in vitro and in vivo models. *Life Sci* 256, p. 117860.

96. Kato, J. et al. 2014. Ischemia/reperfusion of unilateral kidney exaggerates aging-induced damage to the heart and contralateral kidney. *Nephron Exp Nephrol* 126(4), pp. 183-190.

97. Su, M. Y. et al. 2015. MRI evaluation of the adaptive response of the contralateral kidney following nephrectomy in patients with renal cell carcinoma. *J Magn Reson Imaging* 41(3), pp. 822-828.

98. Harwood, R. et al. 2022. Murine models of renal ischemia reperfusion injury: An opportunity for refinement using noninvasive monitoring methods. *Physiol Rep* 10(5), p. e15211.

99. Mehta, R. H. et al. 2006. Bedside tool for predicting the risk of postoperative dialysis in patients undergoing cardiac surgery. *Circulation* 114(21), pp. 2208-2216; quiz 2208.

100. Chen, J. J. et al. 2022. Acute Kidney Disease After Acute Decompensated Heart Failure. *Kidney Int Rep* 7(3), pp. 526-536.

101. Jain, A. et al. 2017. Risk factors for developing acute kidney injury in older people with diabetes and community-acquired pneumonia: a population-based UK cohort study. *BMC Nephrol* 18(1), p. 142.

102. Siew, E. D. et al. 2016. Predictors of Recurrent AKI. *J Am Soc Nephrol* 27(4), pp. 1190-1200.

103. Hobson, C. et al. 2017. Perioperative Acute Kidney Injury: Risk Factors and Predictive Strategies. *Crit Care Clin* 33(2), pp. 379-396.

104. Gong, D. J. et al. 2019. Diabetes aggravates renal ischemia and reperfusion injury in rats by exacerbating oxidative stress, inflammation, and apoptosis. *Ren Fail* 41(1), pp. 750-761.

105. Xu, X. et al. 2014. Aging aggravates long-term renal ischemia-reperfusion injury in a rat model. *J Surg Res* 187(1), pp. 289-296.

106. Neugarten, J. and Golestaneh, L. 2022. Sex Differences in Acute Kidney Injury. *Semin Nephrol* 42(2), pp. 208-218.

107. Müller, V. et al. 2002. Sexual dimorphism in renal ischemia-reperfusion injury in rats: possible role of endothelin. *Kidney Int* 62(4), pp. 1364-1371.

108. Ferreiro, A. and Lombardi, R. 2017. Acute kidney injury after cardiac surgery is associated with mid-term but not long-term mortality: A cohort-based study. *PLoS One* 12(7), p. e0181158.

109. Ponticelli, C. 2014. Ischaemia-reperfusion injury: a major protagonist in kidney transplantation. *Nephrol Dial Transplant* 29(6), pp. 1134-1140.

110. Chen, F. and Date, H. 2015. Update on ischemia-reperfusion injury in lung transplantation. *Curr Opin Organ Transplant* 20(5), pp. 515-520.

111. Dar, W. A. et al. 2019. Ischaemia reperfusion injury in liver transplantation: Cellular and molecular mechanisms. *Liver Int* 39(5), pp. 788-801.

112. Epstein, F. H. 1997. Oxygen and renal metabolism. *Kidney Int* 51(2), pp. 381-385.

113. Brezis, M. and Rosen, S. 1995. Hypoxia of the renal medulla--its implications for disease. *N Engl J Med* 332(10), pp. 647-655.

114. Palmer, L. G. and Schnermann, J. 2015. Integrated Control of Na Transport along the Nephron. *Clinical Journal of the American Society of Nephrology* 10(4), pp. 676-687.

115. Zhang, J. L. et al. 2014. Measurement of renal tissue oxygenation with blood oxygen level-dependent MRI and oxygen transit modeling. *Am J Physiol Renal Physiol* 306(6), pp. F579-587.

116. Bastin, J. et al. 1987. Change in energy reserves in different segments of the nephron during brief ischemia. *Kidney Int* 31(6), pp. 1239-1247.

117. Weinberg, J. M. 1991. The cell biology of ischemic renal injury. *Kidney Int* 39(3), pp. 476-500.

118. Yamashita, J. et al. 2003. Attenuation of ischemia/reperfusion-induced renal injury in mice deficient in Na+/Ca2+ exchanger. *J Pharmacol Exp Ther* 304(1), pp. 284-293.

119. Edelstein, C. L. et al. 1996. Modulation of hypoxia-induced calpain activity in rat renal proximal tubules. *Kidney Int* 50(4), pp. 1150-1157.

120. Han, S. J. and Lee, H. T. 2019. Mechanisms and therapeutic targets of ischemic acute kidney injury. *Kidney Res Clin Pract* 38(4), pp. 427-440.

121. Chazelas, P. et al. 2021. Oxidative Stress Evaluation in Ischemia Reperfusion Models: Characteristics, Limits and Perspectives. *Int J Mol Sci* 22(5).

122. Wijermars, L. G. et al. 2017. The hypoxanthine-xanthine oxidase axis is not involved in the initial phase of clinical transplantation-related ischemia-reperfusion injury. *Am J Physiol Renal Physiol* 312(3), pp. F457-f464.

123. Tsuda, H. et al. 2012. Febuxostat suppressed renal ischemia-reperfusion injury via reduced oxidative stress. *Biochem Biophys Res Commun* 427(2), pp. 266-272.

124. Zhang, X. et al. 2021. The Role of Mitochondria in Acute Kidney Injury and Chronic Kidney Disease and Its Therapeutic Potential. *Int J Mol Sci* 22(20).

125. Lee, H. L. et al. 2012. Biphasic modulation of the mitochondrial electron transport chain in myocardial ischemia and reperfusion. *Am J Physiol Heart Circ Physiol* 302(7), pp. H1410-1422.

126. Chouchani, E. T. et al. 2014. Ischaemic accumulation of succinate controls reperfusion injury through mitochondrial ROS. *Nature* 515(7527), pp. 431-435.

127. Choi, E. K. et al. 2017. Inhibition of Oxidative Stress in Renal Ischemia-Reperfusion Injury. *Anesth Analg* 124(1), pp. 204-213.

128. Simone, S. et al. 2014. Complement-dependent NADPH oxidase enzyme activation in renal ischemia/reperfusion injury. *Free Radic Biol Med* 74, pp. 263-273.

129. Li, C. and Jackson, R. M. 2002. Reactive species mechanisms of cellular hypoxia-reoxygenation injury. *Am J Physiol Cell Physiol* 282(2), pp. C227-241.

130. Zhang, S. et al. 2022. Role of Mitochondrial Pathways in Cell Apoptosis during He-Patic Ischemia/Reperfusion Injury. *Int J Mol Sci* 23(4).

131. Shi, Y. et al. 2000. Downregulation of the calpain inhibitor protein calpastatin by caspases during renal ischemia-reperfusion. *Am J Physiol Renal Physiol* 279(3), pp. F509-517.

132. Borkan, S. C. 2016. The Role of BCL-2 Family Members in Acute Kidney Injury. *Semin Nephrol* 36(3), pp. 237-250.

133. Hatok, J. and Racay, P. 2016. Bcl-2 family proteins: master regulators of cell survival. *Biomol Concepts* 7(4), pp. 259-270.

134. Youle, R. J. and Strasser, A. 2008. The BCL-2 protein family: opposing activities that mediate cell death. *Nat Rev Mol Cell Biol* 9(1), pp. 47-59.

135. Priante, G. et al. 2019. Cell Death in the Kidney. *Int J Mol Sci* 20(14).

136. Ueda, N. et al. 2000. Apoptotic mechanisms in acute renal failure. *Am J Med* 108(5), pp. 403-415.

137. Jan, R. and Chaudhry, G. E. 2019. Understanding Apoptosis and Apoptotic Pathways Targeted Cancer Therapeutics. *Adv Pharm Bull* 9(2), pp. 205-218.

138. Proskuryakov, S. Y. et al. 2002. Necrosis is an active and controlled form of programmed cell death. *Biochemistry (Mosc)* 67(4), pp. 387-408.

139. Lau, A. et al. 2013. RIPK3-mediated necroptosis promotes donor kidney inflammatory injury and reduces allograft survival. *Am J Transplant* 13(11), pp. 2805-2818.

140. Linkermann, A. et al. 2012. Rip1 (receptor-interacting protein kinase 1) mediates necroptosis and contributes to renal ischemia/reperfusion injury. *Kidney Int* 81(8), pp. 751-761.

141. Newton, K. et al. 2016. RIPK3 deficiency or catalytically inactive RIPK1 provides greater benefit than MLKL deficiency in mouse models of inflammation and tissue injury. *Cell Death Differ* 23(9), pp. 1565-1576.

142. Rabb, H. et al. 1997. Leukocytes, cell adhesion molecules and ischemic acute renal failure. *Kidney Int* 51(5), pp. 1463-1468.

143. Molitoris, B. A. et al. 2002. Endothelial injury and dysfunction in ischemic acute renal failure. *Crit Care Med* 30(5 Suppl), pp. S235-240.

144. Summers, W. K. and Jamison, R. L. 1971. The no reflow phenomenon in renal ischemia. *Lab Invest* 25(6), pp. 635-643.

145. Legrand, M. et al. 2008. Renal hypoxia and dysoxia after reperfusion of the ischemic kidney. *Mol Med* 14(7-8), pp. 502-516.

146. Rabb, H. et al. 2016. Inflammation in AKI: Current Understanding, Key Questions, and Knowledge Gaps. *J Am Soc Nephrol* 27(2), pp. 371-379.

147. Ochando, J. et al. 2023. Trained immunity - basic concepts and contributions to immunopathology. *Nat Rev Nephrol* 19(1), pp. 23-37.

148. Rosin, D. L. and Okusa, M. D. 2011. Dangers within: DAMP responses to damage and cell death in kidney disease. *J Am Soc Nephrol* 22(3), pp. 416-425.

149. Ludes, P. O. et al. 2021. Role of Damage-Associated Molecular Patterns in Septic Acute Kidney Injury, From Injury to Recovery. *Front Immunol* 12, p. 606622.

150. Rusai, K. et al. 2010. Toll-like receptors 2 and 4 in renal ischemia/reperfusion injury. *Pediatr Nephrol* 25(5), pp. 853-860.

151. Li, Q. and Lan, P. 2023. Activation of immune signals during organ transplantation. *Signal Transduct Target Ther* 8(1), p. 110.

152. Stasi, A. et al. 2017. Emerging role of Lipopolysaccharide binding protein in sepsis-induced acute kidney injury. *Nephrol Dial Transplant* 32(1), pp. 24-31.

153. Vasselon, T. et al. 2004. TLR2 recognizes a bacterial lipopeptide through direct binding. *J Immunol* 173(12), pp. 7401-7405.

154. Shigeoka, A. A. et al. 2007. TLR2 is constitutively expressed within the kidney and participates in ischemic renal injury through both MyD88-dependent and -independent pathways. *J Immunol* 178(10), pp. 6252-6258.

155. Zhao, H. et al. 2014. Role of Toll-like receptor-4 in renal graft ischemia-reperfusion injury. *Am J Physiol Renal Physiol* 306(8), pp. F801-811.

156. Wang, S. et al. 2016. Necroptosis in acute kidney injury: a shedding light. *Cell Death Dis* 7(3), p. e2125.

157. Wu, H. et al. 2007. TLR4 activation mediates kidney ischemia/reperfusion injury. *J Clin Invest* 117(10), pp. 2847-2859.

158. Bolisetty, S. and Agarwal, A. 2009. Neutrophils in acute kidney injury: not neutral any more. *Kidney Int* 75(7), pp. 674-676.

159. Awad, A. S. et al. 2009. Compartmentalization of neutrophils in the kidney and lung following acute ischemic kidney injury. *Kidney Int* 75(7), pp. 689-698.

160. Li, L. and Okusa, M. D. 2010. Macrophages, dendritic cells, and kidney ischemia-reperfusion injury. *Semin Nephrol* 30(3), pp. 268-277.

161. Huen, S. C. and Cantley, L. G. 2017. Macrophages in Renal Injury and Repair. *Annu Rev Physiol* 79, pp. 449-469.

162. Li, L. et al. 2008. The chemokine receptors CCR2 and CX3CR1 mediate monocyte/macrophage trafficking in kidney ischemia-reperfusion injury. *Kidney Int* 74(12), pp. 1526-1537.

163. Jin, J. et al. 2022. Novel insights into NOD-like receptors in renal diseases. *Acta Pharmacol Sin* 43(11), pp. 2789-2806.

164. Keestra-Gounder, A. M. and Tsolis, R. M. 2017. NOD1 and NOD2: Beyond Peptidoglycan Sensing. *Trends Immunol* 38(10), pp. 758-767.

165. Keestra-Gounder, A. M. et al. 2016. NOD1 and NOD2 signalling links ER stress with inflammation. *Nature* 532(7599), pp. 394-397.

166. Shigeoka, A. A. et al. 2010. Nod1 and nod2 are expressed in human and murine renal tubular epithelial cells and participate in renal ischemia reperfusion injury. *J Immunol* 184(5), pp. 2297-2304.

167. Kasimsetty, S. G. et al. 2020. TLR2 and NODs1 and 2 cooperate in inflammatory responses associated with renal ischemia reperfusion injury. *Transpl Immunol* 58, p. 101260.

168. Jo, S. K. et al. 2006. Macrophages contribute to the initiation of ischaemic acute renal failure in rats. *Nephrol Dial Transplant* 21(5), pp. 1231-1239.

169. Okusa, M. D. and Li, L. 2012. Dendritic cells in acute kidney injury: cues from the microenvironment. *Trans Am Clin Climatol Assoc* 123, pp. 54-62; discussion 62-53.

170. McCullough, J. W. et al. 2013. The role of the complement system in acute kidney injury. *Semin Nephrol* 33(6), pp. 543-556.

171. Danobeitia, J. S. et al. 2014. The role of complement in the pathogenesis of renal ischemia-reperfusion injury and fibrosis. *Fibrogenesis Tissue Repair* 7, p. 16.

172. Sacks, S. H. 2010. Complement fragments C3a and C5a: the salt and pepper of the immune response. *Eur J Immunol* 40(3), pp. 668-670.

173. Peng, Q. et al. 2012. C3a and C5a promote renal ischemia-reperfusion injury. *J Am Soc Nephrol* 23(9), pp. 1474-1485.

174. Zhou, W. et al. 2000. Predominant role for C5b-9 in renal ischemia/reperfusion injury. *J Clin Invest* 105(10), pp. 1363-1371.

175. Bhat, M. Y. et al. 2018. Comprehensive network map of interferon gamma signaling. *J Cell Commun Signal* 12(4), pp. 745-751.

176. Dellepiane, S. et al. 2020. T Cells and Acute Kidney Injury: A Two-Way Relationship. *Front Immunol* 11, p. 1546.

177. Burne, M. J. et al. 2001. Identification of the CD4(+) T cell as a major pathogenic factor in ischemic acute renal failure. *J Clin Invest* 108(9), pp. 1283-1290.

178. Bulkley, G. B. 1987. Free radical-mediated reperfusion injury: a selective review. *Br J Cancer Suppl* 8, pp. 66-73.

179. Murry, C. E. et al. 1986. Preconditioning with ischemia: a delay of lethal cell injury in ischemic myocardium. *Circulation* 74(5), pp. 1124-1136.

180. Reimer, K. A. et al. 1986. Four brief periods of myocardial ischemia cause no cumulative ATP loss or necrosis. *Am J Physiol* 251(6 Pt 2), pp. H1306-1315.

181. Zhu, X. et al. 2007. Ischemic preconditioning prevents in vivo hyperoxygenation in postischemic myocardium with preservation of mitochondrial oxygen consumption. *Am J Physiol Heart Circ Physiol* 293(3), pp. H1442-1450.

182. Shen, S. et al. 2017. The protective effects of ischemic preconditioning on rats with renal ischemia-reperfusion injury and the effects on the expression of Bcl-2 and Bax. *Exp Ther Med* 14(5), pp. 4077-4082.

183. Kume, M. et al. 1996. Ischemic preconditioning of the liver in rats: implications of heat shock protein induction to increase tolerance of ischemia-reperfusion injury. *J Lab Clin Med* 128(3), pp. 251-258.

184. Herajarvi, J. et al. 2017. Exploring effects of remote ischemic preconditioning in a pig model of hypothermic circulatory arrest. *Scand Cardiovasc J* 51(4), pp. 233-241.

185. Takaoka, A. et al. 1999. Renal ischemia/reperfusion remotely improves myocardial energy metabolism during myocardial ischemia via adenosine receptors in rabbits: effects of "remote preconditioning". *J Am Coll Cardiol* 33(2), pp. 556-564.

186. Cochrane, J. et al. 1999. Ischemic preconditioning attenuates functional, metabolic, and morphologic injury from ischemic acute renal failure in the rat. *Ren Fail* 21(2), pp. 135-145.

187. Islam, C. F. et al. 1997. Ischaemia-reperfusion injury in the rat kidney: the effect of preconditioning. *Br J Urol* 79(6), pp. 842-847.

188. Toosy, N. et al. 1999. Ischaemic preconditioning protects the rat kidney from reperfusion injury. *BJU Int* 84(4), pp. 489-494.

189. Wever, K. E. et al. 2012. Ischemic preconditioning in the animal kidney, a systematic review and meta-analysis. *PLoS One* 7(2), p. e32296.

190. Khalid, U. 2016. The role of microRNAs and Ischaemic Preconditioning in Kidney Ischaemia Reperfusion Injury.

191. Khalid, U. et al. 2015. A Localized Ischemic Preconditioning Regimen Increases Tumor Necrosis Factor alpha Expression in a Rat Model of Kidney Ischemia-Reperfusion Injury. *Exp Clin Transplant* 13(6), pp. 535-542.

192. Khalid, U. et al. 2021. Determination of a microRNA signature of protective kidney ischemic preconditioning originating from proximal tubules. *Sci Rep* 11(1), p. 9862.

193. Seyama, Y. et al. 2013. Intermittent clamping is superior to ischemic preconditioning and its effect is more marked with shorter clamping cycles in the rat liver. *J Gastroenterol* 48(1), pp. 115-124.

194. Ebrahimi, S. M. et al. 2012. Consequences of Ischemic Preconditioning of Kidney: Comparing between Male and Female Rats. *Iran J Basic Med Sci* 15(6), pp. 1148-1153.

195. Fan, L. H. et al. 2012. Effect of ischemia preconditioning on renal ischemia/reperfusion injury in rats. *Int Braz J Urol* 38(6), pp. 842-854.

196. Lazaris, A. M. et al. 2009. Protective effect of remote ischemic preconditioning in renal ischemia/reperfusion injury, in a model of thoracoabdominal aorta approach. *J Surg Res* 154(2), pp. 267-273.

197. Hussein, A. M. et al. 2016. Possible Underlying Mechanisms of the Renoprotective Effect of Remote Limb Ischemic Preconditioning Against Renal Ischemia/Reperfusion Injury: A Role of Osteopontin, Transforming Growth Factor-Beta and Survivin. *Nephron* 133(4).

198. Wever, K. E. et al. 2011. Remote ischaemic preconditioning by brief hind limb ischaemia protects against renal ischaemia-reperfusion injury: the role of adenosine. *Nephrol Dial Transplant* 26(10), pp. 3108-3117.

199. Huang, C. H. et al. 2015. Myocardial preconditioning reduces kidney injury and apoptosis induced by myocardial ischaemia and reperfusion. *Eur J Cardiothorac Surg* 48(3), pp. 382-391.

200. Liu, X. et al. 2007. Attenuation of reperfusion injury by renal ischemic postconditioning: the role of NO. *Biochem Biophys Res Commun* 359(3), pp. 628-634.

201. Chen, H. et al. 2008. Ischemic postconditioning inhibits apoptosis after renal ischemia/reperfusion injury in rat. *Transpl Int* 21(4), pp. 364-371.

202. Jiang, H. et al. 2015. Protective effects of three remote ischemic conditioning procedures against renal ischemic/reperfusion injury in rat kidneys: a comparative study. *Ir J Med Sci* 184(3), pp. 647-653.

203. Rabadi, M. M. and Lee, H. T. 2015. Adenosine receptors and renal ischaemia reperfusion injury. *Acta Physiol (Oxf)* 213(1), pp. 222-231.

204. Habibey, R. and Pazoki-Toroudi, H. 2008. Morphine dependence protects rat kidney against ischaemia-reperfusion injury. *Clin Exp Pharmacol Physiol* 35(10), pp. 1209-1214.

205. Hausenloy, D. J. and Yellon, D. M. 2004. New directions for protecting the heart against ischaemia-reperfusion injury: targeting the Reperfusion Injury Salvage Kinase (RISK)-pathway. *Cardiovasc Res* 61(3), pp. 448-460.

206. Zha, J. et al. 1996. Serine phosphorylation of death agonist BAD in response to survival factor results in binding to 14-3-3 not BCL-X(L). *Cell* 87(4), pp. 619-628.

207. Grenz, A. et al. 2008. The reno-vascular A2B adenosine receptor protects the kidney from ischemia. *PLoS Med* 5(6), p. e137.

208. Lee, H. T. and Emala, C. W. 2000. Protective effects of renal ischemic preconditioning and adenosine pretreatment: role of A(1) and A(3) receptors. *Am J Physiol Renal Physiol* 278(3), pp. F380-387.

209. Kim, M. et al. 2009. Kidney-specific reconstitution of the A1 adenosine receptor in A1 adenosine receptor knockout mice reduces renal ischemia-reperfusion injury. *Kidney Int* 75(8), pp. 809-823.

210. Lee, H. T. and Emala, C. W. 2001. Protein kinase C and G(i/o) proteins are involved in adenosine- and ischemic preconditioning-mediated renal protection. *J Am Soc Nephrol* 12(2), pp. 233-240.

211. Kakoki, M. et al. 2007. Bradykinin B1 and B2 receptors both have protective roles in renal ischemia/reperfusion injury. *Proc Natl Acad Sci U S A* 104(18), pp. 7576-7581.

212. Jang, H. S. et al. 2013. Activation of ERK accelerates repair of renal tubular epithelial cells, whereas it inhibits progression of fibrosis following ischemia/reperfusion injury. *Biochim Biophys Acta* 1832(12), pp. 1998-2008.

213. Ban, K. et al. 2013. Inhibition of ERK1/2 worsens intestinal ischemia/reperfusion injury. *PLoS One* 8(9), p. e76790.

214. Costa, A. D. et al. 2005. Protein kinase G transmits the cardioprotective signal from cytosol to mitochondria. *Circ Res* 97(4), pp. 329-336.

215. Chujo, K. et al. 2010. Atrial natriuretic peptide enhances recovery from ischemia/reperfusion-induced renal injury in rats. *J Biosci Bioeng* 109(6), pp. 526-530.

216. Tulafu, M. et al. 2014. Atrial natriuretic peptide attenuates kidney-lung crosstalk in kidney injury. *J Surg Res* 186(1), pp. 217-225.

217. Li, Y. et al. 2012. Overexpression of cGMP-dependent protein kinase I (PKG-I) attenuates ischemia-reperfusion-induced kidney injury. *Am J Physiol Renal Physiol* 302(5), pp. F561-570.

218. Simkhovich, B. Z. et al. 2013. Role of protein kinase C in ischemic "conditioning": from first evidence to current perspectives. *J Cardiovasc Pharmacol Ther* 18(6), pp. 525-532.

219. Gholampour, F. et al. 2018. The role of nitric oxide in the protective action of remote ischemic per-conditioning against ischemia/reperfusion-induced acute renal failure in rat. *Iran J Basic Med Sci* 21(6), pp. 600-606.

220. Ling, H. et al. 1999. Attenuation of renal ischemia-reperfusion injury in inducible nitric oxide synthase knockout mice. *Am J Physiol* 277(3), pp. F383-390.

221. Ogawa, T. et al. 2001. Contribution of nitric oxide to the protective effects of ischemic preconditioning in ischemia-reperfused rat kidneys. *J Lab Clin Med* 138(1), pp. 50-58.

222. Mahfoudh-Boussaid, A. et al. 2012. Ischemic preconditioning reduces endoplasmic reticulum stress and upregulates hypoxia inducible factor-1alpha in ischemic kidney: the role of nitric oxide. *J Biomed Sci* 19, p. 7.

223. Liu, Z. and Gong, R. 2015. Remote ischemic preconditioning for kidney protection: GSK3β-centric insights into the mechanism of action. *Am J Kidney Dis* 66(5), pp. 846-856.

224. Wang, Z. et al. 2010. GSK3beta promotes apoptosis after renal ischemic injury. *J Am Soc Nephrol* 21(2), pp. 284-294.

225. Nezu, M. et al. 2017. Transcription factor Nrf2 hyperactivation in early-phase renal ischemia-reperfusion injury prevents tubular damage progression. *Kidney Int* 91(2), pp. 387-401.

226. Li, J. R. et al. 2019. Ischemic preconditioning improved renal ischemia/reperfusion injury and hyperglycemia. *IUBMB Life* 71(3), pp. 321-329.

227. Liu, M. et al. 2014. The Nrf2 triterpenoid activator, CDDO-imidazolide, protects kidneys from ischemia-reperfusion injury in mice. *Kidney Int* 85(1), pp. 134-141.

228. Shokeir, A. A. et al. 2014. Activation of nuclear factor erythroid 2-related factor 2 (Nrf2) and Nrf-2-dependent genes by ischaemic pre-conditioning and post-conditioning: new adaptive endogenous protective responses against renal ischaemia/reperfusion injury. *Acta Physiol (Oxf)* 210(2), pp. 342-353.

229. Choi, H. S. et al. 2017. The optimal duration of ischemic preconditioning for renal ischemia-reperfusion injury in mice. *Ann Surg Treat Res* 93(4), pp. 209-216.

230. Shen, Y. et al. 2018. Renal ischemia-reperfusion injury attenuated by splenic ischemic preconditioning. *Eur Rev Med Pharmacol Sci* 22(7), pp. 2134-2142.

231. Hou, L. et al. 2016. Small interfering RNA targeting TNF-α gene significantly attenuates renal ischemia-reperfusion injury in mice. *J Huazhong Univ Sci Technolog Med Sci* 36(5), pp. 634-638.

232. Patel, N. S. et al. 2005. Endogenous interleukin-6 enhances the renal injury, dysfunction, and inflammation caused by ischemia/reperfusion. *J Pharmacol Exp Ther* 312(3), pp. 1170-1178.

233. Lee, J. A. et al. 2012. Hepatic ischemic preconditioning provides protection against distant renal ischemia and reperfusion injury in mice. *J Korean Med Sci* 27(5), pp. 547-552.

234. Kelly, K. J. et al. 1994. Antibody to intercellular adhesion molecule 1 protects the kidney against ischemic injury. *Proc Natl Acad Sci U S A* 91(2), pp. 812-816.

235. Zou, G. et al. 2021. Pioglitazone Ameliorates Renal Ischemia-Reperfusion Injury via Inhibition of NF-κB Activation and Inflammation in Rats. *Front Physiol* 12, p. 707344.

236. Kapitsinou, P. P. and Haase, V. H. 2015. Molecular mechanisms of ischemic preconditioning in the kidney. *Am J Physiol Renal Physiol* 309(10), pp. F821-834.

237. Zimmerman, R. F. et al. 2011. Ischemic preconditioning at a remote site prevents acute kidney injury in patients following cardiac surgery. *Kidney Int* 80(8), pp. 861-867.

238. Zarbock, A. et al. 2015. Effect of remote ischemic preconditioning on kidney injury among high-risk patients undergoing cardiac surgery: a randomized clinical trial. *Jama* 313(21), pp. 2133-2141.

239. Pinaud, F. et al. 2016. Remote ischemic preconditioning in aortic valve surgery: Results of a randomized controlled study. *J Cardiol* 67(1), pp. 36-41.

240. Kahlert, P. et al. 2017. No protection of heart, kidneys and brain by remote ischemic preconditioning before transfemoral transcatheter aortic valve implantation: Interim-analysis of a randomized single-blinded, placebo-controlled, single-center trial. *Int J Cardiol* 231, pp. 248-254.

241. Kim, T. K. et al. 2017. Effects of delayed remote ischemic preconditioning on peri-operative myocardial injury in patients undergoing cardiac surgery - A randomized controlled trial. *Int J Cardiol* 227, pp. 511-515.

242. Zhou, F. et al. 2018. Effects of remote ischemic preconditioning on contrast induced nephropathy after percutaneous coronary intervention in patients with acute coronary syndrome. *Medicine (Baltimore)* 97(2), p. e9579.

243. Hong, D. M. et al. 2014. Does remote ischaemic preconditioning with postconditioning improve clinical outcomes of patients undergoing cardiac surgery? Remote Ischaemic Preconditioning with Postconditioning Outcome Trial. *Eur Heart J* 35(3), pp. 176-183.

244. Hausenloy, D. J. et al. 2015. Remote Ischemic Preconditioning and Outcomes of Cardiac Surgery. *N Engl J Med* 373(15), pp. 1408-1417.

245. Meybohm, P. et al. 2015. A Multicenter Trial of Remote Ischemic Preconditioning for Heart Surgery. *N Engl J Med* 373(15), pp. 1397-1407.

246. Deftereos, S. et al. 2013. Renoprotective effect of remote ischemic post-conditioning by intermittent balloon inflations in patients undergoing percutaneous coronary intervention. *J Am Coll Cardiol* 61(19), pp. 1949-1955.

247. Zarbock, A. et al. 2017. Long-term Effects of Remote Ischemic Preconditioning on Kidney Function in High-risk Cardiac Surgery Patients: Follow-up Results from the RenalRIP Trial. *Anesthesiology* 126(5), pp. 787-798.

248. Li, B. et al. 2017. Effect of remote ischemic preconditioning on postoperative acute kidney injury among patients undergoing cardiac and vascular interventions: a meta-analysis. *J Nephrol* 30(1), pp. 19-33.

249. Yang, Y. et al. 2014. Remote ischemic preconditioning for prevention of acute kidney injury: a meta-analysis of randomized controlled trials. *Am J Kidney Dis* 64(4), pp. 574-583.

250. Sardar, P. et al. 2016. Remote ischemic preconditioning in patients undergoing cardiovascular surgery: Evidence from a meta-analysis of randomized controlled trials. *Int J Cardiol* 221, pp. 34-41.

251. Zhang, L. et al. 2016. Remote ischemic conditioning for kidney protection: A meta-analysis. *J Crit Care* 33, pp. 224-232.

252. Zhang, Y. et al. 2016. Remote Ischemic Preconditioning for Prevention of Acute Kidney Injury in Patients Undergoing On-Pump Cardiac Surgery: A Systematic Review and Meta-Analysis. *Medicine (Baltimore)* 95(37), p. e3465.

253. Haji Mohd Yasin, N. A. et al. 2014. The role of remote ischemic preconditioning in organ protection after cardiac surgery: a meta-analysis. *J Surg Res* 186(1), pp. 207-216.

254. Zhang, B. et al. 2014. Remote ischemic preconditioning does not improve the clinical outcomes in patients undergoing coronary artery bypass grafting: a meta-analysis of randomized controlled trials. *Int J Cardiol* 172(1), pp. e36-38.

255. Wang, S. et al. 2017. Impact of remote ischaemic preconditioning on major clinical outcomes in patients undergoing cardiovascular surgery: A meta-analysis with trial sequential analysis of 32 randomised controlled trials. *Int J Cardiol* 227, pp. 882-891.

256. Zuo, B. et al. 2015. Using remote ischemic conditioning to reduce acute kidney injury in patients undergoing percutaneous coronary intervention: a meta-analysis. *Curr Med Res Opin* 31(9), pp. 1677-1685.

257. Hu, J. et al. 2016. Protection of remote ischemic preconditioning against acute kidney injury: a systematic review and meta-analysis. *Crit Care* 20(1), p. 111.

258. Zhou, C. C. et al. 2017. Limited Clinical Utility of Remote Ischemic Conditioning in Renal Transplantation: A Meta-Analysis of Randomized Controlled Trials. *PLoS One* 12(1), p. e0170729.

259. Cao, Z. et al. 2017. Effects of remote ischemic preconditioning on acute myocardial injury in patients undergoing valve replacement. *Ir J Med Sci* 186(4), pp. 889-893.

260. Hou, Y. Y. et al. 2017. Effects of differential-phase remote ischemic preconditioning intervention in laparoscopic partial nephrectomy: A single blinded, randomized controlled trial in a parallel group design. *J Clin Anesth* 41, pp. 21-28.

261. Guerra, G. G. et al. 2017. Pilot randomized controlled trial on early and late remote ischemic preconditioning prior to complex cardiac surgery in young infants. *Paediatr Anaesth* 27(4), pp. 433-441.

262. Balbir Singh, G. et al. 2016. Remote Ischemic Preconditioning for the Prevention of Contrast-Induced Acute Kidney Injury in Diabetics Receiving Elective Percutaneous Coronary Intervention. *PLoS One* 11(10), p. e0164256.

263. Garcia, S. et al. 2016. Cardiac Remote Ischemic Preconditioning Prior to Elective Vascular Surgery (CRIPES): A Prospective, Randomized, Sham-Controlled Phase II Clinical Trial. *J Am Heart Assoc* 5(10).

264. Walsh, M. et al. 2016. Effects of remote ischemic preconditioning in high-risk patients undergoing cardiac surgery (Remote IMPACT): a randomized controlled trial. *Cmaj* 188(5), pp. 329-336.

265. Menting, T. P. et al. 2015. Remote Ischemic Preconditioning To Reduce Contrast-Induced Nephropathy: A Randomized Controlled Trial. *Eur J Vasc Endovasc Surg* 50(4), pp. 527-532.

266. Gallagher, S. M. et al. 2015. Remote ischemic preconditioning has a neutral effect on the incidence of kidney injury after coronary artery bypass graft surgery. *Kidney Int* 87(2), pp. 473-481.

267. Candilio, L. et al. 2015. Effect of remote ischaemic preconditioning on clinical outcomes in patients undergoing cardiac bypass surgery: a randomised controlled clinical trial. *Heart* 101(3), pp. 185-192.

268. Yamanaka, T. et al. 2015. Remote ischemic preconditioning reduces contrast-induced acute kidney injury in patients with ST-elevation myocardial infarction: a randomized controlled trial. *Int J Cardiol* 178, pp. 136-141.

269. Savaj, S. et al. 2014. Remote ischemic preconditioning for prevention of contrast-induced acute kidney injury in diabetic patients. *Iran J Kidney Dis* 8(6), pp. 457-460.

270. Murphy, N. et al. 2014. Remote ischemic preconditioning does not affect the incidence of acute kidney injury after elective abdominal aortic aneurysm repair. *J Cardiothorac Vasc Anesth* 28(5), pp. 1285-1292.

271. McCrindle, B. W. et al. 2014. Remote ischemic preconditioning in children undergoing cardiac surgery with cardiopulmonary bypass: a single-center double-blinded randomized trial. *J Am Heart Assoc* 3(4).

272. Lavi, S. et al. 2014. Remote ischemic postconditioning during percutaneous coronary interventions: remote ischemic postconditioning-percutaneous coronary intervention randomized trial. *Circ Cardiovasc Interv* 7(2), pp. 225-232.

273. Igarashi, G. et al. 2013. Remote ischemic pre-conditioning alleviates contrast-induced acute kidney injury in patients with moderate chronic kidney disease. *Circ J* 77(12), pp. 3037-3044.

274. Chen, Y. et al. 2013. Remote ischemic preconditioning fails to improve early renal function of patients undergoing living-donor renal transplantation: a randomized controlled trial. *Transplantation* 95(2), pp. e4-6.

275. Meybohm, P. et al. 2013. Postoperative neurocognitive dysfunction in patients undergoing cardiac surgery after remote ischemic preconditioning: a double-blind randomized controlled pilot study. *PLoS One* 8(5), p. e64743.

276. Luo, S. J. et al. 2013. Remote ischemic preconditioning reduces myocardial injury in patients undergoing coronary stent implantation. *Can J Cardiol* 29(9), pp. 1084-1089.

277. Er, F. et al. 2012. Ischemic preconditioning for prevention of contrast medium-induced nephropathy: randomized pilot RenPro Trial (Renal Protection Trial). *Circulation* 126(3), pp. 296-303.

278. Young, P. J. et al. 2012. A pilot study investigating the effects of remote ischemic preconditioning in high-risk cardiac surgery using a randomised controlled double-blind protocol. *Basic Res Cardiol* 107(3), p. 256.

279. Hong, D. M. et al. 2012. Effects of remote ischemic preconditioning with postconditioning in patients undergoing off-pump coronary artery bypass surgery--randomized controlled trial. *Circ J* 76(4), pp. 884-890.

280. Kim, J. C. et al. 2012. Effect of combined remote ischemic preconditioning and postconditioning on pulmonary function in valvular heart surgery. *Chest* 142(2), pp. 467-475.

281. Pedersen, K. R. et al. 2012. Failure of remote ischemic preconditioning to reduce the risk of postoperative acute kidney injury in children undergoing operation for complex

congenital heart disease: a randomized single-center study. *J Thorac Cardiovasc Surg* 143(3), pp. 576-583.

282. Choi, Y. S. et al. 2011. Effect of remote ischemic preconditioning on renal dysfunction after complex valvular heart surgery: a randomized controlled trial. *J Thorac Cardiovasc Surg* 142(1), pp. 148-154.

283. Rahman, I. A. et al. 2010. Remote ischemic preconditioning in human coronary artery bypass surgery: from promise to disappointment? *Circulation* 122(11 Suppl), pp. S53-59.

284. Venugopal, V. et al. 2010. Effect of remote ischemic preconditioning on acute kidney injury in nondiabetic patients undergoing coronary artery bypass graft surgery: a secondary analysis of 2 small randomized trials. *Am J Kidney Dis* 56(6), pp. 1043-1049.

285. Walsh, S. R. et al. 2010. Remote ischemic preconditioning for renal protection during elective open infrarenal abdominal aortic aneurysm repair: randomized controlled trial. *Vasc Endovascular Surg* 44(5), pp. 334-340.

286. Walsh, S. R. et al. 2009. Remote ischemic preconditioning for renal and cardiac protection during endovascular aneurysm repair: a randomized controlled trial. *J Endovasc Ther* 16(6), pp. 680-689.

287. Hoole, S. P. et al. 2009. Cardiac Remote Ischemic Preconditioning in Coronary Stenting (CRISP Stent) Study: a prospective, randomized control trial. *Circulation* 119(6), pp. 820-827.

288. Ali, Z. A. et al. 2007. Remote ischemic preconditioning reduces myocardial and renal injury after elective abdominal aortic aneurysm repair: a randomized controlled trial. *Circulation* 116(11 Suppl), pp. I98-105.

289. Ozbilgin, S. et al. 2016. Renal Ischemia/Reperfusion Injury in Diabetic Rats: The Role of Local Ischemic Preconditioning. *Biomed Res Int* 2016, p. 8580475.

290. Wider, J. et al. 2018. Remote ischemic preconditioning fails to reduce infarct size in the Zucker fatty rat model of type-2 diabetes: role of defective humoral communication. *Basic Res Cardiol* 113(3), p. 16.

291. Jankauskas, S. S. et al. 2017. The age-associated loss of ischemic preconditioning in the kidney is accompanied by mitochondrial dysfunction, increased protein acetylation and decreased autophagy. *Sci Rep* 7, p. 44430.

292. Chen, H. et al. 2008. Similarities between ozone oxidative preconditioning and ischemic preconditioning in renal ischemia/reperfusion injury. *Arch Med Res* 39(2), pp. 169-178.

293. Wever, K. E. et al. 2013. Humoral signalling compounds in remote ischaemic preconditioning of the kidney, a role for the opioid receptor. *Nephrol Dial Transplant* 28(7), pp. 1721-1732.

294. Julier, K. et al. 2003. Preconditioning by sevoflurane decreases biochemical markers for myocardial and renal dysfunction in coronary artery bypass graft surgery: a double-blinded, placebo-controlled, multicenter study. *Anesthesiology* 98(6), pp. 1315-1327.

295. Ambrosi, N. et al. 2016. alpha-Lipoic Acid Protects Against Ischemia-Reperfusion Injury in Simultaneous Kidney-Pancreas Transplantation. *Transplantation* 100(4), pp. 908-915.

296. Hombach, S. and Kretz, M. 2016. Non-coding RNAs: Classification, Biology and Functioning. *Adv Exp Med Biol* 937, pp. 3-17.

297. Liu, Z. et al. 2019. Non-coding RNAs in kidney injury and repair. *Am J Physiol Cell Physiol* 317(2), pp. C177-c188.

298. Manzoni, C. et al. 2018. Genome, transcriptome and proteome: the rise of omics data and their integration in biomedical sciences. *Brief Bioinform* 19(2), pp. 286-302.

299. Medicine, C. o. t. R. o. O.-B. T. f. P. P. O. i. C. T. B. o. H. C. S. B. o. H. S. P. I. o. 2012. *Evolution of Translational Omics: Lessons Learned and the Path Forward.* Washington (DC): National Academies Press (US).

300. Lowe, R. et al. 2017. Transcriptomics technologies. *PLoS Comput Biol* 13(5), p. e1005457.

301. Wang, Z. et al. 2009. RNA-Seq: a revolutionary tool for transcriptomics. *Nat Rev Genet* 10(1), pp. 57-63.

302. Kukurba, K. R. and Montgomery, S. B. 2015. RNA Sequencing and Analysis. *Cold Spring Harb Protoc* 2015(11), pp. 951-969.

303. Giraud, S. et al. 2018. Dynamic transcriptomic analysis of Ischemic Injury in a Porcine Pre-Clinical Model mimicking Donors Deceased after Circulatory Death. *Sci Rep* 8(1), p. 5986.

304. Park, M. et al. 2020. RNA-Seq identifies condition-specific biological signatures of ischemia-reperfusion injury in the human kidney. *BMC Nephrol* 21(Suppl 1), p. 398.

305. Correa-Costa, M. et al. 2012. Transcriptome analysis of renal ischemia/reperfusion injury and its modulation by ischemic pre-conditioning or hemin treatment. *PLoS One* 7(11), p. e49569.

306. Johnsen, M. et al. 2020. The Integrated RNA Landscape of Renal Preconditioning against Ischemia-Reperfusion Injury. *J Am Soc Nephrol* 31(4), pp. 716-730.

307. Khalid, U. et al. 2016. Kidney ischaemia reperfusion injury in the rat: the EGTI scoring system as a valid and reliable tool for histological assessment. *Journal of Histology and Histopathology* 3(1), p. 1.

308. S, A. 2010. *FastQC: a quality control tool for high throughput sequence data.* [Online]. Available at: http://www.bioinformatics.babraham.ac.uk/projects/fastqc [Accessed: 16/Mar/2017].

309. Mehta, R. L. et al. 2004. Spectrum of acute renal failure in the intensive care unit: the PICARD experience. *Kidney Int* 66(4), pp. 1613-1621.

310. Palevsky, P. M. et al. 2008. Intensity of renal support in critically ill patients with acute kidney injury. *N Engl J Med* 359(1), pp. 7-20.

311. Basile, D. P. et al. 2012. Pathophysiology of acute kidney injury. *Compr Physiol* 2(2), pp. 1303-1353.

312. Sharfuddin, A. A. and Molitoris, B. A. 2011. Pathophysiology of ischemic acute kidney injury. *Nat Rev Nephrol* 7(4), pp. 189-200.

313. Malek, M. and Nematbakhsh, M. 2015. Renal ischemia/reperfusion injury; from pathophysiology to treatment. *J Renal Inj Prev* 4(2), pp. 20-27.

314. Mehta, R. L. et al. 2004. Spectrum of acute renal failure in the intensive care unit: the PICARD experience. *Kidney Int* 66(4), pp. 1613-1621.

315. Coca, S. G. et al. 2009. Long-term risk of mortality and other adverse outcomes after acute kidney injury: a systematic review and meta-analysis. *Am J Kidney Dis* 53(6), pp. 961-973.

316. Joo, J. D. et al. 2006. Ischemic preconditioning provides both acute and delayed protection against renal ischemia and reperfusion injury in mice. *J Am Soc Nephrol* 17(11), pp. 3115-3123.

317. Chen, X. et al. 2009. Ischemic preconditioning attenuates renal ischemia-reperfusion injury by inhibiting activation of IKKbeta and inflammatory response. *Am J Nephrol* 30(3), pp. 287-294.

318. Liu, H. et al. 2013. Ischemic preconditioning increases endothelial progenitor cell number to attenuate partial nephrectomy-induced ischemia/reperfusion injury. *PLoS One* 8(1), p. e55389.

319. Yoon, Y. E. et al. 2015. Preconditioning strategies for kidney ischemia reperfusion injury: implications of the "time-window" in remote ischemic preconditioning. *PLoS One* 10(4), p. e0124130.

320. Bromage, D. I. et al. 2017. Remote ischaemic conditioning reduces infarct size in animal in vivo models of ischaemia-reperfusion injury: a systematic review and meta-analysis. *Cardiovasc Res* 113(3), pp. 288-297.

321. Menting, T. P. et al. 2017. Ischaemic preconditioning for the reduction of renal ischaemia reperfusion injury. *Cochrane Database Syst Rev* 3, p. Cd010777.

322. Ates, E. et al. 2002. Renal protection by brief liver ischemia in rats. *Transplantation* 74(9), pp. 1247-1251.

323. Williams, P. et al. 1997. Characterization of renal ischemia-reperfusion injury in rats. *J Pharmacol Toxicol Methods* 37(1), pp. 1-7.

324. Skrypnyk, N. I. et al. 2013. Ischemia-reperfusion model of acute kidney injury and post injury fibrosis in mice. *J Vis Exp* (78).

325. Jablonski, P. et al. 1983. An experimental model for assessment of renal recovery from warm ischemia. *Transplantation* 35(3), pp. 198-204.

326. Finn, W. F. et al. 1984. Attenuation of injury due to unilateral renal ischemia: delayed effects of contralateral nephrectomy. *J Lab Clin Med* 103(2), pp. 193-203.

327. Kierulf-Lassen, C. et al. 2017. Unilateral nephrectomy diminishes ischemic acute kidney injury through enhanced perfusion and reduced pro-inflammatory and pro-fibrotic responses. *PLoS One* 12(12), p. e0190009.

328. Jang, H. S. et al. 2012. Bone marrow derived cells and reactive oxygen species in hypertrophy of contralateral kidney of transient unilateral renal ischemia-induced mouse. *Free Radic Res* 46(7), pp. 903-911.

329. Fatemikia, H. et al. 2016. Distant effects of unilateral renal ischemia/reperfusion on contralateral kidney but not lung in rats: the roles of ROS and iNOS. *Can J Physiol Pharmacol* 94(5), pp. 477-487.

330. Zhao, H. et al. 2018. Ischemia-Reperfusion Injury Reduces Long Term Renal Graft Survival: Mechanism and Beyond. *EBioMedicine* 28, pp. 31-42.

331. Evans, K. et al. 2018. UK Renal Registry 20th Annual Report: Introduction. *Nephron* 139 Suppl 1, pp. 1-12.

332. Pine, J. K. et al. 2010. Impact of cold ischemia on renal transplant outcomes following donation after cardiac death. *Transplant Proc* 42(10), pp. 3951-3953.

333. Philipponnet, C. et al. 2018. Ischemia reperfusion injury in kidney transplantation: A case report. *Medicine (Baltimore)* 97(52), p. e13650.

334. Gassanov, N. et al. 2014. Remote ischemic preconditioning and renoprotection: from myth to a novel therapeutic option? *J Am Soc Nephrol* 25(2), pp. 216-224.

335. Schumacher, L. et al. 2014. Bihemispheric ischemic tolerance induced by a unilateral focal cortical lesion. *Brain Res* 1570, pp. 54-60.

336. Belayev, L. et al. 1996. Bilateral ischemic tolerance of rat hippocampus induced by prior unilateral transient focal ischemia: relationship to c-fos mRNA expression. *Neuroreport* 8(1), pp. 55-59.

337. Fan, C. et al. 2017. Reduced Severity of Outcome of Recurrent Ipsilateral Transient Cerebral Ischemia Compared with Contralateral Transient Cerebral Ischemia in Rats. *J Stroke Cerebrovasc Dis* 26(12), pp. 2915-2925.

338. Shimizu, S. et al. 2011. Protective effect of ischaemic post-conditioning on ipsilateral and contralateral testes after unilateral testicular ischaemia-reperfusion injury. *Int J Androl* 34(3), pp. 268-275.

339. Charlotte Victoria Maynard Brown, G. P.-C., Aeliya Zaidi, Irina Grigorieva, Emma Woods, Robert Steadman, Rafael Chavez, Soma Meran, Usman Khalid. 2023. Ischaemic Preconditioning attenuates Chronic Renal Damage following Ischaemia Reperfusion Injury. *bioRxiv*.

340. Moledina, D. G. et al. 2017. Performance of Serum Creatinine and Kidney Injury Biomarkers for Diagnosing Histologic Acute Tubular Injury. *Am J Kidney Dis* 70(6), pp. 807-816.

341. Parekh, D. J. et al. 2013. Tolerance of the human kidney to isolated controlled ischemia. *J Am Soc Nephrol* 24(3), pp. 506-517.

342. Santoriello, D. et al. 2020. Postmortem Kidney Pathology Findings in Patients with COVID-19. *J Am Soc Nephrol* 31(9), pp. 2158-2167.

343. Langenberg, C. et al. 2014. Renal histopathology during experimental septic acute kidney injury and recovery. *Crit Care Med* 42(1), pp. e58-67.

344. Trevisani, F. et al. 2021. Renal histology across the stages of chronic kidney disease. *J Nephrol* 34(3), pp. 699-707.

345. Park, K. M. et al. 2001. Prevention of kidney ischemia/reperfusion-induced functional injury and JNK, p38, and MAPK kinase activation by remote ischemic pretreatment. *J Biol Chem* 276(15), pp. 11870-11876.

346. Al-Hashimi, M. and Thompson, J. 2013. Anaesthesia for elective open abdominal aortic aneurysm repair. *BJA Education* 13(6), pp. 208-212.

347. Bedir, S. et al. 2015. Ineffectiveness of remote ischemic renal preconditioning in a porcine solitary-kidney model. *J Endourol* 29(5), pp. 590-594.

348. Khatri, P. et al. 2012. Ten years of pathway analysis: current approaches and outstanding challenges. *PLoS Comput Biol* 8(2), p. e1002375.

349. Yoshida, T. et al. 2002. Monitoring changes in gene expression in renal ischemia-reperfusion in the rat. *Kidney Int* 61(5), pp. 1646-1654.

350. Supavekin, S. et al. 2003. Differential gene expression following early renal ischemia/reperfusion. *Kidney Int* 63(5), pp. 1714-1724.

351. Kim, T. M. et al. 2011. Gene expression analysis reveals the cell cycle and kinetochore genes participating in ischemia reperfusion injury and early development in kidney. *PLoS One* 6(9), p. e25679.

352. Tammaro, A. et al. 2017. TREM-1 and its potential ligands in non-infectious diseases: from biology to clinical perspectives. *Pharmacol Ther* 177, pp. 81-95.

353. Tammaro, A. et al. 2016. Effect of TREM-1 blockade and single nucleotide variants in experimental renal injury and kidney transplantation. *Sci Rep* 6, p. 38275.

354. Tampella, G. et al. 2015. The Tec Kinase-Regulated Phosphoproteome Reveals a Mechanism for the Regulation of Inhibitory Signals in Murine Macrophages. *J Immunol* 195(1), pp. 246-256.

355. Zhang, M. J. et al. 2010. Stress signaling by Tec tyrosine kinase in the ischemic myocardium. *Am J Physiol Heart Circ Physiol* 299(3), pp. H713-722.

356. Zhao, J. et al. 2021. Bruton's tyrosine kinase regulates macrophage-induced inflammation in the diabetic kidney via NLRP3 inflammasome activation. *Int J Mol Med* 48(3).

357. Zhang, W. et al. 2020. Negative Regulation of Tec Kinase Alleviates LPS-Induced Acute Kidney Injury in Mice via theTLR4/NF-κB Signaling Pathway. *Biomed Res Int* 2020, p. 3152043.

358. Luan, Z. L. et al. 2022. Nuclear receptors in renal health and disease. *EBioMedicine* 76, p. 103855.

359. Yang, M. et al. 2015. The liver X receptor agonist TO901317 protects mice against cisplatin-induced kidney injury. *Exp Biol Med (Maywood)* 240(12), pp. 1717-1727.

360. Ding, H. et al. 2016. LXR agonist T0901317 upregulates thrombomodulin expression in glomerular endothelial cells by inhibition of nuclear factor-κB. *Mol Med Rep* 13(6), pp. 4888-4896.

361. Nezu, M. and Suzuki, N. 2020. Roles of Nrf2 in Protecting the Kidney from Oxidative Damage. *Int J Mol Sci* 21(8).

362. Tejchman, K. et al. 2021. Assessment of Oxidative Stress Markers in Hypothermic Preservation of Transplanted Kidneys. *Antioxidants (Basel)* 10(8).

363. Tan, K. P. et al. 2008. NRF2 as a determinant of cellular resistance in retinoic acid cytotoxicity. *Free Radic Biol Med* 45(12), pp. 1663-1673.

364. Prieto-Moure, B. et al. 2017. Allopurinol Protective Effect of Renal Ischemia by Downregulating TNF-α, IL-1β, and IL-6 Response. *J Invest Surg* 30(3), pp. 143-151.

365. Zagler, A. et al. 2006. N-acetylcysteine and contrast-induced nephropathy: a meta-analysis of 13 randomized trials. *Am Heart J* 151(1), pp. 140-145.

366. Hall, A. 1998. Rho GTPases and the actin cytoskeleton. *Science* 279(5350), pp. 509-514.

367. Han, S. J. et al. 2016. Inhibition of microtubule dynamics impedes repair of kidney ischemia/reperfusion injury and increases fibrosis. *Sci Rep* 6, p. 27775.

368. Bowers, S. L. K. et al. 2019. Inhibition of fibronectin polymerization alleviates kidney injury due to ischemia-reperfusion. *Am J Physiol Renal Physiol* 316(6), pp. F1293-f1298.

369. McCurley, A. et al. 2017. Inhibition of αvβ5 Integrin Attenuates Vascular Permeability and Protects against Renal Ischemia-Reperfusion Injury. *J Am Soc Nephrol* 28(6), pp. 1741-1752.

370. Cano-Peñalver, J. L. et al. 2016. Renal Integrin-Linked Kinase Depletion Induces Kidney cGMP-Axis Upregulation: Consequences on Basal and Acutely Damaged Renal Function. *Mol Med* 21(1), pp. 873-885.

371. Prakash, J. et al. 2008. Inhibition of renal rho kinase attenuates ischemia/reperfusion-induced injury. *J Am Soc Nephrol* 19(11), pp. 2086-2097.

372. Zhang, J. et al. 2020. Elucidating the molecular pathways and immune system transcriptome during ischemia-reperfusion injury in renal transplantation. *Int Immunopharmacol* 81, p. 106246.

373. Zhou, W. et al. 2020. Roles of TRAFs in Ischemia-Reperfusion Injury. *Front Cell Dev Biol* 8, p. 586487.

374. Li, M. et al. 2010. The effect of PACAP38 on MyD88-mediated signal transduction in ischemia-/hypoxia-induced acute kidney injury. *Am J Nephrol* 32(6), pp. 522-532.

375. Zhang, Y. et al. 2022. HSP70 Ameliorates Septic Acute Kidney Injury via Binding with TRAF6 to Inhibit of Inflammation-Mediated Apoptosis. *J Inflamm Res* 15, pp. 2213-2228.

376. Dai, Y. et al. 2016. miR-146a is essential for lipopolysaccharide (LPS)-induced cross-tolerance against kidney ischemia/reperfusion injury in mice. *Sci Rep* 6, p. 27091.

377. Yang, J. and Yan, H. 2017. TLR5: beyond the recognition of flagellin. *Cell Mol Immunol* 14(12), pp. 1017-1019.

378. Yoon, S. I. et al. 2012. Structural basis of TLR5-flagellin recognition and signaling. *Science* 335(6070), pp. 859-864.

379. Elloumi, N. et al. 2017. Relevant genetic polymorphisms and kidney expression of Toll-like receptor (TLR)-5 and TLR-9 in lupus nephritis. *Clin Exp Immunol* 190(3), pp. 328-339.

380. Feng, Y. et al. 2015. Role of Toll-like receptors in diabetic renal lesions in a miniature pig model. *Sci Adv* 1(5), p. e1400183.

381. Fukuzawa, N. et al. 2011. A TLR5 agonist inhibits acute renal ischemic failure. *J Immunol* 187(7), pp. 3831-3839.

382. Kawai, T. and Akira, S. 2010. The role of pattern-recognition receptors in innate immunity: update on Toll-like receptors. *Nat Immunol* 11(5), pp. 373-384.

383. Kawasaki, T. and Kawai, T. 2014. Toll-like receptor signaling pathways. *Front Immunol* 5, p. 461.

384. Huang, Y. et al. 2019. TLR7 mediates increased vulnerability to ischemic acute kidney injury in diabetes. *Rev Assoc Med Bras (1992)* 65(8), pp. 1067-1073.

385. Yayi, H. et al. 2016. Toll-like receptor 7 involves the injury in acute kidney ischemia/reperfusion of STZ-induced diabetic rats. *Acta Cir Bras* 31(7), pp. 448-455.

386. Kim, J. et al. 2023. TLR7 activation by miR-21 promotes renal fibrosis by activating the pro-inflammatory signaling pathway in tubule epithelial cells. *Cell Commun Signal* 21(1), p. 215.

387. Tan, R. S. et al. 2014. TLR cross-talk confers specificity to innate immunity. *Int Rev Immunol* 33(6), pp. 443-453.

388. Hussain, S. et al. 2020. TLR5 participates in the TLR4 receptor complex and promotes MyD88-dependent signaling in environmental lung injury. *Elife* 9.

389. Rusai, K. et al. 2008. Administration of interleukin-1 receptor antagonist ameliorates renal ischemia-reperfusion injury. *Transpl Int* 21(6), pp. 572-580.

390. Register, E. C. T. 2015. *Dose response study of a new treatment "gevokizumab" in patients with type 2 diabetes and diabetic kidney disease* [Online]. Available at: https://www.clinicaltrialsregister.eu/ctr-search/trial/2013-003610-41/DK [Accessed: 26/03/2023].

391. Leemans, J. C. et al. 2005. Renal-associated TLR2 mediates ischemia/reperfusion injury in the kidney. *J Clin Invest* 115(10), pp. 2894-2903.

392. Pulskens, W. P. et al. 2008. Toll-like receptor-4 coordinates the innate immune response of the kidney to renal ischemia/reperfusion injury. *PLoS One* 3(10), p. e3596.

393. Farrar, C. A. et al. 2012. Inhibition of TLR2 promotes graft function in a murine model of renal transplant ischemia-reperfusion injury. *Faseb j* 26(2), pp. 799-807.

394. Liu, M. et al. 2010. Protective effects of Toll-like receptor 4 inhibitor eritoran on renal ischemia-reperfusion injury. *Transplant Proc* 42(5), pp. 1539-1544.

395. Vázquez-Carballo, C. et al. 2021. Toll-Like Receptors in Acute Kidney Injury. *Int J Mol Sci* 22(2).

396. Lv, Y. et al. 2023. Therapeutic potential of fucosyltransferases in cancer and recent development of targeted inhibitors. *Drug Discov Today* 28(1), p. 103394.

397. Furuichi, K. et al. 2008. Chemokine receptor CCR1 regulates inflammatory cell infiltration after renal ischemia-reperfusion injury. *J Immunol* 181(12), pp. 8670-8676.

398. Cui, J. et al. 2016. Macrophage migration inhibitory factor promotes cardiac stem cell proliferation and endothelial differentiation through the activation of the PI3K/Akt/mTOR and AMPK pathways. *Int J Mol Med* 37(5), pp. 1299-1309.

399. Li, J. H. et al. 2019. Macrophage migration inhibitory factor promotes renal injury induced by ischemic reperfusion. *J Cell Mol Med* 23(6), pp. 3867-3877.

400. Li, J. et al. 2018. Blocking Macrophage Migration Inhibitory Factor Protects Against Cisplatin-Induced Acute Kidney Injury in Mice. *Mol Ther* 26(10), pp. 2523-2532.

401. Jin, X. et al. 2022. Phosphoinositide 3 Kinase γ Plays a Critical Role in Acute Kidney Injury. *Cells* 11(5).

402. Liu, H. B. et al. 2015. Nephroprotective Effects of Polydatin against Ischemia/Reperfusion Injury: A Role for the PI3K/Akt Signal Pathway. *Oxid Med Cell Longev* 2015, p. 362158.

403. Wei, Q. et al. 2019. Propofol can suppress renal ischemia-reperfusion injury through the activation of PI3K/AKT/mTOR signal pathway. *Gene* 708, pp. 14-20.

404. Klausner, J. M. et al. 1989. Postischemic renal injury is mediated by neutrophils and leukotrienes. *Am J Physiol* 256(5 Pt 2), pp. F794-802.

405. Kelly, K. J. et al. 1996. Intercellular adhesion molecule-1-deficient mice are protected against ischemic renal injury. *J Clin Invest* 97(4), pp. 1056-1063.

406. Xu, L. et al. 2019. Tubular GM-CSF Promotes Late MCP-1/CCR2-Mediated Fibrosis and Inflammation after Ischemia/Reperfusion Injury. *J Am Soc Nephrol* 30(10), pp. 1825-1840.

407. Harper, S. et al. 2006. Leucocyte depletion improves renal function during reperfusion using an experimental isolated haemoperfused organ preservation system. *Br J Surg* 93(5), pp. 623-629.

408. Long, C. et al. 2016. Attenuation of renal ischemia/reperfusion injury by oleanolic acid preconditioning via its antioxidant, anti-inflammatory, and anti-apoptotic activities. *Mol Med Rep* 13(6), pp. 4697-4704.

409. Sedaghat, Z. et al. 2013. Remote preconditioning reduces oxidative stress, downregulates cyclo-oxygenase-2 expression and attenuates ischaemia-reperfusion-induced acute kidney injury. *Clin Exp Pharmacol Physiol* 40(2), pp. 97-103.

410. Kim, J. et al. 2010. Reactive oxygen species generated by renal ischemia and reperfusion trigger protection against subsequent renal ischemia and reperfusion injury in mice. *Am J Physiol Renal Physiol* 298(1), pp. F158-166.

411. Wang, Y. et al. 2005. Downregulation of liver X receptor-alpha in mouse kidney and HK-2 proximal tubular cells by LPS and cytokines. *J Lipid Res* 46(11), pp. 2377-2387.

412. Wang, Y. et al. 2012. Vitamin D receptor signaling in podocytes protects against diabetic nephropathy. *J Am Soc Nephrol* 23(12), pp. 1977-1986.

413. Azak, A. et al. 2013. Effect of novel vitamin D receptor activator paricalcitol on renal ischaemia/reperfusion injury in rats. *Ann R Coll Surg Engl* 95(7), pp. 489-494.

414. Xu, S. et al. 2015. Vitamin D3 pretreatment alleviates renal oxidative stress in lipopolysaccharide-induced acute kidney injury. *J Steroid Biochem Mol Biol* 152, pp. 133-141.

415. Xu, S. et al. 2015. Vitamin D3 pretreatment regulates renal inflammatory responses during lipopolysaccharide-induced acute kidney injury. *Sci Rep* 5, p. 18687.

416. Wang, T. T. et al. 2023. 14-3-3ζ inhibits maladaptive repair in renal tubules by regulating YAP and reduces renal interstitial fibrosis. *Acta Pharmacol Sin* 44(2), pp. 381-392.

417. Wang, F. et al. 2022. Stratifin promotes renal dysfunction in ischemic and nephrotoxic AKI mouse models via enhancing RIPK3-mediated necroptosis. *Acta Pharmacol Sin* 43(2), pp. 330-341.

418. Pang, Y. et al. 2015. Ischemia preconditioning protects astrocytes from ischemic injury through 14-3-3γ. *J Neurosci Res* 93(10), pp. 1507-1518.

419. Schenning, K. J. et al. 2015. Hyperglycemia abolishes the protective effect of ischemic preconditioning in glomerular endothelial cells in vitro. *Physiol Rep* 3(3).

420. Wouters, O. J. et al. 2020. Estimated Research and Development Investment Needed to Bring a New Medicine to Market, 2009-2018. *Jama* 323(9), pp. 844-853.

421. Committee, J. F. *Sidenafil* [Online]. BMJ Group and Pharmaceutical Press. Available at: https://bnf.nice.org.uk/drugs/sildenafil/ [Accessed: 07/03/2023].

422. Hansen, N. T. et al. 2009. Generating genome-scale candidate gene lists for pharmacogenomics. *Clin Pharmacol Ther* 86(2), pp. 183-189.

423. Lussier, Y. A. and Chen, J. L. 2011. The emergence of genome-based drug repositioning. *Sci Transl Med* 3(96), p. 96ps35.

424. Dudley, J. T. et al. 2011. Computational repositioning of the anticonvulsant topiramate for inflammatory bowel disease. *Sci Transl Med* 3(96), p. 96ra76.

425. Sirota, M. et al. 2011. Discovery and preclinical validation of drug indications using compendia of public gene expression data. *Sci Transl Med* 3(96), p. 96ra77.

426. Chatterjee, P. K. et al. 2003. Pyrrolidine dithiocarbamate reduces renal dysfunction and injury caused by ischemia/reperfusion of the rat kidney. *Eur J Pharmacol* 482(1-3), pp. 271-280.

427. Mallick, I. H. et al. 2005. Pyrrolidine dithiocarbamate reduces ischemia-reperfusion injury of the small intestine. *World J Gastroenterol* 11(46), pp. 7308-7313.

428. Tian, X. F. et al. 2006. Protective effect of pyrrolidine dithiocarbamate on liver injury induced by intestinal ischemia-reperfusion in rats. *Hepatobiliary Pancreat Dis Int* 5(1), pp. 90-95.

429. Kabay, B. et al. 2007. Pyrrolidine dithiocarbamate reduces lung injury caused by mesenteric ischemia/reperfusion in a rat model. *World J Surg* 31(8), pp. 1707-1715.

430. Teke, Z. et al. 2007. Pyrrolidine dithiocarbamate prevents 60 minutes of warm mesenteric ischemia/reperfusion injury in rats. *Am J Surg* 194(2), pp. 255-262.

431. Lee, C. H. et al. 2008. Effect of pyrrolidine dithiocarbamate on hepatic vascular stress gene expression during ischemia and reperfusion. *Eur J Pharmacol* 595(1-3), pp. 100-107.

432. Zeng, M. et al. 2012. Suppression of NF-kappaB reduces myocardial no-reflow. *PLoS One* 7(10), p. e47306.

433. Zhu, T. et al. 2012. Pyrrolidine dithiocarbamate enhances hepatic glycogen synthesis and reduces FoxO1-mediated gene transcription in type 2 diabetic rats. *Am J Physiol Endocrinol Metab* 302(4), pp. E409-416.

434. Ta, M. H. et al. 2014. Pyrrolidine dithiocarbamate reduces the progression of total kidney volume and cyst enlargement in experimental polycystic kidney disease. *Physiol Rep* 2(12).

435. Kan, M. H. et al. 2016. Pyrrolidine Dithiocarbamate Prevents Neuroinflammation and Cognitive Dysfunction after Endotoxemia in Rats. *Front Aging Neurosci* 8, p. 175.

436. Zhao, H. et al. 2017. Suppression of TLR4/NF-kappaB Signaling Pathway Improves Cerebral Ischemia-Reperfusion Injury in Rats. *Mol Neurobiol*.

437. Yang, N. et al. 2008. Blockage of JAK/STAT signalling attenuates renal ischaemia-reperfusion injury in rat. *Nephrol Dial Transplant* 23(1), pp. 91-100.

438. Neria, F. et al. 2009. Inhibition of JAK2 protects renal endothelial and epithelial cells from oxidative stress and cyclosporin A toxicity. *Kidney Int* 75(2), pp. 227-234.

439. Si, Y. et al. 2013. Dexmedetomidine protects against renal ischemia and reperfusion injury by inhibiting the JAK/STAT signaling activation. *J Transl Med* 11, p. 141.

440. Gent, S. et al. 2017. Ischemic preconditioning in pigs: a causal role for signal transducer and activator of transcription 3. *Am J Physiol Heart Circ Physiol* 312(3), pp. H478-h484.

441. Shimizu, T. et al. 1997. Pirfenidone prevents collagen accumulation in the remnant kidney in rats with partial nephrectomy. *Kidney Int Suppl* 63, pp. S239-243.

442. Wang, F. et al. 2008. Protective effects of pirfenidone on D-galactosamine and lipopolysaccharide-induced acute hepatotoxicity in rats. *Inflamm Res* 57(4), pp. 183-188.

443. Takakura, K. et al. 2014. Antiproteinuric effect of pirfenidone in a rat model of anti-glomerular basement membrane glomerulonephritis. *Eur J Pharmacol* 737, pp. 106-116.

444. Yu, W. et al. 2017. Effects and mechanisms of pirfenidone, prednisone and acetylcysteine on pulmonary fibrosis in rat idiopathic pulmonary fibrosis models. *Pharm Biol* 55(1), pp. 450-455.

445. Alderliesten, M. et al. 2007. Extracellular signal-regulated kinase activation during renal ischemia/reperfusion mediates focal adhesion dissolution and renal injury. *Am J Pathol* 171(2), pp. 452-462.

446. Wang, T. et al. 2015. Picroside II Inhibits the MEK-ERK1/2-COX2 Signal Pathway to Prevent Cerebral Ischemic Injury in Rats. *J Mol Neurosci* 57(3), pp. 335-351.

447. Wang, A. et al. 2016. U0126 attenuates ischemia/reperfusion-induced apoptosis and autophagy in myocardium through MEK/ERK/EGR-1 pathway. *Eur J Pharmacol* 788, pp. 280-285.

448. Wang, Y. et al. 2007. SP600125, a selective JNK inhibitor, protects ischemic renal injury via suppressing the extrinsic pathways of apoptosis. *Life Sci* 80(22), pp. 2067-2075.

449. de Borst, M. H. et al. 2009. c-Jun NH2-terminal kinase is crucially involved in renal tubulo-interstitial inflammation. *J Pharmacol Exp Ther* 331(3), pp. 896-905.

450. Xu, Y. F. et al. 2011. Protective effects of SP600125 on renal ischemia-reperfusion injury in rats. *J Surg Res* 169(1), pp. e77-84.

451. Bai, M. et al. 2016. Inhibition of c-Jun N-terminal kinase signaling suppresses skin flap apoptosis in a rat ischemia and/or reperfusion model. *J Surg Res* 206(2), pp. 337-346.

452. Hasegawa, T. et al. 2005. Generation of hypochlorite-modified proteins by neutrophils during ischemia-reperfusion injury in rat liver: attenuation by ischemic preconditioning. *Am J Physiol Gastrointest Liver Physiol* 289(4), pp. G760-767.

453. Nagel, S. et al. 2012. Suppression of the inflammatory response by diphenyleneiodonium after transient focal cerebral ischemia. *J Neurochem* 123 Suppl 2, pp. 98-107.

454. Ostergaard, M. et al. 2014. ROS dependence of cyclooxygenase-2 induction in rats subjected to unilateral ureteral obstruction. *Am J Physiol Renal Physiol* 306(2), pp. F259-270.

455. Pei, H. et al. 2015. TNF-alpha inhibitor protects against myocardial ischemia/reperfusion injury via Notch1-mediated suppression of oxidative/nitrative stress. *Free Radic Biol Med* 82, pp. 114-121.

456. DiMasi, J. A. et al. 2016. Innovation in the pharmaceutical industry: New estimates of R&D costs. *J Health Econ* 47, pp. 20-33.

457. Fogel, D. B. 2018. Factors associated with clinical trials that fail and opportunities for improving the likelihood of success: A review. *Contemp Clin Trials Commun* 11, pp. 156-164.

458. Dhillon, S. 2019. Dapagliflozin: A Review in Type 2 Diabetes. *Drugs* 79(10), pp. 1135-1146.

459. Wheeler, D. C. et al. 2020. The dapagliflozin and prevention of adverse outcomes in chronic kidney disease (DAPA-CKD) trial: baseline characteristics. *Nephrol Dial Transplant* 35(10), pp. 1700-1711.

460. McMurray, J. J. V. et al. 2019. Dapagliflozin in Patients with Heart Failure and Reduced Ejection Fraction. *N Engl J Med* 381(21), pp. 1995-2008.

461. Collij, V. et al. 2016. Drug Repositioning in Inflammatory Bowel Disease Based on Genetic Information. *Inflamm Bowel Dis* 22(11), pp. 2562-2570.

462. Pushpakom, S. et al. 2019. Drug repurposing: progress, challenges and recommendations. *Nat Rev Drug Discov* 18(1), pp. 41-58.

463. Nozaki, Y. et al. 2017. Lipopolysaccharide-Induced Acute Kidney Injury Is Dependent on an IL-18 Receptor Signaling Pathway. *Int J Mol Sci* 18(12).

464. Huang, H. et al. 2020. Gentamicin-Induced Acute Kidney Injury in an Animal Model Involves Programmed Necrosis of the Collecting Duct. *J Am Soc Nephrol* 31(9), pp. 2097-2115.

465. Kan, W. C. et al. 2022. Vancomycin-Associated Acute Kidney Injury: A Narrative Review from Pathophysiology to Clinical Application. *Int J Mol Sci* 23(4).

466. Tapping, R. I. et al. 2000. Toll-like receptor 4, but not toll-like receptor 2, is a signaling receptor for Escherichia and Salmonella lipopolysaccharides. *J Immunol* 165(10), pp. 5780-5787.

467. Cunningham, P. N. et al. 2004. Role of Toll-like receptor 4 in endotoxin-induced acute renal failure. *J Immunol* 172(4), pp. 2629-2635.

468. Sung, F. L. et al. 2002. Enhanced MCP-1 expression during ischemia/reperfusion injury is mediated by oxidative stress and NF-kappaB. *Kidney Int* 62(4), pp. 1160-1170.

469. Humes, H. D. 1986. Role of calcium in pathogenesis of acute renal failure. *Am J Physiol* 250(4 Pt 2), pp. F579-589.

470. Smith, M. W. et al. 1992. Injury-induced changes in cytosolic Ca2+ in individual rabbit proximal tubule cells. *Am J Physiol* 262(4 Pt 2), pp. F647-655.

471. Wu, Z. et al. 2019. CD14: Biology and role in the pathogenesis of disease. *Cytokine Growth Factor Rev* 48, pp. 24-31.

472. Grigoryev, D. N. et al. 2008. The local and systemic inflammatory transcriptome after acute kidney injury. *J Am Soc Nephrol* 19(3), pp. 547-558.

473. Own, J. et al. 2022. CD14 blockade to prevent ischemic injury to donor organs. *Transpl Immunol* 72, p. 101580.

474. Lewington, A. J. et al. 2000. Expression of CD44 in kidney after acute ischemic injury in rats. *Am J Physiol Regul Integr Comp Physiol* 278(1), pp. R247-254.

475. Rouschop, K. M. et al. 2005. Protection against renal ischemia reperfusion injury by CD44 disruption. *J Am Soc Nephrol* 16(7), pp. 2034-2043.

476. Rampanelli, E. et al. 2013. CD44-deficiency attenuates the immunologic responses to LPS and delays the onset of endotoxic shock-induced renal inflammation and dysfunction. *PLoS One* 8(12), p. e84479.

477. Yucel, M. et al. 2013. Protective effects of the nuclear factor kappa B inhibitor pyrrolidine dithiocarbamate in bladder ischemia-reperfusion injury in rats. *Mol Biol Rep* 40(10), pp. 5733-5740.

478. Lima-Posada, I. et al. 2019. Pirfenidone prevents acute kidney injury in the rat. *BMC Nephrol* 20(1), p. 158.

479. Chen, J. X. et al. 2007. NADPH oxidase modulates myocardial Akt, ERK1/2 activation, and angiogenesis after hypoxia-reoxygenation. *Am J Physiol Heart Circ Physiol* 292(4), pp. H1664-1674.

480. Lee, I. T. et al. 2012. Role of TLR4/NADPH oxidase/ROS-activated p38 MAPK in VCAM-1 expression induced by lipopolysaccharide in human renal mesangial cells. *Cell Commun Signal* 10(1), p. 33.

481. Zhang, K. et al. 2023. Renal Endothelial Cell-Targeted Extracellular Vesicles Protect the Kidney from Ischemic Injury. *Adv Sci (Weinh)* 10(3), p. e2204626.

482. Baran, D. et al. 2000. Cell adhesion molecule expression in murine lupus-like nephritis induced by lipopolysaccharide. *Nephron* 84(2), pp. 167-176.

483. Yang, H. et al. 2017. Inhibition of nuclear factor-κB signal by pyrrolidine dithiocarbamate alleviates lipopolysaccharide-induced acute lung injury. *Oncotarget* 8(29), pp. 47296-47304.

484. Krupickova, L. et al. 2021. Chemokine Profiles Are Affected in Serum of Patients with Acute Rejection of Kidney Allograft. *Mediators Inflamm* 2021, p. 5513690.

485. Moledina, D. G. et al. 2023. Identification and validation of urinary CXCL9 as a biomarker for diagnosis of acute interstitial nephritis. *J Clin Invest* 133(13).

486. Jo, S. K. et al. 2005. MEK inhibitor, U0126, attenuates cisplatin-induced renal injury by decreasing inflammation and apoptosis. *Kidney Int* 67(2), pp. 458-466.

487. Tao, Z. et al. 2015. JAK2/STAT3 pathway mediating inflammatory responses in heatstroke-induced rats. *Int J Clin Exp Pathol* 8(6), pp. 6732-6739.

488. Wang, S. et al. 2010. Jak/STAT signaling is involved in the inflammatory infiltration of the kidneys in MRL/lpr mice. *Lupus* 19(10), pp. 1171-1180.

489. Sartiani, L. et al. 2022. Pharmacological basis of the antifibrotic effects of pirfenidone: Mechanistic insights from cardiac in-vitro and in-vivo models. *Front Cardiovasc Med* 9, p. 751499.

490. Yamagami, K. et al. 2015. Pirfenidone exhibits cardioprotective effects by regulating myocardial fibrosis and vascular permeability in pressure-overloaded hearts. *Am J Physiol Heart Circ Physiol* 309(3), pp. H512-522.

491. García, L. et al. 2002. Pirfenidone effectively reverses experimental liver fibrosis. *J Hepatol* 37(6), pp. 797-805.

492. RamachandraRao, S. P. et al. 2009. Pirfenidone is renoprotective in diabetic kidney disease. *J Am Soc Nephrol* 20(8), pp. 1765-1775.

493. Sharma, K. et al. 2011. Pirfenidone for diabetic nephropathy. *J Am Soc Nephrol* 22(6), pp. 1144-1151.

494. Lewis, G. A. et al. 2021. Pirfenidone in heart failure with preserved ejection fraction: a randomized phase 2 trial. *Nat Med* 27(8), pp. 1477-1482.

495. Poo, J. L. et al. 2020. Benefits of prolonged-release pirfenidone plus standard of care treatment in patients with advanced liver fibrosis: PROMETEO study. *Hepatol Int* 14(5), pp. 817-827.

496. Sen, K. et al. 2011. Periostin is induced in glomerular injury and expressed de novo in interstitial renal fibrosis. *Am J Pathol* 179(4), pp. 1756-1767.

497. Stribos, E. G. D. et al. 2016. Precision-cut human kidney slices as a model to elucidate the process of renal fibrosis. *Transl Res* 170, pp. 8-16.e11.

498. Zhang, S. et al. 1998. Pirfenidone reduces fibronectin synthesis by cultured human retinal pigment epithelial cells. *Aust N Z J Ophthalmol* 26 Suppl 1, pp. S74-76.

499. Song, X. et al. 2018. Pirfenidone suppresses bleomycin-induced pulmonary fibrosis and periostin expression in rats. *Exp Ther Med* 16(3), pp. 1800-1806.

500. Rudman-Melnick, V. et al. 2020. Single-Cell Profiling of AKI in a Murine Model Reveals Novel Transcriptional Signatures, Profibrotic Phenotype, and Epithelial-to-Stromal Crosstalk. *J Am Soc Nephrol* 31(12), pp. 2793-2814.

501. Morevati, M. et al. 2021. Effect of NAD+ boosting on kidney ischemia-reperfusion injury. *PLoS One* 16(6), p. e0252554.

502. Muratsu, J. et al. 2022. Blocking Periostin Prevented Development of Inflammation in Rhabdomyolysis-Induced Acute Kidney Injury Mice Model. *Cells* 11(21).

503. Sheng, L. and Zhuang, S. 2020. New Insights Into the Role and Mechanism of Partial Epithelial-Mesenchymal Transition in Kidney Fibrosis. *Front Physiol* 11, p. 569322.

504. Kumar, S. 2018. Cellular and molecular pathways of renal repair after acute kidney injury. *Kidney Int* 93(1), pp. 27-40.

505. Xu-Dubois, Y. C. et al. 2014. Expression of the transcriptional regulator snail1 in kidney transplants displaying epithelial-to-mesenchymal transition features. *Nephrol Dial Transplant* 29(11), pp. 2136-2144.

506. Grande, M. T. et al. 2015. Snail1-induced partial epithelial-to-mesenchymal transition drives renal fibrosis in mice and can be targeted to reverse established disease. *Nat Med* 21(9), pp. 989-997.

507. Tang, T. T. et al. 2021. Kim-1 Targeted Extracellular Vesicles: A New Therapeutic Platform for RNAi to Treat AKI. *J Am Soc Nephrol* 32(10), pp. 2467-2483.

508. Pourgholamhossein, F. et al. 2018. Pirfenidone protects against paraquat-induced lung injury and fibrosis in mice by modulation of inflammation, oxidative stress, and gene expression. *Food Chem Toxicol* 112, pp. 39-46.

509. Ma, Y. et al. 2021. Pirfenidone mediates cigarette smoke extract induced inflammation and oxidative stress in vitro and in vivo. *Int Immunopharmacol* 96, p. 107593.

510. Chen, J. F. et al. 2013. Improved mitochondrial function underlies the protective effect of pirfenidone against tubulointerstitial fibrosis in 5/6 nephrectomized rats. *PLoS One* 8(12), p. e83593.

511. Munshi, R. et al. 2011. MCP-1 gene activation marks acute kidney injury. *J Am Soc Nephrol* 22(1), pp. 165-175.

512. Chen, J. F. et al. 2013. Pirfenidone inhibits macrophage infiltration in 5/6 nephrectomized rats. *Am J Physiol Renal Physiol* 304(6), pp. F676-685.

513. Bizargity, P. et al. 2012. Inhibitory effects of pirfenidone on dendritic cells and lung allograft rejection. *Transplantation* 94(2), pp. 114-122.

514. Sharawy, M. H. and Serrya, M. S. 2020. Pirfenidone attenuates gentamicin-induced acute kidney injury by inhibiting inflammasome-dependent NLRP3 pathway in rats. *Life Sci* 260, p. 118454.

515. Szukiewicz, D. et al. 2014. CX3CL1 (fractalkine) and TNFα production by perfused human placental lobules under normoxic and hypoxic conditions in vitro: the importance of CX3CR1 signaling. *Inflamm Res* 63(3), pp. 179-189.

516. Oh, D. J. et al. 2008. Fractalkine receptor (CX3CR1) inhibition is protective against ischemic acute renal failure in mice. *Am J Physiol Renal Physiol* 294(1), pp. F264-271.

517. Stroo, I. et al. 2010. Chemokine expression in renal ischemia/reperfusion injury is most profound during the reparative phase. *Int Immunol* 22(6), pp. 433-442.

518. Ishani, A. et al. 2009. Acute kidney injury increases risk of ESRD among elderly. *J Am Soc Nephrol* 20(1), pp. 223-228.

519. Silver, S. A. et al. 2018. Causes of Death after a Hospitalization with AKI. *J Am Soc Nephrol* 29(3), pp. 1001-1010.

520. Shi, S. et al. 2007. Single- and multiple-dose pharmacokinetics of pirfenidone, an antifibrotic agent, in healthy Chinese volunteers. *J Clin Pharmacol* 47(10), pp. 1268-1276.

521. Agency, E. M. 2023. *Esbriet (pirfenidone) hard capsules: EU summary of product characteristics* [Online]. Available at: http://www.ema.europa.eu [Accessed: 01 Dec 2023].

522. Togami, K. et al. 2015. Pharmacokinetic evaluation of tissue distribution of pirfenidone and its metabolites for idiopathic pulmonary fibrosis therapy. *Biopharm Drug Dispos* 36(4), pp. 205-215.

Appendix

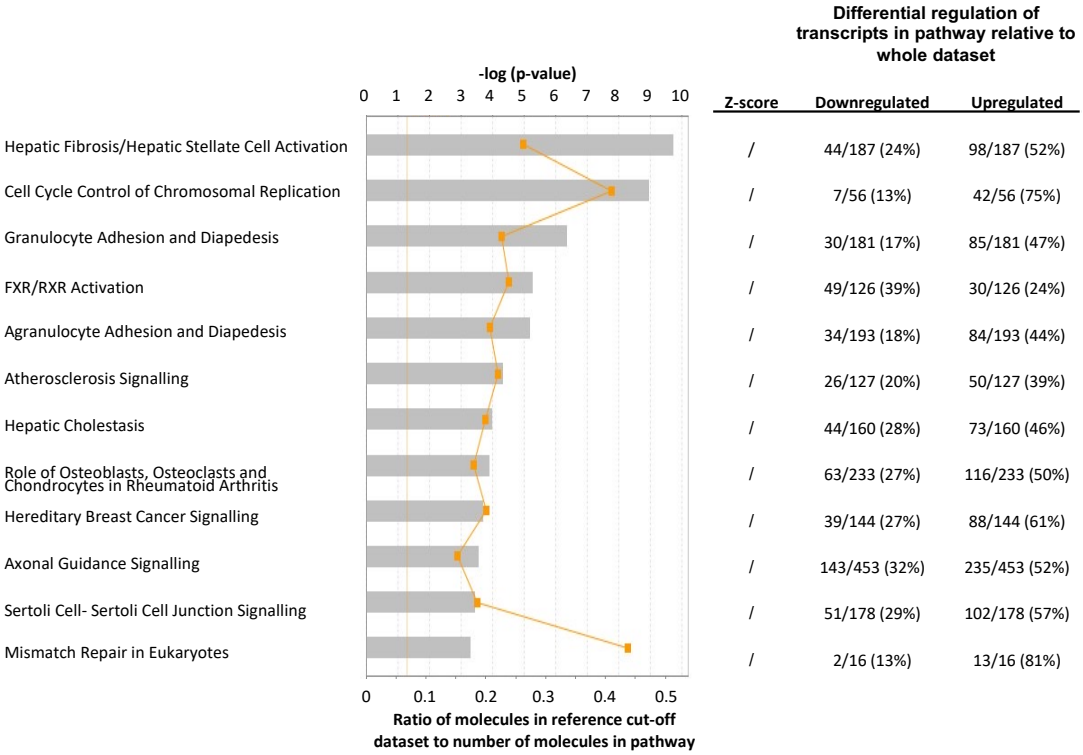

Appendix 1 Ingenuity Pathway Analysis: Signalling Pathways of the IRI Dataset

IPA is currently unable to provide z-scores for a number of pathways owing to insufficient information continued within the IPA knowledge base. As such the IPA Canonical Pathways were further examined for those pathways which demonstrated a significant p-value of overlap between the pathway and dataset but a z-score could not be calculated. Those with a $p<0.05$ and no z-score calculated were examined. The pathway ranked by p-value of overlap are displayed above. In total twelve pathways fulfilled selection criteria.

Upstream Regulator	z-score	p-value	Upstream Regulator	z-score	p-value	Upstream Regulator	z-score	p-value	Upstream Regulator	z-score	p-value	Upstream Regulator	z-score	p-value	Upstream Regulator	z-score	p-value	Upstream Regulator	z-score	p-value
TGFB1	8.34	4E-46	PTEN	-2.29	8E-11	SOX4	2.08	5E-07	IL1R1	2.38	5E-05	TICAM1	5.15	0.0005	EPHB1	2.22	0.003	TNFRSF12A	2.22	0.0181
ERBB2	7.22	2E-43	S100A9	2.96	8E-11	IL1A	4.94	6E-07	IL17RA	2.57	5E-05	MSTN	2.25	0.0005	CHRM3	2.21	0.003	DEF6	2.21	0.0181
CDKN1A	-3.23	3E-41	RBL1	-4.48	9E-11	THRA	-2.22	7E-07	AIF1	2.61	6E-05	IL12 (complex)	3.17	0.0005	TSLP	2.58	0.0031	VIPR1	2.21	0.0181
CSF2	9.09	3E-36	E2F2	2.79	1E-10	SPP1	3.47	7E-07	Mapk	2.31	6E-05	PRKCB	2.82	0.0005	AMH	2.73	0.0033	FCGR2A	2.60	0.0194
TNF	9.21	1E-34	RETNLB	3.92	1E-10	INSIG1	-3.67	7E-07	FN1	3.99	6E-05	SMAD1	2.39	0.0006	MAC	2.72	0.0033	miR-26a-5p	-2.58	0.0194
IL1B	7.85	2E-29	HNF1B	-2.95	2E-10	MED1	2.81	7E-07	BMP2	2.60	6E-05	EIF2AK2	3.47	0.0006	AHI1	-2.12	0.0033	EIF4G1	2.45	0.0196
Vegf	7.31	2E-28	Irgm1	-4.57	3E-10	SMAD3	5.21	7E-07	TRPV4	3.13	6E-05	FOXL2	3.55	0.0006	COL18A1	-2.76	0.0033	miR-204-5p	-2.45	0.0196
IL6	6.42	3E-27	STAT3	4.80	3E-10	TGFA	3.08	1E-06	ERCC1	-2.22	6E-05	FGF10	2.60	0.0006	Fibrinogen	2.16	0.0036	POU2F2	2.67	0.0205
HGF	7.04	1E-26	INHA	-2.48	3E-10	PDGF-AA	2.14	1E-06	KLF5	2.16	6E-05	FOXP3	-2.11	0.0007	IFI16	2.22	0.0036	ATF2	2.64	0.0205
CDKN2A	-3.95	2E-24	HDAC1	-3.10	3E-10	cytokine	3.62	1E-06	NFYA	2.95	6E-05	TNFSF14	2.61	0.0007	UXT	-2.42	0.0037	FGF7	2.46	0.0205
CCND1	6.03	5E-24	TCF4	2.60	3E-10	LIF	3.47	1E-06	ATF4	2.14	7E-05	GHR	-2.21	0.0007	ICAM1	2.44	0.0038	TAC1	2.99	0.0214
RABL6	5.69	7E-24	ERK1/2	4.19	5E-10	INHBA	3.07	1E-06	NELFA	2.00	7E-05	Nr1h	-3.66	0.0007	STAT4	4.08	0.0038	TCR	3.82	0.0228
TBX2	4.85	2E-23	MYD88	5.62	7E-10	Ptprd	-2.33	1E-06	DNMT1	-2.05	8E-05	EIF4E	3.13	0.0007	CD14	3.37	0.0041	IRF6	2.07	0.0231
let-7	-7.64	2E-23	MTPN	4.32	8E-10	MAPK14	2.80	1E-06	KITLG	2.75	8E-05	Ifn gamma	3.30	0.0007	ETS1	3.20	0.0041	SMTNL1	-2.05	0.0234
HRAS	3.13	3E-22	P38 MAPK	4.82	8E-10	TGFB2	2.73	2E-06	WNT1	2.36	8E-05	IL21	4.36	0.0008	FBXO32	-2.16	0.0042	ITGB6	2.19	0.0236
SP1	3.17	1E-21	CD44	4.26	9E-10	E2F6	-2.50	2E-06	TGM2	2.95	9E-05	AVP	2.90	0.0008	Fcer1	2.46	0.0044	IL27	3.15	0.0237
PDGF BB	5.42	5E-21	BNIP3L	-2.32	1E-09	CIP2A	-2.64	2E-06	ACKR3	2.00	9E-05	TOB1	-2.14	0.0008	RAC1	2.63	0.0047	ELK1	2.52	0.0238
IKBKB	4.30	8E-21	CEBPA	2.11	1E-09	SRC	3.07	2E-06	MAP2K1	3.87	9E-05	HNF4A	-3.53	0.0009	MAP3K7	2.21	0.0047	FGF4	2.16	0.0243
IFNG	6.79	2E-19	IKBKG	4.83	1E-09	Tnf (family)	3.87	2E-06	EIF3E	-2.54	0.0001	F7	3.10	0.0009	TRAF6	2.38	0.0048	HTATIP2	-2.16	0.0243
MYC	2.35	2E-19	CD40LG	4.44	1E-09	Insulin	2.10	3E-06	IGFBP2	2.04	0.0001	SCUBE3	2.22	0.001	STAT1	4.39	0.0049	SIM1	2.34	0.0247
E2f	4.18	1E-18	PTGS2	4.05	1E-09	SRF	3.25	3E-06	HDAC4	-2.18	0.0001	CD28	-2.20	0.001	KLK5	2.45	0.0051	TWIST2	2.78	0.0256
SMARCA4	3.74	2E-18	CSF1	4.19	2E-09	MEOX2	-2.66	3E-06	S1PR2	2.75	0.0001	GATA1	-2.34	0.001	IL11RA	2.43	0.0051	TNFRSF1B	2.33	0.0257
EGFR	4.04	2E-18	estrogen receptor	-4.14	2E-09	NOTCH1	2.62	3E-06	TNFAIP3	-2.38	0.0001	BMX	2.43	0.001	LAMA5	2.41	0.0051	GFI1	-2.19	0.0257
FOXM1	5.59	3E-18	ACOX1	-4.14	2E-09	NFKB1	4.20	4E-06	CAV1	3.17	0.0001	NDUFA13	-2.23	0.001	PDGFRA	2.19	0.0051	IRF4	-2.50	0.026
Alpha catenin	-5.86	8E-18	CSF3	3.03	2E-09	Pdgfr	2.81	4E-06	TAF4B	2.37	0.0001	I kappa b kinase	-2.44	0.001	HCAR2	-2.45	0.0051	NPC1	-2.13	0.0267
NFKBIA	3.08	1E-17	HIF1A	2.93	2E-09	CCL5	3.08	4E-06	NPR1	-2.59	0.0001	PLAU	3.51	0.0011	PPP2R5C	-2.45	0.0051	MIF	2.11	0.0269
PTGER2	5.45	2E-17	FOXO1	4.14	3E-09	NOS2	2.61	4E-06	ROCK2	2.92	0.0001	TLR7	4.46	0.0011	ID1	2.33	0.0051	CLEC1B	2.00	0.0271
EP400	4.35	3E-17	AKT1	3.23	3E-09	ABCB4	-3.57	4E-06	Ifn	4.11	0.0002	Ifnar	3.86	0.0012	TSH	2.32	0.0051	CTBP1	-2.20	0.0279
E2F1	4.88	1E-16	CD38	3.04	3E-09	PDX1	2.42	5E-06	miR-29b-3p	-3.64	0.0002	EHF	2.39	0.0012	SRC (family)	3.13	0.0051	PLAUR	2.57	0.0298
ESR1	2.21	1E-16	ADAMTS12	-3.85	3E-09	CXCL12	2.71	5E-06	DUSP1	-2.60	0.0002	SELPLG	2.53	0.0012	NELFCD	2.00	0.0053	Pdgf Ab	2.22	0.03
TCF3	-2.14	2E-16	TGFB3	4.35	4E-09	JAK2	3.27	5E-06	MYB	2.70	0.0002	Nfat (family)	3.45	0.0012	AQP7	2.00	0.0053	ITGAL	2.16	0.03
CTNNB1	3.44	2E-16	LDL	4.34	4E-09	PIK3CA	2.32	5E-06	ECSIT	2.54	0.0002	PLK1	-2.27	0.0013	FOXA1	-2.75	0.0057	RNF20	-2.00	0.03
IL4	4.62	7E-16	SMAD7	-3.04	6E-09	GDF2	2.82	6E-06	PGF	2.73	0.0002	ADA	-2.18	0.0013	let-7a-5p	-4.67	0.0057	NR4A2	-2.20	0.03
Cg	4.46	9E-16	PRL	4.13	7E-09	SMAD4	2.07	6E-06	MDM4	-2.18	0.0002	TNFSF13B	2.45	0.0013	miR-34a-5p	-3.41	0.006	miR-122-5p	-2.81	0.0327
RB1	-5.15	2E-15	MET	3.62	1E-08	BRD4	3.81	7E-06	HDL-cholesterol	-2.88	0.0002	AGTR1	2.31	0.0013	IL18	4.20	0.0061	NFATC3	2.24	0.0338
E2F3	3.74	3E-15	PRKCD	2.73	1E-08	Ap1	3.09	7E-06	SYVN1	3.29	0.0002	CPXM1	2.00	0.0014	TYROBP	2.63	0.0065	miR-21-5p	-2.72	0.0338
MITF	6.15	4E-15	IGF2BP1	3.56	1E-08	NTRK2	3.49	8E-06	MAP3K1	2.70	0.0002	AQP11	-2.00	0.0014	STAT5a/b	2.74	0.0068	TLR5	2.57	0.0345
IL10RA	-2.99	9E-15	Ras	2.84	1E-08	Cdkn1c	-2.24	8E-06	SPIB	3.40	0.0002	SEMA7A	2.83	0.0014	FGFR1	3.36	0.0069	PPRC1	2.97	0.0349
NFkB (complex)	6.64	1E-14	RAF1	4.26	1E-08	IKZF1	-2.57	9E-06	ZNF217	-2.33	0.0002	SOCS1	-3.31	0.0015	ADRB3	2.30	0.0069	GRP	2.37	0.0358
JUN	3.59	2E-14	Mek	3.34	2E-08	CD40	2.75	9E-06	Collagen type I	2.53	0.0002	SELP	2.53	0.0015	PDCD4	-2.42	0.0069	NTRK1	2.18	0.0358
AHR	-2.03	2E-14	CREBBP	2.38	2E-08	F2R	3.37	9E-06	ELAVL1	3.02	0.0003	TRAF3IP2	2.28	0.0017	ETV5	2.20	0.0076	TBXT	2.24	0.0374
F2	7.31	8E-14	ZFP36	-4.17	2E-08	EWSR1	2.88	1E-05	HNRNPK	2.03	0.0003	Gm-csf	2.31	0.0017	F3	2.83	0.0077	BACH1	2.22	0.0374
APP	2.82	2E-13	NKX2-1	-2.60	3E-08	SMOC2	2.65	1E-05	REL	3.42	0.0003	MAPK3	3.56	0.0017	CD2	3.14	0.0081	MST1R	2.21	0.0374
Rb	-4.77	2E-13	PKD1	-3.95	3E-08	CDK9	2.53	1E-05	CAMP	2.98	0.0003	EIF4G2	2.24	0.0018	Bcl9-Cbp	2.00	0.0088	GABPB1	2.19	0.0374
EGF	6.48	2E-13	SFTPA1	-3.54	3E-08	TRIM24	-2.89	1E-05	PPARGC1A	-2.37	0.0003	RLIM	2.24	0.0018	NELFE	2.00	0.0088	EIF2AK3	2.13	0.0389
CHUK	4.91	3E-13	RBL2	-3.60	4E-08	JUNB	2.78	1E-05	miR-483-3p	-2.51	0.0003	SAMSN1	3.44	0.0018	ARHGAP21	3.16	0.0097	PTPN6	-2.38	0.0397
CREB1	4.20	3E-13	IL1	5.17	4E-08	TGFBR1	2.33	2E-05	BCR (complex)	3.90	0.0003	IL15	3.31	0.0018	F2RL1	2.21	0.0098	TRIM37	-2.45	0.0426
IGF1	3.61	3E-13	MAP2K1/2	2.68	4E-08	RHOA	3.03	2E-05	CYR61	2.85	0.0003	RPS6KA5	2.58	0.0019	mir-196	-2.20	0.0099	HMGB1	2.91	0.0433
OSM	5.47	4E-13	PI3K (complex)	4.06	5E-08	ANGPT2	4.80	2E-05	IFNAR1	2.68	0.0003	CSF1R	3.14	0.002	HNF4α dimer	-2.21	0.0099	Cdk	2.43	0.0449
ERK	5.49	4E-13	EDN1	4.40	7E-08	INS	2.43	2E-05	GLI1	3.97	0.0003	MBD2	2.59	0.002	GNA12	3.57	0.01	SMARCD3	2.24	0.0458
NUPR1	-4.32	7E-13	HTT	3.45	7E-08	VEGFA	3.93	2E-05	ZNF281	2.39	0.0003	Pka	2.81	0.002	SAA	2.95	0.0102	PRKCE	2.79	0.046
mir-21	-4.07	8E-13	YAP1	2.55	7E-08	CFTR	-3.46	2E-05	NOD2	3.24	0.0003	PTPRJ	2.11	0.0021	STAT	2.60	0.0102	HIRA	2.00	0.0465
S100A8	2.62	1E-12	FFAR3	2.20	8E-08	NCF1	2.55	2E-05	LGALS1	2.07	0.0004	PRKCA	2.51	0.0021	ARNT2	2.48	0.0108	LATS2	2.00	0.0465
AGT	6.68	1E-12	TREM1	2.43	8E-08	TET2	3.27	2E-05	Pro-inflammatory Cytokine	2.14	0.0004	OLR1	2.19	0.0021	miR-145-5p	-2.39	0.0109	mir-208	-2.00	0.0465
AREG	4.08	2E-12	TLR3	5.32	9E-08	GLIS2	-3.00	2E-05	C3	2.12	0.0004	PI3K (family)	2.41	0.0021	IRF8	2.36	0.0111			
CEBPB	2.55	2E-12	IL2	6.73	1E-07	IPMK	3.13	2E-05	PDGFB	3.69	0.0004	TLR2	3.08	0.0021	JAK1/2	2.14	0.0113			
IL5	5.47	2E-12	TSC2	-4.35	1E-07	NRG1	3.30	3E-05	Stat3-Stat3	2.95	0.0004	CCNK	2.91	0.0023	H2AFB3	2.71	0.0121			
TNFSF11	5.67	3E-12	SPDEF	-2.77	1E-07	PTGER4	-2.54	3E-05	CD3	2.81	0.0004	NPPB	-2.96	0.0023	mir-34	-2.80	0.0121			
APOE	-3.27	3E-12	Akt	2.61	1E-07	STK11	-2.56	3E-05	IL17F	2.20	0.0004	Creb	3.08	0.0024	MKNK1	3.75	0.0128			
SPARC	-2.93	3E-12	CR1L	-3.85	1E-07	IFN alpha/beta	2.64	4E-05	RET	3.40	0.0004	PADI2	2.43	0.0024	RBM5	-2.02	0.0133			
FGF2	4.11	4E-12	SPI1	3.38	1E-07	CBX5	-2.08	4E-05	TMEM173	3.46	0.0004	ITGA9	2.43	0.0024	ANKRD17	2.00	0.0135			
NR3C1	-3.16	7E-12	DYRK1A	-2.98	3E-07	KLF4	2.77	4E-05	SPHK1	2.33	0.0004	NOTCH3	2.02	0.0025	Nos	2.22	0.0136			
IL17A	5.96	8E-12	TLR9	3.43	3E-07	EDNRA	2.65	4E-05	ZNF106	-3.05	0.0004	miR-24-3p	-2.79	0.0025	miR-503-5p	-2.24	0.0136			
IL13	2.66	8E-12	Pdgf (complex)	4.47	4E-07	Pkc(s)	2.98	4E-05	ATM	2.68	0.0004	BCL3	-2.07	0.0026	C5	2.85	0.0146			
HNF1A	-3.19	1E-11	TNFSF12	4.22	4E-07	Rock	2.56	5E-05	CTLA4	-3.39	0.0004	CDKN1B	-2.79	0.0026	OGT	2.79	0.0155			
FAS	-2.19	1E-11	TNFRSF1A	3.24	4E-07	Interferon alpha	5.82	5E-05	SNCA	2.23	0.0004	IL7	2.13	0.0027	FBN1	-2.20	0.0156			
RELA	3.63	1E-11	BMP6	3.08	4E-07	TRADD	3.32	5E-05	TRAF2	2.05	0.0005	MYCN	-2.69	0.0027	miR-124-3p	-3.44	0.0158			
Tgf beta	2.35	4E-11	MMP9	2.15	4E-07	IL3	3.00	5E-05	TFDP1	2.62	0.0005	NGF	2.87	0.0027	PTTG1	3.40	0.016			
TFRC	-3.45	4E-11	EGR1	2.97	5E-07	RIPK2	2.70	5E-05	Brd4	2.89	0.0005	P2RY4	2.00	0.0029	CXCR4	2.32	0.0163			
Jnk	5.53	6E-11	TLR4	4.41	5E-07	miR-199a-5p	-3.46	5E-05	AGA	-2.00	0.0005	TMPO	2.00	0.0029	ABL1	2.35	0.017			
LHX1	-4.62	7E-11	KDM5B	-4.18	5E-07	JAK1	2.74	5E-05	KLF6	2.77	0.0005	PLAG1	3.07	0.0029	CCR5	2.19	0.017			

Appendix 2 Ingenuity Pathway Analysis: Upstream Regulators of the IRI Dataset

IPA Upstream Regulator analysis links the dataset molecule's whose differential regulation can be linked to a single regulator. P-values are calculated by analysing the overlap between genes in the dataset and what is known targets regulated by the transcriptional regulator. The activation Z-score is calculated to predict the activation state of the regulator. In total 480 regulators with a p<0.05 and a z-score of >2 or <-2 was predicted are displayed.

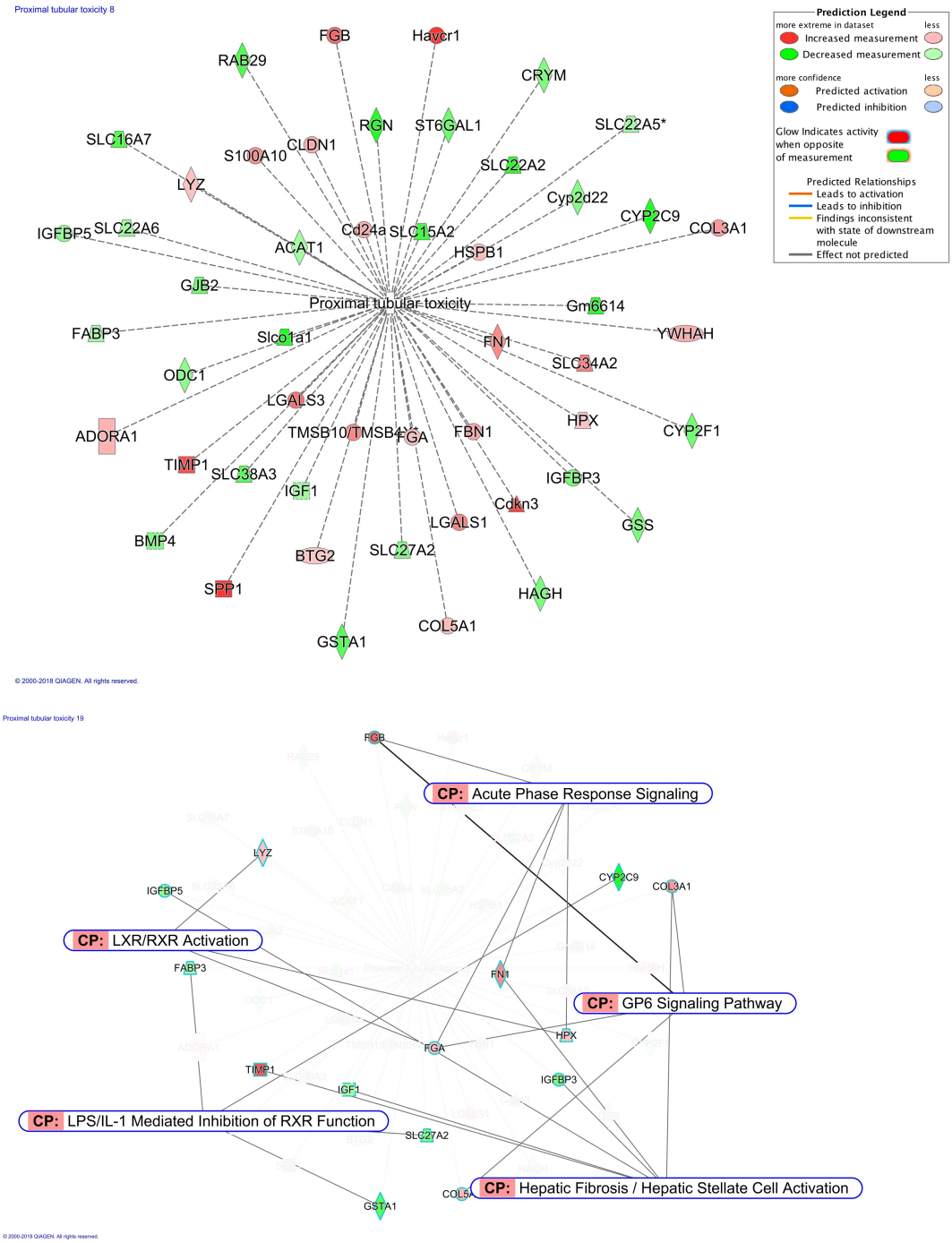

Appendix 3 Ingenuity Pathway Analysis: Tox Function the Principle Ranked Pathway

The IRI dataset linked to 654 tox function annotations contained within the IPA tox functions knowledge base. The top ranked by p-value clinical pathology endpoint predicted from the Tox Function was that of Renal Proximal Tubular Toxicity p=5.24E-26 (p-value of overlap). The function contains 50 dataset molecules and is displayed in image **(A)**. IPA was further interrogated to view the principle 5 canonical signalling pathways which overlap with the functional annotation of Proximal Tubular Toxicity. The Canonical pathways and their corresponding connections with the dataset molecules in the Renal Proximal Tubular Toxicity annotation is shown in image **(B)**.

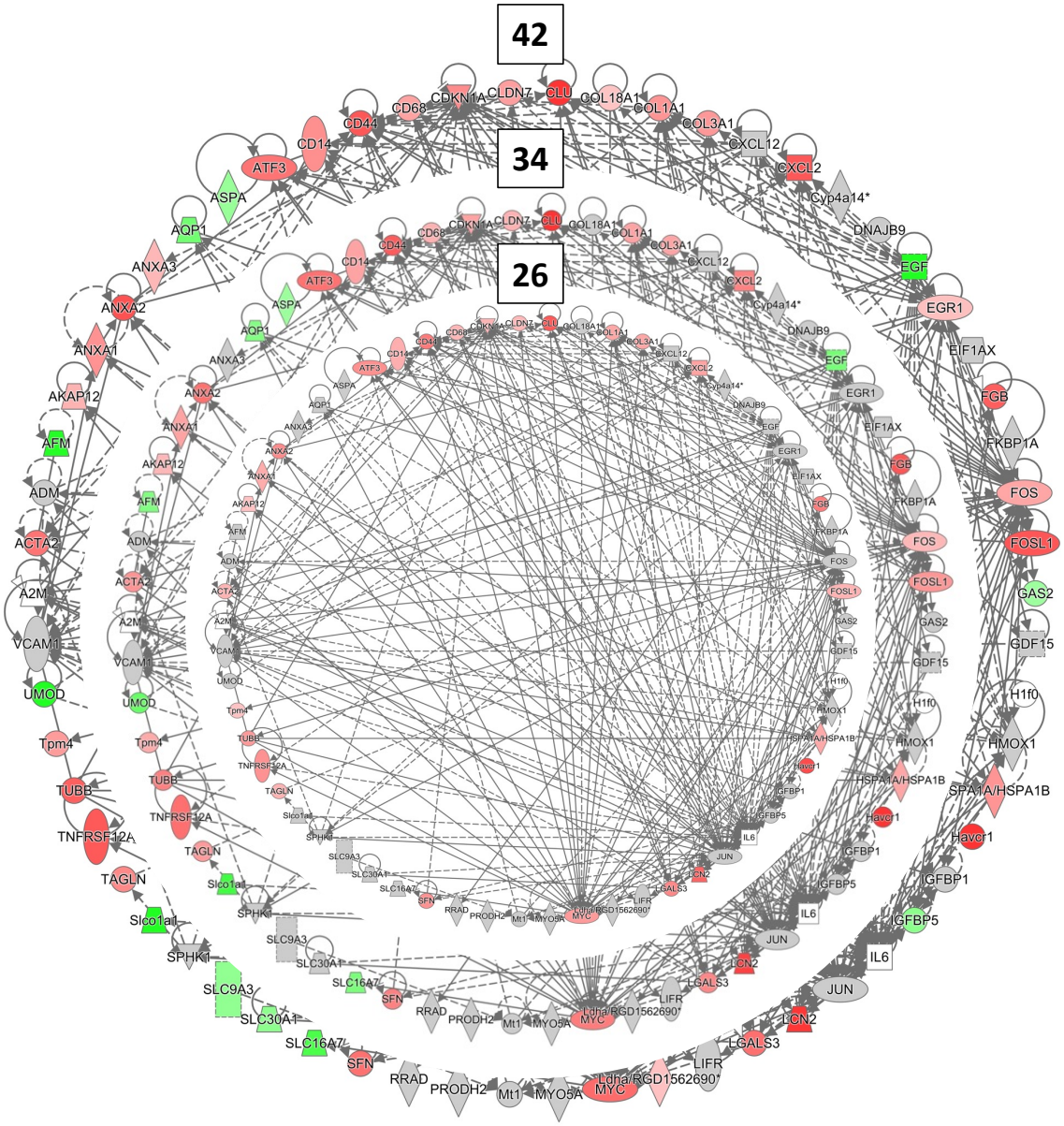

Appendix 4 Ingenuity Pathway Analysis: Acute Renal Failure Panel (Rat)

IPA tox list for the phenotype of Acute Renal Failure Panel (Rat) was examined. In all the tox list comprises of 62 genes whose transcriptional response has been shown to be associated with acute renal failure in the rat kidney. The datasets of IRI, indirect-IPC and direct-IPC were each compared relative to the background expression level of Sham and those transcripts with a corrected $p<0.05$ and $\log_2$FC of >1 or <-1 were uploaded to IPA. The number of statistically significant transcripts which linked to the panel of Acute Renal Failure Panel (Rat) in the IRI dataset was 42. This number reduced in both preconditioning groups to 34 and 26 respectively. The image above describes the interconnecting nature of each transcript (represented by solid and doted lines). Those transcripts coloured red are activated and those green inhibited. The outer most circle demonstrates the transcript expression change observed in the IRI group. The the middle circle is overlaid with the transcript expression change in the indirect-IPC dataset and finally the innermost circle is the transcriptional expression change of the direct-IPC dataset.

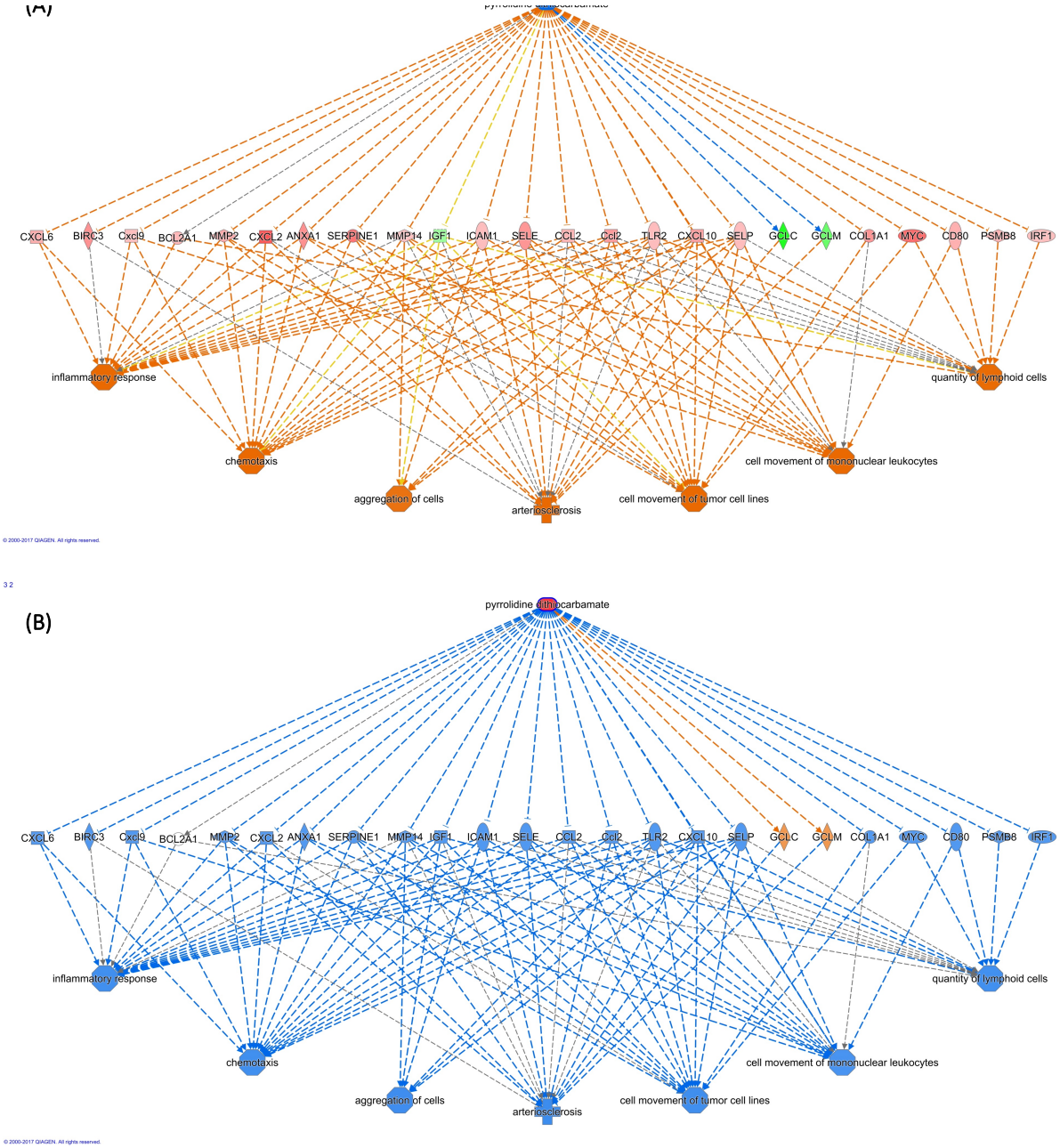

Appendix 5 Pyrrolidine Dithiocarbamate Targets in the IRI Dataset

The Regulatory Effects Network algorithm was set to examine for connections between known compounds (contained in IPA knowledge base), the dataset molecules and finally the phenotype. The compound pyrrolidine dithiocarbamate (PDTC) was predicted to demonstrate a high consistency score of 14.711. Image **(A)** demonstrates the anti-correlation between PDTC and IRI dataset. Image **(B)** demonstrates the activation of PDTC (coloured red) and hypothesized regulator effect and function.

Node key Compound: blue (not administered), red (administered)
Upstream regulator: red and orange (activated), blue and green (inhibited)
Function: orange (activated), blue (inhibited)

(A)

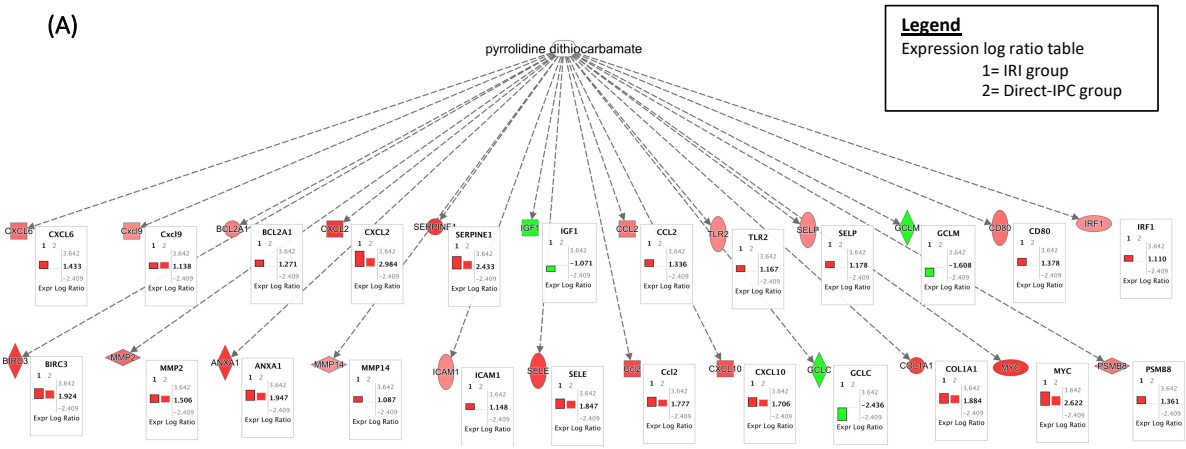

(B)

Diseases/Toxicity/Bio Functions	Z-score		Dirrection of Chemical Prediction
PDTC	IRI	D-IPC	
Aggregation of cells	2.7	0.0	Inhibition
Atherosclerosis	2.0	3.0	Inhibition
Cell movement of mononuclear leukocytes	6.0	0.0	Inhibition
Cell movement of tumor cell lines	6.1	5.5	Inhibition
Chemotaxis	4.9	3.6	Inhibition
Inflammatory response	3.4	2.0	Inhibition
Quantity of lymphoid cells	2.5	0.0	Inhibition

Appendix 6 Pyrrolidine Dithiocarbamate IPC Transcriptional Comparison

(A) Those upstream regulators predicted to be targeted by pyrrolidine dithiocarbamate (PDTC) in the IRI dataset are displayed. The log_2FC of each upstream regulator in the IRI and direct-IPC datasets are displayed relative to sham. **(B)** The downstream directional change of the function of the network was further examined for concordance with the direct-IPC. PDTC was predicted to inhibit 7 functions of the network. Direct-IPC shared concordance with PDTC functional changes in 6 of the 7 functions.

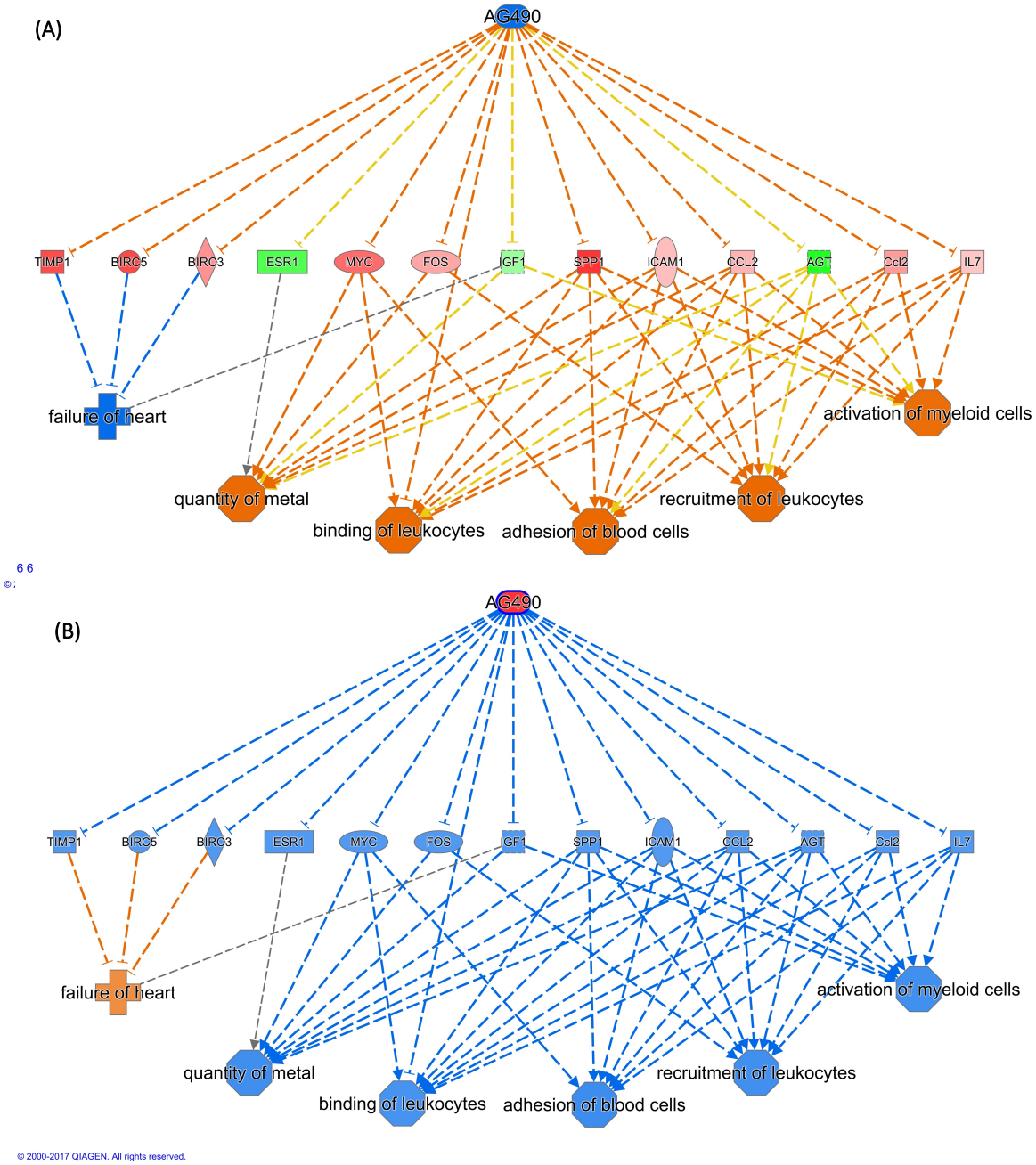

Appendix 7 AG490 Targets in the IRI Dataset

The Regulatory Effects Network algorithm was set to examine for connections between known compounds (contained in IPA knowledge base), the dataset molecules and finally the phenotype. The compound AG490 was predicted to demonstrate a high consistency score of 11.068. Image **(A)** demonstrates the anti-correlation between AG490 and IRI dataset. Image **(B)** demonstrates the activation of AG490 (coloured red) and hypothesized regulator effect and function.

Node key
Compound: blue (not administered), red (administered)
Upstream regulator: red and orange (activated), blue and green (inhibited)
Function: orange (activated), blue (inhibited)

(A)

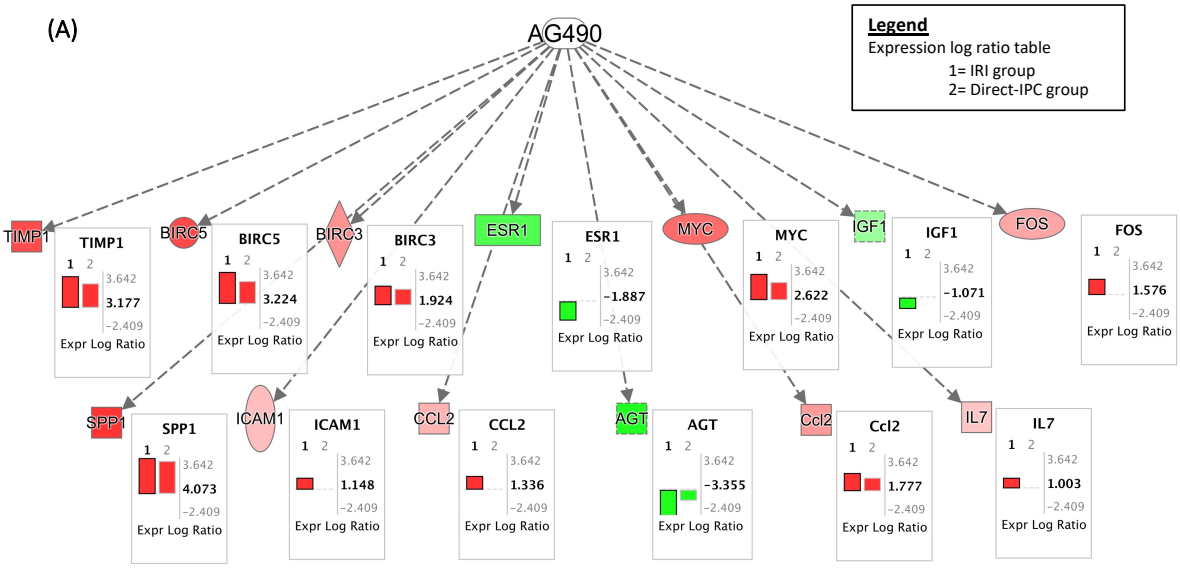

(B)

Diseases/Toxicity/Bio Functions	Z-score		Direction of Chemical Prediction
AG490	IRI	D-IPC	
Failure of heart	-2.4	-2.1	Activation
Activation of myeloid cells	2.1	2.2	Inhibition
Adhesion of blood cells	4.8	2.7	Inhibition
Binding of leukocytes	4.8	2.7	Inhibition
Quantity of metal	2.5	0.0	Inhibition
Recruitment of leukocytes	4.9	3.3	Inhibition

Appendix 8 AG490 IPC Transcriptional Comparison

(A) Those upstream regulators predicted to be targeted by AG490 in the IRI dataset are displayed. The log_2FC of each upstream regulator in the IRI and direct-IPC datasets are displayed relative to sham. **(B)** The downstream directional change of the function of the network was further examined for concordance with the direct-IPC. AG490 was predicted to inhibit 4 functions and activate 1 function of the network. Direct-IPC shared concordance with AG490 functional changes in 5 of the 6 functions.

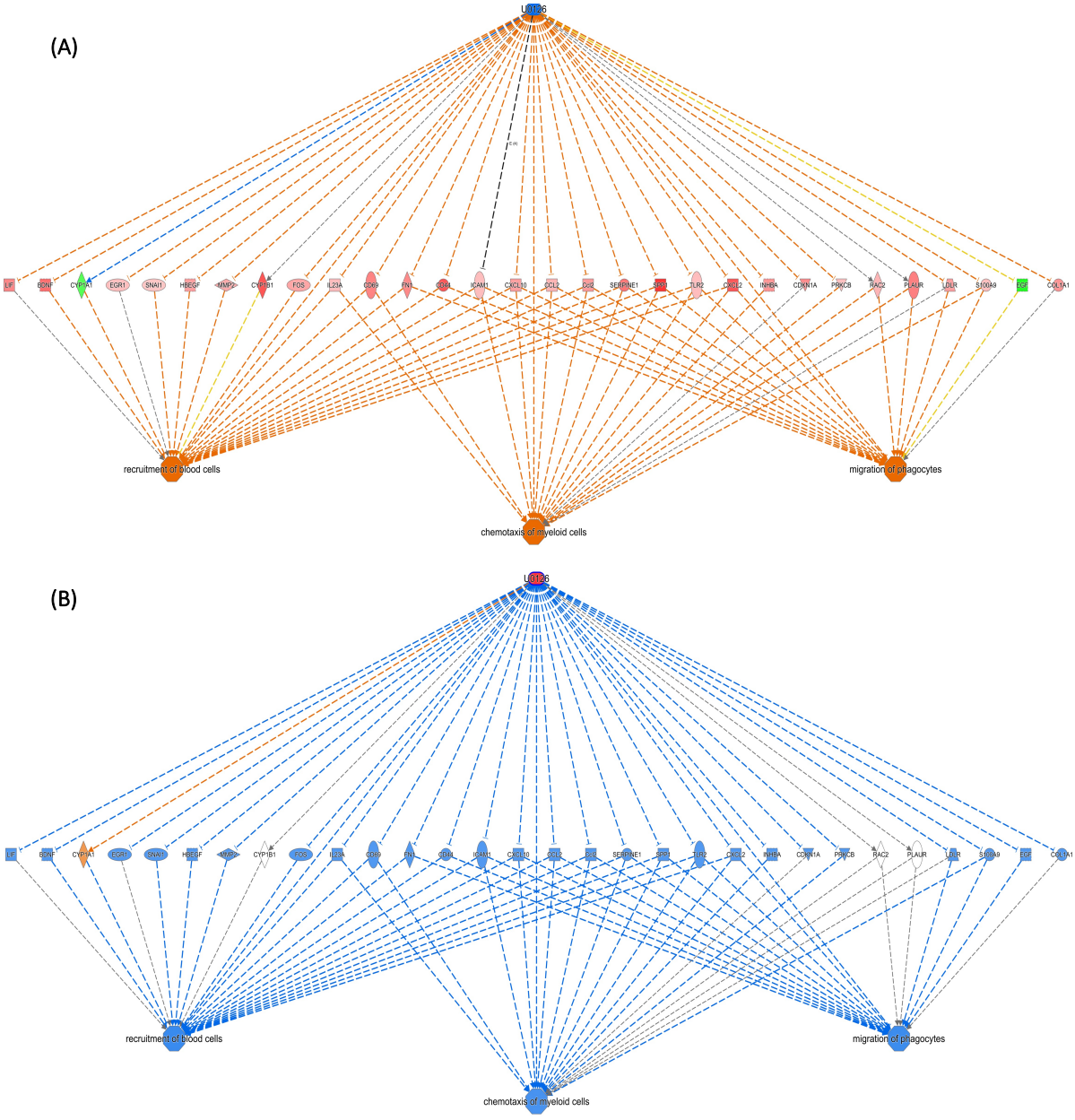

Appendix 9 U0126 Targets in the IRI Dataset

The Regulatory Effects Network algorithm was set to examine for connections between known compounds (contained in IPA knowledge base), the dataset molecules and finally the phenotype. The compound U0126 was predicted to demonstrate a high consistency score of 8.033. Image **(A)** demonstrates the anti-correlation between U0126 and IRI dataset. Image **(B)** demonstrates the activation of U0126 (coloured red) and hypothesized regulator effect and function.

Node key
Compound: blue (not administered), red (administered)
Upstream regulator: red and orange (activated), blue and green (inhibited)
Function: orange (activated), blue (inhibited)

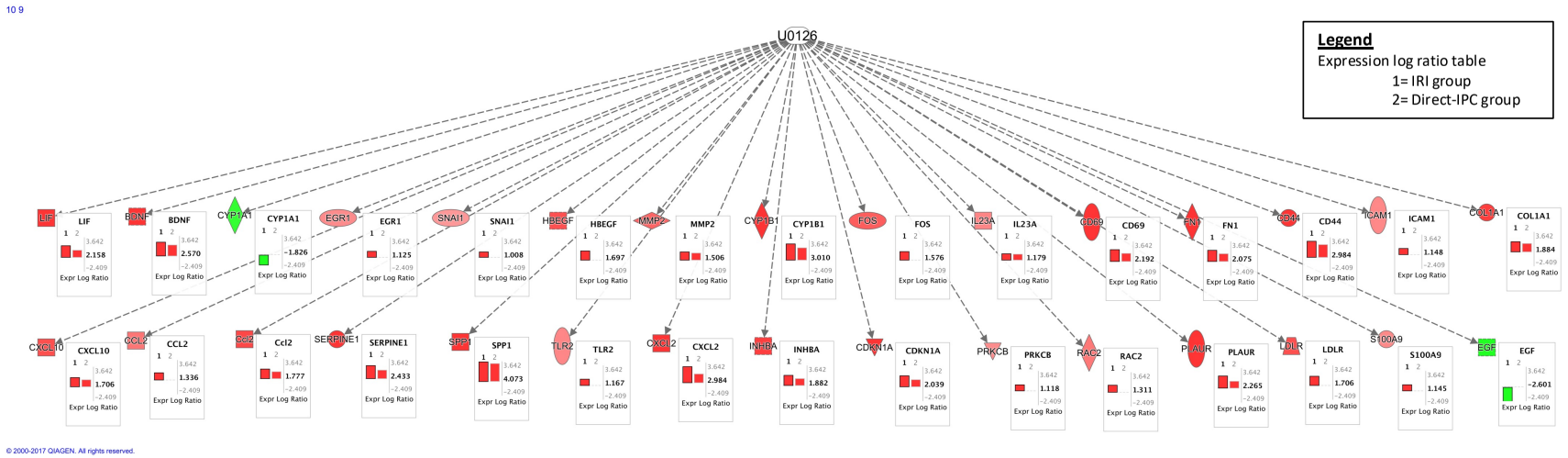

Diseases/Toxicity/Bio Functions	Z-score		Dirrection of Chemical Prediction
U0126	IRI	D-IPC	
Chemotaxis of myeloid cells	4.6	0.0	Inhibition
Migration of phagocytes	4.0	0.0	Inhibition
Recruitment of blood cells	4.8	3.4	Inhibition

Appendix 10 U0126 IPC Transcriptional Comparison

(A) Those upstream regulators predicted to be targeted by U0126 in the IRI dataset are displayed. The log_2FC of each upstream regulator in the IRI and direct-IPC datasets are displayed relative to sham. **(B)** The downstream directional change of the function of the network was further examined for concordance with the direct-IPC. U0126 was predicted to inhibit 3 functions . Direct-IPC shared concordance with U0126 functional changes in 3 of the 3 functions.

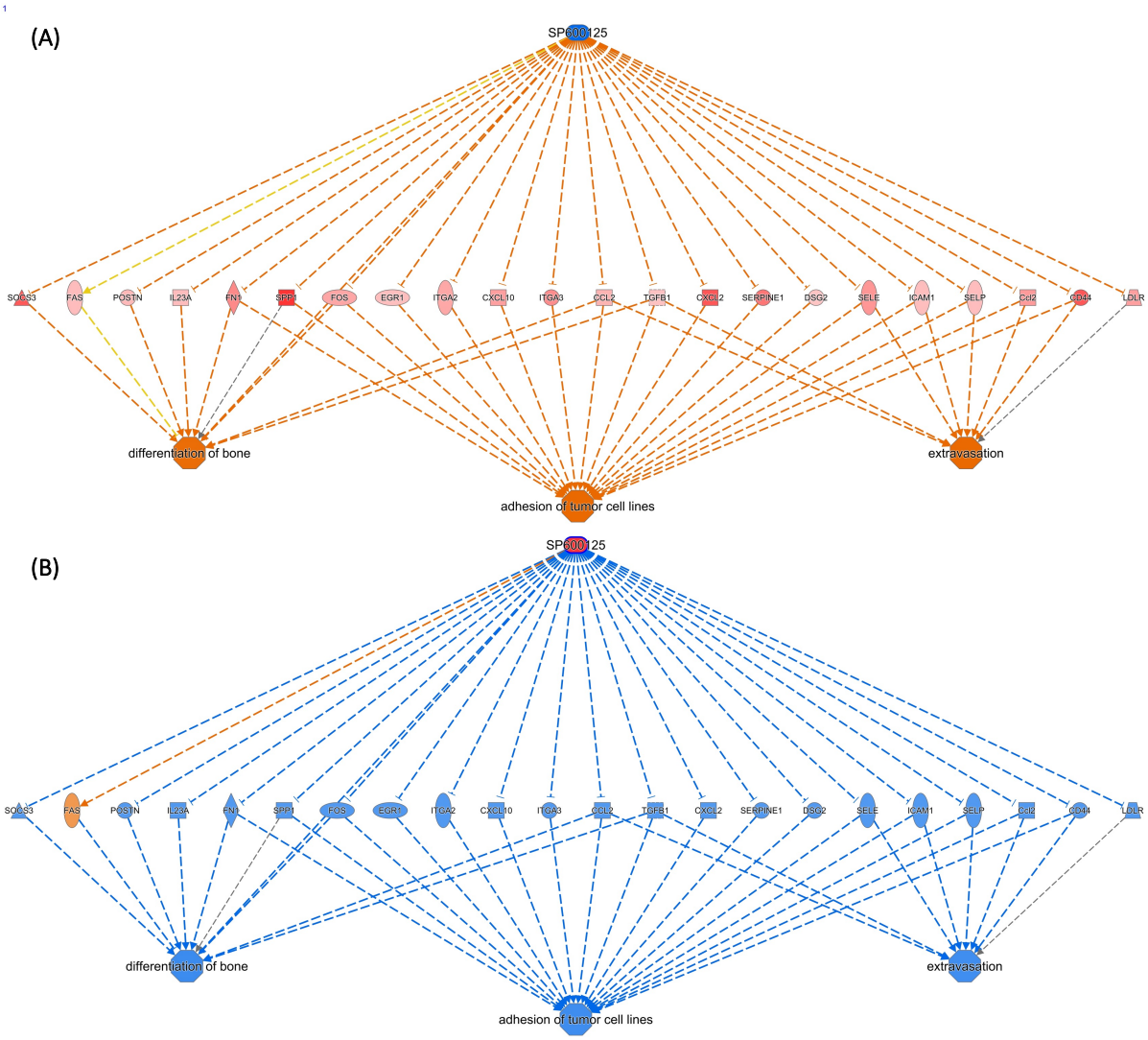

Appendix 11 SP600125 Targets in the IRI Dataset

The Regulatory Effects Network algorithm was set to examine for connections between known compounds (contained in IPA knowledge base), the dataset molecules and finally the phenotype. The compound SP600125 was predicted to demonstrate a high consistency score of 6.822. Image **(A)** demonstrates the anti-correlation between SP600125 and IRI dataset. Image **(B)** demonstrates the activation of SP600125 (coloured red) and hypothesized regulator effect and function.

Node key
Compound: blue (not administered), red (administered)
Upstream regulator: red and orange (activated), blue and green (inhibited)
Function: orange (activated), blue (inhibited)

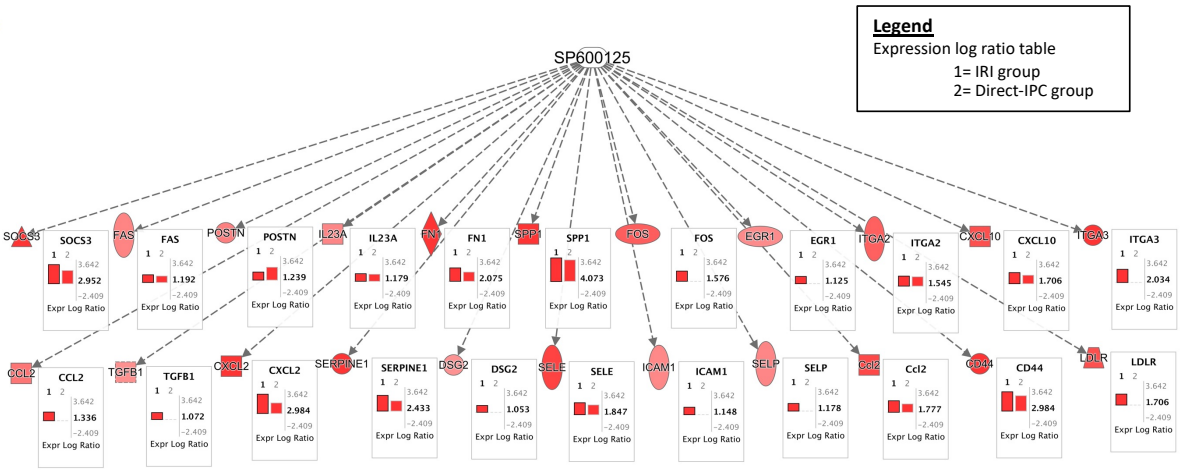

Diseases/Toxicity/Bio Functions	Z-score		Dirrection of Chemical Prediction
SP600125	IRI	D-IPC	
Adhesion of tumor cell lines	4.6	3.7	Inhibition
Differentiation of bone	2.2	1.7	Inhibition
Extravasation	4.1	0.0	Inhibition

Appendix 12 SP600125 IPC Transcriptional Comparison

(A) Those upstream regulators predicted to be targeted by SP600125 in the IRI dataset are displayed. The log_2FC of each upstream regulator in the IRI and direct-IPC datasets are displayed relative to sham. **(B)** The downstream directional change of the function of the network was further examined for concordance with the direct-IPC. SP600125 was predicted to inhibit 3 functions of the network. Direct-IPC shared concordance with SP600125 functional changes in 3 of the 3 functions.

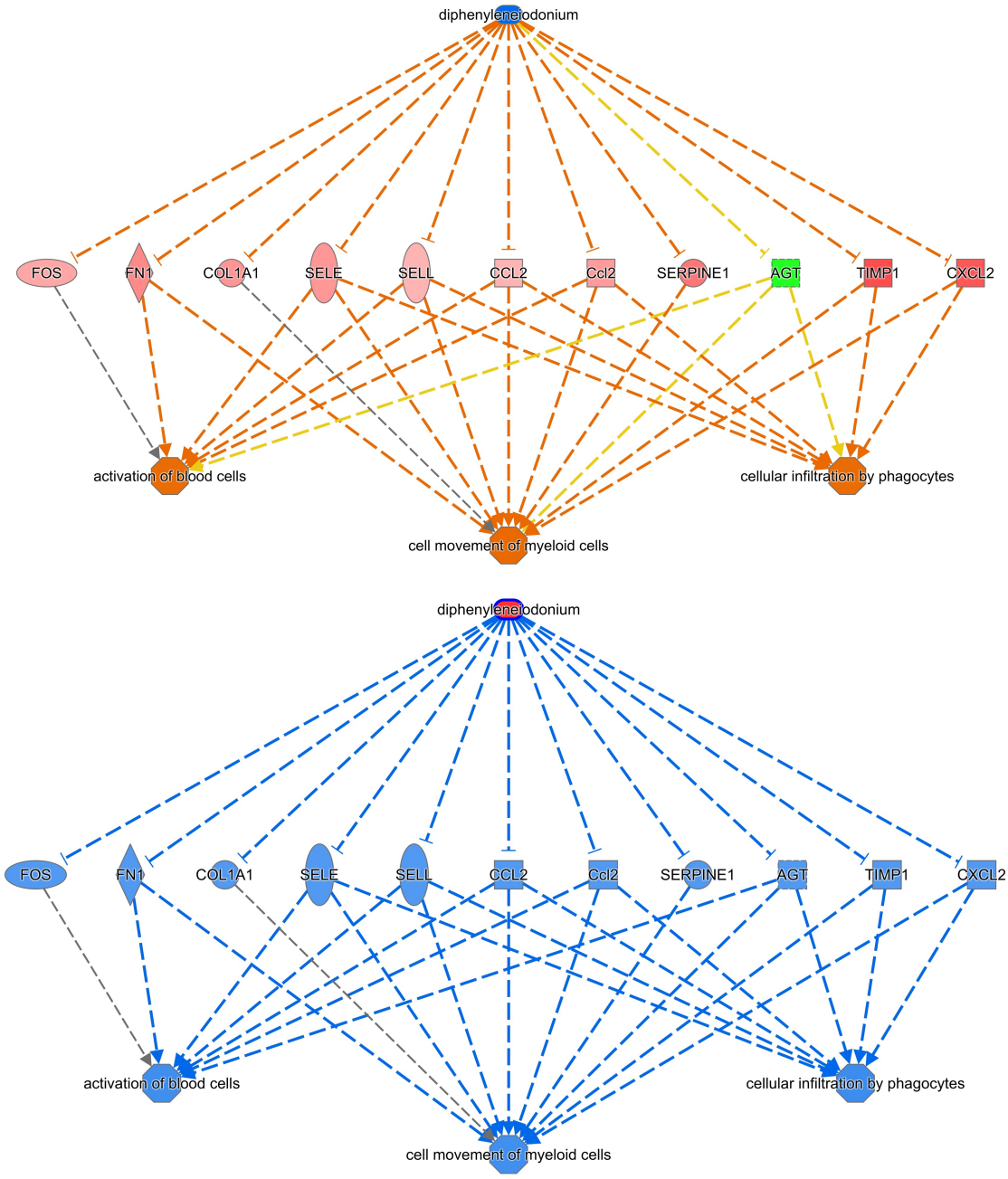

Appendix 13 Diphenyleneiodonium Targets in the IRI Dataset

The Regulatory Effects Network algorithm was set to examine for connections between known compounds (contained in IPA knowledge base), the dataset molecules and finally the phenotype. The compound diphenyleneiodonium was predicted to demonstrate a high consistency score of 6.633. Image **(A)** demonstrates the anti-correlation between diphenyleneiodonium and IRI dataset. Image **(B)** demonstrates the activation of diphenyleneiodonium (coloured red) and hypothesized regulator effect and function.

Node key Compound: blue (not administered), red (administered)
Upstream regulator: red and orange (activated), blue and green (inhibited)
Function: orange (activated), blue (inhibited)

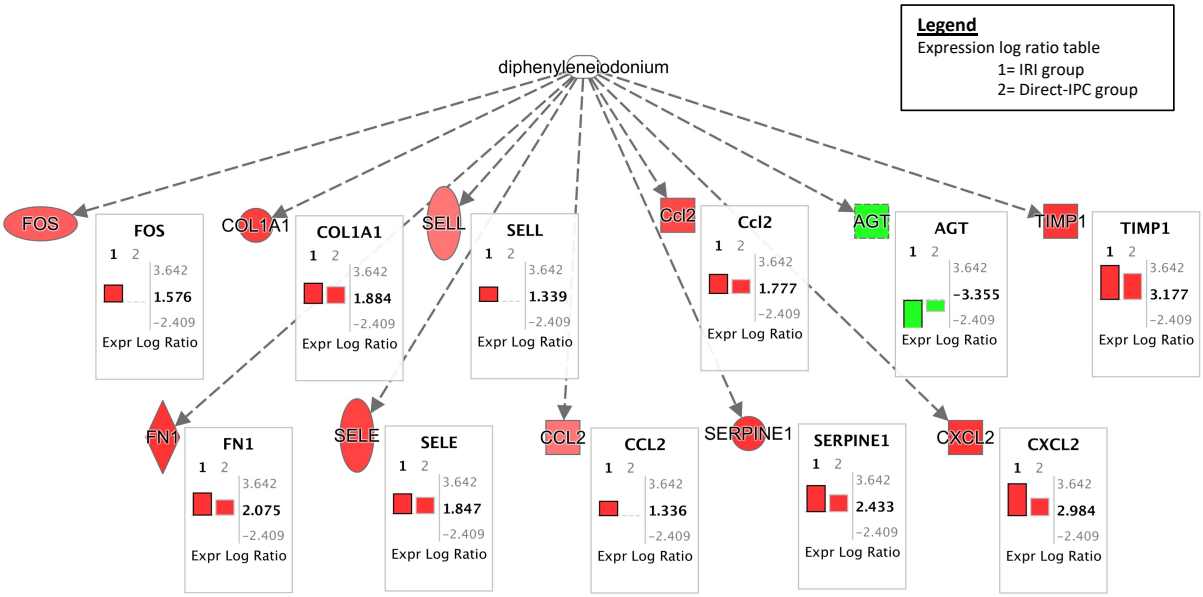

Diseases/Toxicity/Bio Functions	Z-score		Dirrection of Chemical Prediction
Diphenyleneiodonium	IRI	D-IPC	
Activation of blood cells	2.4	1.2	Inhibition
Cell movement of myeloid cells	4.5	3.5	Inhibition
Cellular infiltration by phagocytes	2.4	1.5	Inhibition

Appendix 14 Diphenyleneiodonium IPC Transcriptional Comparison

(A) Those upstream regulators predicted to be targeted by diphenyleneiodonium in the IRI dataset are displayed. The log_2FC of each upstream regulator in the IRI and direct-IPC datasets are displayed relative to sham. **(B)** The downstream directional change of the function of the network was further examined for concordance with the direct-IPC. Diphenyleneiodonium was predicted to inhibit 3 functions of the network. Direct-IPC shared concordance with diphenyleneiodonium functional changes in 3 of the 3 functions.

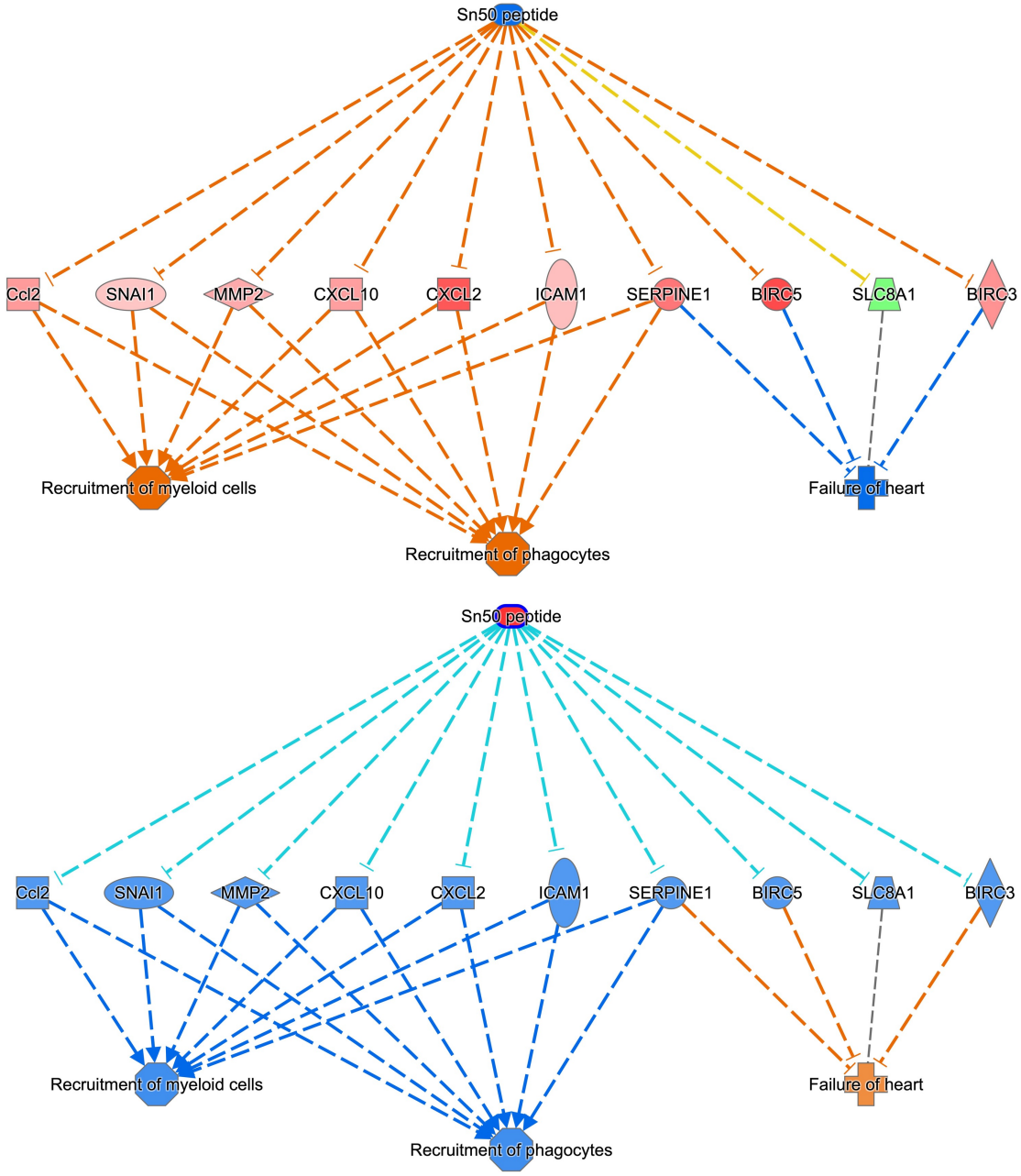

Appendix 15 Sn50 Targets in the IRI Dataset

The Regulatory Effects Network algorithm was set to examine for connections between known compounds (contained in IPA knowledge base), the dataset molecules and finally the phenotype. The compound Sn50 was predicted to demonstrate a high consistency score of 5.292. Image **(A)** demonstrates the anti-correlation between Sn50 and IRI dataset. Image **(B)** demonstrates the activation of Sn50 (coloured red) and hypothesized regulator effect and function.

Node key Compound: blue (not administered), red (administered)
Upstream regulator: red and orange (activated), blue and green (inhibited)
Function: orange (activated), blue (inhibited)

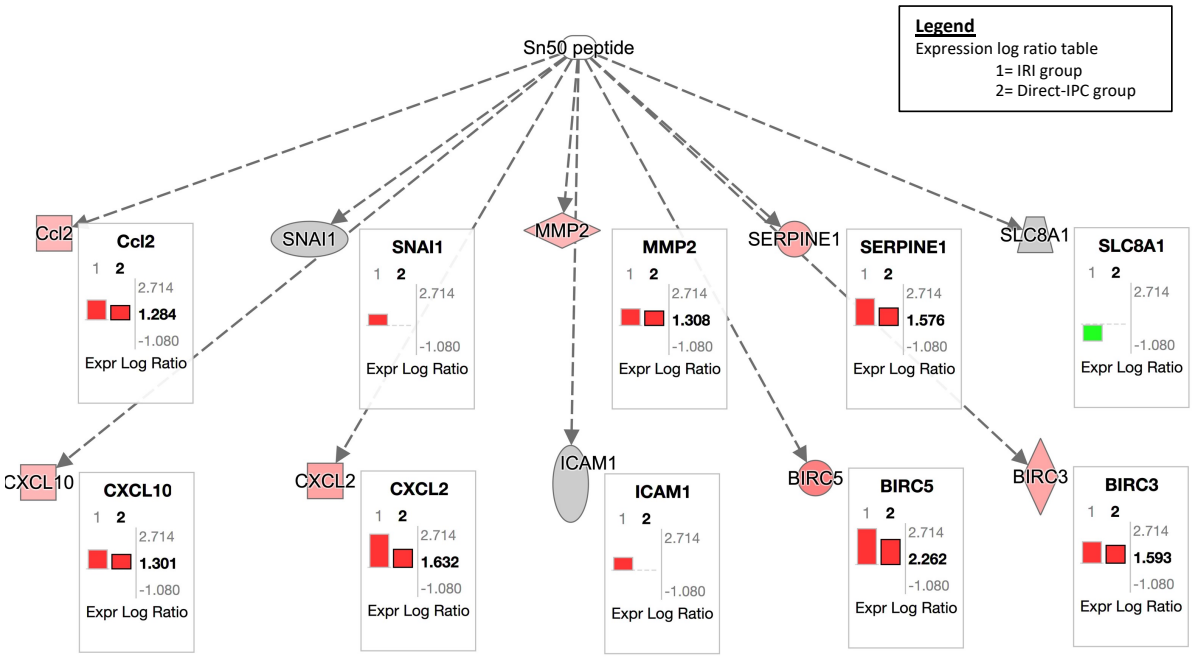

Diseases/Toxicity/Bio Functions	Z-score		Dirrection of Chemical Prediction
Sn50	IRI	D-IPC	
Failure of heart	-2.4	-2.1	Inhibition
Recruitment of myeloid cells	4.0	2.1	Inhibition
Recruitment of phagocytes	4.5	2.7	Activation

Appendix 16 Sn50 IPC Transcriptional Comparison

(A) Those upstream regulators predicted to be targeted by Sn50 in the IRI dataset are displayed. The log_2FC of each upstream regulator in the IRI and direct-IPC datasets are displayed relative to sham. **(B)** The downstream directional change of the function of the network was further examined for concordance with the direct-IPC. Sn50 was predicted to inhibit 2 functions and activate 1 function in the network. Direct-IPC shared concordance with Sn50 functional changes in 1 of the 3 functions.